ELECTRODEPOSITION OF PALLADIUM AND INDIUM

By

Anjum Razaq

A thesis submitted for the degree of

DOCTOR OF PHILOSOPHY

November , 1983

Department of Chemistry
University of Southampton

To my parents

and

to Razaq and Rabia

UNIVERSITY OF SOUTHAMPTON

ABSTRACT

FACULTY OF SCIENCE

CHEMISTRY

Doctor of Philosophy

ELECTRODEPOSITION OF PALLADIUM AND INDIUM

by Anjum Razaq

A study has been made of the electrochemical deposition of palladium and indium onto a vitreous carbon electrode from acidic aqueous solutions, pH 0-5, containing chloride ion. The two major techniques used were cyclic voltammetry and potential step. Although scanning electron scan microscopy and experiments with Platinum and carbon microelectrodes provided essential confirmation of the conclusion. It has been shown for both metals that good deposits could be obtained and that the deposition process involves instantaneous nucleation and three dimensional growth of the nuclei. The potential, concentration and pH dependences of the kinetic parameters are reported.

Electrocatalysis of H_2 of formic acid oxidation at freshly deposited palladium centers on platinum and carbon substrates was also studied. The results would suggest that very small palladium centers (<0.6 μ) are less active for H_2 evolution than bulk Pd. In contrast the palladium centers on a platinum substrate appeared to be excellent catalyst for formic acid oxidation (this is in contrast to carbon when the palladium centers are almost totally inactive).

Finally, the oxidation of HCOOH and DCOOH was studied at platinum partially covered by Pb adatoms. It was confirmed that the oxidation of HCOOH is partially diffusion and partially kinetically controlled. The chemical step reflects the coverage by Pb and shows a strong kinetic isotopes effect, $k_{HCOOH}/k_{DCOOH} = 2.6$. Such an effect is compatible with cleavage of the C-H bond in a dissociative adsorption reaction at adjacent Pt centers as the rate determining step.

ACKNOWLEDGEMENTS

I am indebted to Professor G.J.Hills for providing me with the opportunity to work in his research group. My thanks are also due to Dr. G.A.Gunawardena, not only for introducing me to this work but also for his continuous advice, supervision and constant encouragement throughout this research. I wish to express my sincere appreciation and gratitude to Dr.D.Pletcher for his consistent help, inspiration and "speedy" guidance, when I needed it most during the last and important stages of this work. My thanks are extended to the members of the glassblowing section and the other workshops who have always been very helpful to me.

I should like to express my heartfelt gratitude to Razaq for his continuous support, enthusiasm and patience without which this work would have been impossible. At this stage I must not forget to thank sweet Rabia, my daughter, for being so understanding and patient and hence making it possible for me to continue this work. I owe a special thanks to my parents who are extremely keen to see me successful, particularly in education and, despite every kind of problem, providing me with the chance to reach this stage.

My thanks are extended to all of my friends and colleagues for making my stay in the Department so pleasant. When speaking of friends, it is impossible to forget all those who have been very understanding and made me feel at home, never getting tired of looking after my daughter (which is quite a hard job I must admit). Their memories and help will be unforgettable.

Finally, I would like to thank Mrs. P.A.Dawson for her typing skills and helpfulness in the completion of this thesis so quickly and so well.

CONTENTS

CHAPTER 1

INTRODUCTION

CHAPTER 2

EXPERIMENTAL

CHAPTER 3

DEPOSITION OF PALLADIUM AND INDIUM

CHAPTER 4

APPENDIX

CHAPTER 1

INTRODUCTION

CHAPTER ONE

INTRODUCTION

The electrodeposition of metals has been of great interest in many branches of science for many years. A wide range of experimental techniques have been used to gain an insight into the mechanism and kinetics of the deposition of metals such as silver, mercury and nickel onto a conducting substrate (vitreous carbon is particularly convenient choice in the laboratory). Palladium, despite its importance as a precious metal and potential catalyst, has not received the attention it deserves. In electrodeposited form, it can be corrosion and tarnish resistant and is considered as a material for electrical contacts; certainly interest in its deposition has increased during the last decade.

Hence an objective of this work was to study the mechanism and kinetics of deposition of palladium onto vitreous carbon. It was also intended to investigate the catalysis, hydrogen evolution and formic acid oxidation being used as model reactions, at growing centers of palladium. It was hoped to answer questions such as the effect of the size of the catalyst center on the rate of catalysis. Moreover during the study of the deposition of palladium from chloride media, some unexpected results were obtained and some experiments were also carried out on indium deposition to see whether the phenomena is general.

Many of the experiments use cyclic voltammetry or potential step techniques. The latter method is particularly useful for the determination of the nucleation and growth parameters as a function of experimental conditions, e.g. Pd^{2+} concentration and pH.

Experiments at microelectrodes can give very detailed information on electrode reactions. On electrodes with a diameter of a few micron, one obtains a very high steady state rate of diffusion and with many electrodeposition systems, one only observes a single or at most, a very small number of nuclei. This is helpful in the study of metal deposition since one does not record the integral behaviour of a large

number of centers sometimes formed by progressive nucleation. It was also expected that such advantages would extend to the studies of electrocatalysis at such centers. Hence in this thesis, studies of the deposition of both indium and palladium on platinum and carbon microelectrodes are reported as are studies of hydrogen evolution at palladium centers on microelectrodes.

1.1 SOLUTION CHEMISTRY

1.1.1 Solution Chemistry of Palladium

Palladium almost always exists in aqueous solution as a complex; it hydrolyses readily. Pd(II) is the only common stable oxidation state. The other oxidation states such as Pd(0) and Pd(IV) are known but they are not normally stable and generally only exist as reaction intermediates. The Pourbaix diagram for non-complexing, aqueous solution is given in figure 1.1.

In aqueous solution and at all pH, palladium metal is thermodynamically stable in the absence of reducing, oxidizing or complexing agents. Palladium (II) forms hydroxides in aqueous solution at all pH. Pourbaix(1) also reports that in aqueous solutions palladium forms stable hydrides while only at low pH $\lesssim$ 1.0 is it stable as Pd^{2+} ions, see figure 1.1 but again in the presence of a ligand it forms complexes in solution. Droll etal(2) have demonstrated that a number of species exist in palladium chloride solution. They are Pd^{2+}, $PdOH^{+}$, $PdCl^{+}$, $PdCl_2$, $PdCl_3^{-}$ and $PdCl_4^{2-}$. All the species were seen spectroscropically in $PdCl_2/Cl^{-}$ / perchlorate media. The variation of all these possible species in chloride solution when the ratio of chloride and palladium varies from 0.6 to 4.8 is shown in figure 1.2, taken from the reference (2). For the chloride and total palladium concentrations used in this work it has been assumed that only the species $PdCl_2$, $PdCl_3^{-}$ and $PdCl_4^{--}$ are present. Droll etal(2) have calculated stability constants for the equilibria,

$$PdCl_2 + Cl^{-} \rightleftharpoons PdCl_3^{-} \quad \log K_1 = 2.5$$

$$PdCl_3^{-} + Cl^{-} \rightleftharpoons PdCl_4^{2-} \quad \log K_2 = 2.6$$

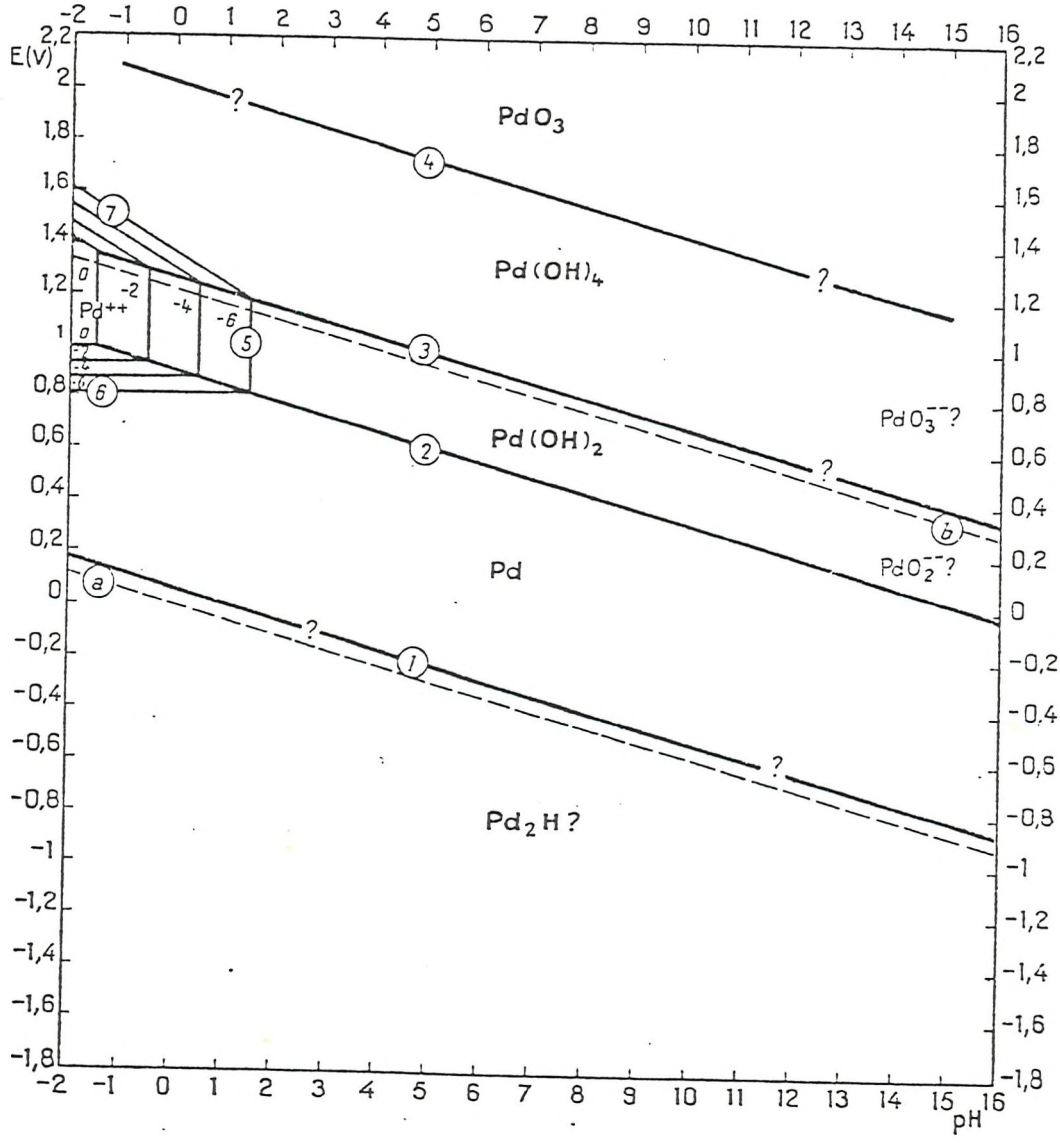

Figure 1.1 Potential - pH diagram for the system palladium - water at 25°C

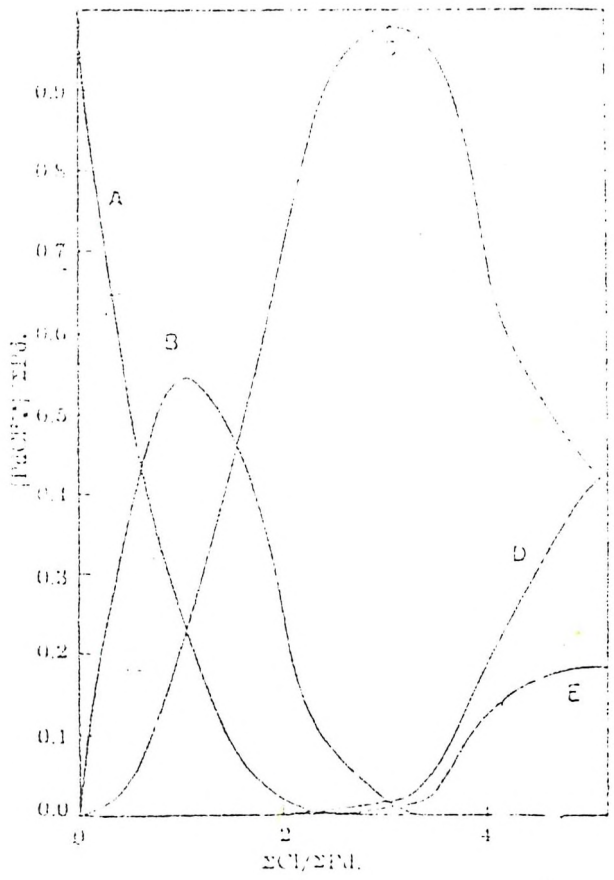

Figure 1.2 Distribution of palladium(II) chloride complexes at 21°C with $\Sigma Pd = 7.86 \times 10^{-4}$ mol dm^{-3} $[HClO_4] = 0.208$ mol dm^{-3} and $\mu = 0.440$. Curve A represents Pd^{++} + $Pd(OH)_x^{+2-x}$, B-$PdCl^+$, C-$PdCl_2$, $PdCl_3^-$, E-$PdCl_4^{--}$

At higher Cl^-/Pd ratios, the species $PdCl_5^{3-}$ and $PdCl_6^{4-}$ have been postulated by Sundaram and Sandell(3) but both species are of minor importance. Assuming that the four equilibria and their stability constants shown in table 1.1, the palladium chloride species present in chloride solution (1 mol dm^{-3}) have been computed see figure 1.3. $PdCl_4^{2-}$ is the predominant species but Pd^{2+}, $PdCl^+$, $PdCl_2$, $PdCl_3^-$, are also present.

1.1.2 Solution Chemistry of Indium

The most stable oxidation state of indium is In(III) although it also exists in the In(I) oxidation state. Indium readily forms complexes in aqueous solutions and figure 1.4 shows the potential-pH equilibria for indium in an aqueous non-complexing medium. At all pH the dissolution of indium is a favourable reaction and indium (In^{3+}) in aqueous solution hydrolyses to some extent. The Pourbaix diagram indicates that the upper limit of the stability region of indium (In^{3+}) in aqueous solution is about pH 2.5 and at pH 5-11 forms a film of In_2O_3. Busev(5) and Beidermann(6) has studied the behaviour of indium ions in solution and it is clear that the ions $(In(H_2O)\ OH)^{2+}$ and $(In(H_2O)(OH)_2)^+$ exist in the solutions of indium salts. The hydrolysis of indium is readily demonstrated. Moeller (7,8) has calculated the degree of hydrolysis of In^{3+} ions at high concentration in chloride solution and at pH 3.42 and the precipitation of a hydroxide could be detected. Radioactive techniques have also been used to determine the hydrolysis constants of the indium (In^{3+}) ions in aqueous solution.

In complexing media (e.g. halide ion solution) the complexes of indium are formed; indium chloride complexes are well known. Carlson and Irving(9) have examined the equilibria in halide ion solutions and report that indium exists as the complex, InX^{2+}, InX_2^+ and InX_3 (where X is Cl^-, Br^-, I^-). The stability constants decreased in the order $Cl>Br>I^-$, The equilibria between In^{3+} and chloride ions is given (10).

Equilibria for palladium(II) in chloride media	log K
$K_1 = \frac{[PdCl^+]}{[Pd^{2+}][Cl^-]}$	4.47
$K_2 = \frac{[PdCl_2]}{[Pd^{2+}][Cl^-]^2}$	7.74
$K_3 = \frac{[PdCl_3^-]}{[Pd^{2+}][Cl^-]^3}$	10.2
$K_4 = \frac{[PdCl_4^{--}]}{[Pd^{2+}][Cl^-]^4}$	11.5

Table 1.1 Various palladium equilibria in chloride media and corresponding stability constants

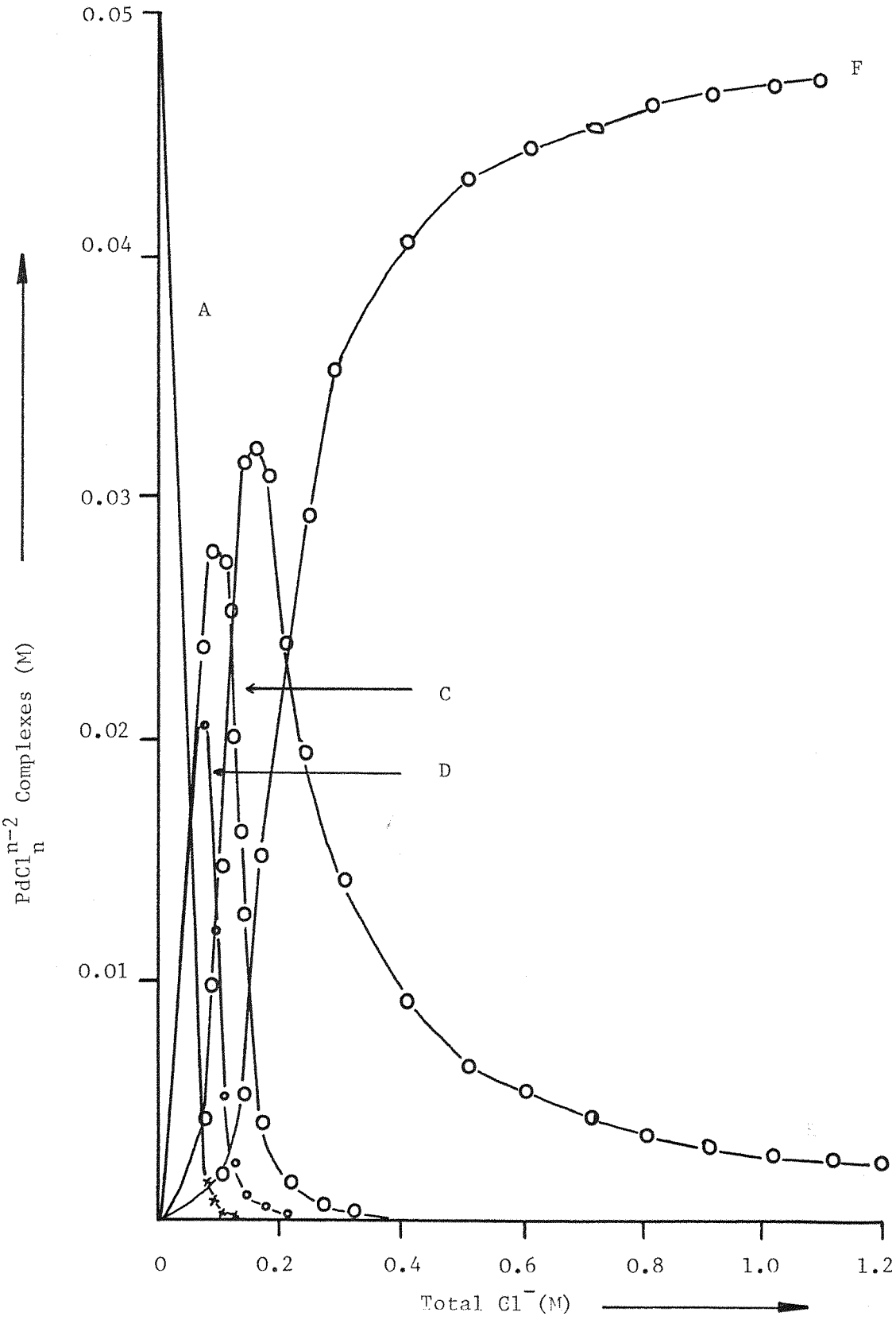

Figure 1.3 Distribution of palladium(II) chloride complexes in 50 mmol dm^{-3} $PdCl_2$ + 1 mol dm^{-3}KCl. Curve A represents Pd^{2+}, C- $PdCl^+$, D- $PdCl_2$ E- $PdCl_3^-$, F- $PdCl_4^{-2}$

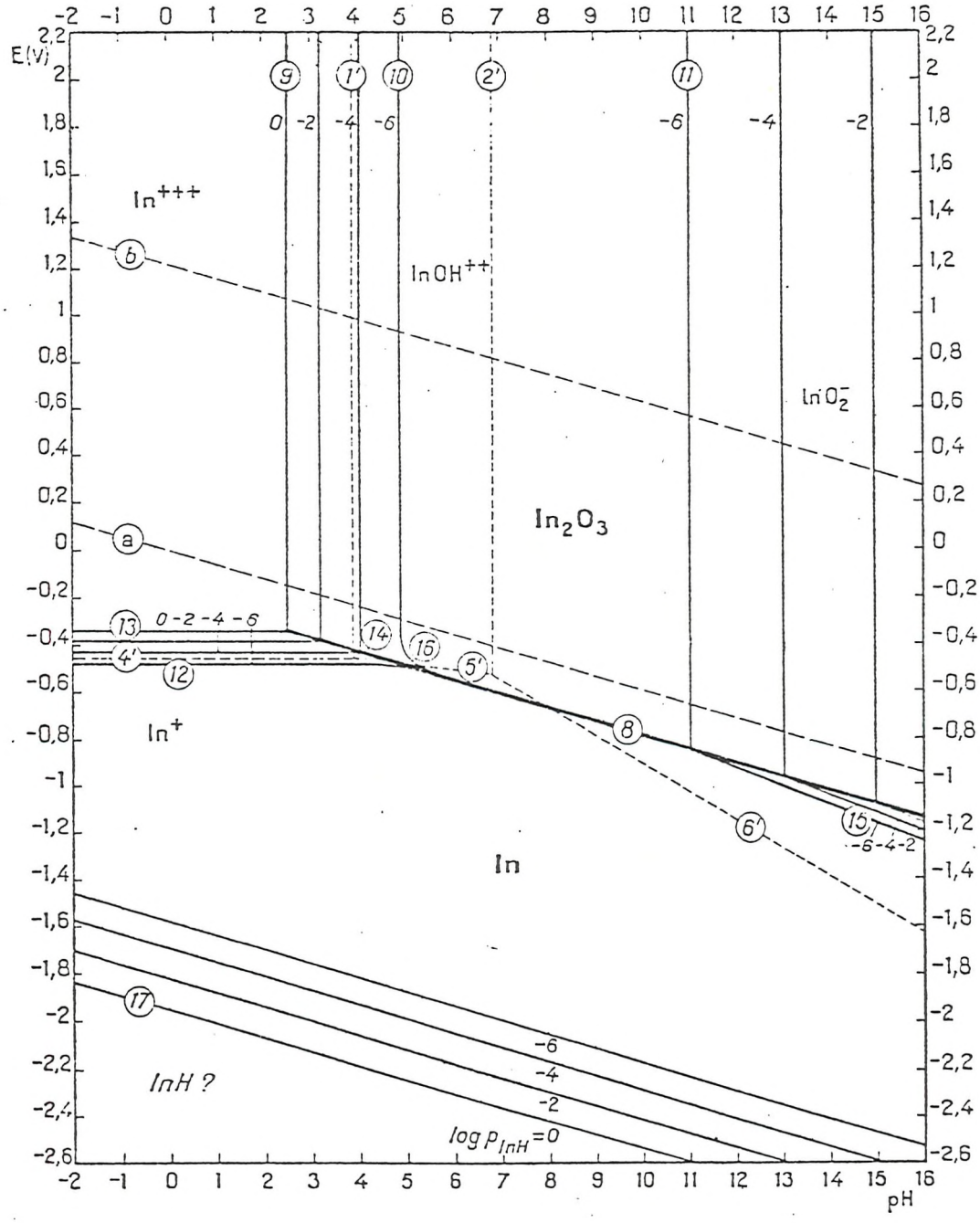

Figure 1.4 Potential - pH diagram for the system indium - water, at 25°C

$$In^{3+} + Cl^{-} \rightleftharpoons InCl^{2+}$$

$$In^{3+} + 2Cl^{-} \rightleftharpoons InCl_2^{+}$$

$$In^{3+} + 3Cl^{-} \rightleftharpoons InCl_3$$

In fact, the solution is more complicated since some hydrolysis will occur. Moeller(7) has shown that mixed complexes of Cl^- and OH^- are present.

Moreover in high chloride ion concentrations, higher complexes such as $InCl_4^-$, $InCl_5^{2-}$ and $InCl_6^{3-}$ are also present. Certainly $In(CNS)_6^{3-}$ dominates in concentrated CNS media see figure 1.5 (11), as shown spectrometically. However assuming only the three equilibria shown above and the stability constants (4)(table 1.2), the indium chloride species present in chloride solution have been calculated, see figure 1.6. In the chloride solutions used in this work (1 mol dm^{-3}), $InCl_3$ is the major speciesbut $InCl_2^+$ and $InCl^+$ are also present in substantial amounts. HCl was always added to suppress hydrolysis.

1.2 METAL DEPOSITION

1.2.1 Mechanism of Deposition - Electrocrystallization

Gibbs(12) studied the growth of solid crystals from the vapour phase and showed the similarities between electrodeposition and gas phase crystal growth. He formalized the thermodynamic quantities, enthalpies and entropies, as effecting forces in phase transformation in the equilibrium state between liquid and crystal; the essential driving force for nucleation and crystal growth is the difference in the free energies of the two phases i.e. liquid and crystal.

Kossel(13) presented a model of crystal growth based on a "KINK SITE" atomic model. The atomic or molecular species from the vapour phase absorb on the regular crystalline lattice, diffuse along the surface as an absorbed species or adion, until it reaches a monomolecular step. Then these adspecies travel along the step, still free to diffuse, until they find a kink, where they add into

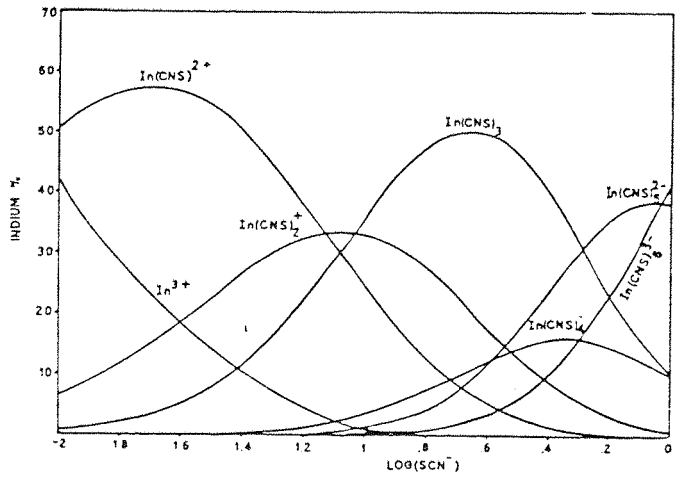

Figure 1.5 Percentage of indium in various forms as a function of free thiocyanate concentration

Equilibria for indium(III) in chloride media	log K
$K_1 = \frac{[InCl^+]}{[In^{3+}][Cl^-]}$	2.45
$K_2 = \frac{[InCl_2]}{[In^{3+}][Cl^-]^2}$	3.4
$K_3 = \frac{[InCl_3]}{[In^{3+}][Cl^-]^3}$	3.7

Table 1.2 Indium equilibria in chloride media and corresponding stability constants.

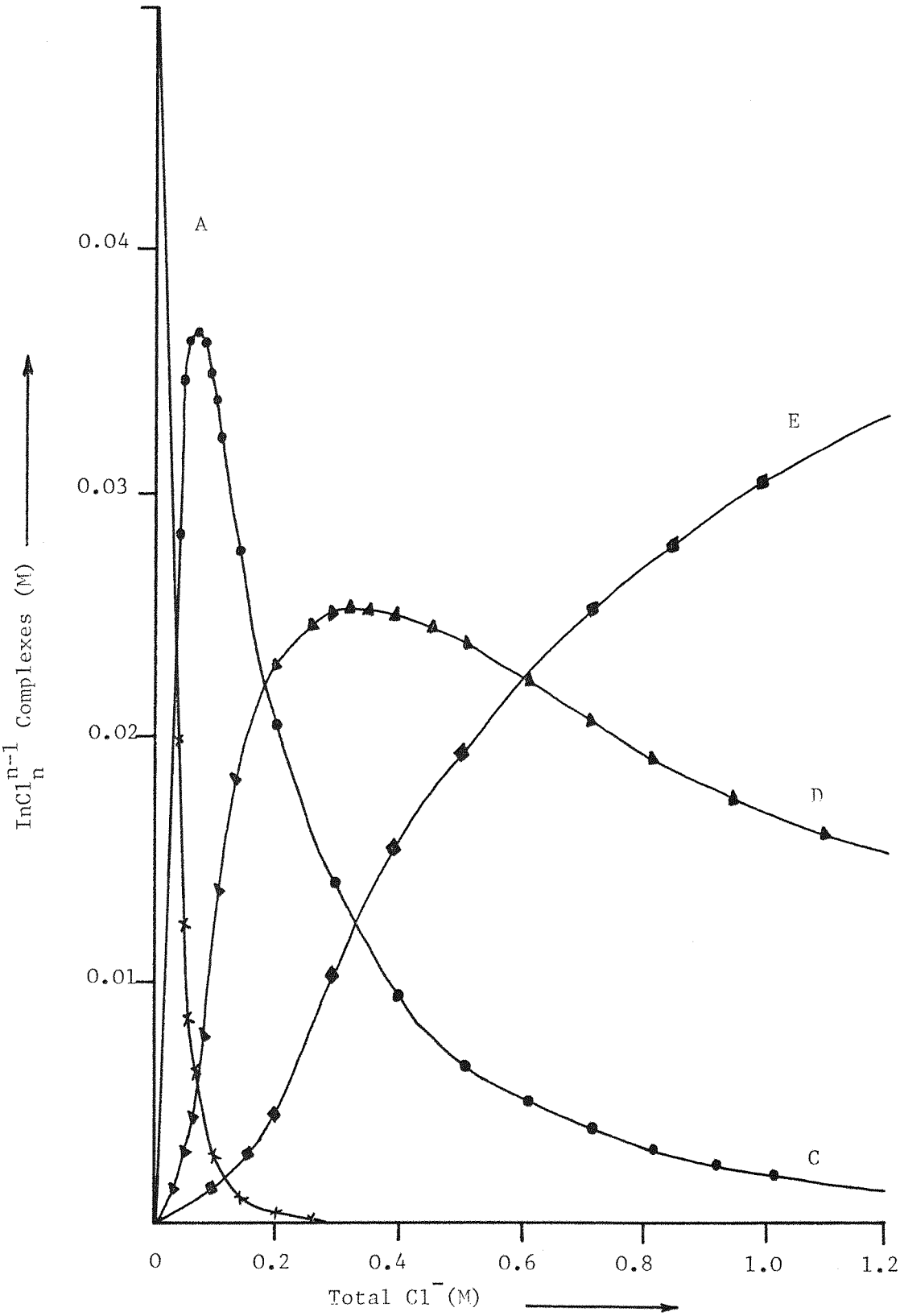

Figure 1.6 Distribution of In(III) chloride complexes in 50 mmol dm^{-3} $InCl_3$ + 1 mol dm^{-3} KCl. Curve A represents In^{3+}, C-$InCl^{+2}$, D-$InCl_2^{+1}$, E-$InCl_3$.

the surface lattice. This theory was combined with two dimensional nucleation and further developed by Stranski and Kaishev(14). When the surface is covered with two dimensional nuclei, another step is required for further nucleation and growth of another layer. The model of the growth plane is illustrated in figure 1.7(a) This well known "KINK SITE MODEL" is still widely used.

Bewick, Fleischmann and Thirsk(15), have experimentally demonstrated layer formation from a two dimensional nucleation. A screw dislocation model was demonstrated by Frank etal(16). and then Seiter and Fischer[17] who introduced spiral growth forms on the growing crystal. On the surface of the crystal an atom diffuses into a screw dislocation and creates a step line in the surface as shown in figure 1.7(b).A complete layer has not been formed but the spiral growth has been followed and the dislocation is always present one layer higher than before. Spiral growth has been observed in many cases (18). A "bunching mechanism" leading to the formation of microsteps can only occur in the region of a high concentration of adatoms. These microsteps can only be observed in the presence of adsorbed impurities (18,19). Then even more complex models of crystallization, whiskers (20) and dentrites (21), were introduced. Most of the theoretical work deals with homogeneous nucleation from the vapour phase, a well justified position in view of its relevance to the general theories of nucleation. However the difference between vapour phase growth and electrochemical growth is the presence at the metal solution interface of the potential field. Electrochemical nucleation and growth is a heterogenous process where the super-saturation for crystal growth results from the strong driving force for reduction and for the formation of metal adatoms.

1.2.2 NUCLEATION AND GROWTH

A nucleus is defined as a small cluster of atoms or molecules, which under the prevailing conditions, have developed to a size, sufficiently large, to grow spontaneously, thereby ensuring the viability and, eventually, the stability of the new phase. Their intensive properties differ from those of the bulk by virtue of their small size. Electrochemical free energy is the essential force to

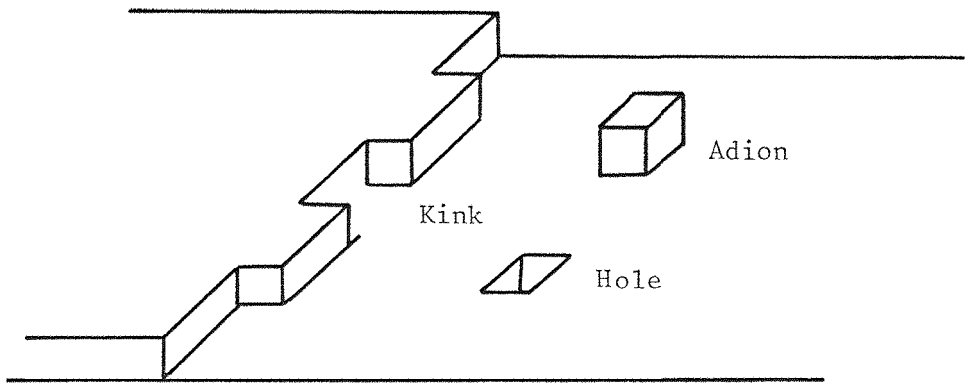

Figure 1.7 (a) KINK SITE model for the crystal growth

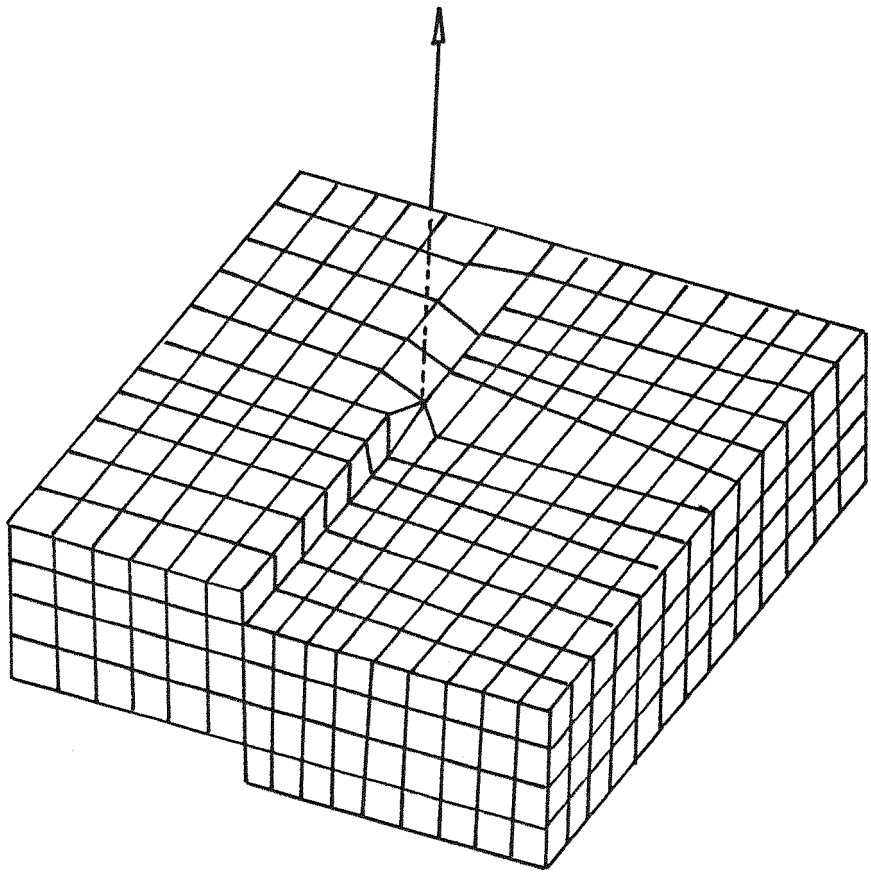

Figure 1.7 (b) Model for the screw dislocation intersecting the surface.

start the process of nucleation. The free energy, in the form of a potential applied to a conducting substrate, results in a current, and hence the growth of the nucleus. Before going into further details of the growth of nuclei and developing the current-time relations obtained at constant applied overpotential, it is better to distinguish between instantaneous and progressive nucleation, since these terms will be used frequently.

(a) Instantaneous nucleation
The nuclei all form in a very short time compared to that taken to grow the phase

(b) Progressive nucleation
The nuclei appear continuously with time with a constant average rate of formation

$$N = AN_o t$$

where N_o is the number density of available sites at the electrode surface

A is the nucleation rate constant.

Experimental studies of the nucleation process and of the growth morphology have commonly employed a potential step technique with analysis of the current-time transients. When an appropriate potential is applied to an electrode surface and after an initial decaying current which charges the double layer, the current will increase with time as the centers form and then grow. Eventually the current rises more slowly or even decreases as individual centers overlap. But the observed I-t response of the system will be influenced by a number of processes,

(a) The rate of formation of growth sites
(b) The geometery of the growing centers
(c) The number of growth sites
(d) The rate of propagation of growth sites in various dimensions
(e) The overlapping of centers

The number of these factors will reduce the number of parameters which can be evaluated. More recently the transient technique has extensively been used to formulate the growth model, and to study the

potential dependence of the rate constants for growth and for nucleation (22) under circumstances where the mass transport is large compared to the growth rate.

Jeager etal(23) and Frank and co-workers have, however, considered the rate of mass transport in an electrocrystallization process in unstirred solution and the diffusion to the electrode was considered to be a combination of planar and spherical diffusion. At high overpotentials where the concentration of species at the electrode is reduced to zero immediately after electrolysis has started, the overall current density for the reaction at a planar electrode is given by

$$I = \frac{nFD^{\frac{1}{2}}C^{\infty}}{\pi^{\frac{1}{2}}t^{\frac{1}{2}}} \qquad (1.1)$$

and when the spherical diffusion is also considered (necessary when the electrode is a small sphere or a nucleus is spherical) the equivalent equation is

$$I = nFD^{\frac{1}{2}}C^{\infty}\frac{1}{\pi^{\frac{1}{2}}t^{\frac{1}{2}}} + nFC^{\infty}\frac{1}{r_o}D \qquad (1.2)$$

This equation is extensively used to describe the transient current for growing hemispherical nuclei. As Jeager etal and Frank and co-workers have considered the planar and spherical diffusion, the flux obtained by them is the combination of

(a) hemispherical diffusion
or (b) hemicyclindrical
and (c) planar diffusion

Generally in such situations $I \propto t^{\frac{1}{2}}$ during early growth of nuclei and values of N_o can be evaluated and will be considered in detail later on. At long times the flux is planar (because r_o has become large) and $I \propto t^{-\frac{1}{2}}$; the value of diffusion coefficient D can then be evaluated.

1.2.3 NUCLEATION AND DIFFUSION CONTROLLED GROWTH

Astley etal(25) have considered that linear diffusion is the dominant form of mass transport at all t, and then the current at a

single hemispherical nucleus is given by the equation

$$I = 2\pi r_t^2 \, ZFC\left(\frac{D}{r_t}\right)^{\frac{1}{2}} \tag{1.3}$$

where

I = the current
r_t = the radius of effective surface area
Z = the number of electron transfer involved in the reaction
F = Faraday's constant
C = the concentration
D = the diffusion coefficient and
t = the time

and $$r_t = \frac{2MCD^{\frac{1}{2}}t^{\frac{1}{2}}}{\rho\pi^{\frac{1}{2}}} \tag{1.4}$$

substituting the value of r_t in equation (1.3)

$$I = \frac{8ZFM^2C^3D^{3/2}t^{\frac{1}{2}}}{\rho^2} \tag{1.5}$$

where Z,F,D,C and t have their usual meanings
and
M is the molecular weight of the depositing material
and ρ is its density

And hence a linear dependence between I and $t^{\frac{1}{2}}$ is predicted. On the other hand Hills etal(26 have given more importance to hemispherical diffusion in the growth of nuclei. Neglecting linear diffusion, the flux for hemispherical diffusion at small value of r is given by

$$I = 2\pi r^2 ZFC\frac{1}{r_t} \tag{1.6}$$

where

$$r = \frac{2DMCt}{\rho} \tag{1.7}$$

Then the final expression for the current is

$$I = \frac{ZF\pi(2DC)^{3/2}M^{\frac{1}{2}}t^{\frac{1}{2}}}{\rho^{\frac{1}{2}}} \qquad (1.8)$$

Again a linear dependence of I vs $t^{\frac{1}{2}}$ is obtained but with a different slope. The equations so far obtained are for a mass transfer controlled process (the overpotential was high so that the concentration at the surface is zero).

When there are N_o nuclei formed instantaneously at the beginning of the pulse, N_o must be added in the R.H.S. of all the equations (1,5, 1.8). If nucleation is progressive the equations are more complex.

1.2.4 NUCLEATION AND KINETICALLY CONTROLLED GROWTH

The other school of thought (27,28) believe that charge transfer is the rate determining step in the growth of a nuclei. Fleischmann etal(27) have considered the case when the growth of a nucleus is controlled solely by the rate of charge transfer (i.e. the mass transfer is relatively fast). Then the current time relationship depends on

(a) a geometeric factor
(b) the rate of appearance of nuclei

When a suitable potential is applied to an inert electrode, the growth centres (nuclei) will appear at the surface and then grow. Assuming that the rates are time invarient and the resultant current is due to the quantity of the material transformed, the current at any time t is given by

$$I = ZFkS \qquad (1.9)$$

Where k is the electrochemical rate constant at particular overpotential
S is the surface area of deposit which is expanding (cm^2).

The surface area of one center will increase with time. In the interval, dt, the center expands dr in one dimension then

$$dr = \frac{Mkdt}{\rho} \qquad (1.10)$$

Integrating the equation (1.10) within the limits

$$r = o \text{ at } t = o$$

$$r = \frac{Mkt}{\rho} \qquad (1.10)$$

and the current into a hemispherical nucleus is

$$I = ZFk\ 2\pi r^2 \qquad (1.11)$$

Therefore substituting the value of r in equation (1.11) gives

$$I = \frac{ZF\pi M^2 k^3 t^2}{\rho^2} \qquad (1.12)$$

Hence the current is linearly proportional to . Similarly the current obtained for two dimensional cylindrical growth is

$$I = \frac{2ZF\pi MLk^2 t}{\rho} \qquad (1.13)$$

Derivation for other geometeries have also been reported in the literature (28).

In all the above mentioned equations the currents are for the growth of single nuclei before the overlapping of individual diffusion zones.

1.2.5 COMBINATION OF GROWTH CURRENT WITH THE NUCLEATION LAW

The overall behaviour of the whole electrode surface can be obtained by combining the growth current for each nucleus with the nucleation law. If the age of the center is denoted by U, the following equation summarizes the growth model

$$I = f_1(U) \qquad (1.14)$$

and the law of nucleation is

$$N = f_2(t) \qquad (1.15)$$

where

N = the nucleation rate (s^{-1})

U = the age of the given center (sec)

Then overall current is given by

$$I = f_1(U)\left(\frac{df_2}{dt}\right)_{t = (t-U)} \qquad (1.16)$$

Equation (1.16) gives the behaviour of all centers in the time range where overlap has not started.

The surface energy is the major factor opposing the formation of nuclei. Therefore it is possible that particular sites on the electrode surface offer a lower barrier to nucleation; these sites are termed "preferred sites". Such sites all have an equal chance of becoming nuclei, and the nucleation process will be represented by first order rate law.

$$N = N_o \left[1-\exp(-At)\right] \qquad (1.17)$$

N = the number of nuclei at time t (cm^{-2})

N_o = the number of preferred sites (cm^{-2})

A = nucleation rate constant (s^{-1})

Two limiting forms of eq (1.17) are commonly used

(a) When A is large (with respect to the experimental time scale)

$$N \simeq N_o \text{ (instantaneous nucleation)} \qquad (1.18)$$

(b) When A is small

$$N \simeq N_o At \quad \text{(progressive nucleation)} \tag{1.19}$$

With different probabilities of nucleation, more complex models for the distribution of preferred sites have been reported(17).

By substitution of N in eq (1.12) and (1.13) gives for

instantaneous nucleation of centres growing in two dimensions

$$I = \frac{2ZF\pi MhN_o k^2}{\rho} t \tag{1.20}$$

instantaneous nucleation of centres growing in 3-dimensions as hemispheres

$$I = \frac{2ZF\pi M^2 N_o k^3}{\rho} t^2 \tag{1.21}$$

Similarly for progressive nucleation

progressive nucleation of centres growing in 2-dimensions

$$I = \frac{ZF\pi MLAN_o k^2}{\rho} t^2 \tag{1.22}$$

progressive nucleation of centres growing in 3-dimensions as hemispheres

$$I = \frac{ZF\pi MAN_o k^3}{3\rho^2} t^3 \tag{1.23}$$

A similar treatment of the diffusion controlled case using Astley's equations gives for

instantaneous nucleation of centres growing as 3 - D hemispheres

$$I = \frac{8ZFM^2 C^3 D^{3/2} N_o}{\rho^2 \pi^{\frac{1}{2}}} t^{\frac{1}{2}} \tag{1.24}$$

progressive nucleation of 3 - D centres growing as hemispheres

$$I = \frac{16ZFM^2AC^3D^{3/2}N_o\, t^{3/2}}{3\rho^2\pi^{1/2}} \qquad (1.25)$$

Likewise the Hills equations become, after similar substitution for

instantaneous nucleation of 3 - D centres growing as hemispheres

$$I = \frac{ZF\pi M^{1/2}(2DC)^{3/2}N_o\, t^{\frac{1}{2}}}{\rho^{1/2}} \qquad (1.26)$$

progressive nucleation of 3 - D centres growing as hemispheres

$$I = \frac{2ZF\pi M^{1/2}(2DC)^{3/2}N_o\, t^{3/2}}{3\rho^{1/2}} \qquad (1.27)$$

All these analytical expressions derived here involve approximations. The power law of I vs t is not alone diagnostic of the type of nucleation and growth. For characterizing the system in detail one needs optical microscopy or electron scanning microscopy as well. Moreover, it is commonly difficult to be certain of the power law from experimental data particularly as the approximations used in their derivation are only appropriate over part of the I - t transient. Anyway the slope of I vs t^n plots gives the combination of the potential dependent rate constant for the growth of nuclei and the formation of nuclei. The overlap factor can be considered and has been discussed for different geometeries.

1.3 THE REDUCTION OF Pd(II) and In(III)

1.3.1 THE REDUCTION OF Pd(II)

Polarographic studies of the reduction of various palladium (II) complexes have been made by a number of authors(29-43). Willis(29) seems to be the first to make an extensive polarographic study of the cyanide, ammonia, and pyridine complexes of platinum group metals. He claimed that palladium is the only metal in the platinum group which gives

satisfactory results on a mercury surface and showed the direct reduction of Pd(II) complexes to palladium. Formation of palladium from ammonical solution was also studied by Wilson and Daniel(35). Reduction of the Pd(II)/pyridine complex on a hanging mercury drop has been reported by Douglas and Magee(32,34). They have shown that the process involves two electrons and have proposed a full mechanism of the reduction process (32,34). Woodburn and co-workers(36) have reported the chronopotentiometry of the pyridine, ethylene diamine and ammonia complexes of palladium and again a two electron irreversible process was proposed. Several techniques have been used by a Soviet group of electrochemists in the study of reduction of palladium from its chloro and bromo complexes. The deposition and dissolution of palladium on a palladium disc electrode have been studied by Zelenskii and co-workers(37-41). They have reported that in palladium chloride solution, the major reducible specie is $PdCl_4^{2-}$. The deposition of palladium was found to be first order. Electro-reduction of palladium from its chloro-complexes have been studied galvanostatically. Zellenskii and Kravstov(44) showed that the deposition of palladium was proceeded by a chemical reaction.

$$PdCl_4^{2-} \rightleftharpoons PdCl_3^- + Cl^- \qquad (1.28)$$

followed by

$$PdCl_3^- \xrightarrow{+2\bar{e}} Pd + 3Cl^- \qquad (1.29)$$

This was demonstrated by the linear dependence of $\frac{\partial(i\tau^{\frac{1}{2}})}{\partial i}$ on chloride ion concentration, where τ is the transition time. During the last decade Harrison etal(45-48) has published a number of papers on the electrodeposition of palladium from a chloride solution. The techniques mainly used are based on the application of a potential pulse to a metal substrate and polarography. Astley and Harrison(45) have shown that the deposition of mercury, silver and palladium does not follow the same pathway partly because of the different nature of the deposits. Mercury does not have a crystalline lattice, therefore leads to transients which exhibit an $I \propto t^{\frac{1}{2}}$ dependence, as expected for diffusion controlled growth of the centres. On the other hand, the

silver deposit has a crystal structure and the growth is kinetically controlled. Palladium shows different behaviour again. Harrison and Thompson(46) studied the deposition of palladium from a chloride solution onto a palladium rotating disc electrode. During the potential pulse growth of palladium the rate was found to be time and potential dependent. Nucleation and growth steps are also shown by linear sweep voltammetry. A two electron irreversible charge transfer process giving rise to a Tafel slope of 60 mV was proposed as the mechanism for the deposition of palladium. The proposed reaction pathway is as follows:

$$\rightleftharpoons PdCl_4^{2-} \xrightleftharpoons{-Cl^-} PdCl_3^- \xrightleftharpoons{-Cl^-} PdCl_2 \rightleftharpoons \qquad (1.30)$$

$$\downarrow 2e$$

$$Pd + 2Cl^-$$

Moreover this behaviour is similar to that observed by Harrison and Bell(49) who studied the deposition of palladium onto vitreous carbon by cyclic voltammetry. The nucleation is slow and progressive but the growth is three dimensional at longer times. Similar results were obtained for the reduction of tetramine complexes. The number of nuclei were the same in both systems and therefore it is evident that the nucleation is controlled by the structure of the electrode surface.

During the electrodeposition of palladium from hydrochloric acid(50) it was found that with increase in Cl^- ion concentration the discharge potential of palladium was shifted towards more negative potential.

The effect of Cl^- ions on the anodic behaviour of palladium in moderately acidic solution is reported by Domenech and co-workers(51).

1.3.2 REDUCTION OF In(III)

The polarographic studies of indium have been reported by

Lingane(52). He observed that the reduction of indium ions in aqueous solution and in the presence of perchloric acid is irreversible. On the addition of halide ions, the wave shifts to more positive potentials and becomes steeper and better defined. This shows that the chloro-complex ions reduce more reversibly. Tuck etal(53) conclude that the polarographic reduction takes place in successive one electron transfer step, from indium complexes. It was then reported that the Cl^- ions have an accelerating effect upon the polarographic reaction of In^{3+}, and the polargraphic wave shifts towards more positive potential along with the sharp increase in height(54). Kiss etal (55) have demonstrated the reduction of In^{3+} ion onto a rotating disc electrode, and it occurs in one-electron steps, the rate-determining reaction depends on the release of the second electron. From the study of the electrode process on indium amalagum using a radioactive technique, Budov and Losev(56) have concluded that both cathodic and anodic process are step-wise.

$$In \longrightarrow In^+ + e \qquad (1.31)$$

$$In^+ \longrightarrow In^{2+} + e \qquad (1.32)$$

$$In^{2+} \longrightarrow In^{3+} + e \qquad (1.33)$$

The effect of pH on the anodic dissolution of indium has also been examined by Losev and Molodov(57). The formation of In(I) species during the anodic dissolution was suggested by Pchl-Nikov and Losev(58), and In(III) is then formed either by chemical reaction with H^+ in solution or by direct oxidation at the electrode. The addition of Cl^- ions to a perchlorate solution increases the apparent valency of dissolving indium. The participation of In(I) species have also been shown by Visco and co-workers(59-61). In Visco's(59,60) experiments In(I) formed during the anodization could be swept away from the electrode surface and detected polarographically in the bulk of the solution. Later on Miller and Visco(61) verified the mechanism of anodic dissolution of indium by using the rotating ring-disc electrode in perchloric acid media and showed a rapid one electron reaction to an In(I) species. The kinetics of reaction of In amalgam in chloride electrolyte have been investigated by Markovac and Lovrecek(62) and

Wright(63). Again the disproportionation reactions are likely to occur during anodic polarization while the first step

$$In^{3+} \longrightarrow In^{2+} \qquad (1.34)$$

in the cathodic reaction is the rate determining step.

1.4 THE ELECTROPLATING OF PALLADIUM AND INDIUM

1.4.1 PALLADIUM PLATING

Electroplating is of considerable practical interest. Many metals, e.g. tin, nickel, copper, zinc, gold, are electroplated commercially. The objective is always to modify the surface properties to fulfil a particular need, e.g. improve the corrosion resistance or conductivity of the surface. The art of electroplating is therefore to select the conditions (e.g. the bath composition, current density, temperature) to deposit the metal with the desired properties.

Platinum group metals are characterized by a high corrosion and tarnish resistance and when electrodeposited by hardness. This combination of properties has led to the widespread use of plated rhodium and palladium. Because of its relatively low cost, it is attractive to use palladium in place of other metals of the group such as platinum and gold. Recently Tedeschi etal(64) have reported palladium plating to be five times cheaper than rhodium plating. In view of its high hardness, good contact properties, excellent solderability and relatively low cost, palladium is used in many applications in place of gold, particularly for printed circuits and connectors where the areas of copper are isolated and it is difficult to make electrical connections(65).

Palladium deposits have also been used in the plastics industry, as an undercoat for sensitising plastics prior to further electrodeposition, and to form a range of electronic inks and components(66). Another use of palladium is in the communication industry. Deposited palladium is reported to be highly stable in artificial atmospheres(67) while an electrodeposited thin layer of palladium increases the corrosion resistance of titanium(68).

Deposition of palladium onto a foreign substrate from Pd(II) solution is generally done by one of two methods.

(a) An electrolytic method where the electrons are supplied by an external source (electroplating)

(b) Non-electrolytic methods, where the electrons are supplied by a chemical reducing agent (electroless plating) or by the dissolution of the base metal (immersion plating)

At the discharge potential for palladium (II), hydrogen evolution is very close and most of the plating so far reported is therefore based on palladium diammonium dinitrite (P-Salts)(69,70) in an ammonical media and with the addition of ammonium phosphate, sulphamate(70,71) and formate(72) as conducting salts which also influence the nature of the deposit. Recently halide electrolytes have been introduced and they are found to be 90% current efficient whereas the P-Salt bath is only 60% efficient. Acid palladous chloride and palladasoammine - chloride are other newly developed prototype, acid type baths(73). In $PdCl_2$/HCl media the electrodeposition of palladium can occur easily as the palladium is only loosely bound in a series of chlorocomplexes. This electrolyte is suitable for thick plating of palladium at the current density of 0.1 —— $10A/dm^2$. The corrosion resistance of palladium electrodeposits on nickel are somewhat better than that of gold deposits. It has been proved that palladium forms a thin passive oxide layer on the surface(74).

In their original configuration, the palladium baths were used with a cyclic organic amide as a brightening agent, but the drawback in these systems was the presence of microcracks in the product. A revised brightening method which leads to a less porous and cracked surface has been proposed by Ronald(74).

The pH of the electroplating bath also plays an important role in determining the form of deposit. In basic media palladium ion precipitates as hydroxides, therefore most of the plating solutions are acidic. As the hydrogen is discharged at low pH, the addition of a buffering agent is essential to maintain the pH at a suitable value.

The use of a buffering agent is demonstrated in a British patent(75) for palladium electroplating. The method gives a mirror bright deposit over a wide range of pH, 4———12. Acid electrolytes for bright plating have also been developed based on dinitrosulphate palladous acid and its salts(76,77). A number of other plating baths and conditions are summarised in table 1.3. It is noticeable that most of the baths used lately are based on aqueous complexing solutions.

Electroless plating or deposition is a term suggested by Brenner and Riddel(78) (1946). Gutziet(79) is more explicit and calls it "selective deposition by catalysed reduction on metallic substrate from aqueous solution".

A limited number of metals can be reduced to the metallic state by chemical means and palladium is one of them. Useful electroless deposits have been obtained for gold, silver, chromium, iron, nickel, cobalt, copper, antimony and palladium. The chemical reducing agents commonly used are hypophosphite, formaldelyde, hydrazine, borohydrides, aminoboranes and certain derivatives.

Brenner(80) recognised that the electroless deposition of palladium can be accomplished but there was a tendency for homogeneous reduction of the palladium ions to occur. This problem of bath instability has been controlled by proper selection of additives.

Rhoda(81,82) have introduced several electroless palladium baths based on hydrazine as the reducing agent for tetramine palladium complexes. The general reaction is illustrated as follows,

$$2Pd(NH_3)_4^{++} + N_2H_4 + 4OH^- \longrightarrow 2Pd^o + 8NH_3 + 4H_2O + N_2$$

The typical composition of solutions for hydrazine baths are listed in table 1.4. Electroless palladium deposits have been achieved on aluminium, chromium, cobalt, gold, iron, molybdenum, nickel, palladium, platinum, ruthenium, silver, steel, tin and tungsten.

Bath Constituents	Amount/gdm^{-3}	pH	Temp/C^{o}	Current Density A/dm^2	References
1. HALIDE TYPE					
$Pd(NH_3)_4 Br_2$	30	9.2	50^{o}	4	88
Ammonium bromide	45				
2. Palladium as amino chloride	30	9 - 9.5	25 - 50	4 - 10	70
Halide Conducting salt	45				
3. SULFAMATE TYPE					
Palladium diammonium dinitrite	12	7.5 - 8.5	25 - 35	4 - 10	70
Sulfamate	100				
4. $K_2(Pd(NO_2)_4)$	10	8.9	60	20	89
N-(2-aminoethyl) -1,3-diaminopropane.	60				
$NaNO_3$	30				
Potassium citrate	5				

Table 1.3 Bath constituents and conditions used for palladium electroplating

Pearlstein and Weightman(83,84) have demonstrated hypophospite as a reducing agent and the bath compositions are also illustrated in table 1.4. Glass or plastic activated by stannous chloride and palladium chloride(85) immersion are also readily plated with palladium. Recently palladium plating has been of a great interest and many other bath compositions have been reported(88-90).

1.4.2 INDIUM PLATING

Indium has been plated onto nearly all the metals and alloys, such as cast iron, stainless steel, steel, cadmium, nickel, copper, tin, silver and lead(93). Indium itself is a soft metal but on addition to gold and silver, it increases their hardness(94). It has been reported that a thin indium deposit on aircraft engine bearings reduces their corrosion. The corrosion of silver copper bearings was also reduced up to 30% by indium plating. Indium plating is very important in protection of aircraft engines(95). Indium and its alloys with other metals are extensively used in the electronics industry, to provide a low melting surface for soldering or joining(96-101). Many other authors have reported indium as a good corrosion resistant finish(101-105).

The most favoured electrolyte for the electrodeposition of indium is the sulphate solution. However difficulties may arise. Rakhmalullaev etal(106) found that at high current densities, the $In(OH)_3$ species was involved in the deposition of indium whereas at low current densities oxygen was reduced and indium was redissolved. The passivation of the electrode surface could arise by an acid film $In_2(SO_4)_3.H_2SO_4 \cdot 7H_2O$(107). This passivation was indicated by a low limiting current which depends on the electrolyte. The best electrolysis condition in sulphate solution was reported to be pH>1.6 with a current density below 1 A dm^{-2}.

Gershov and Purin(108) have studied the effect of halide ions on the process of electrodeposition of the metal, and have reported the increase in reaction rate on addition of halide ions.

Bath Composition	Amount/gdm^{-3}	pH	Temp/C^{o}	Application and form of plating obtained	References
1. HYDRAZINE BATH					
Tetramine palladium chloride	5.4		80	Electroless palladium has been deposited on number of metals and printed circuits as well as plastics	81
EDTA (disodium salt)	33.6				
Ammonium hydroxide	350.0				
Hydrazine	0.3				
2. Tetramine palladium chloride	7.5		35	useful for barrel plating	82
EDTA (disodium salt)	8				
Ammonium hydroxide	28				
Hydrazine (1 mol dm^{-3} soln	8 ml/hr/1				
3. Palladium chloride	1 - 5.5			Corrosion and wear resistance coating used for elect. contact or precision instruments	85
NH_4OH (28%)	50-250ml/1				
EDTA (disodium salt)	10-30				
$Na_2\ CO_3$	10-40				
$(H_2N)_2CSO$	.005-0.0001				
N_2H_4	0.2-0.45				

contd/

4.	HYPOPHOSPHITE-BASED BATH					
	$PdCl_2$	2		55	palladium is deposited on copper, brass, gold and nickel	84
	HCl (38%)	4				
	NH_4OH	160				
	NH_4Cl	27				
	$Na_2HPO_2.H_2O$	10				
5.	$Pd(NH_3)_2(NO_2)_2$	2	9.2		White palladium plating used at various metal surfaces	86
	$NH_4H_2PO_2$	95				
	NH_3	24 ml/l				

Table 1.4 Bath compositions and conditions for electroless palladium plating.

Indium plating is very simple, in contrast to that of many other metals, such as chromium, for which there is only one method. For indium there are quite a few baths available and used to some extent commercially. They are summarized in table 1.5.

1.5 CORROSION OF PALLADIUM AND INDIUM

The corrosion of metals can be a complex process with the formation of low valency intermediates as well as the stable product M^{n+} ions and the final corrosion product may be free in solution and/or be a solid phase on the metal surface. If the anodic dissolution of a metal

$$M \longrightarrow M^{n+} + e \qquad (1.35)$$

proceeds in one step then its corrosion rate can be determined by the usual electrochemical method of extrapolating the Tafel lines, to the corrosion potential. For the common electrochemical mechanism this extrapolated value should coincide with the open circuit corrosion rate.

The open circuit corrosion of metals, dissolving stepwise with the formation of unstable low-valency intermediates, in general proceed by a complex electrochemical-chemical mechanism, comprising several steps(116).

(a) Electrochemical formation of M^{+} ions, compensated by cathodic reduction of an oxidant (oxygen or water)

$$O + e \longrightarrow O^{-} \qquad (1.36)$$

(b) Electrochemical oxidation of M^{+} ions.

(c) Oxidation of M^{+} ions by solution components.

(d) Formation of solid phases

The anodic dissolution of both palladium and indium have been studied, and as has been mentioned earlier, both of them form stable

Bath Composition	Amount/gdm^{-3}	pH	Temp/C^{o}	Current density A/dm^{2}	References
1. CYANIDE BATH					
(a) Indium hydroxide	30 - 60		20 - 30	1 - 16	103-105
D-Glucose	15 - 30				
NaCN	150				
(b) Indium hydroxide	15 - 30		20 - 30	1 - 4	105-108
D - Glucose	20 - 30				
KCN	140- 160				
KOH	30 - 40				
2. SULFATE BATH					
Indium sulfate	20	2 - 2.7	20 - 30	2 - 8	112
3. SULFAMATE BATH					
Indium sulfamate	20		20 - 30	2 - 10	
Sulfamic acid					
4. TARTRATE BATH					
Indium hydroxide	15 - 25		20 - 30	1 - 5	113
Chloride, sulfate, nitrate or carbonate salt and tartrate					

Contd/

5. FLUOROBORATE BATH					
Indium metal	236	1.0	20 - 30	1 - 16	112,114, 115
Ammonium flouro-borate	272				
Boric acid	40 - 50				
Flouroboric acid	22 - 30				

Table 1.5 Bath compositions and various corresponding conditions for indium electroplating.

oxide and hydroxides. Anodic oxidation of indium in aqueous sodium hydroxide solution, under conditions where passivation readily occurs has been reported(117). The mechanism of oxygen evolution on the electrode has also been studied(118,119). Salem and Ismail(117) considered that the anodic polarization occurred in two stages.

(a) formation of indate ions, and
(b) the formation of indium hydroxide.

The initial discharge of hydroxide ions governed the overall reaction rate and led to the formation of InO_2^- on the electrode

$$In + 2H_2O \longrightarrow InO_2 + 4\overset{+}{H}+3e \qquad (1.37)$$

The linear potential sweep curve given in figure 1.8 shows the active and passive region and after saturation by the indate ions, the second phase of oxidation starts with the deposition of hydroxide on the electrode surface and the following process is involved.

$$InO_2^- + 2H_2O \longrightarrow In(OH)_3 + OH^- \qquad (1.38)$$

The anodic decay curve suggests the formation of a layer of indium hydroxide. From the results shown in the figure it is evident that there are two anodic arrests, attributed to the formation of indium oxide. At higher current densities indate formation occurs at more positive potential and direct passivation leads to oxygen evolution. Anodic passivation occurred as a result of a second surface oxide film, situated directly on the metal under the oxide film. Peircy etal(121) agreed with the previous workers, that the anodic reaction led to passivation due to the progressive growth of a solid film on the electrode surface.

In acidic solutions the anodic dissolution of indium is a stepwise process via unstable In^+ ions(116).

$$In \longrightarrow In^+ + e \qquad (1.39)$$

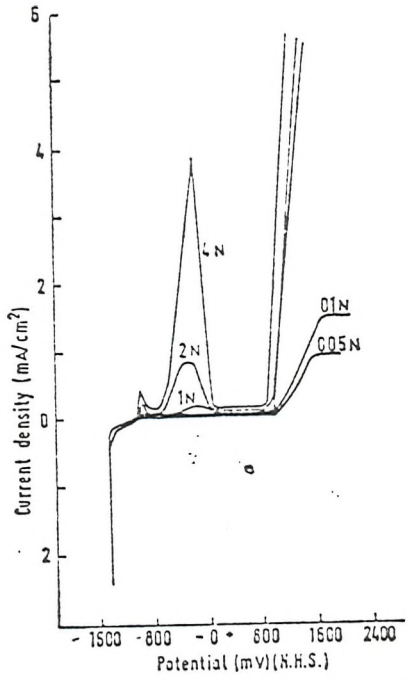

Figure 1.8 Current potential curve for anodic dissolution of indium in NaOH solution

The ions further oxidised to stable In^{3+} ions, both on the electrode

$$In^{+} \longrightarrow In^{3+} + e \qquad (1.40)$$

and in the solution by hydrogen ions.

$$In^{+} + 2H^{+} \longrightarrow In^{3+} + H_2 \qquad (1.41)$$

The effective valency of indium ions passing into the solution depends on the ratio of the rates of the reactions 1.40, 1.41 and at the low pH the indium dissolution potential shifts towards negative potential(122). In the presence of chloride ions the process of anodic oxidation of In^{+} to In^{3+} is accelerated and the effective valency increased to 3(123).

Similarly the polarization curves for a palladium electrode in acidic solution shows an active and passive region with corrosion commencing at 0.8 V(123). Figure 1.9 shows the current potential curve on a bright palladium electrode while figure 1.10 illustrates the corrosion of palladium for an electrode with a range of palladium loadings. Two distinct anodic peaks can be observed in figure 1.10-b, where the palladium black loading is in order a<b<c. More usually the second peak occurred as a shoulder as in figure 1.10-a and 1.10-c. The possible $2\bar{e}$ transfer mechanism is proposed for the reaction,

$$Pd \longrightarrow Pd^{2+} + 2e \qquad (1.42)$$

$$Pd \xrightarrow{k_1} Pd^{+} + e \qquad (1.43)$$

$$Pd^{+} \xrightarrow{k_2} Pd^{2+} + e \qquad (1.44)$$

$$Pd^{2+} \xrightarrow{H_2O} Pd^{2+} \qquad (1.45)$$

The rate constants k_1 and k_2 must be of similar magnitude. It is also observed that the pH of the solution also effects the separation of the two anodic peaks. The reaction scheme for

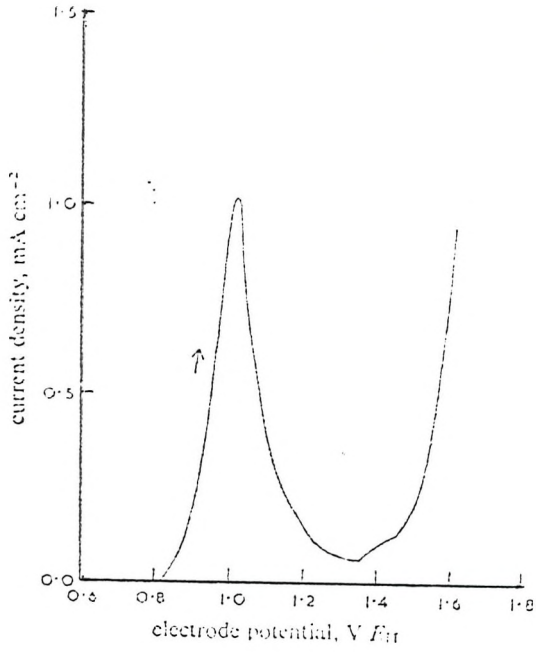

Figure 1.9 Polarization of a bright palladium electrode in 2 N H_2SO_4, potential sweep rate 100mVmin^{-1}.

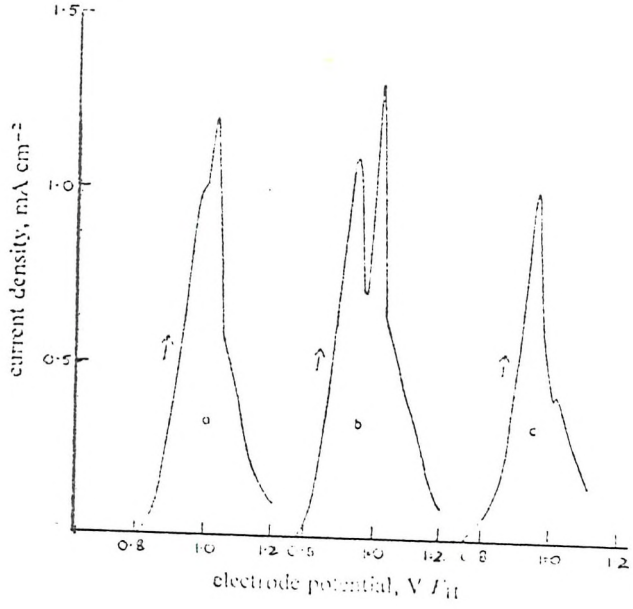

Figure 1.10 Polarization of palladium electrodes in 2N H_2SO_4, potential sweep rate 100mVmin^{-1}, Pd black loading order a<b<c.

anodic dissolution in aqueous solution can be written as follows(125),

$$Pd \longrightarrow Pd^{+2} + 2e \quad \text{(Direct dissolution)} \tag{1.45}$$

$$Pd + H_2O \longrightarrow PdO + 2H^{+} + 2e \quad \text{(formation of the surface oxide)} \tag{1.46}$$

$$PdO + 2H^{+} \longrightarrow Pd^{2+} + H_2O \quad \text{(Breakdown of the oxide layer)} \tag{1.47}$$

The overall rate of dissolution will depend on reaction 1.46 and 1.47. Reaction 1.46 leads to the formation of the surface oxide film(passive layer) which is responsible for the retardation of the dissolution process(126), and reaction 1.47 involves the breakdown of the passive layer. The presence of agressive anions such as Cl^- can lead to the pitting of metals, even when the potential is maintained in the passive potential region(127-129). The role of Cl^- ions in the pitting is related to its ability to effectively destroy the passive oxide film. Therefore the dissolution of palladium in presence of Cl^- ions is accelerated.

1.6 IMPORTANCE OF MICROELECTRODES IN ELECTROCHEMICAL STUDIES

The low currents and high mass transfer rate on a microelectrode make them excellent for the study of electrochemical kinetics. Because of the small size of the electrode a spherical diffusion field is superimposed upon planer diffusion to the surface. Therefore under potentiostatic conditions in unstirred solutions, the current density is given by the equation

$$I_d = \underbrace{\frac{ZFD^{\frac{1}{2}}C_o}{\pi^{\frac{1}{2}}t^{\frac{1}{2}}}}_{(a)} + \underbrace{\frac{ZFDC_o}{r_o}}_{(b)} \tag{1.48}$$

where (a) is the component due to planar diffusion and

(b) is that due to spherical diffusion

and I_d = the current density

D = the diffusion coefficient

Z = the number of electrons involved in the electron transfer process

F = the Faraday constant

C_o = the concentration

t = the time

The current at a spherical electrode of area, $A=4\pi r_o^2$, is given by

$$I = \frac{ZFD^{\frac{1}{2}}C_oA}{\pi^{\frac{1}{2}}t^{\frac{1}{2}}} + 4\pi r_o ZFDC_o \qquad (1.49)$$

This equation has two limiting forms, at short times and at long times.

1. At short times - The second term in equation 1.49 is negligible and the current is equivalent to that of normal planer electrode

$$I = \frac{ZFD^{\frac{1}{2}}C_oA}{\pi^{\frac{1}{2}}t^{\frac{1}{2}}} >> \frac{4\pi ZFDC_o}{r_o} \qquad (1.50)$$

or

$$I_d = \frac{ZFD^{\frac{1}{2}}C_oA}{\pi^{\frac{1}{2}}t^{\frac{1}{2}}} \qquad \text{(short time)} \qquad (1.51)$$

I_d is the diffusion current

2. At long times - At longer times and for small value of r_o, the first term in equation (1.49) is negligible as compared to the second

$$\frac{ZFD^{\frac{1}{2}}C_oA}{\pi^{\frac{1}{2}}t^{\frac{1}{2}}} << 4\pi r_o ZFDC_o \qquad (1.52)$$

Then the current becomes time independent and is now determined by the steady state (I_s) term.

$$I_s = 4\pi r_o ZFDC_o \qquad (1.53)$$

In the case of very small electrodes the current reaches a steady state value, whereas at a large electrode, at longer times the current should reach zero (in the total absence of convection). Note also the steady state current density at a microelectrode is proportional to $1/r_o$ and that the time to transfer to complete control by term (b) in equation 1.48 also depends on $1/r_o$.

1.6.1 THE DETERMINATION OF KINETICS UNDER STEADY STATE CONDITIONS

At a microelectrode, the steady state rate of diffusion is very high and it should therefore be possible to study the kinetics of fast electron transfer reactions.

For a totally reversible system Swan(130) has given the steady state current at a hemispherical electrode, as follows,

$$I_s = \frac{ZFD(C_b - C_o)}{r_o} \qquad (1.54)$$

Where C_b is the bulk concentration
and C_o is the concentration at the electrode surface

In this case, the curve will reach a diffusion limiting current but for a slightly slower electron transfer process, the rising part of the I-E curve can be analysed to give the electron transfer kinetics.

Because the area of the electrode is very small, the rate of mass transfer is large compared to the electron transfer process. For sufficiently small values of the standard rate constant the reaction must be under full kinetic control so that k can be determined. A reaction having a relatively small value of k has been investigated, and the availability of information about the rate constant, depends on the electrode radius used. The value of the rate constant for Hg/Hg^{2+} system has been reported by Fleishmann etal(131,132).

An experimental advantage of microelectrodes is that the set up can be made more straightforward. The low currents can be monitored in a two electrode cell (the reference electrode serves also as counter

electrode) without significant IR drop. Moreover the double layer charging current is proportional to the electrode area, so that in the case of microelectrodes this double layer charging capacity is low and this reduces the charging time. Therefore very rapid time dependent measurements of electrochemical events can be made.

1.6.2 NUCLEATION OF A SINGLE CENTER

The surface area of a normal macroelectrode is the order of cm^2 and the process of electrodeposition which is the result of wide spread nucleation leads to a large number of nuclei. This type of electrode also gives a large background current because of the large surface area and a high double layer charging current. But at a microelectrode, the area can be such that only a single nucleus is formed and it is therefore possible to watch the growth of only one nucleus. Moreover, as mentioned earlier, the double layer charging in the case of microelectrode is very small and hence the current associated with a single or small number of nuclei can now be observed and analysed.

On such a small electrode area, up to 10^{-7} cm^2, under potentiostatic conditions the growth current of a single nucleus can be directly observed. The currents corresponding to such a small nucleus are very small in the order 10^{-10}A so a special, rather sensitive ammeter is required to read the currents.

Nucleation is considered to be a stochastic process as the nucleation consists in the propagation of clusters through the distribution. If the current time transients for the formation and growth of a single nucleus is observed, a large fluctuation of individual transients from the mean of the ensemble are to be seen. Kinetic information can also be taken from the transients. The measurement of the rate of formation of α-PbO_2 on platinum microelectrode has been performed successfully(133).

A number of different kind of microelectrodes have been extensively used by the Electrochemistry Group at Southampton to study the rate of electron transfer(130,134-136). Lately attention

has been given to the investigation of nucleation and catalytic phenomena on microelectrodes. The formation and growth of the single nuclei have been studied in our laboratories while the catalytic activity of such small electrode covered by a foreign metal (ruthenium) have been demonstrated(135).

Recently the use of microelectrodes to measure the chemical concentration inside the nueral tissues (the brain) has been demonstrated(135). The application of microelectrodes have been reported for in vivo electrochemistry, the measured current is very small (nA) and does not damage the living cell.

A carbon fibre microelectrode was first introduced by Ponchon(138). Several other microelectrodes made by coating wires with an insulating film or the use of integrated microcircuit technology have been reported. McCreary(139) has used carbon fibres and 7 μm gold as cyclindrical electrodes in spectrophotometrical studies. The charging current is small and rapidly dies to zero. So the measurement on a timescale as short as 5 μs can be obtained.

1.7 MECHANISM OF THE HYDROGEN EVOLUTION REACTION

Gas evolution reactions usually involve the discharge of ions in solution or of the solvent molecules and in most cases involve two or more consecutive steps. The hydrogen evolution reaction is typical and has been studied on many electrode materials. It is of great importance in water electrolysis, chlor - alkali technology and corrosion and in the deposition of metals and organic reductions where it occurs as a side reaction. The reaction follows the pathway shown below and adsorbed hydrogen plays a key role. The hydrogen evolution reaction on metals follows the following steps(140).

$$\text{(a)} \quad M + H^+ + e \longrightarrow M(H)_{ads} \qquad (1.56)$$

followed by

$$\text{(b)} \quad M(H)_{ads} + H^+ + e \longrightarrow M + H_2\uparrow \qquad (1.57)$$

or

$$\text{(c)} \quad 2M(H)_{ads} \longrightarrow 2M + H_2\uparrow \qquad (1.58)$$

Each of these steps can be the rate determining step at an appropriate cathode and each step leads to a different Tafel slope and reaction order with respect to proton. The values predicted for such mechanisms are summarised in table 1.6.

Platinum metals have been widely studied and the dependence of the rate of hydrogen evolution reaction on the strength of the metal-hydrogen bond, was first discussed by Horiuti and Polanyi(141) and was further developed quantitatively by Parson and Bockris(142).

For the hydrogen evolution reaction on platinum metal, two types of hydrogen must be considered.

(a) Strongly adsorbed hydrogen
(b) Weakly adsorbed hydrogen

Evidence indicating the hydrogen exists in both weakly and strongly bound states on platinum has been shown by several workers(143-145). Thus two peaks can be seen on a cyclic voltammogram for a platinum electrode in an acid solution. Strongly adsorbed hydrogen leads to the peak at a more positive potential whereas the peak for weakly adsorbed hydrogen can be seen at a less positive potential. The mechanism for hydrogen evolution on platinum was shown to be (1.56) followed by (1.57) by Conway and Bockris(146);(1.57) is the rate determining step for hydrogen evolution in acid solution at high current density. Hence experiments lead to a Tafel slope of 120 mV and a first order dependence of current on proton-concentration. Azzam and Bockris(147) has also suggested that at low current density hydrogen evolution occurs by the slow recombination of H atoms and, in that case, rate determing step will be

$$2\ Pt(H)_{ads} \longrightarrow 2Pt + H_2\uparrow \qquad (1.59)$$

Hydrogen adsorption has been studied on other Pt group metals e.g. Rh, Ir, and Pd. The potential for the formation and the sharpness of the peaks corresponding to the hydrogen adsorption depends on the metal and the concentration of the acid. The mechanism for the

Rate determining step	Voltage range	Tafel slope $\frac{d \log I}{dE}$ /mV	Reaction order $\left(\frac{d \log I}{d \log C_H}\right)_E$
a	all	120	1
b	low	30	2
c	low	40	2
	high	120	1

Table. 1.6 Summary of the Tafel slopes and the reaction orders calculated for various possible mechanisms for hydrogen evolution.

hydrogen evolution at palladium is more complicated than the others. Capon and Parsons(148) has reported that the formation of molecular hydrogen involves the adsorbed hydrogen as an intermediate step

$$Pd + H^+ + e \longrightarrow Pd(H)_{ads} \qquad (1.60)$$

$$2Pd(H)_{ads} \longrightarrow 2Pd + H_2 \qquad (1.61)$$

and at the same time the adsorbed hydrogen diffuses into the bulk of the metal, hydrogen enters the lattice and its electrons become "collectivized" with the metallic electrons(149). Due to the absorption of hydrogen on palladium, the linear potential sweep voltammetry gives (in contrast to the sharp peaks observed on Pt) a broad peak for the hydrogen absorption and an ill defined diffused hydrogen oxidation region, especially at fast sweep rates. The double layer charging and the oxide formation region on Pd and Pt are very similar. However on Pd, the double layer charging region is found to extend with decreasing pH of the solution. In the case of palladium black a very small hump at slightly more positive potential can be observed, which may be because of adsorbed hydrogen(150).

1.8 CATALYTIC EFFECT OF DEPOSITED PALLADIUM ONTO METAL SUBSTRATE

The study of a thin layer of platinum metals on other substrate has shown that their behaviour is not the same as the bulk metals. It is reported that platinum on carbon does not show characteristic hydrogen adsorption until quite thick layers of platinum have been formed, while on gold, even a thin deposit show normal behaviour towards hydrogen adsorption(151).

It has been reported that a palladium electrode shows quite different behaviour with regard to hydrogen adsorption when it is covered with a thin evaporated film of palladium. The behaviour of a variety of grain sizes of palladium towards hydrogen adsorption has been studied by Horkan and Jean(152). A greater quantity of hydrogen was adsorbed by a thin layer of palladium on a palladium substrate than on palladium itself. On the bulk palladium the hydrogen adsorption region is well defined and

the process is irreversible. The results obtained from the palladium electrode covered with 0.025 - 1000mm thickness of film confirms that the hydrogen absorption occurs to a larger extent than with bulk palladium. The desorption peak is broadened at slow sweep rates, while at fast sweep rate the desorption peak disappears and the absorption process becomes irreversible. The broadening of the desorption peak is due to the slow diffusion of hydrogen in the metal lattice. On the other hand, an annealled (thick) film of palladium gives the similar results as bulk palladium.

Gold itself does not adsorb hydrogen but a monoatomic layer of palladium on gold behaves as palladium metal(153). The exchange current density increased rapidly with the deposit thickness. It is evident that the effect of palladium either on bulk palladium(152), gold(153) or pyrolytic graphite(154-156) depends on the form it is present. In either of these cases the results obtained are not similar. For instance, contrary to the results reported by Motoo and co-workers(153) no adsorption peaks are reported by Morcos(156) etal when studying the effect of palladium deposition on pyrolytic graphite, although the activity of the palladium for hydrogen evolution is twice higher than that of bulk palladium.

Studies were also made by Keren and Soffer(157) for hydrogen absorption rate and discharge mechanism on a palladium/carbon suspension electrode and again the behaviour of this kind of electrode is different from that reported by other workers.

The effect of the surface structure of a palladized platinum electrode upon the hydrogen sorption and catalytic properties have been reported by Shtrev and Glozhshka(158). The electrode coated with palladium at higher current density adsorb more hydrogen and displays a higher catalytic activity, although the real surface of both types of electrodes are the same order of magtitude.

1.9 MECHANISM FOR THE OXIDATION OF FORMIC ACID

The mechanisms for the catalytic oxidation of small organic molecules such as formic acid and methanol on metal electrodes, mainly

of the platinum group, have been the subject of extensive investigations for many years. Platinum is initially a good catalyst, but the metal surface is rapidly poisoned by strongly adsorbing intermediates. Several mechanisms have been proposed for the oxidation of formic acid but the mechanism, generally accepted, is that proposed by Capon and Parsons(159).

$$HCOOH \longrightarrow *COOH + *H \qquad (1.61)$$

$$*H \longrightarrow H^+ + e \qquad (1.63)$$

$$*COOH \longrightarrow CO_2 + H^+ + e \qquad (1.64)$$

Where * indicates the number of platinum sites bonded to the carbon.

The poison is formed by a parallel reaction, possibly

$$*COOH + HCOOH \longrightarrow \overset{*}{\underset{*}{*}}COH + H_2O + CO_2 \qquad (1.65)$$

They also suggested that the poison could also be formed by a different pathway, if the potential is held in the hydrogen adsorption region.

$$HCOOH \longrightarrow *H + *COOH \qquad (1.66)$$

$$H^+ + e \longrightarrow *H \qquad (1.67)$$

$$*COOH + 2*H \longrightarrow \overset{*}{\underset{*}{*}}COH + H_2O \qquad (1.68)$$

This mechanism was important in non steady - state experiments, where the potential is swept or pulsed from the hydrogen adsorption region. The oxidation of formic acid then occurs at a surface already partially covered by poison and hence only at a low rate.

The formic acid oxidation leads to the production of CO_2 and some workers have suggested that reduced CO_2 poisons the electrocatalytic oxidation of formic acid(160. The identification of the structure of the poison is still not regarded as fully resolved. Recently the use

of in situ electrochemically modulated infra red spectroscopy (EMIRS) has made it possible to elucidate the molecular structure of the species adsorbed at the electrode surface(161-163). Bewick etal have investigated in detail the electrosorbtion of formic acid and reduced CO_2 in aqueous solutions(163-165). Two infra red absorption bands observed in each case were assigned to a carbonyl species bonded to one surface platinum atoms (I.R. band centered at 2060 cm^{-1}) and to three surface platinum atoms (I.R. band centered at 1860 cm^{-1}).

It was reported by several workers that submonolayers of lead adatoms catalyse the oxidation of formic acid. The role of the adatoms is believed to be twofold.

(a) The formation of poison by reaction (1.65) requires several adjacent platinum atoms (the sites where the adsorption occurs) and the role of lead is to isolate adjacent platinum atoms in the surface and hence slow down the formation of poison.

(b) When the electrode potential is in the hydrogen adsorption region the reaction (1.66) and (1.67) is inhibited because hydrogen does not adsorb on lead (which is present as a complex monolayer at these potentials)

Bewick and co-workers have also reported that in the presence of Pb^{++} ions the IR band centered at 1860 cm^{-1} disappeared while the IR band centered at 2060 cm^{-1} was uneffected which suggested that the main poison during the oxidation of formic acid was a carbonyl species, presumably $(CO)_{ads}$, bonded to three surface platinum atoms.

At Pd, the same type of mechanism of oxidation of formic acid has been proposed and the effect of foreign adatoms should again be observed although palladium is known to be poisoned to a less extent by the adsorbing intermediate(166,167). Voltammograms for the oxidation of formic acid on palladium shows very little resemblence with platinum. A typical linear potential sweep voltammogram for the oxidation of formic acid on platinum is shown in figure (1.11). The voltammogram has identical features to those reported by other workers(168-170). On the anodic sweep there are three peaks, at 0.5 to 0.6V, 0.9V, 1.4 to 1.5V,

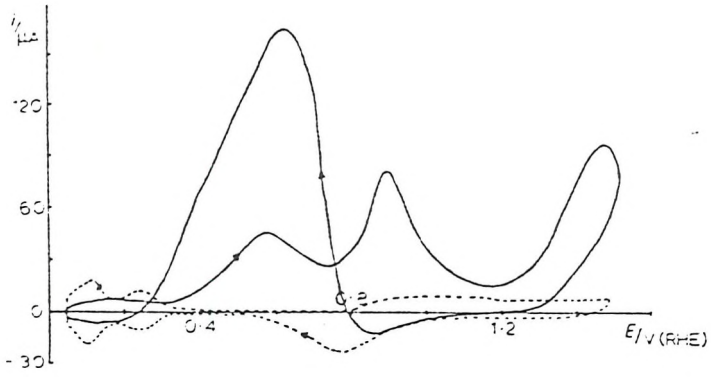

Figure 1.11 Cyclic voltammogram for platinum electrode in (....) 0.5mol dm^{-3} H_2SO_4, (——) 0.5 mol dm^{-3} H_2SO_4 + 0.1 mol dm^{-3} HCOOH. Sweep rate 140 mVs^{-1}

termed as first, second and third anodic peaks respectively. On the reverse sweep a single large peak is observed at the potential close to the first anodic peak. The cyclic voltammogram for the oxidation of formic acid on a palladium electrode (figure 1.12b) shows that there are no peaks in the potential range between 0.9 and 1.5V equivalent to the second and third anodic peaks as observed on platinum electrode. A single oxidation peak occurs at a potential close to the first anodic peak observed on platinum. The shape of the oxidation peaks on both the positive and negative going sweeps(166) are similar. However the oxidation current on the cathodic sweep is a little higher than that on the anodic sweep. This shows that there is no or a very little removal of the active sites by strongly adsorbed intermediates, as occurs on Pt, and the proportion of the surface available during the positive and negative going sweeps is the same. The disappearance of the oxidation peaks equivalent to the second and third anodic peaks observed on platinum, is probably due to the fact that formic acid does not react with the adsorbed palladium oxide species(171), although the palladium oxide is known to form in this potential range.

Poliak(172) has also interpreted the equality of the shape and size of the oxidation peaks on both the positive and negative going sweeps on the basis that no strongly adsorbed intermediates are present on palladium.

For palladium the oxidation of formic acid on the negative going sweep starts after the palladium oxide, reduction peak. Formic acid has the tendancy to react with platinum oxide(s) to form chemisorbed intermediate, thus accelerating its removal as soon as the threshold of oxide reduction peak is reached, and as a result a large increase in oxidation current is observed on the cathodic sweep. Formic acid does not form the chemisorbed intermediates by reacting with palladium oxide(s);therefore it cannot accelerate the removal of oxide and hence there is no appreciable increase in the oxidation current on the negative going sweep.

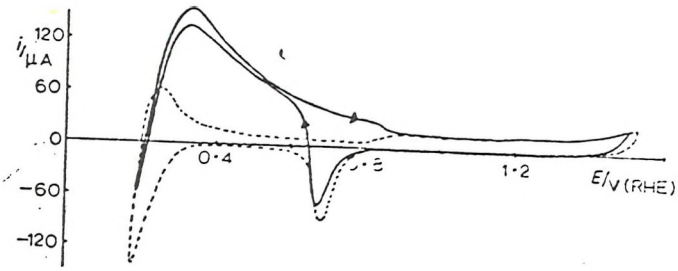

(a)

Figure 1.12-a Cyclic voltammogram for palladium electrode in (....) 0.5 mol dm^{-3} H_2SO_4, (——) 0.5 mol dm^{-3} H_2SO_4 + 0.1 mol dm^{-3} HCOOH. Sweep rate 70 mVs^{-1}

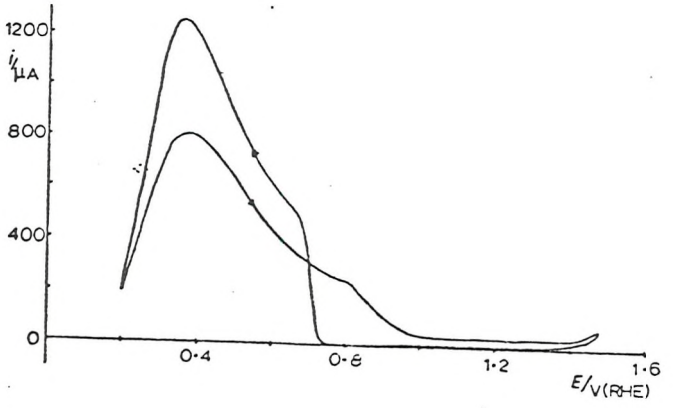

(b)

Figure 1.12 -b Cyclic voltammogram for palladium electrode in 0.5 mol dm^{-3} H_2SO_4 + 1 mol dm^{-3} HCOOH.
Sweep rate 70 mVs^{-1}.

CHAPTER 2

EXPERIMENTAL

CHAPTER TWO

EXPERIMENTAL

2.1 The Cells

All the experiments using vitreous carbon, platinum or palladium disc electrodes of normal size (macroelectrodes) were carried out in a cell shown in figure 2.1. It was a conventional type of two compartment, three electrode cell. The disc working electrode was inserted into the cell from the top in such a way that the electrode surface faced downwards. The height of the electrode was adjusted to make the distance between the electrode surface and the fixed luggin capillary as small as possible. The fixed capillary was attached to a separate reference electrode compartment. A circular (spiral) platinum wire used as secondary electrode was inserted into the working compartment from the side towards the bottom of the cell.

All the experiments using a carbon or platinum microelectrode were carried out in cell shown in figure 2.2. It was a single compartment two electrode cell. The microelectrode was inserted into the cell from the top in such a way that the electrode surface faced downwards, towards the secondary electrode. A platinum or palladium spiral secondary electrode (which was also acting as the reference electrode) was inserted from the bottom of the cell. The distance between the working electrode and platinum or palladium spiral was maintained as small as possible (about 0.5cm).

2.2 Electrodes

(a) Reference Electrodes

In all the experiments carried out on normal size (large) electrode a Radiometer K.401 saturated calomel electrode was used as the reference electrode. In the experiments using micro working electrodes, the platinum or palladium spiral electrode was used as a counter/reference electrode, being placed parallel to the microelectrode.

(b) Working Electrodes

The vitreous carbon disc electrode was made by sealing under vacuum

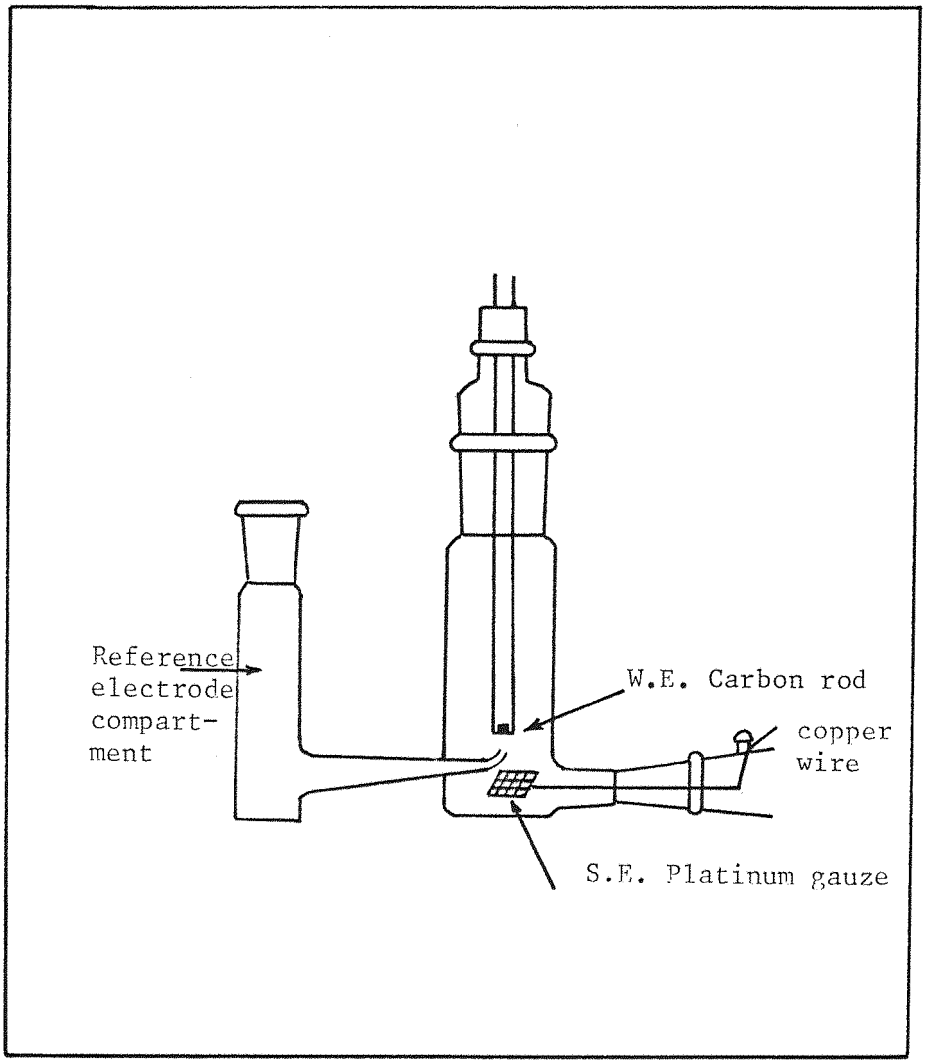

Figure 2.1 Sketch of the cell used for electrodeposition on macroelectrodes

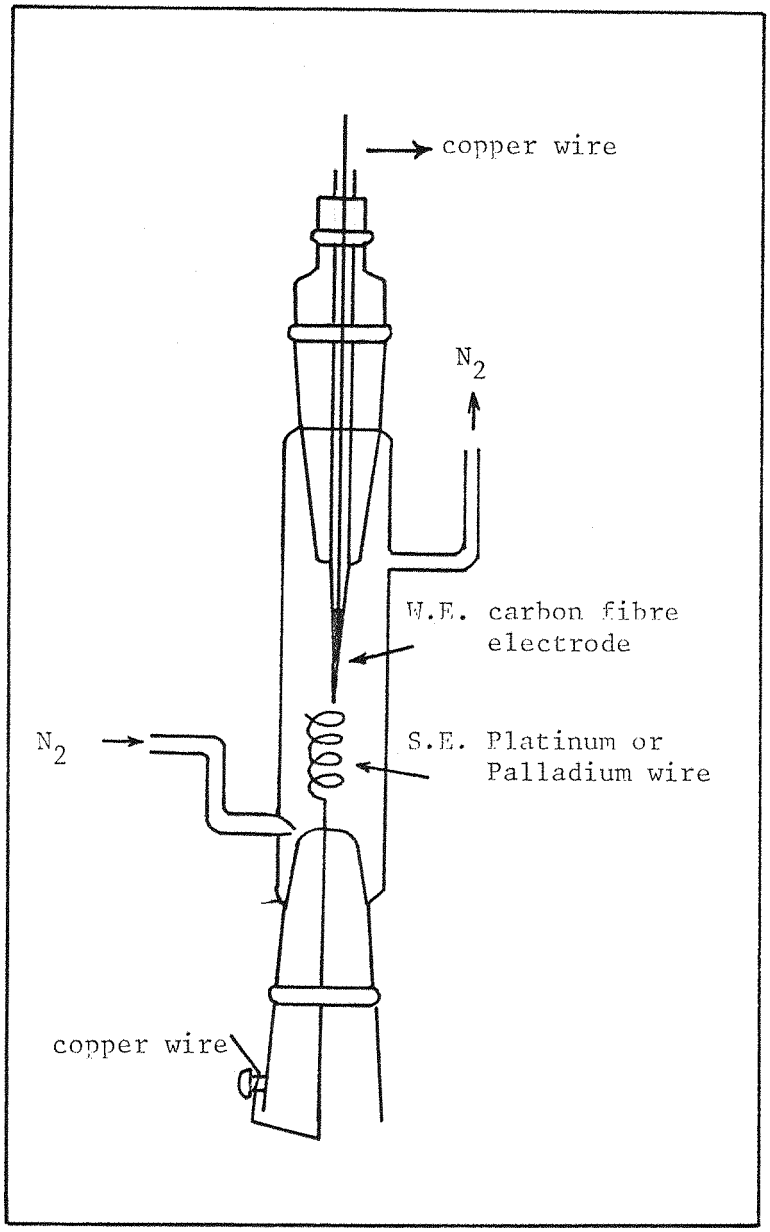

Figure 2.2 Sketch of the cell used for microelectrode system

the carbon rod (0.35cm diameter) with an exposed area (A= 0.07cm^2), into a soda glass tube in such a way that only one side, of a disc was exposed, figure (2.3b).

The vitreous carbon disc electrodes used for preparing samples for electron microscopy were made by mounting a carbon disc into perspex. The carbon discs of 2-3 mm in height were cut and mounted into a button shaped perspex holder with Araldite with an exposed area of 0.07cm^2. After a couple of hours, when the Araldite is completely dry, a copper wire was then sealed to the surface of carbon disc using thermo-setting silver conducting Araldite (Johnson Matthey Co.Ltd) with the ordinary hardening Araldite. This part (figure 2.3a) with an electrode at one end can be fixed into a perspex rod and was used as a working electrode. For the electron scan microscopy, the bottom half of the electrode (with the actual electrode surface)can easily be taken out and fitted into another metal disc, which is of the actual and exact size required to fit into the scanning electron microscope.

The platinum disc was made by soldering a copper wire onto the back of the platinum disc (0.4 cm diameter) which was then sealed into glass, with only the front side of the disc exposed. The palladium disc electrode was made in a similar way.

Carbon microelectrodes were made from carbon fibers (8-10μm diameter) sealed in a glass capillary under vacuum, with an exposed area A = 5×10^{-7} cm^2. The electrical contact was made by filling the capillary with lead beads, a copper wire was inserted from the top and then the tube was heated to about 100^{o}C. When the lead melted, a small vacuum was applied to remove the air bubble and the system was then allowed to cool.

Platinum microelectrodes were made from a platinum wire (10 or 25μ diameter), with an exposed area of 7.85×10^{-7} cm^2 or 4.9×10^{-6} cm^2. The platinum wire was flame welded with a copper wire and sealed in a glass capillary in such a way that only one face of the platinum wire was exposed. Both platinum and carbon microelectrodes are sketched in figure 2.4

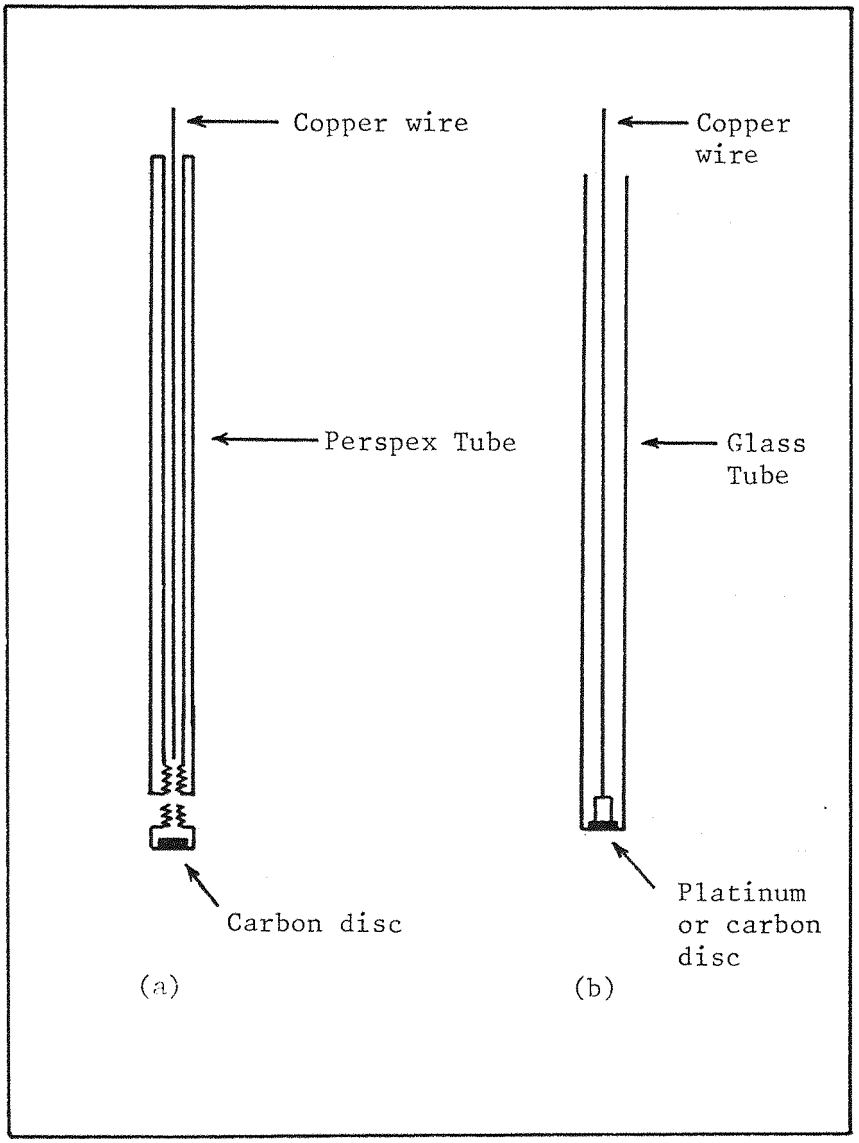

Figure 2.3 Sketch of the working electrodes used for electrodeposition of palladium and indium on macroelectrode

(a) Vitreous carbon electrode used for electron scan microscopy

(b) Vitreous carbon (or platinum) disc electrode

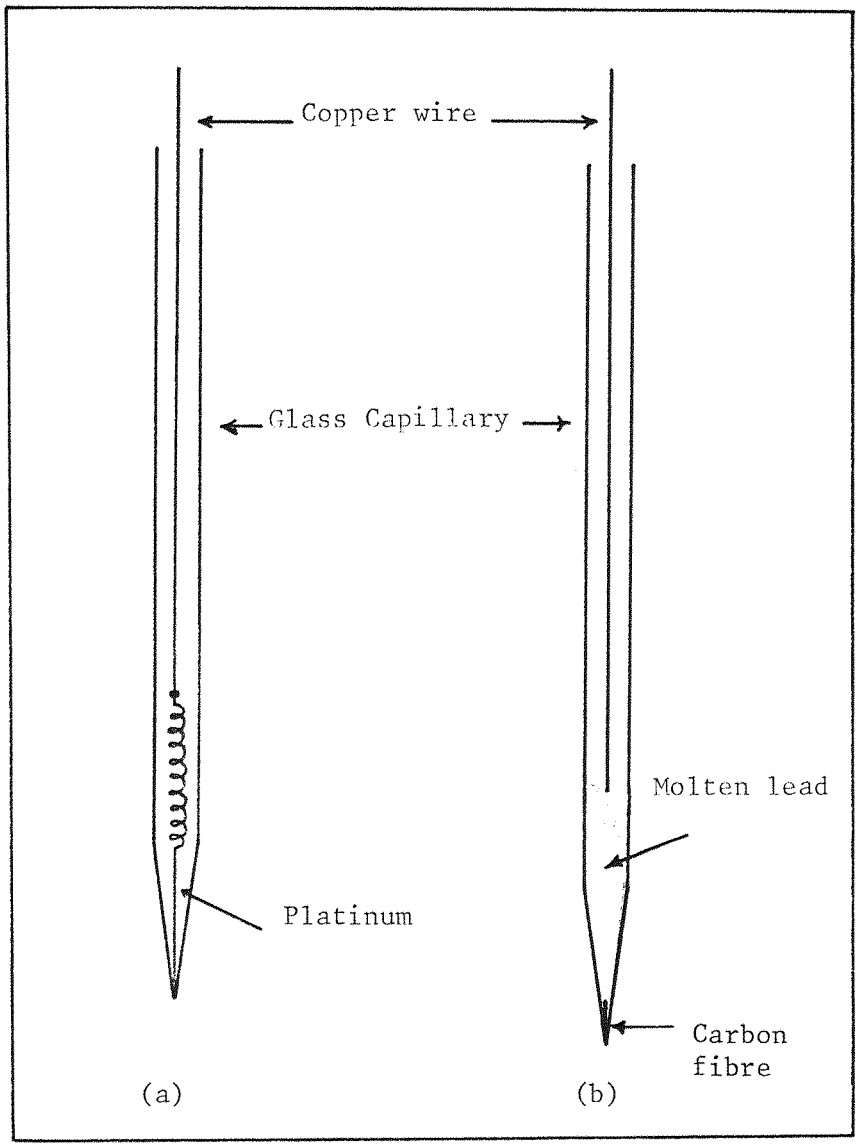

Figure 2.4 Sketch of Carbon and Platinum microelectrodes
(a) Platinum microelectrode, (Area 7.85×10^{-7} cm^2)
(b) Carbon fibre microelectrode, (Area = 5×10^{-7} cm^2)

(c) Secondary Electrode

In most experiments a large platinum wire (spiral) was used as the secondary electrode. In a few experiments such as the oxidation of formic acid, a platinum gauze secondary electrode was used. Occasionally a palladium spiral electrode was used as a secondary/reference electrode in some experiments where the deposition of palladium have been studied on carbon microelectrode.

The platinum or palladium/spiral was soldered onto a copper wire for electrical contact and sealed in a cone glass (Pyrex) tube so that all the platinum wire/spiral was exposed.

2.3 Pretreatment of the Electrodes

(a) Vitreous Carbon

The vitreous carbon disc electrode was first polished to get a smooth, mirror finish on a wet grinding wheel and then on a moist Metron polishing cloth with Banner Scientific alumina of decreasing size (1 micron and 0.3 micron) until the surface looked mirror bright.

The carbon microelectrode was first polished with fine emery papers, 4 and 6 grade, then polishing alumina, 1, 0.3, 0.05 micron (from Banner Scientific Ltd) supported on a Metron polishing cloth lubricated with water. After polishing with the finest grade alumina, the electrode was further polished on a clean wet portion of the cloth only, in order to remove alumina adherring to the electrode, followed by thorough washing with distilled water.

(b) Platinum and Palladium Electrodes

Platinum and palladium disc electrodes were first polished on a moist Metron polishing cloth using Banner Scientific alumina of decreasing grades and then washed with distilled water. Electrodes were then cleaned by immersion in a 50/50 mixture of concentrated nitric acid and sulfuric acid, followed by thorough washing with distilled water.

Platinum microelectrodes were first polished with fine emery paper 6 grade, and then on a moist Metron polishing cloth with alumina of 0.05 and 0.03 micron (Banner Scientific Ltd).

2.4 Cleaning of Glassware

All the glassware used was cleaned by immersion in chromic acid solution followed by washing in distilled water. Then in experiments where the traces of organic materials were critical, the glassware was cleaned by immersion in a 50/50 boiling mixture of nitric acid and sulphuric acid for an hour, then washed with hot water and boiled in triply distilled water.

2.5 Instrumentation

Most of the electrochemical experiments were carried out using a Hi-Tek Instruments potentiostat, Model DT 2101 or DT 131 and a wave form generator Model PPR1. Cyclic voltammograms were recorded on a Farnell X-Y recorder or, in some cases a Bryans X-Y recorder Model 2600. The current/time and potential/time transients were recorded either using a Hi-Tek Instruments multi-purpose signal averager type AAI (with storing capicity of 256 sample points of a analogue signal at a maximum sampling rate of 5 μsec) or a Gould Advance storage oscilloscope. The schematic diagram for the set up is shown in figure 2.5.

For the potential step experiments using microelectrodes, the currents are very low. Therefore potentiostatic control with a three electrode cell is not necessary. Moreover the reference electrode can serve also as a counter electrode and the potential is directly applied by a wave form generator (Hi-Tek PPRI). The potential of the working electrode was kept at virtual ground. The current was measured by a high gain picoammeter (built in this lab; capable of measuring current from 10^{-4} - 10^{-9}A) connected in series with the cell. The output current was then recorded either directly on an X-Y recorder (slow sweep, linear sweep voltammetry) or for transients, on a Gould Advance OS-4000 digital

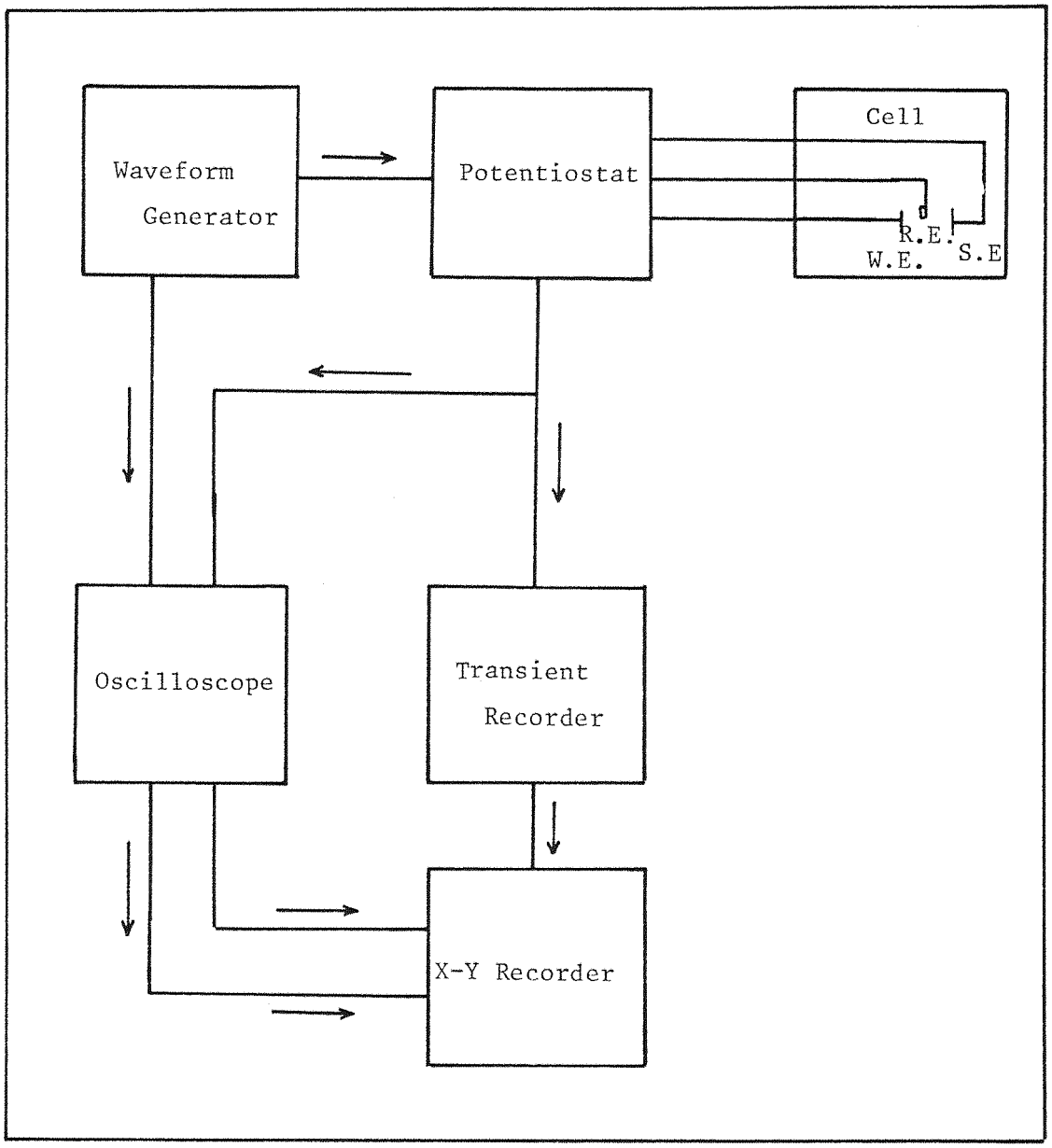

Figure 2.5 Schematic diagram for the three electrode system for the electrodeposition of palladium and indium onto macroelectrode.

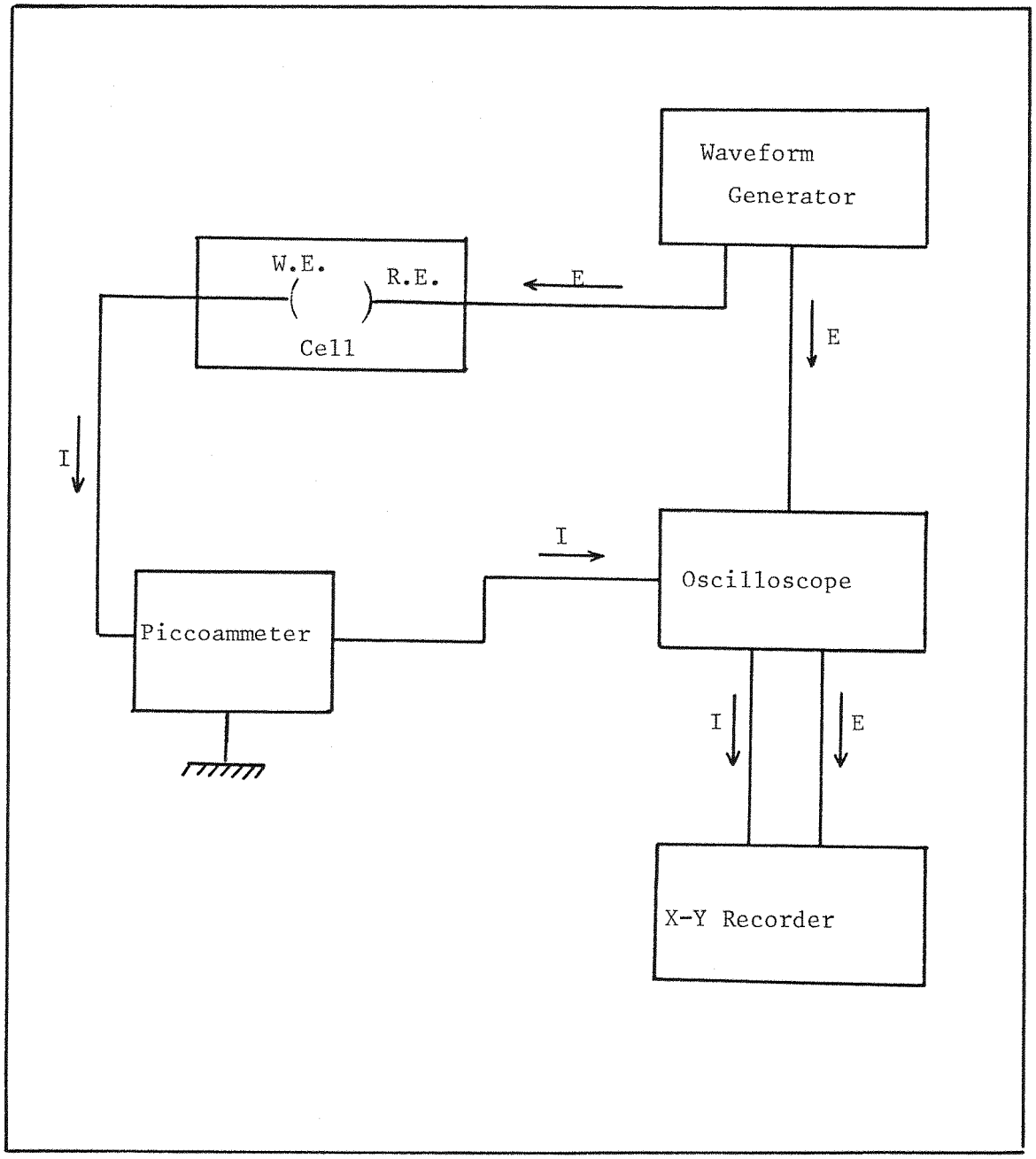

Figure 2.6 Schematic diagram for two electrode system for the deposition phenomena on microelectrodes.

storage oscilloscope, from which the transient could be outputted to X-Y recorder on a longer time scale. The schematic diagram of the circuit used for microelectrode studies is shown in figure 2.6.

In some cyclic voltammograms, the charge under (both cathodic and anodic peaks were measured) as a function of potential. For this purpose a home built charge integrator was used connected in series with the potentiostat and wave form generator.

2.6 Source of Chemicals

The following chemicals were used without further purification.

Abbr;

Analar (A)

Reagent(R)

Chemicals	Grade	Supplier
Hydrochloric Acid	(R)	BDH
Lead Nitrate	(A)	BDH
Nitric Acid	(R)	BDH
Perchloric Acid	(A)	BDH
Potassium Nitrate	(R)	BDH
Potassium Chloride	(A)	BDH
Palladium Chloride	(A)	Fluka
Sodium Perchlorate	(A)	BDH
Sodium Hydroxide	(R)	BDH
Sulfuric Acid	(A)	Cambrian Chemicals
Indium Chloride	(R)	Aldrich Chemical Co.
Formic Acid	(A)	BDH

Water used to make up the solutions was triply distilled. Initial distillation was followed by two other distillations from a weakly alkaline solution of $KMnO_4$ and then from the solution containing a trace amount of orthophosphoric acid. For even more sensitive experiments (oxidation of formic acid) four times distilled water was used, triple distilled water was followed by a simple distilation and was collected straight into the flask which was going to be used to prepare the solution.

The vitreous carbon rod was supplied by"Sigma" Electrographic GMBH, Germany". The platinum and palladium metal used for making electrodes was supplied by Johnson Matthey and Company Ltd , while the thin platinum wire used to make microelectrodes was supplied by Goodfellow Metals , purity 99.9%.

2.7 Experimental procedure

2.7.1 Reduction of Palladium and Indium

Typically linear potential sweep voltammetry for the reduction of palladium was carried out in a cell shown in figure 2.1. The concentration of palladium chloride solutions were 10-50 mmol dm^{-3}. The working electrode used in the experiments on a macroelectrode was vitreous carbon with area 0.07 cm^2. Prior to every series of experiments the vitreous carbon electrode was polished (as mentioned in section 2.3). Moreover the electrode was polished and washed thoroughly with distilled water in between each run. The platinum counter electrode was also always cleaned by putting it on an oxidizing flame before starting the experiments.

Each experiment was repeated, at least twice, until reproducible results were obtained. Electrodes were prepared before each run only by polishing with different grades of alumina as stated earlier. Occasionally when the results became erratic the electrodes were polished again starting from the grinding wheel, especially in the case of microelectrodes. For the reduction of palladium (II) on microelectrodes the cell used for all the experiments is given in figure 2.2. A carbon fiber microelectrode (area $1.5 \times 10^{-7} cm^2$) was used for this purpose. For the small electrodes the difficulties in getting reproducible results, arose from the polishing. This was due to the alumina particles adherring to the electrode surface.

For all the slow sweep experiments the resultant I-E plots were directly recorded on Farnell x - y recorder. For higher sweep rates and for pulse experiments the data was first stored on a Gould OS 4000 digital storage oscilloscope and then played back onto the x - y recorder. For the potential step experiments on microelectrodes, the actual potential step required to grow a small number of nuclei was applied to the counter

electrode. Similar procedures were adapted for the reduction of indium.

2.7.2 Electron Scan Microscopy

This technique provides a powerful method of observing the results of electrodeposition, of its morphology, and of kinetics of nucleation. It was here applied to study the nucleation and growth phenomena of palladium onto vitreous carbon under potentiostatic conditions. The same set up of apparatus was used as in figure 2.1, except the working electrode. The geometery and construction of the working electrode is stated in section 2.2-b. A potential pulse was applied to the vitreous carbon electrode (current time transients were recorded on an x - y recorder) before the electrode was then taken out from the cell (with the deposit on the surface), washed with distilled water, dried and then placed in the electron microscope object holder. The deposit can then be seen on a screen connected electroscan micrograph, then on particular, suitable magnification photographed. The number of growing nuclei can be observed and counted and the pattern of nucleation was also analysed i.e. is it instantaneous nucleation or progressive nucleation? The number density of nuclei were then counted and calculated from the photograph and compared with those calculated from the I - t response.

2.7.3 Catalytic effect of small clusters on hydrogen adsorbtion

In all the experiments carried out to study the catalytic effect of small nuclei on microelectrodes (carbon fiber A = 5×10^{-7} cm and platinum wire A = 7.85 $\times 10^{-7}$ cm^2, 4.9 $\times$ 10^{-6} cm^2) two cells as shown in figure 2.2, with exactly the same design were used. One cell containing palladium chloride solution, where the electrodeposition of palladium was carried out potentiostatically, the other containing either 1 mol dm^{-3} formic acid or 1 mol dm^{-3} sulfuric acid (as required for the experiment). After depositing palladium, the electrode was then taken out from the cell, carefully washed with triply distilled water and transferred to the cell containing formic or sulfuric acid. Linear potential sweep voltammetry was applied to study the catalytic effect of palladium on platinum and carbon microelectrodes. A repetitive ramp was applied to the system

and each time,the most reproducible cyclic voltammogram was recorded, but for the electrode with deposited palladium the first cycle was recorded as the surface might get poisoned by repetitive cycles. Each set of experiments was repeated a number of times and the most reproducible results were recorded and analysed. Before starting each experiment the electrodes were polished as stated earlier and cyclic voltammograms were run for a blank solution i.e. for oxidation of $HClO_4$ acid or H_2SO_4 on a clean platinum or carbon fiber electrode. When the typical voltammograms were observed, (to make sure that there was no palladium left on the electrode surface) deposition and oxidation on the electrode with some deposit, was then followed.

After repeating a large number of experiments it was observed that the electrode became irreproducible. Therefore electrodes were then polished starting from the very first step, i.e. polishing on emery paper followed by decreasing grades of alumina so that a new clean surface could be produced.

CHAPTER 3

DEPOSITION OF PALLADIUM AND INDIUM

Part 1 - Electrodeposition of palladium

Part 2 - Electrodeposition of indium

CHAPTER THREE

DEPOSITION OF PALLADIUM AND INDIUM

PART ONE - ELECTRODEPOSITION OF PALLADIUM

3.1 LINEAR SWEEP VOLTAMMETRY

3.1.1 EFFECT OF CONCENTRATION

Cyclic voltammograms were recorded at a vitreous carbon disc electrode for a series of solutions of 10-50 mmole dm^{-3} palladium chloride at pH 3.5. The supporting electrolyte was 1 mol dm^{-3} potassium chloride. A saturated calomel electrode was used as the reference electrode in all experiments and the working electrode was vitreous carbon sealed in glass with an area of 0.07 cm^2. The electrode was polished to a mirror finish between cyclic voltammograms using 0.05μ alumina.

A cyclic voltammogram recorded for a solution of 10 mmole dm^{-3} palladium chloride in 1 mol dm^{-3} potassium chloride pH3.5, at a potential sweep rate of 100 mV s^{-1} is shown in figure 3.1 a. There is a steeply rising cathodic peak at -105 mV vs S.C.E. and the cathodic peak current density was found to be 6 mA cm^{-2}. The reverse potential sweep shows a current crossover, i.e. between -50 and +250 mV, the cathodic current during the reverse sweep is higher than during forward sweep, and this is prima facie evidence for an electrode reaction where nucleation of a new phase on the electrode surface is an essential step in the cathode reaction. The anodic stripping process leads to two peaks at different potentials. The first anodic peak, current density 6 mA cm^{-2}, was at 420 mV. The second anodic peak was at 500 mV and the current density was also higher, Ip_a = 7mA cm^{-2}. Hence the cyclic voltammogram would suggest that the cathodic reaction is

$$Pd(II) + 2e \longrightarrow Pd$$

where Pd(II) is a chlorocomplex of palladium in solution and that the corrosion reaction is not straightforward, leading at this pH to more than one complex.

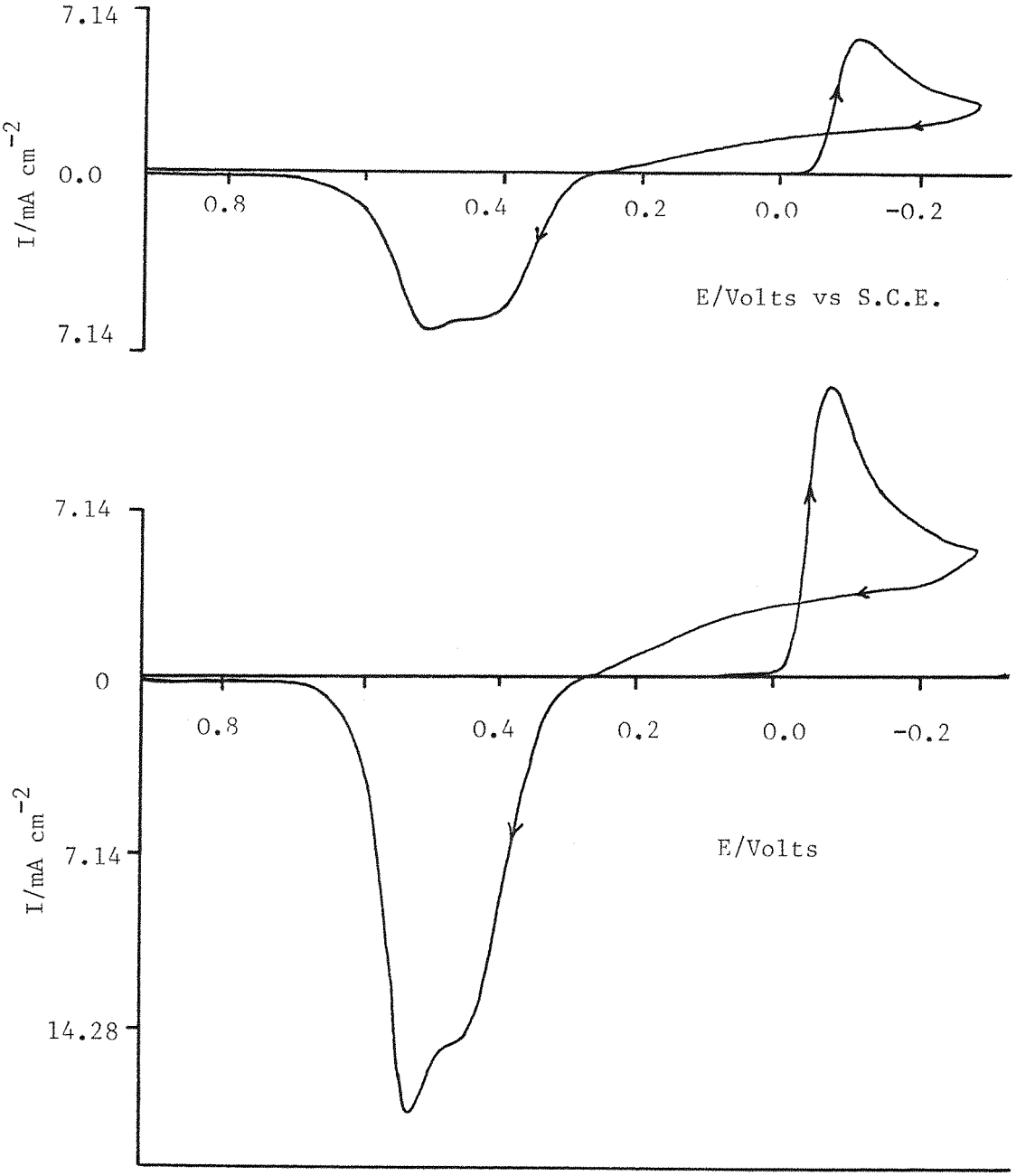

Figures 3.1(a,b) Cyclic voltammograms for the reduction of Pd(II), from (a) 10 mmol dm^{-3}. (b) 20 mmol dm^{-3} $PdCl_2$, in 1 mol dm^{-3} KCl at pH 3.5 on vitreous carbon electrode (Area=0.07 cm^2). Sweep rate = 0.1Vs^{-1}.

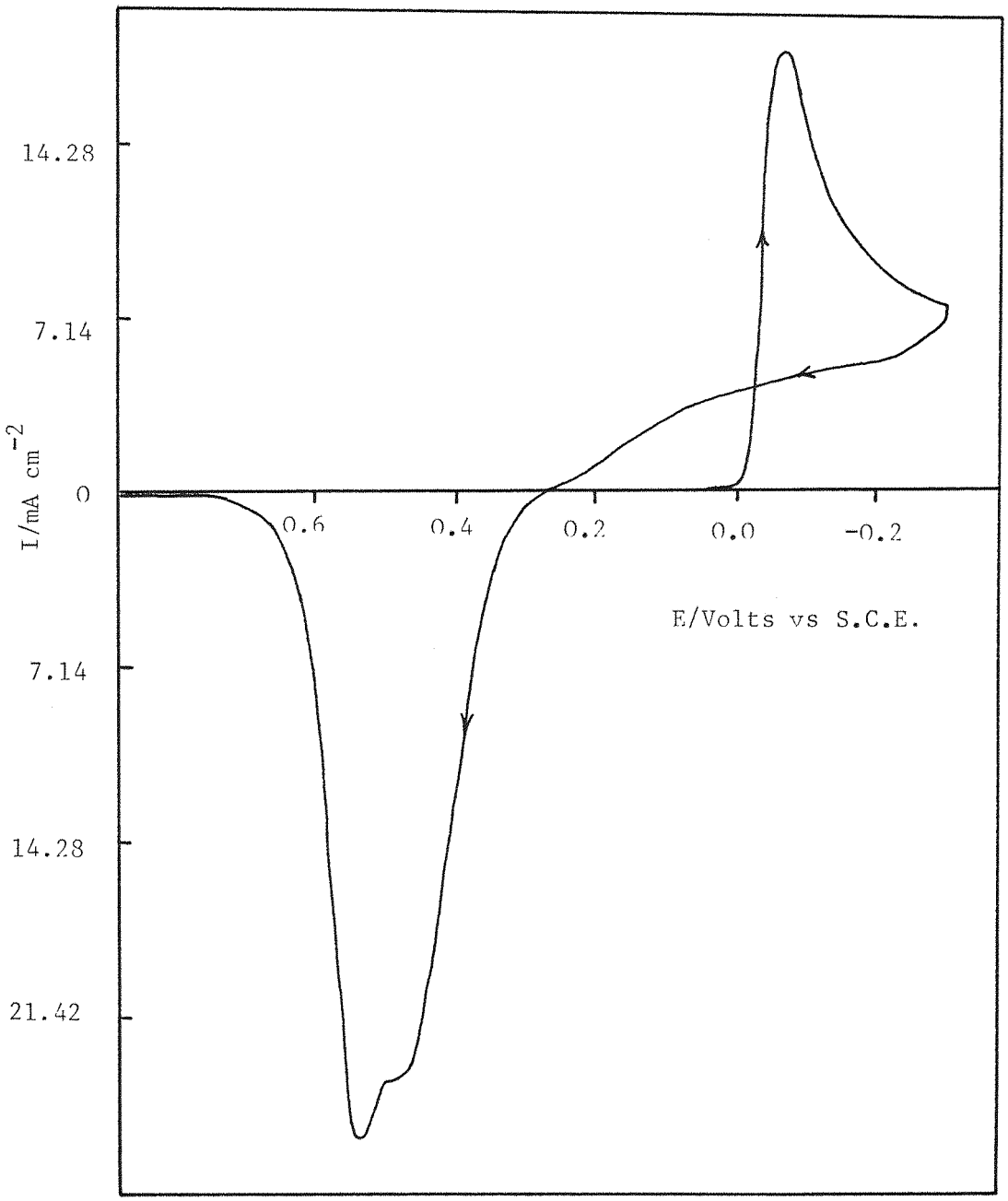

Figure 3.1c. Cyclic voltammogram for the reduction of Pd(II) from 30 mmol dm^{-3} $PdCl_2$ in 1 mol dm^{-3} KCl at pH 3.5, Sweep rate = 0.1Vs^{-1}.

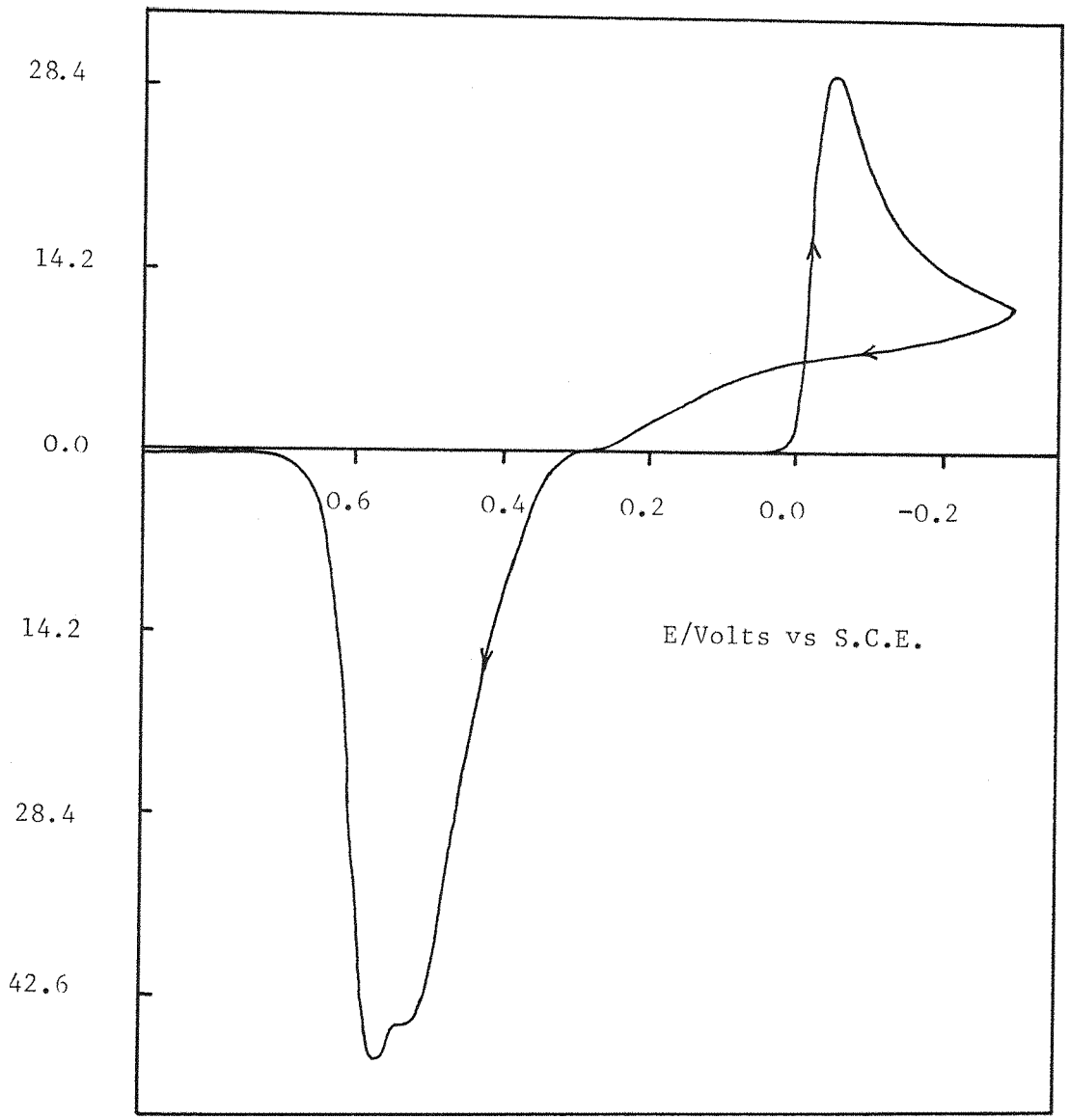

Figure 3.1d. Cyclic voltammogram for 50 mmol dm^{-3} $PdCl_2$ in 1 mol dm^{-3} KCl under similar conditions as for figure 3.1-c

Cyclic voltammograms were also recorded at various potential sweep rates. Only the cathodic part of the voltammograms recorded at various potential sweep rates are shown in figure 3.2-a. With an increase in the scan rate, the cathodic peak was shifted towards more negative potential, while figure 3.2-b shows a plot of cathodic peak current versus the square root of the sweep rate. It is linear showing that the process is diffusion controlled beyond the peak. From the gradient of the plot in figure 3.2-b,a value for diffusion coefficient of Pd(II) was calculated as 1.08×10^{-5} $cm^2 s^{-1}$.

Commonly Q-E plots were recorded simultaneously with the I-E response during cyclic voltammetry and a typical Q-E plot is shown in figure 3.3. The ratio $Q_{anodic}/Q_{cathodic}$ can be seen to be slightly less than unity. Hence it is clear that either

(a) not all the palladium deposited is stripped anodically

or (b) the cathodic charge contains a contribution from another electrode reaction e.g. H_2 evolution.

Cyclic voltammograms were also recorded for 20, 30 and 50 mmole dm^{-3} palladium chloride in 1 mole dm^{-3} potassium chloride, and are shown in figure 3.1-b,c, and d. The potential scan rate was always 100 mV s^{-1}. The cathodic peak potential for the solutions of 10, 20, 30 and 50 mmole dm^{-3} palladium chloride were -105 mV, -80 mV, -55 mV and - 35 mV respectively confirming that nucleation is easier with a higher $PdCl_2$ concentration. Ip_c was found to vary linearly with the concentration of palladium chloride as demonstrated in the plot in figure 3.4.

The peak potentials for both anodic stripping peaks were found to shift to more positive potential at higher concentration of palladium(II); the peak potentials occurred at 420 and 500 mV for 10 mmole dm^{-3} $PdCl_2$ and 505 and 555 mV at 50 mmole dm^{-3} $PdCl_2$. The potential difference between the two anodic peaks potentials was also found to be slightly decreased with increasing concentration of palladium (II).

All data taken from the cyclic voltammograms is summarised in table 3.1. In particular it should be noted that Q_a/Q_c increases with

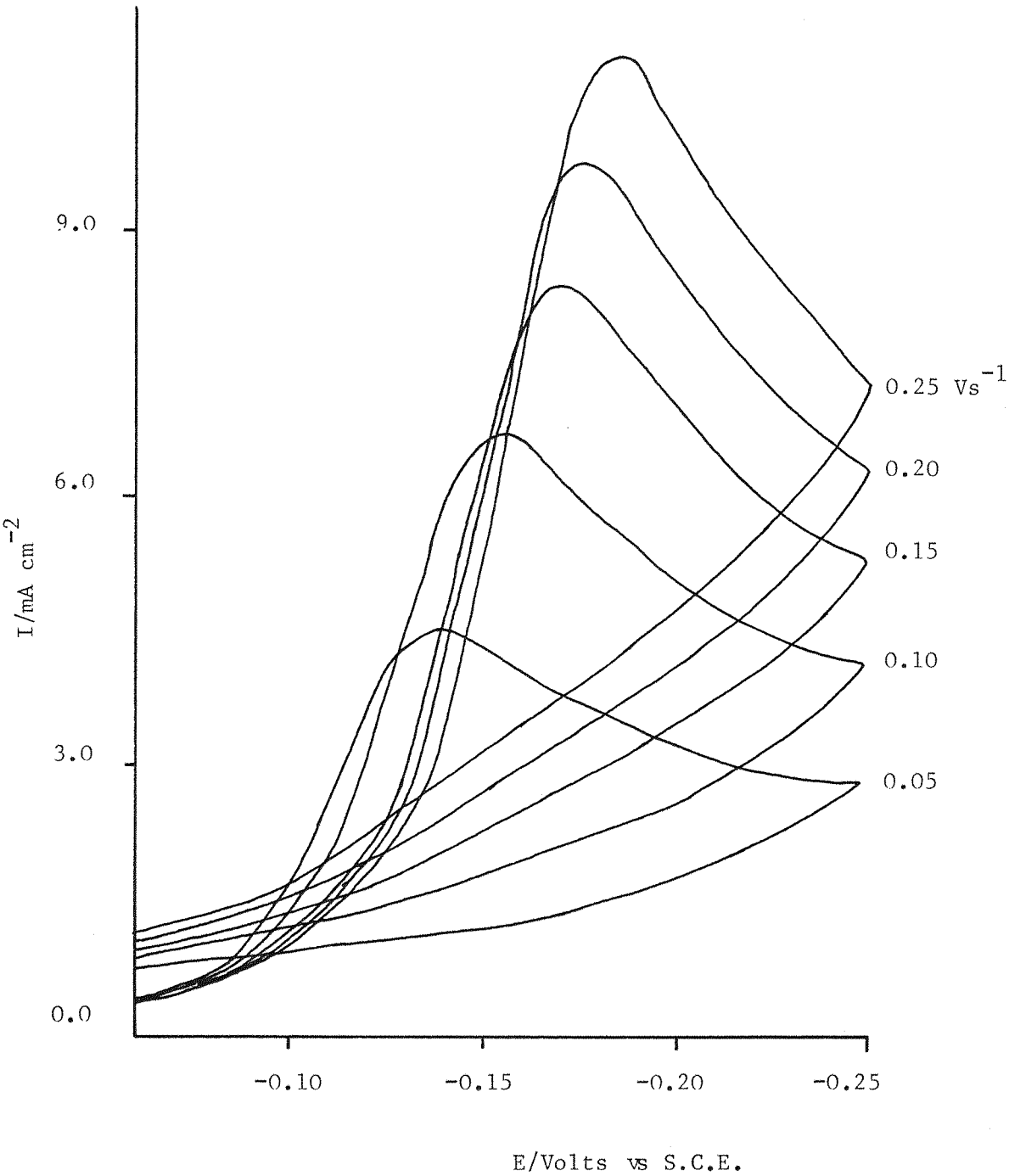

Figure 3.2-a. The cathodic peaks of the cyclic voltammograms for the reduction of Pd(II) from 10 mmol dm^{-3} $PdCl_2$ in 1 mol dm^{-3} KCl at various potential sweep rates.

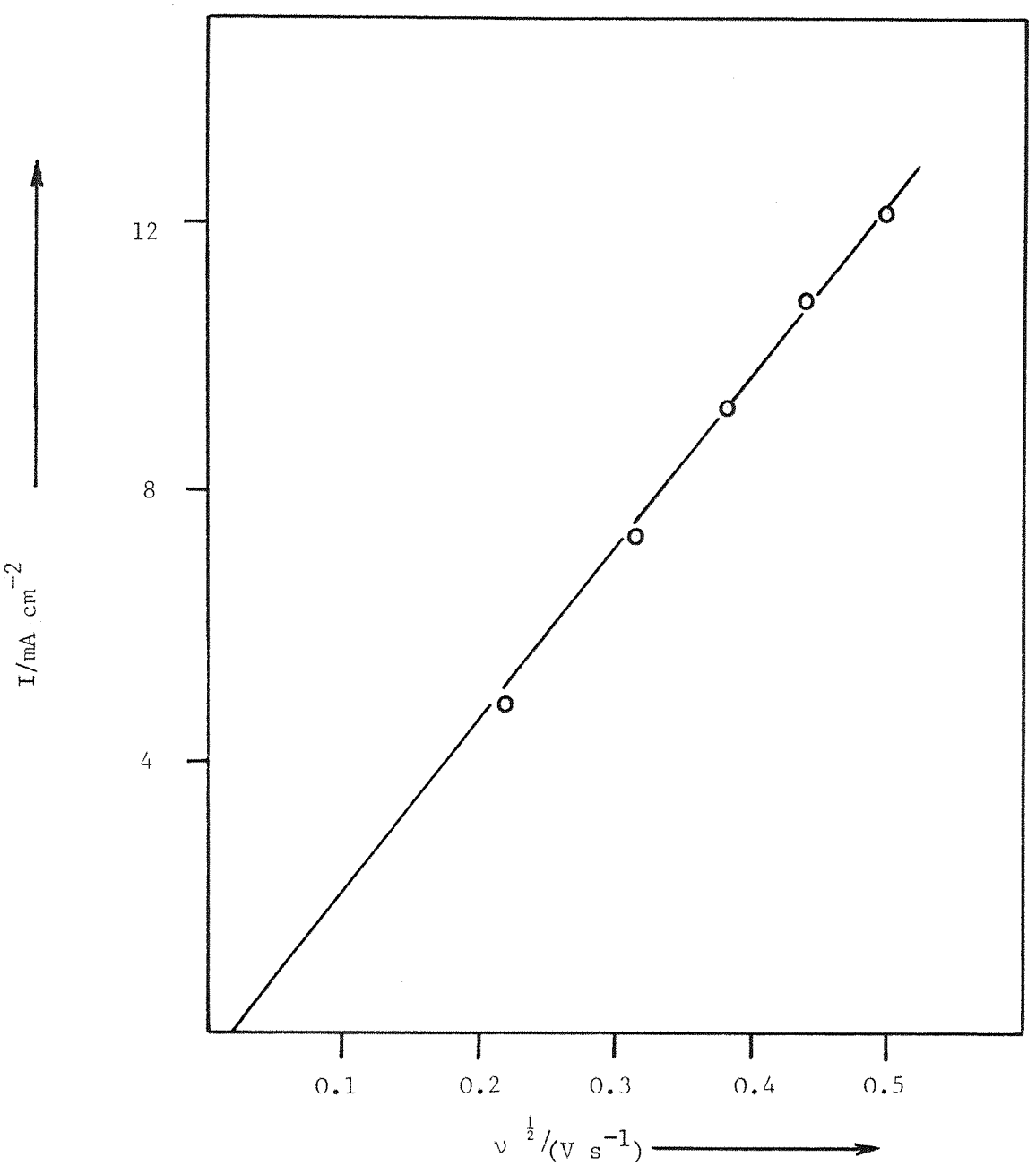

Figures 3.2-b Cathodic peak currents versus square root of a potential sweep rate for the data obtained from figure 3.2-a.

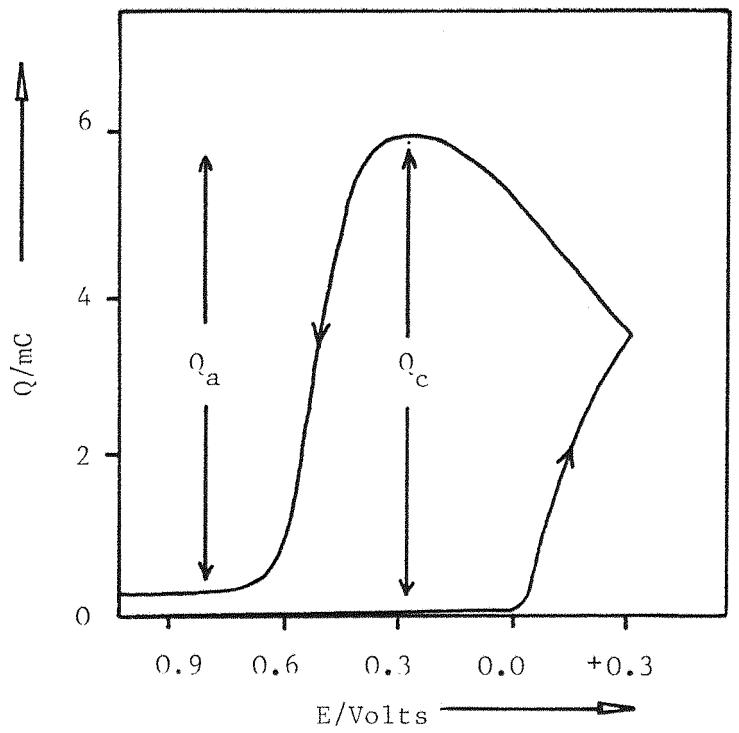

Figure 3.3: Plot showing the change in cathodic and anodic charges along with the potential corresponding to the cyclic voltammogram.

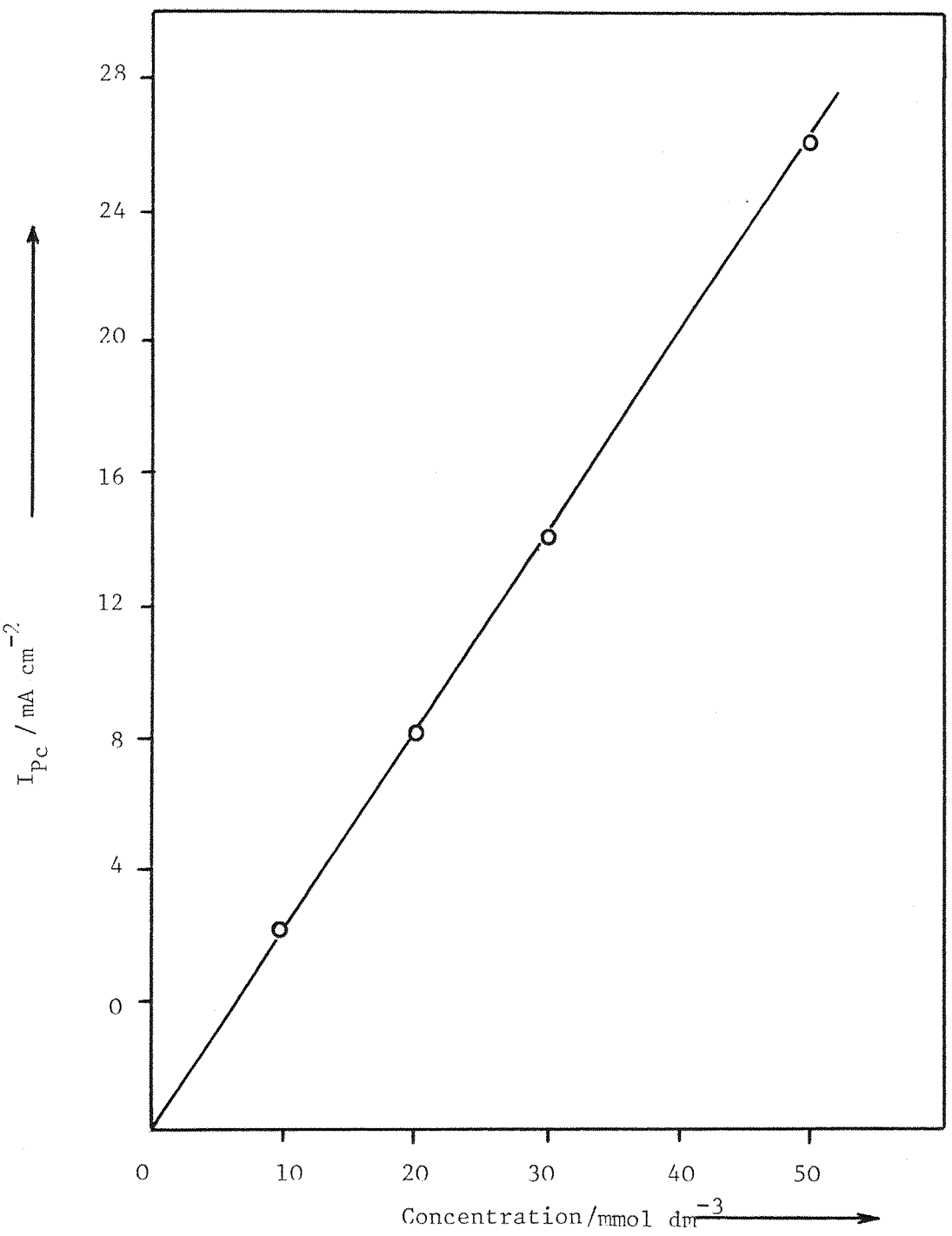

Figure 3.4: Cathodic peak currents vs concentration, for for the data obtained from figures 3.1a,b,c and d.

Conc mmol dm^{-3}	I_{Pc} mA cm^{-2}	I_{Pa_1} mA cm^{-2}	I_{Pa_2} mA cm^{-2}	E_{Pc} mV	E_{Pa_1} mV	E_{Pa_2} mV	Width of anodic peak at half height $(\Delta E_{\frac{1}{2}})_{mV}^{A}$	Q_C mC cm^{-2}	Q_A mC cm^{-2}	Q_A/Q_C
10	6	6	7.0	-105	420	500	215	17.4	14.7	0.89
20	12	15.3	18.3	-80	460	525	170	34.8	32.1	0.92
30	18	23.6	26.6	-55	480	550	175	53.6	50.9	0.94
50	29.8	41.7	48.0	-35	505	555	160	84.3	80.3	0.95

TABLE 3.1 Table of cathodic, anodic peak currents, potentials and charges under the cathodic and anodic peaks as the function of palladium concentration at pH 3.5.

increasing $PdCl_2$ concentration.

3.2.1 EFFECT OF pH

Cyclic voltammograms were also recorded for solution of 10 mmole dm^{-3} $PdCl_2$ in 1 mole dm^{-3} potassium chloride for a range of pH, i.e. 4.9, 4.3, 3, 2, 1 and 0.5; the pH was adjusted by the addition of aqueous HCl. The I-E curves obtained at 100 mV s^{-1} are shown in figure 3.5. Data taken from the cyclic voltammograms is summarised in table 3.2.

The cathodic peak changes only a little with pH. The peak potential did not vary except at the very acid end of the range where the peak potential was significantly more negative suggesting an increase in the nucleation overpotential in these conditions. Moreover the cathodic peak current density and the cathodic charge were almost independent of pH. In contrast, the shape and position of the anodic peak is strongly variable with pH. The peak potentials for the stripping peaks were found to shift to less positive valuesat low solution pH, e.g. 430 mV at pH 0.5 and 700 mV at pH 4.9. At only one pH,3, there were clearly two anodic peaks at 410 mV and 520 mV but in acid solution the stripping peak is always broad. At low pH the charge ratio Q_a/Q_c was found to be higher than at high pH, e.g. at pH 4.9, the charge ratio was 0.28 and for pH=1, the charge ratio was 0.94. This is clearly due to a decrease in the anodic charge. Hence complete dissolution takes place in acid solution but not above pH 3.0.

3.1.3 EFFECT OF SOLVENT

Attempts were made to study the electrodeposition of palladium in a noncomplexing medium. For that purpose palladium nitrate was dissolved in a solution of either aqueous potassium nitrate, sodium perchlorate or perchloric acid.

A cyclic voltammogram recorded for a solution of 50 mmole dm^{-3} $PdCl_2$ in sodium perchlorate is shown in figure 3.6-a. The potential sweep rate was again 100 mV s^{-1}. There was a cathodic peak at -230 mV Vs S.C.E., and the crossing over of the cathodic currents between +100 and -100 mV confirms the deposition of metal. The only anodic peak was a very broad one probably due to the oxidation of palladium into palladium oxide at

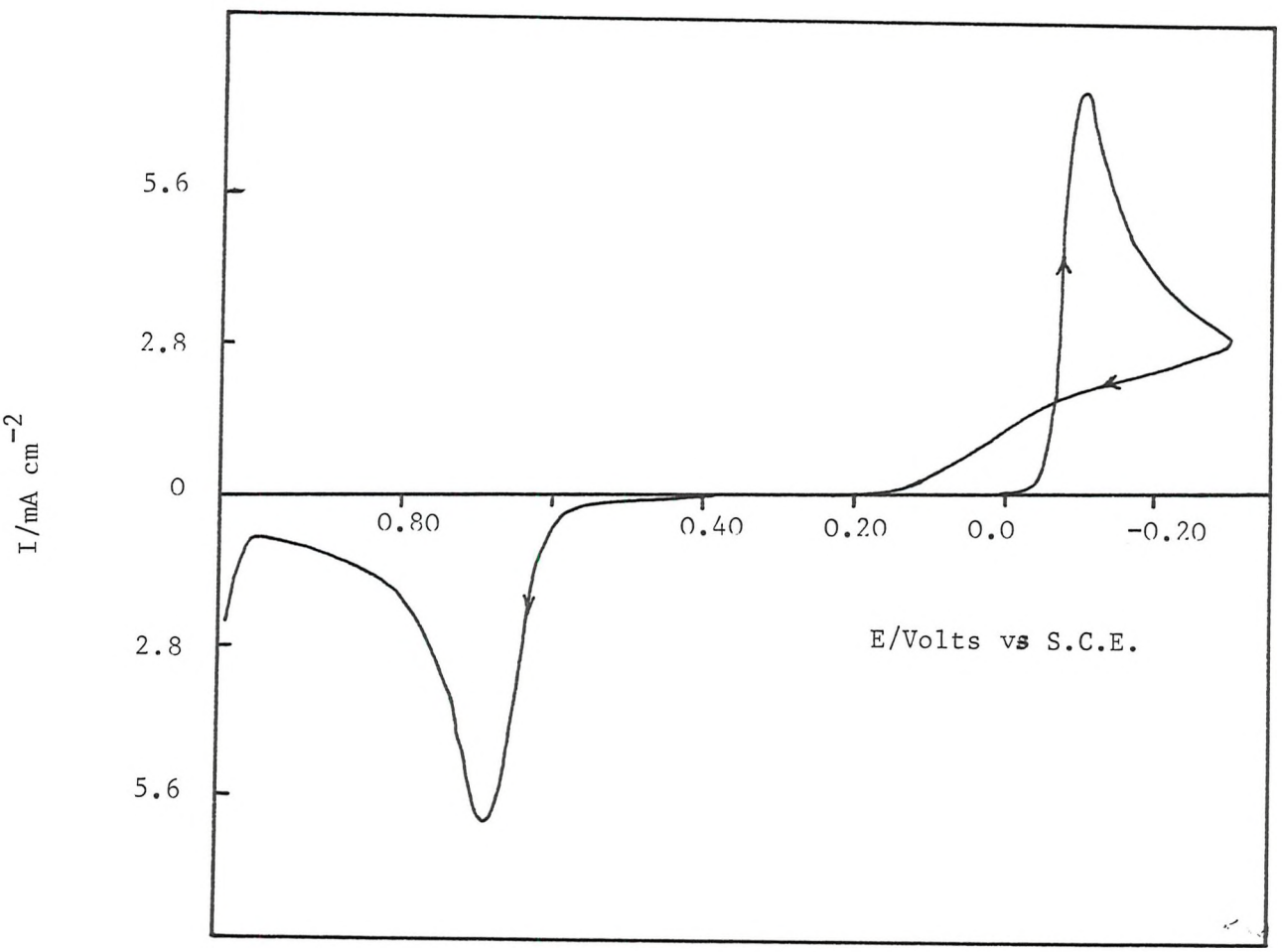

Figure 3.5(a) Cyclic voltammogram for the reduction of Pd(II) from 10 mmol dm^{-3} $PdCl_2$ + 1 mol dm^{-3} KCl at various pH values at sweep rate = 0.1Vs^{-1}

pH = 4.9

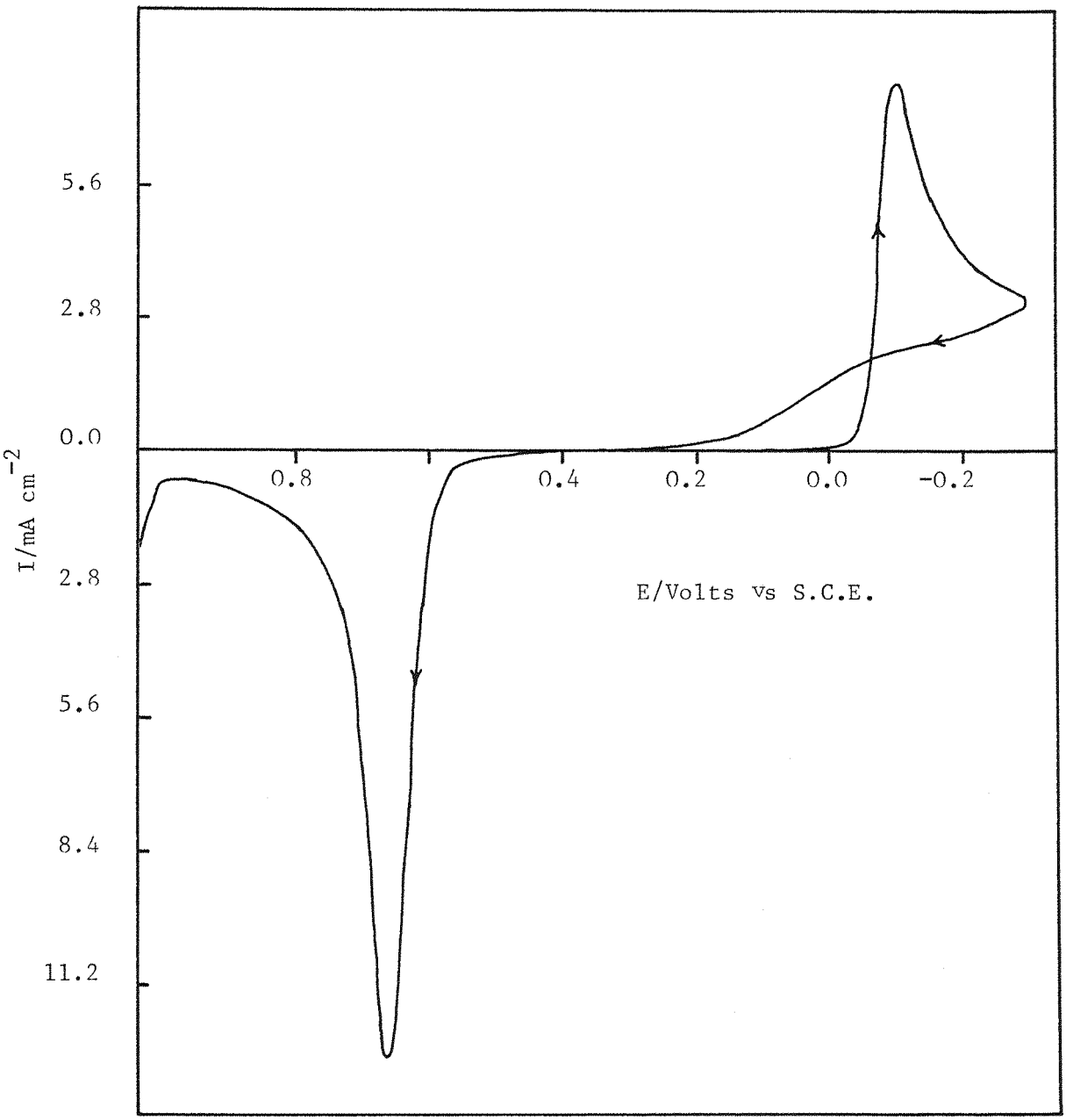

Figure 3.5(b) As Figure 3.5(a)

pH = 4.3

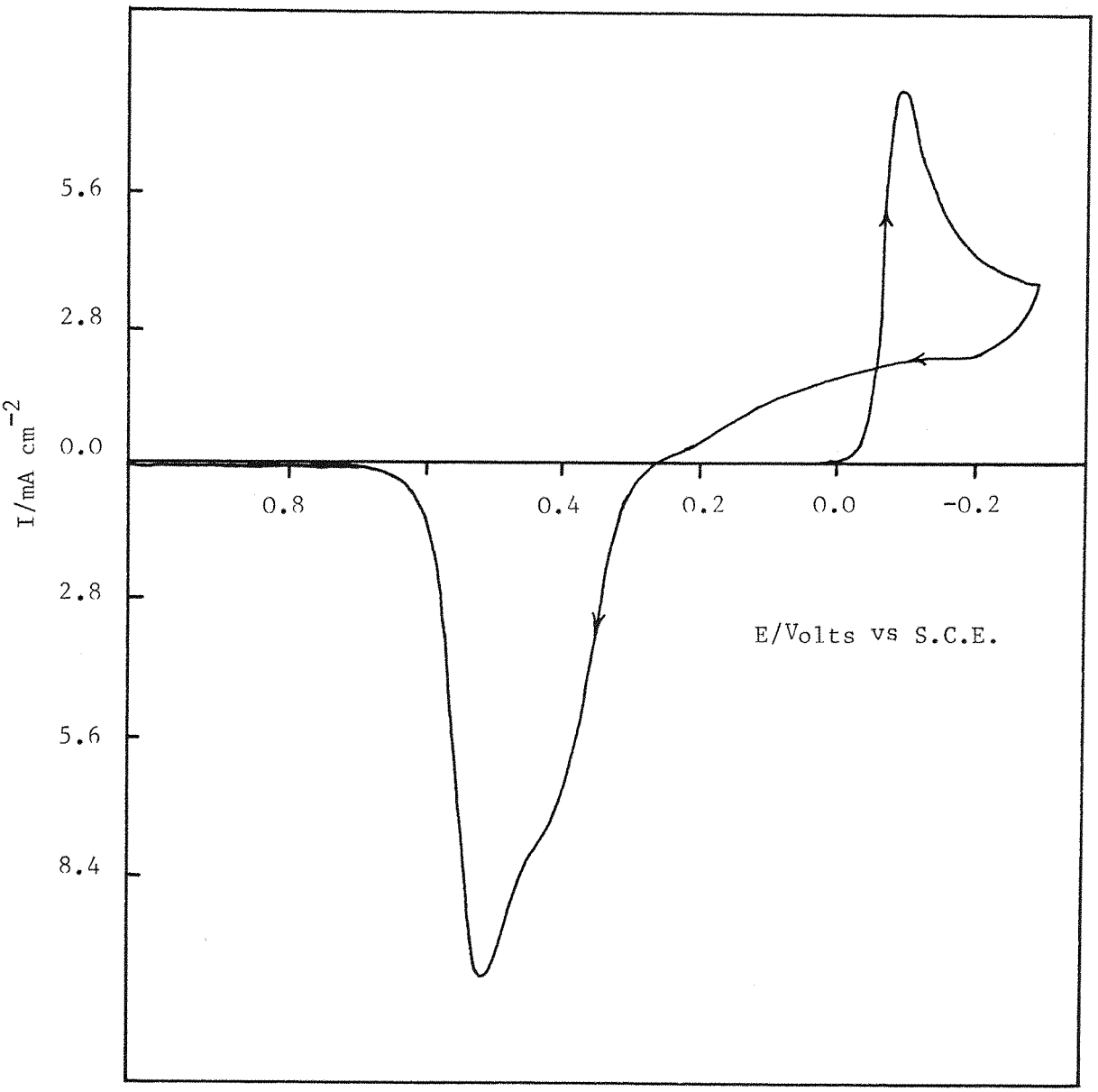

Figure 3.5(c) As Figure 3.5(a)
pH = 3

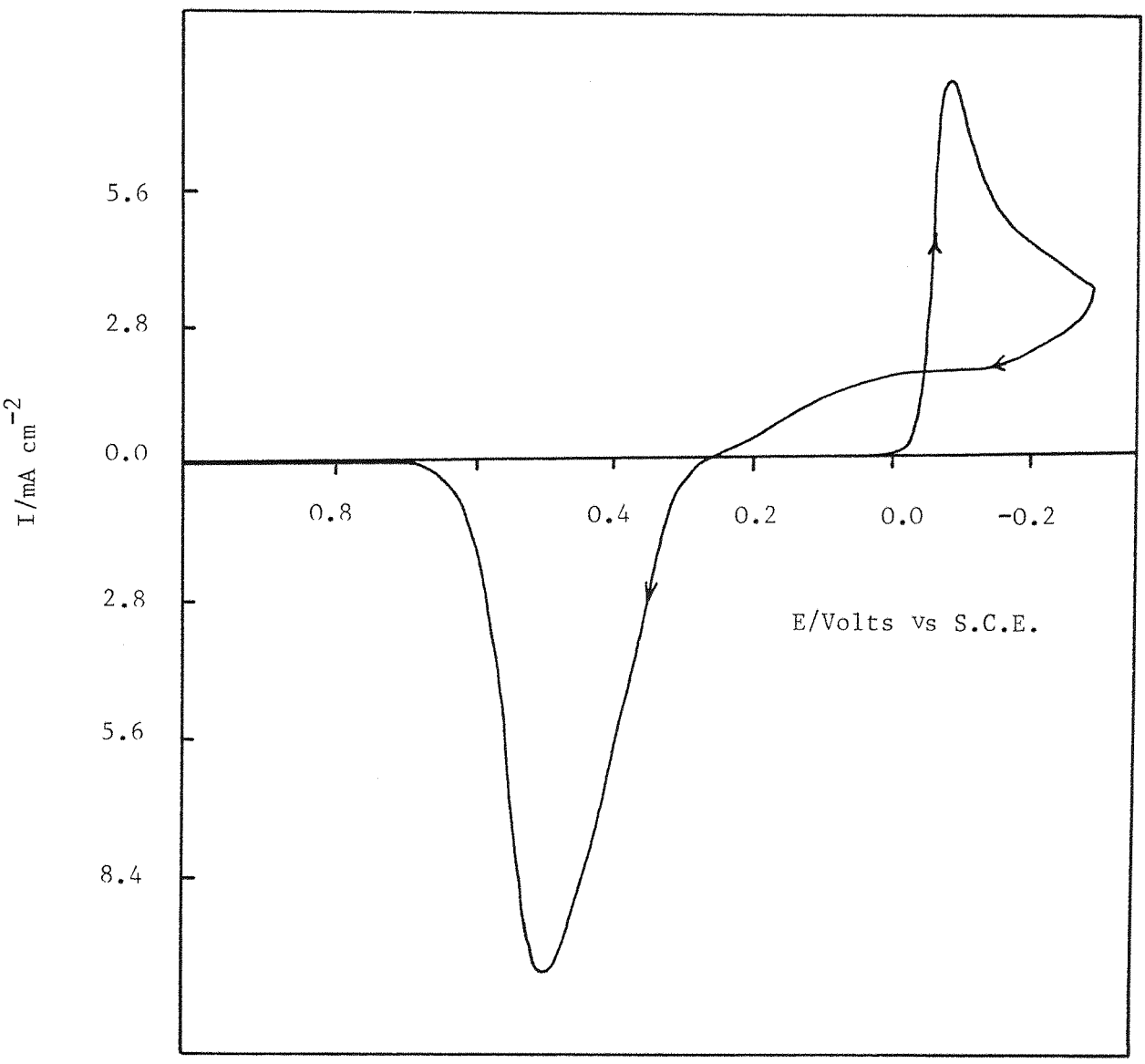

Figure 3.5(d) As Figure 3.5(a)

pH = 2

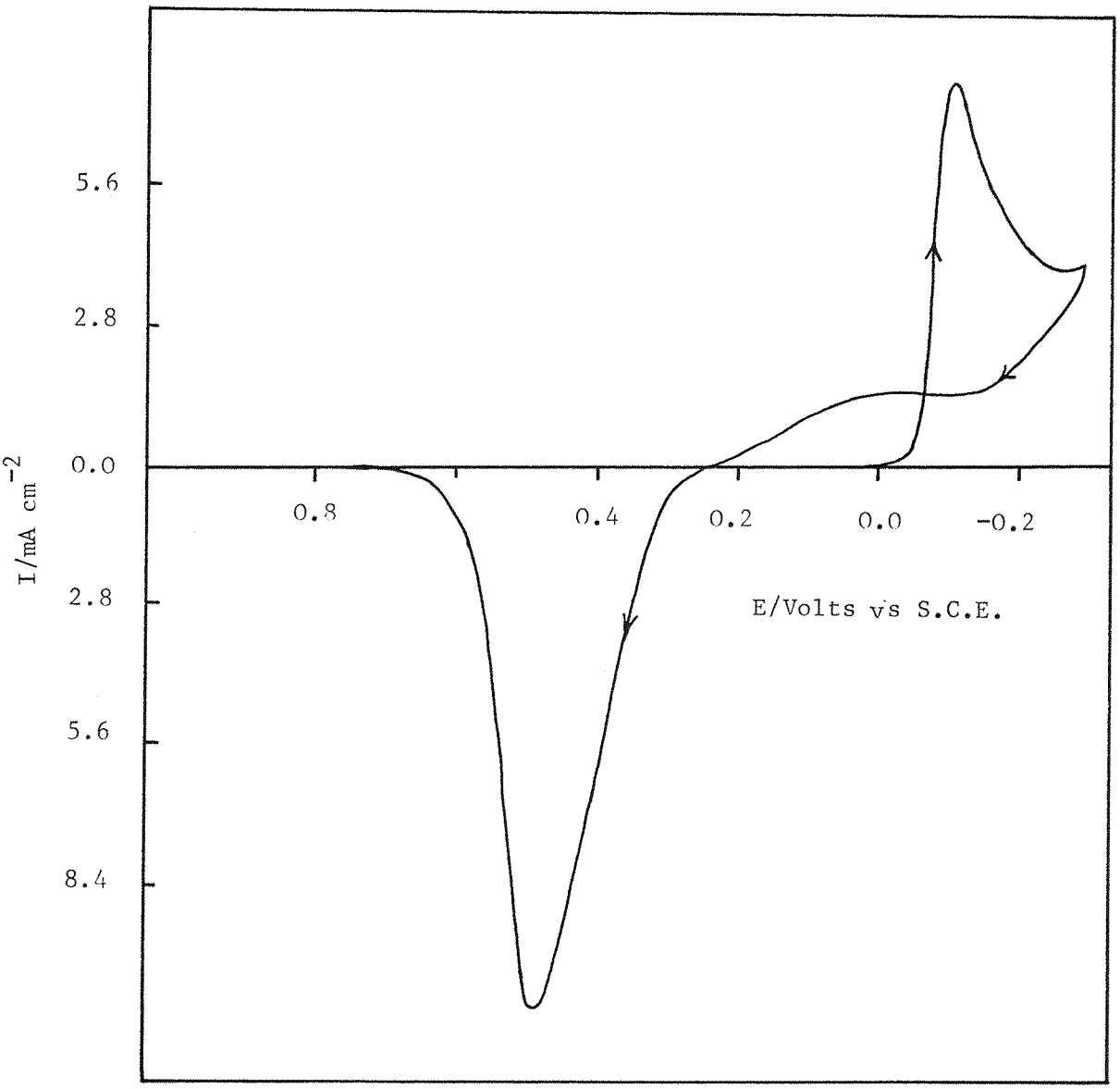

Figure 3.5(e) As Figure 3.5(a)

pH = 1

pH	I_{Pc} mA cm^{-2}	I_{Pa} mA cm^{-2}	E_{Pc} mV	E_{Pa} mV	Width of anodic peak at half height $(\Delta E_{\frac{1}{2}})_A$ mV	Q_C mC cm^{-2}	Q_A mC cm^{-2}	Q_A/Q_C
4.9	7.6	6.3	-100	700	105	18.8	5.4	0.28
4.3	7.6	13.0	-100	680	80	20.0	13.4	0.67
3.0*	7.6	10.7	-100	520	180	20.4	18.9	0.92
2.0	7.6	10.7	-100	510	160	20.4	18.9	0.92
1.0	7.6	11.0	-110	480	150	18.9	17.8	0.94
0.5	8.7	10.0	-145	430	150	19.3	16.3	0.84

TABLE 3.2 Table of the parameters given in table 3.1 for palladium at various pH of solution at a concentration of 50 mmol dm^{-3} $PdCl_2$.

* At pH3 the first anodic peak was observed at 410 mV.

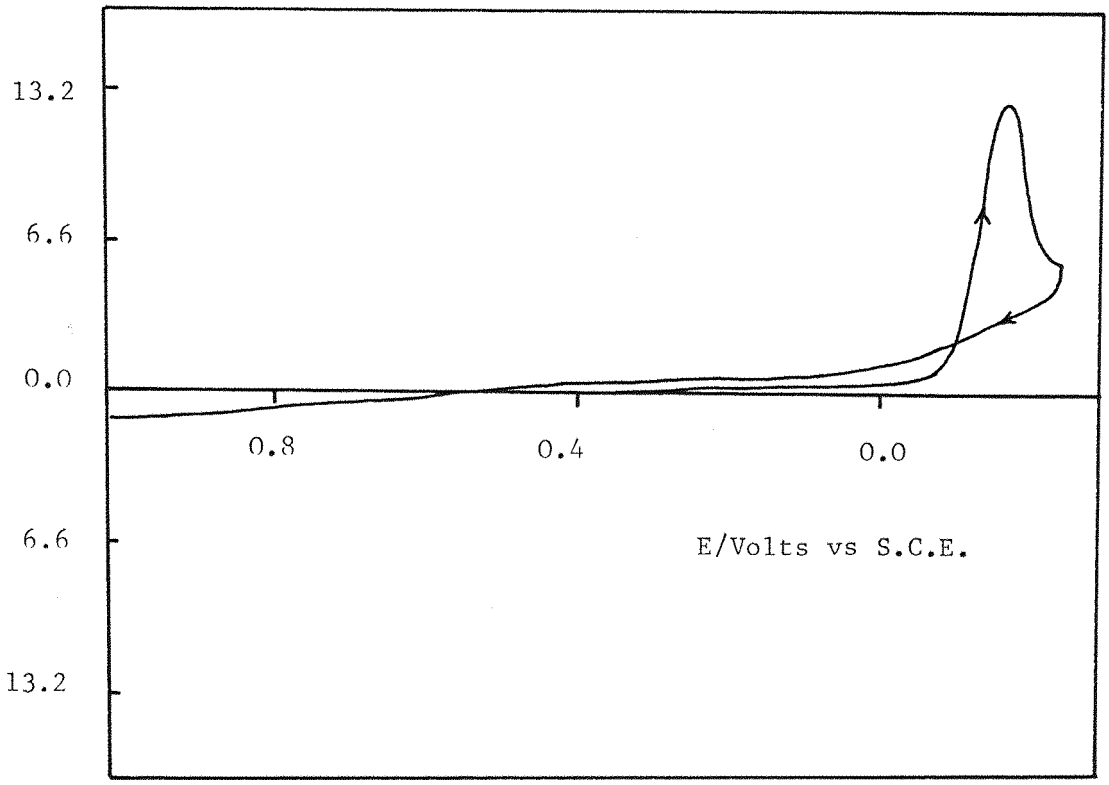

Figure 3.6(a): Linear sweep voltammogram for reduction of palladium(II) from 50 mmol dm^{-3} $Pd(NO_3)_2$ in 20 mmol dm^{-3} $NaClO_4$. Sweep rate = 0.1 Vs^{-1}.

quite positive potential.

The I-E curve at 300mV s^{-1} 50 mmole dm^{-3} palladium chloride in 1 mole dm^{-3} perchloric acid is shown in figure 3.6-b. The cathodic and anodic peaks were found to be quite similar to neutral perchlorate, but the cathodic peak was at low (-10 mV) potential. No peaks were observed in KNO_3 but in all the cases, the curves were not totally reproducible and indeed after a time a precipitate was always observed. Hence it was concluded that solutions of palladium(II) in non-complexing media were insufficiently stable for rigorous study of their electrochemistry.

3.2 POTENTIAL STEP EXPERIMENTS

A set of current transients for a vitreous carbon disc electrode (area 0.07 cm^2) in a solution of 50 mmol dm^{-3} palladium chloride containing 1 mol dm^{-3} potassium chloride at pH 3.5, for a series of potentials is shown in figure 3.7. In all cases at very short times a double layer charging current was observed but it decreases rapidly with time. Thereafter the current started increasing with time until it reaches a peak value and again decreases. The currents in the very early rising part of the transient could be replotted to give linear I-t^2 plots, see figure 3.8. This shape of transient was to be expected if the nucleation process is instantaneous on changing the potential but the rate of three dimensional growth of the centers, was controlled by the kinetics of reduction. On this assumption, the slopes of the lines were used to estimate the rate constants using equation (1.21). The rate constants were found to vary with potential. Indeed a plot of $\log kN_o$ Vs E was a straight line with a slope of 120 mV consistent with a rate determining electron transfer process, figure 3.0. The value of the rate constants as a function of potential are reported in table 3.3.

At longer times the currents increased more gradually and this part of the rising transient seemed to obey the relationship for diffusion to isolated hemispherical centers, equation (1.26) since the I vs $t^{\frac{1}{2}}$ plots were linear, figure 3.10, using the slopes of the lines, nuclear number densities were calculated using equation (1.26) for each potential and are given in table 3.4. At longer times the transients passed through a peak and

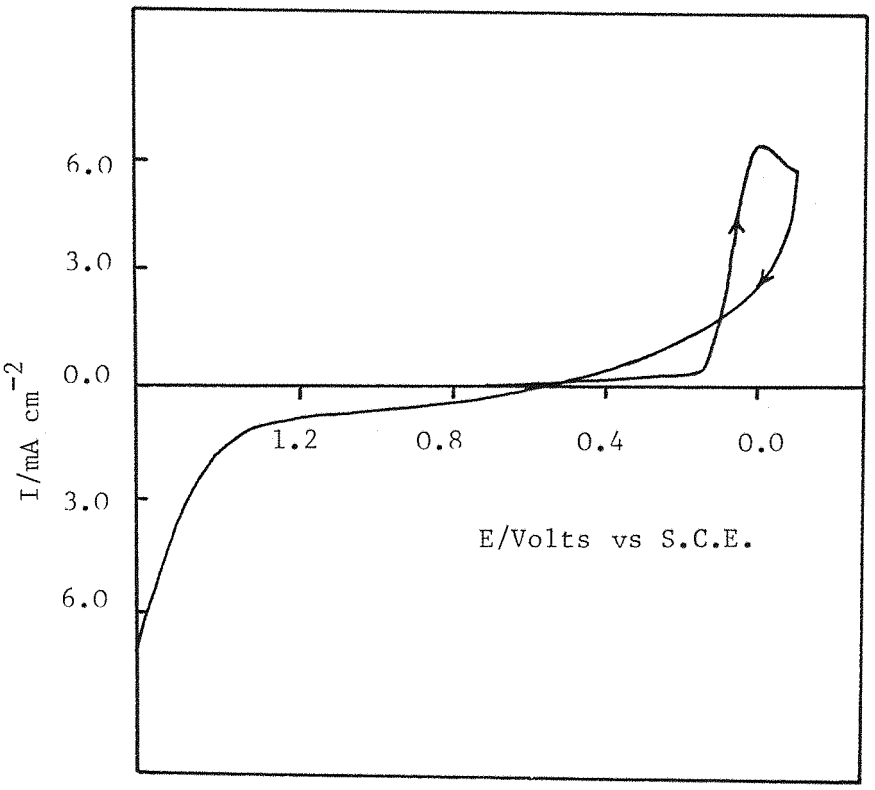

Figure 3.6(b): Cyclic voltammogram for reduction of palladium(II) from 50 mmol dm^{-3} $Pd(NO_3)_2$ + 1 mol dm^{-3} $HClO_4$. Sweep rate = 0.300 Vs^{-1}

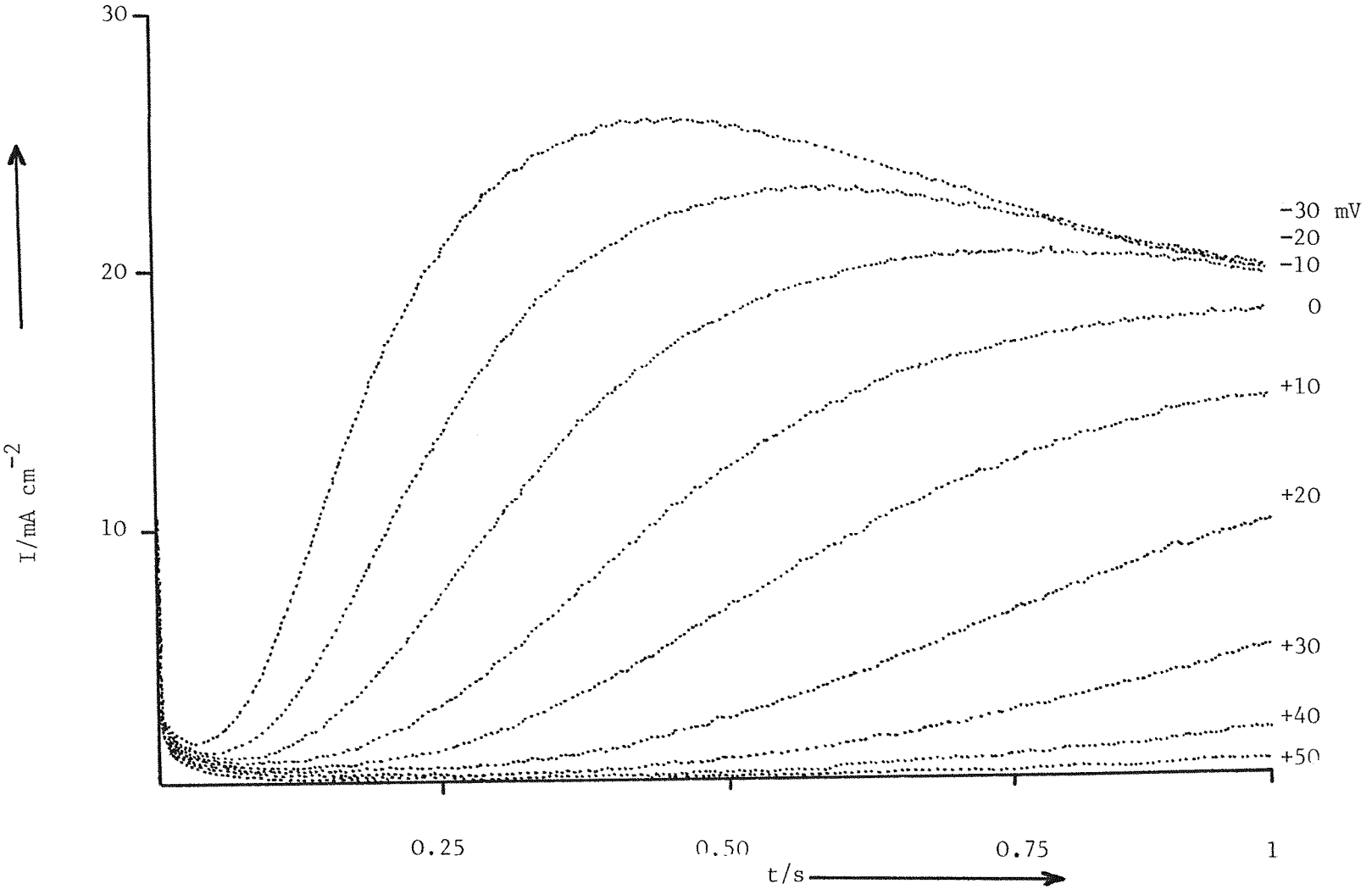

Figure 3.7 Potentiostatic current transients for the deposition of palladium onto vitreous carbon electrode from a solution of 50 mmol dm^{-3} $PdCl_2$ in aqueous 1 mol dm^{-3} KCl at pH ≈ 3.5. Potential as indicated.

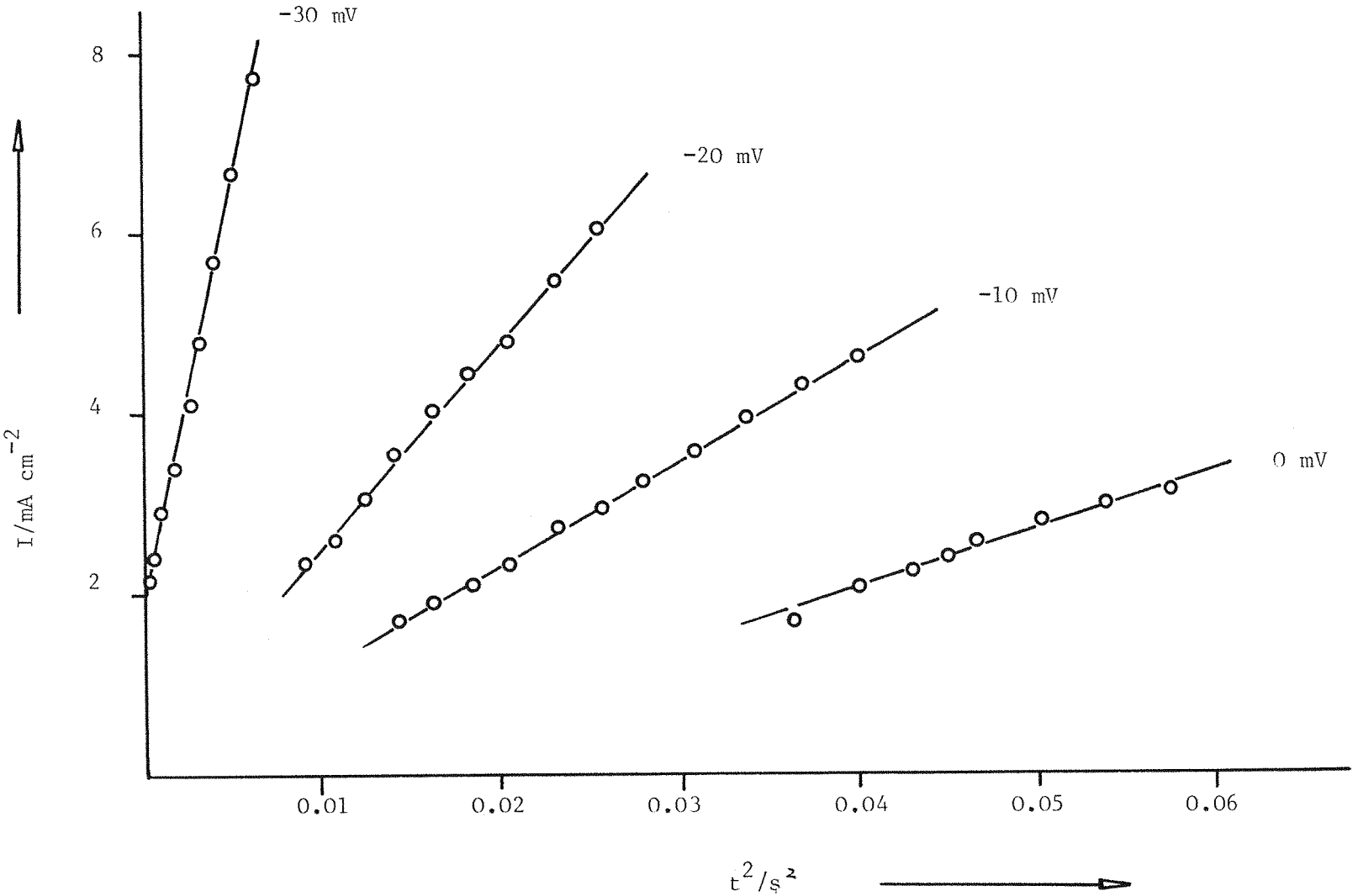

Figure 3.8 I vs t^2 plots for the early parts of the potentiostatic current transients in figure 3.7

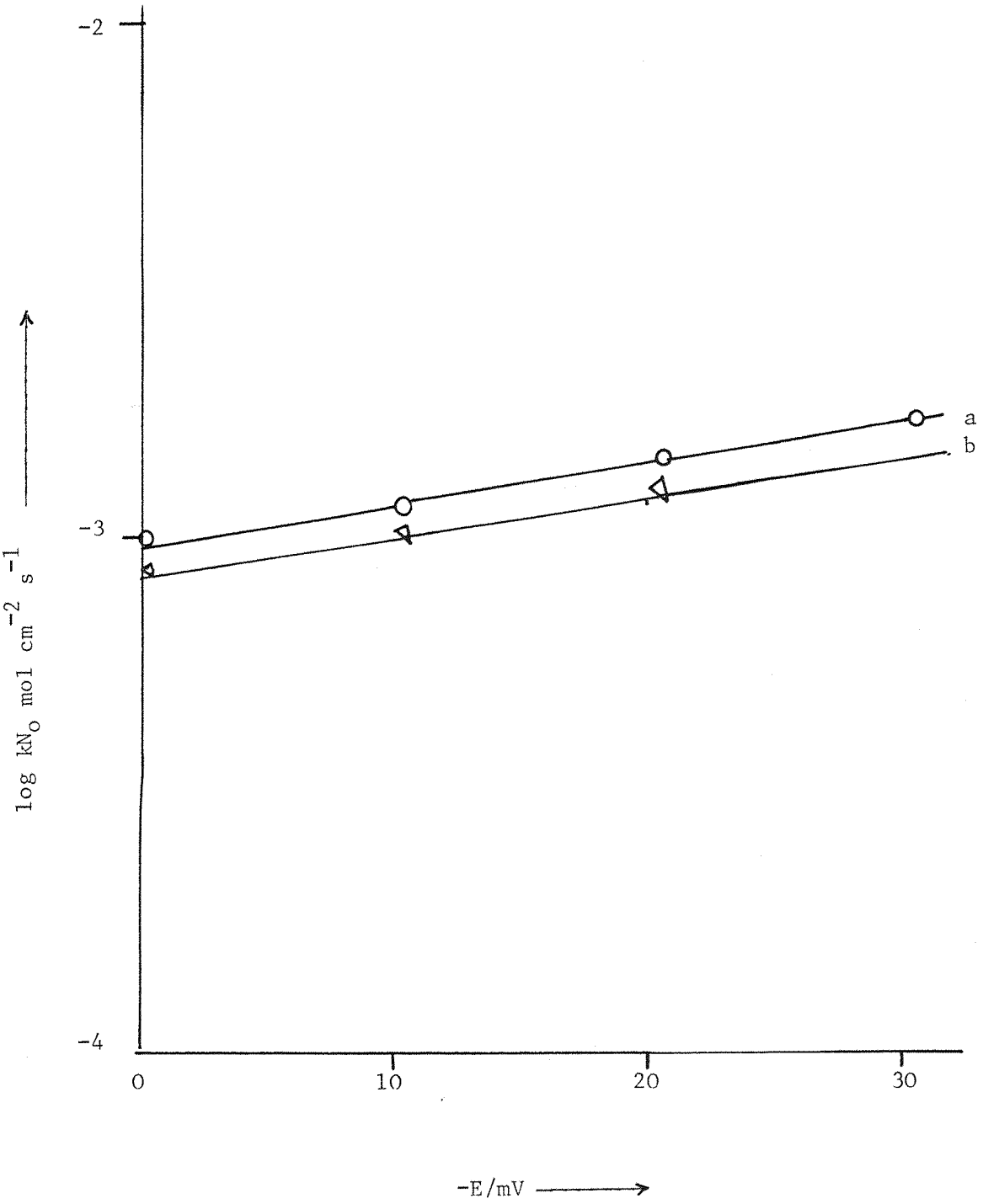

Figure 3.9 log kN_o vs -E plots. The values are calculated from the slopes of the I vs t^2 plots

(a) 50 mmol dm^{-3} $PdCl_2$

(b) 25 mmol dm^{-3} $PDCl_2$

50 mmol dm^{-3} $PdCl_2$ + 1 mol dm^{-3} KCl				25 mmol dm^{-3} $PdCl_2$ + 1 mol dm^{-3}		
-E mV	dI/dt^2 Acm^{-2} s^{-2}	$kN_o x10^{-3}$ mol $cm^{-2}s^{-1}$	log kN_o	dI/dt^2 Acm^{-2} s^{-2}	$10^3 kNo$ mol $cm^{-2}s^{-1}$	log kN_o
0	8×10^{-2}	1	-3.0	5.26×10^{-2}	0.87	-3.06
-10	1.18×10^{-1}	1.13	-2.94	9.6×10^{-2}	1.06	-2.97
-20	2.24×10^{-1}	1.40	-2.85	1.42×10^{-1}	1.20	-2.91
-30	9×10^{-1}	2.23	-2.65			

Table 3.3 log kN_o values calculated for a range of potentials at concentrations,
(a) 50 mmol dm^{-3} $PdCl_2$
(b) 25 mmol dm^{-3} $PdCl_2$
both in 1 mol dm^{-3} KCl.

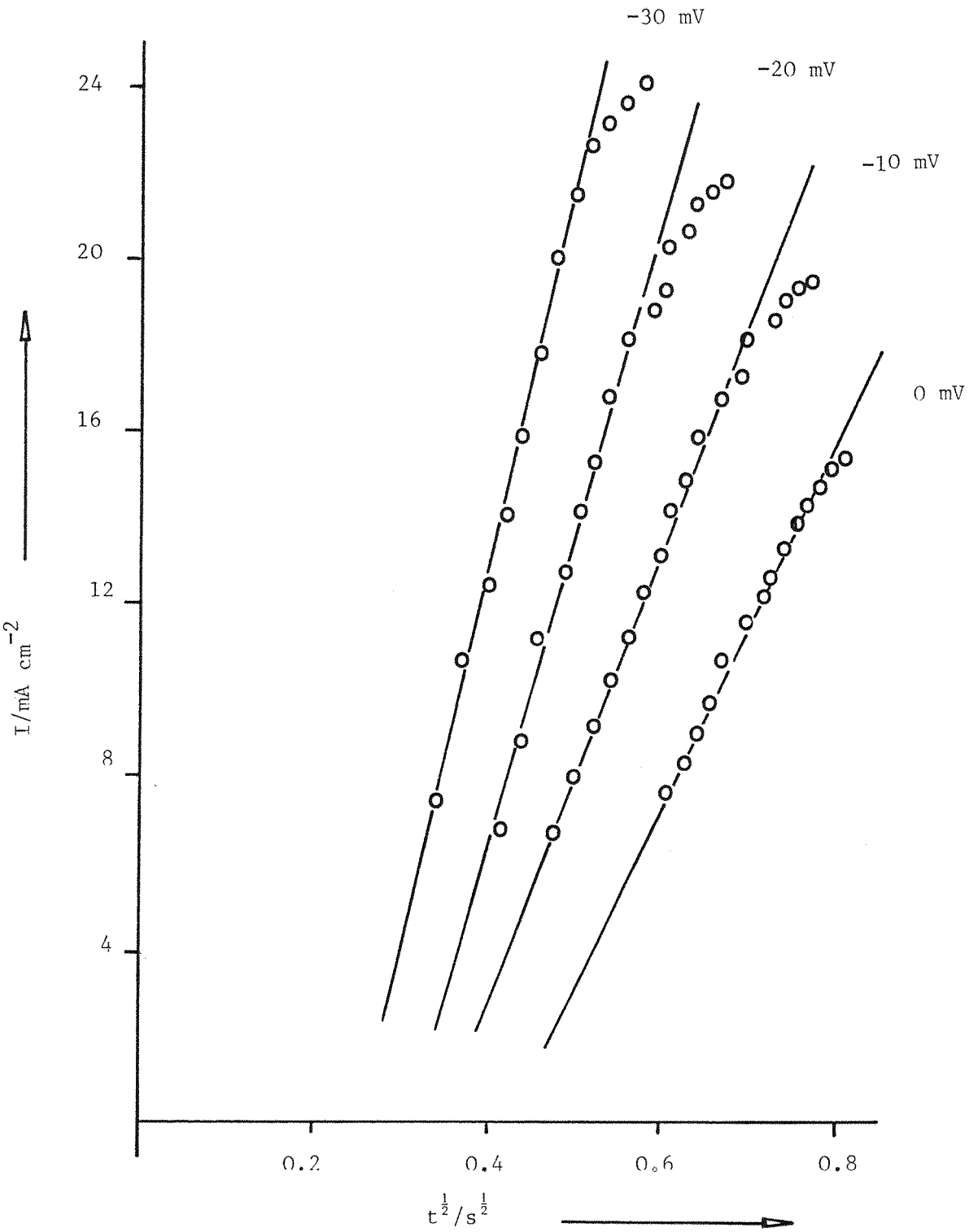

Figure 3.10 I vs $t^{\frac{1}{2}}$ plots for the potentiostatic current transients in figure 3.7

50 mmol dm^{-3} $PdCl_2$			25 mmol dm^{-3}			10 mmol dm^{-3}		
- E mV	$10^2 dI/dt^{\frac{1}{2}}$ A cm^{-2} $s^{-\frac{1}{2}}$	$10^{-5} N_o$ cm^{-2}	-E mV	$10^2 dI/dt^{\frac{1}{2}}$ A $cm^{-2} s^{-\frac{1}{2}}$	$10^{-5} N_o$ cm^{-2}	-E mV	$10^3 dI/dt^{\frac{1}{2}}$ A cm^{-2} $s^{-\frac{1}{2}}$	$10^{-5} N_o$ cm^{-2}
			-50	3.75	17.92			
			-40	3.0	14.34	-40	4.80	9.1
-30	8.93	15.0	-30	2.48	11.86	-30	3.46	6.56
-20	7.2	12.0	-20	1.80	8.60			
-10	5.1	8.61	-10	1.37	6.58			
			0	1.06	5.08			
0	4.12	4.01	+10	0.64	3.04			

Table 3.4 Nuclear number density as a function of potential and for a range of concentrations. 50,25 and 10 mmol dm^{-3} $PdCl_2$ in 1 mol dm^{-3} KCl.

fall on a common curve figure 3.11. The falling part of the transient could be replotted to give a I vs $t^{-\frac{1}{2}}$ plot which was linear, figure 3.12. This shows that beyond the peak, the growth centers have overlapped and further growth obeysthe simple linear diffusion law, equation (1.1). From the slope of the plot the value of diffusion coefficient was calculated to be D= 1.07 x 10^{-5} cm^2 s^{-1}. This value is similar to that obtained by cyclic voltammetry and close to the expected value.

A set of potentiostatic current transients for a solution of 25 mmol dm^{-3} in 1 mol dm^{-3} potassium chloride at pH 3.5 are shown in figure 3.13. The shape of the transient was similar to that of figure 3.7. At short time and low potential I vs t^2 plots were obtained, figure 3.14. From the slopes of the lines the value of rate constants were again calculated, table 3.3. At higher potentials the current was effected by the background current, and hence a similar treatment was not attempted. A plot of logkN_o vs E is shown in figure 3.9. The slope was again 120 mV.

At longer times the I vs $t^{\frac{1}{2}}$ plots were again linear, figure 3.15. Nuclear number densities were again calculated. The plot of N_o vs E is shown in figure 3.16.

A set of potentiostatic current transient was also recorded for 10 mmol dm^{-3} palladium chloride containing 1 mol dm^{-3} potassium chloride is shown in figure 3.17. A higher overpotential was required to initiate the nucleation process and the rising part of the transients were badly effected by background currents but the shapes of the transients were essentially similar to these at higher concentration of palladium(II). At high potentials after a sharp fall in currents, these currents reached to a maxima and fall down to a common branch indicating that the process was diffusion controlled. Nuclear number densities increase with the concentration of Pd(II).

3.3 OBSERVATION OF THE NUCLEATION AND GROWTH OF PALLADIUM USING ELECTRON SCAN MICROSCOPY

Electron scanning microscopy was used to confirm the conclusions from the electrochemical studies. The electrodeposition of palladium onto vitreous carbon electrode was carried out under potentiostatic conditions.

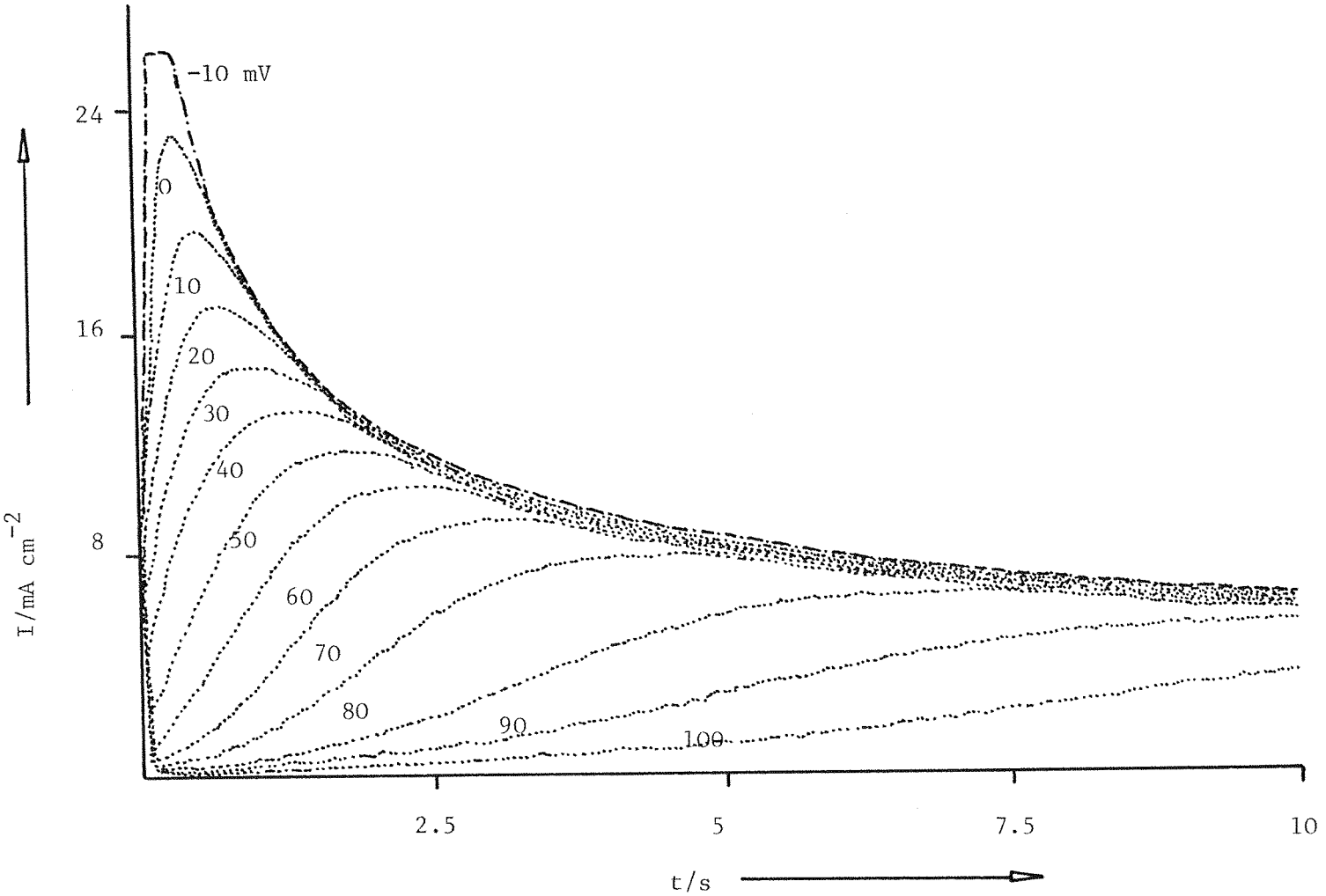

Figure 3.11 Potentiostatic current transients for the deposition of palladium onto vitreous carbon electrode from a solution of 50 mmol dm^{-3} $PdCl_2$ in aqueous 1 mol dm^{-3} KCl, at pH ≈ 3.5. The timescales recorded are much longer than for figure 3.7. Potentials as shown.

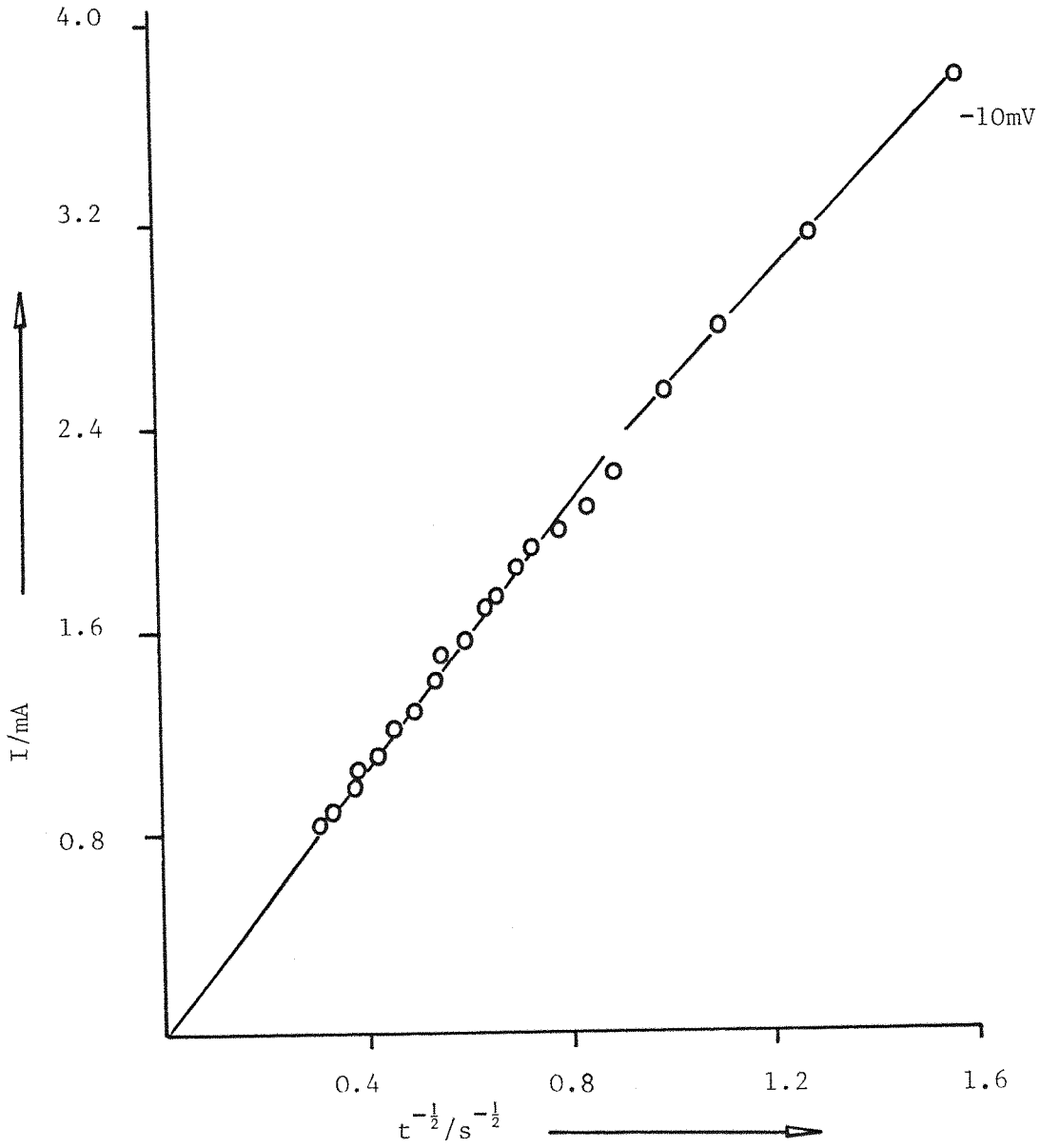

Figure 3.12 I vs $t^{-\frac{1}{2}}$ plot for the potentiostatic current transient at -10 mV (in figure 3.11)

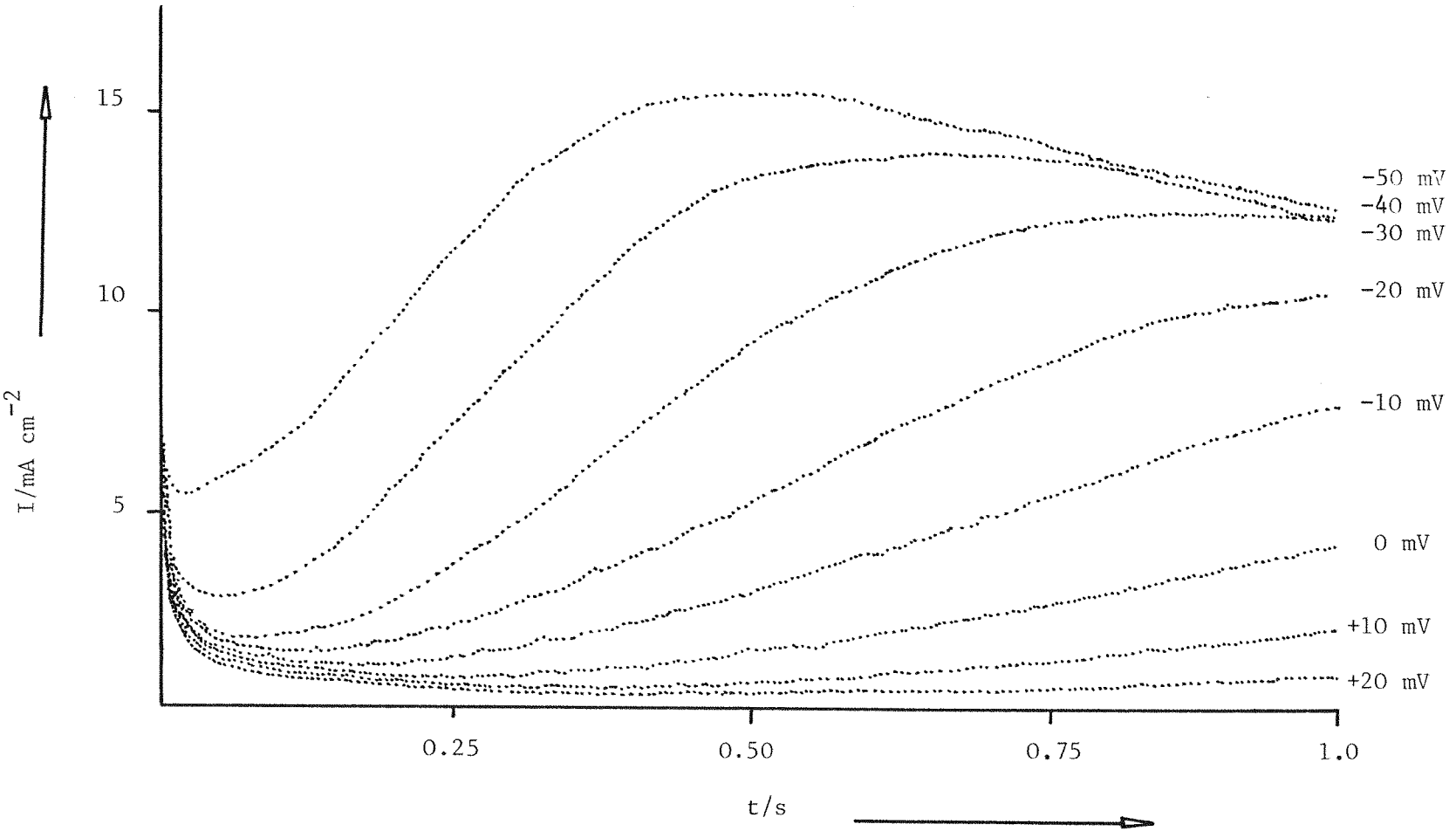

Figure 3.13 Potentiostatic current transients for deposition of palladium onto vitreous carbon electrode from a solution of 25 mmol dm^{-3} $PdCl_2$ in aqueous 1 mol dm^{-3} KCl. Potentials as shown

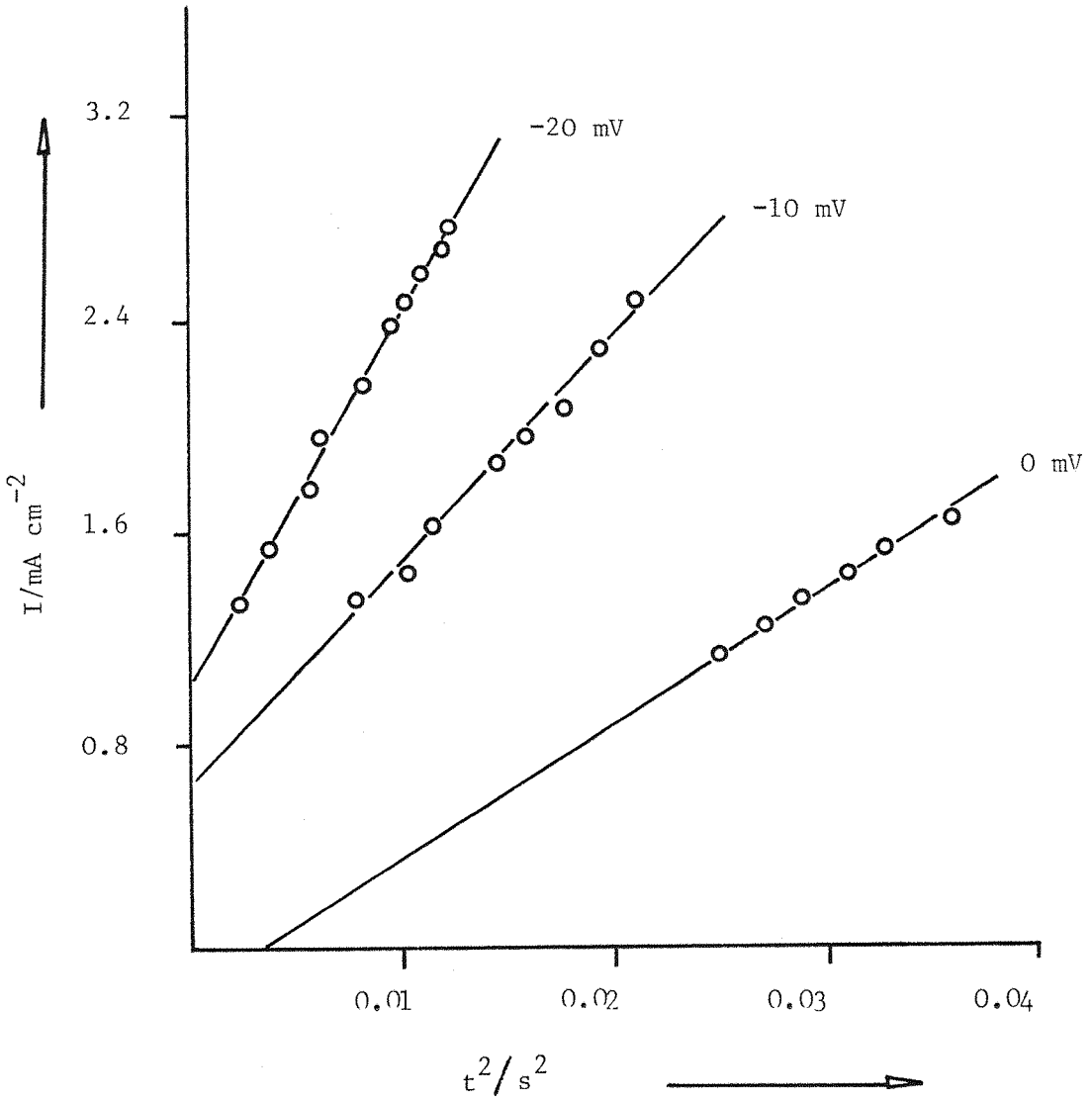

Figure 3.14 I vs t^2 plots for the early parts of the potentiostatic current transients in figure 3.13

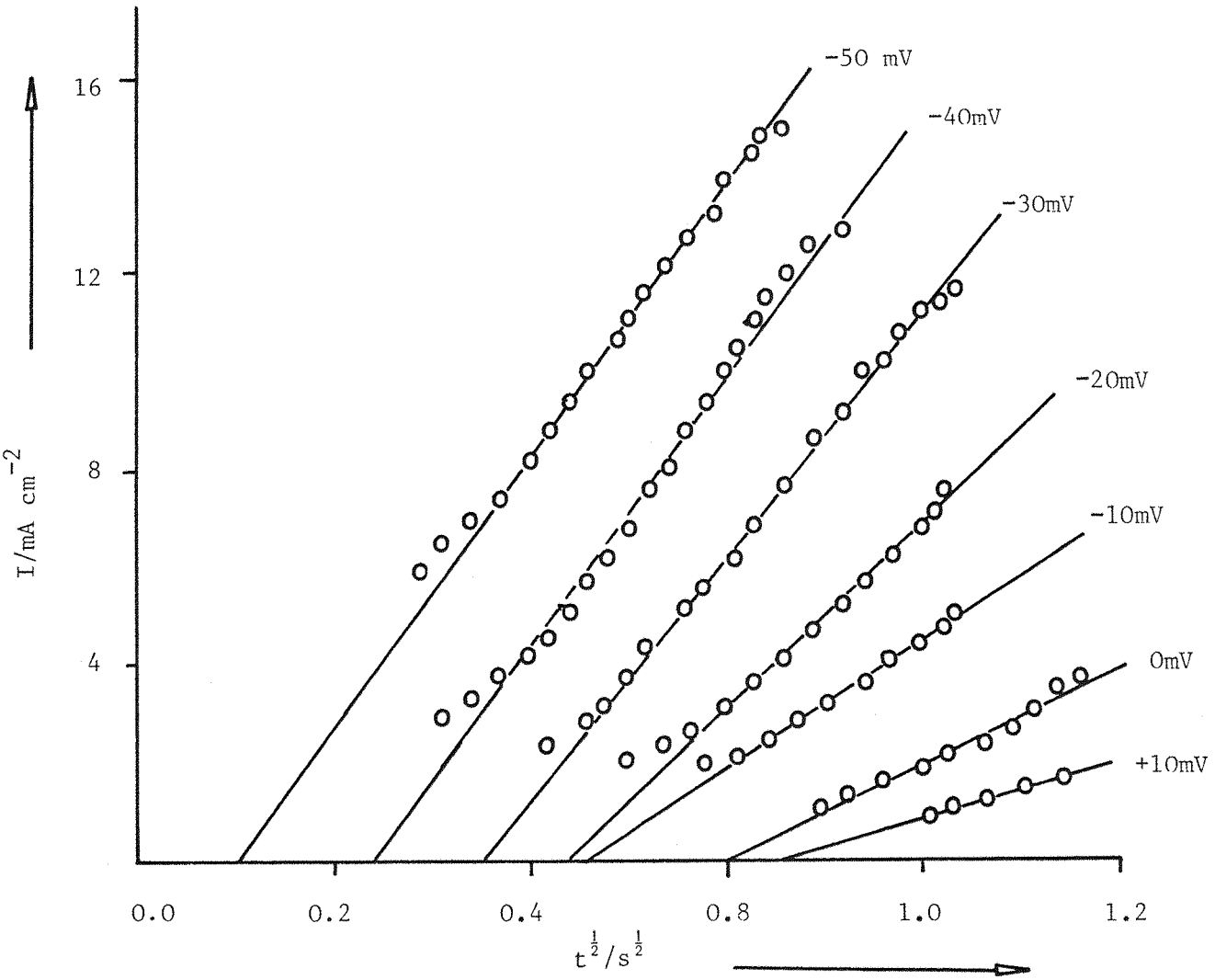

Figure 3.15 I vs $t^{\frac{1}{2}}$ plots for the later rising parts of the potentiostatic current transients in figure 3.13

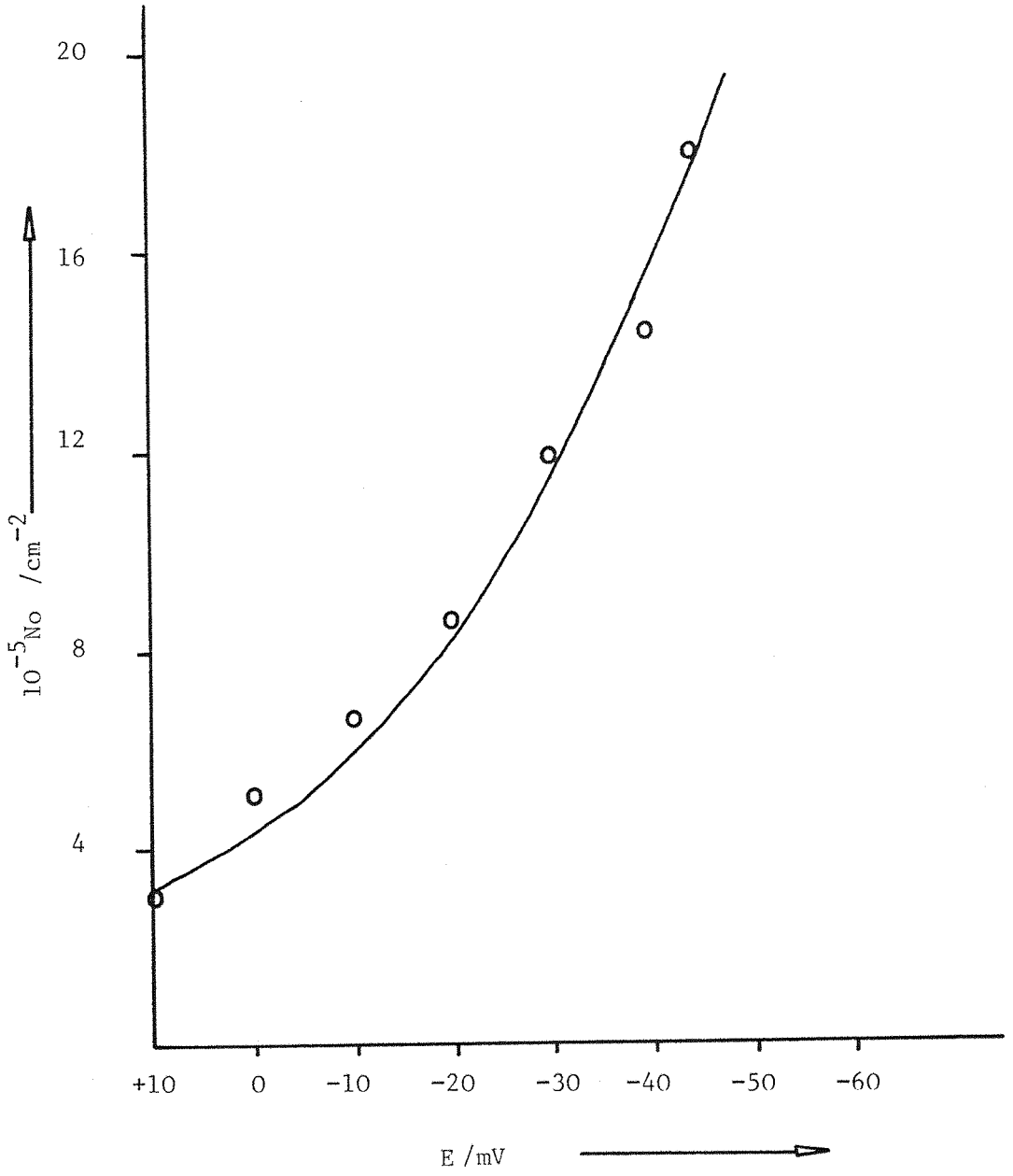

Figure 3.16 Nuclear number density as a function of potential. Data calculated from the plots in figure 3.15

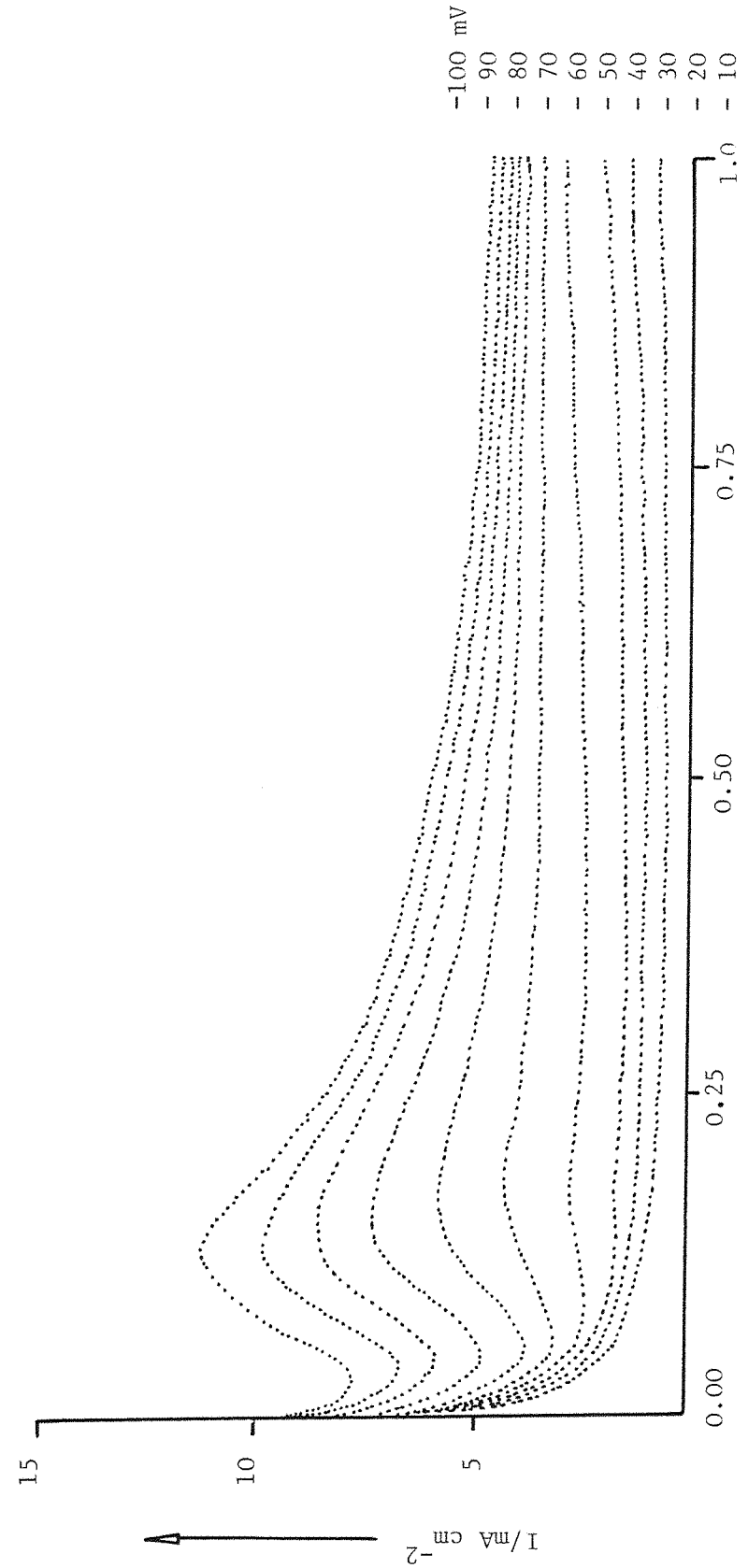

Figure 3.17 Potentiostatic current transients for the deposition of palladium onto vitreous carbon electrode from a solution of 10 mmol dm^{-3} $PdCl_2$ in aqueous 1 mol dm^{-3} KCl

The design and the construction of this specially made electrode is shown in chapter two. A single potentiostatic pulse was applied to a vitreous carbon electrode in a solution of 1 mol dm^{-3} potassium chloride containing 50 mmol dm^{-3} palladium chloride. To study the type of nucleation law, the number density and the growth mode of the nuclei, a constant potential pulse was applied for different times of 2,4 and 9 seconds. The applied potential was low (+120 mV vs S.C.E.) so that the process of nucleation and growth model adopted by the system could be observed during the initial stages. The current time transients were also recorded on an oscilloscope and then onto a X-Y recorder for further analysis.

The electron micrograph in figure 3.18 shows the spatial distribution of the growth centers for palladium at + 120 mV after 9 seconds. The corresponding current time transient is shown in figure 3.19. The centres may be seen, by and large, to be of similar sizes and hence the electron microscopy would support the conclusion that instantaneous nucleation occurs. The electron micrograph at higher magnification, figure 3.20 provides further evidence for this nucleation model since most of the nuclei are of similar size although there are a very few nuclei of smaller size. The diameter of a single nucleus (calculated from the micrograph) was approximately 0.6 micron. The distribution of nuclei is not even, as can clearly be seen from the figure 3.20. Some areas of the electrode were highly covered with nuclei whereas the others are not. The uneven distribution is probably due to nucleation occurring at particular types of sites on the vitreous carbon. The nature of the bulk phase was clearly evident as was the approximation to a spherical shape. The number of clustures could be easily counted and compared with the number density obtained by the analysis of the current time transients, discussed above using equation 1.26. The average value for nucleation number density calculated from I-t transient analysis was 10^6 cm^{-2} (table 3.4) whereas the nucleation number densities by visual counting was 2×10^7 cm^{-2} (average value). This discrepancy will be discussed further later in this thesis.

3.4 THE STUDY OF NUCLEATION AND GROWTH OF PALLADIUM ON MICROELECTRODES

3.4.1 LINEAR SWEEP VOLTAMMETRY

All linear potential sweep experiments using microelectrodes (carbon

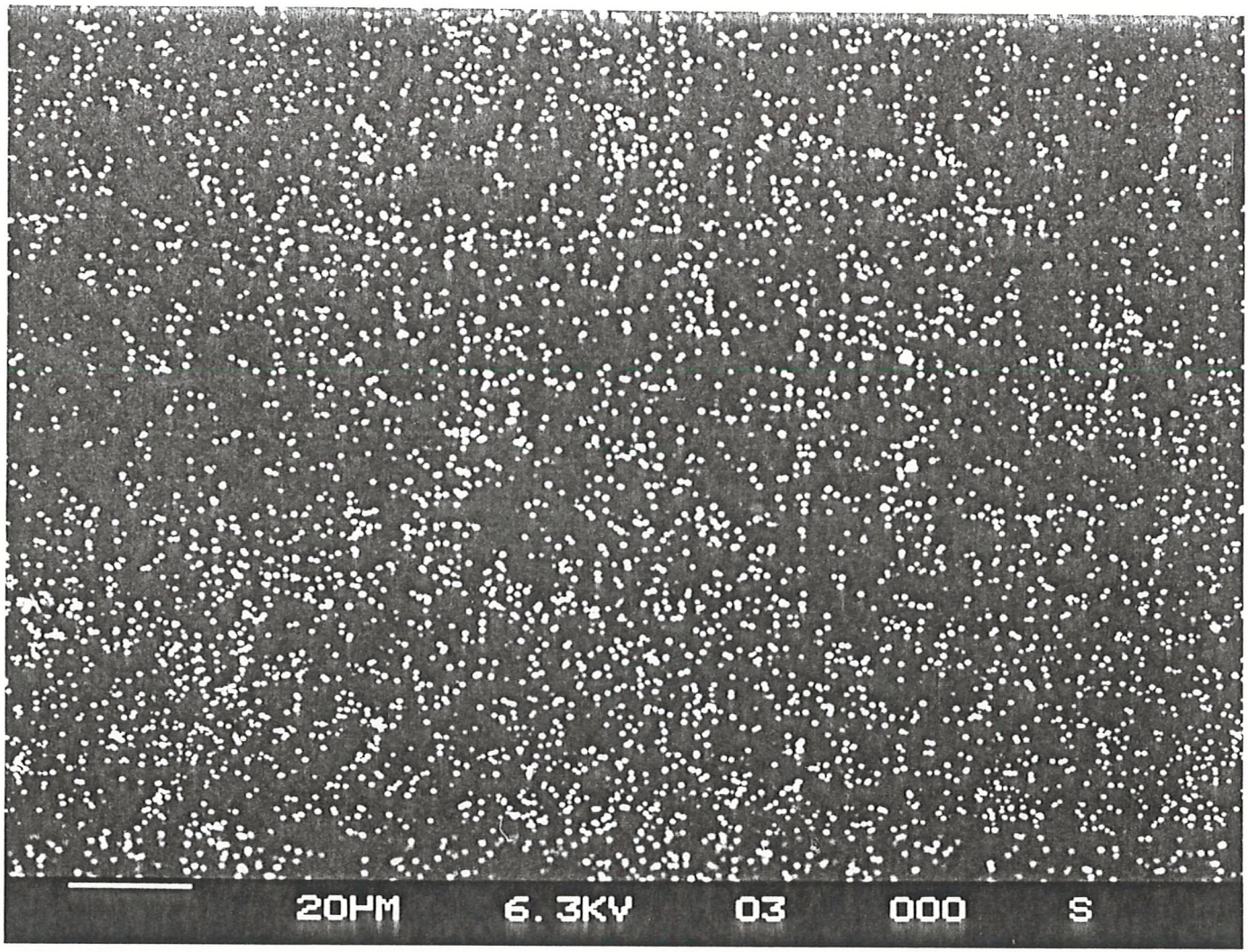

Figure 3.18 Electron micrograph of the palladium deposited onto vitreous carbon from 50 mmol dm^{-3} $PdCl_2$. E = 120 mV. Deposition time = 9 s.

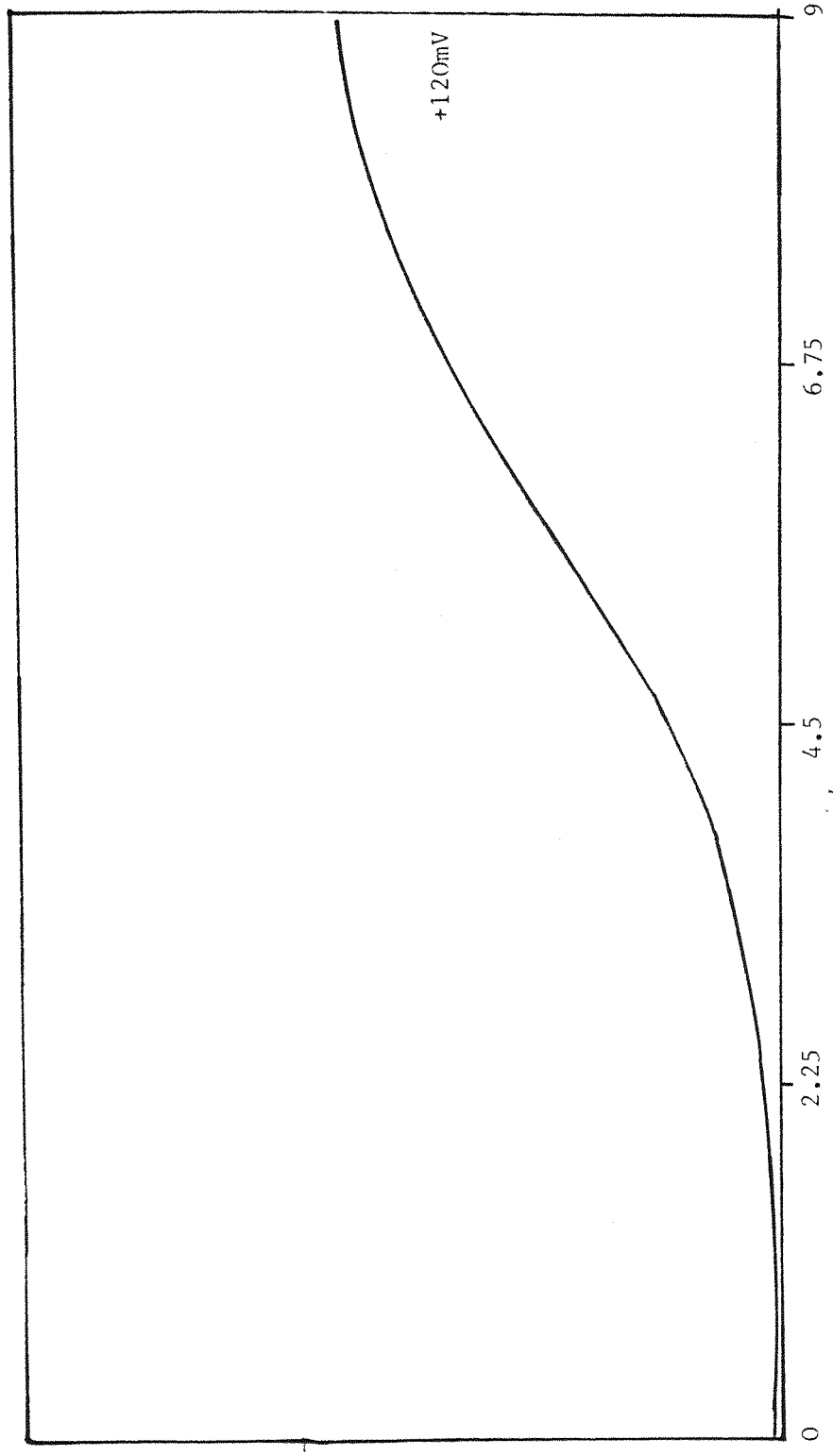

Figure 3.19 The corresponding potentiostatic current transient at -E = 120 mV, for figure 3.18. Solution as for figure 3.7.

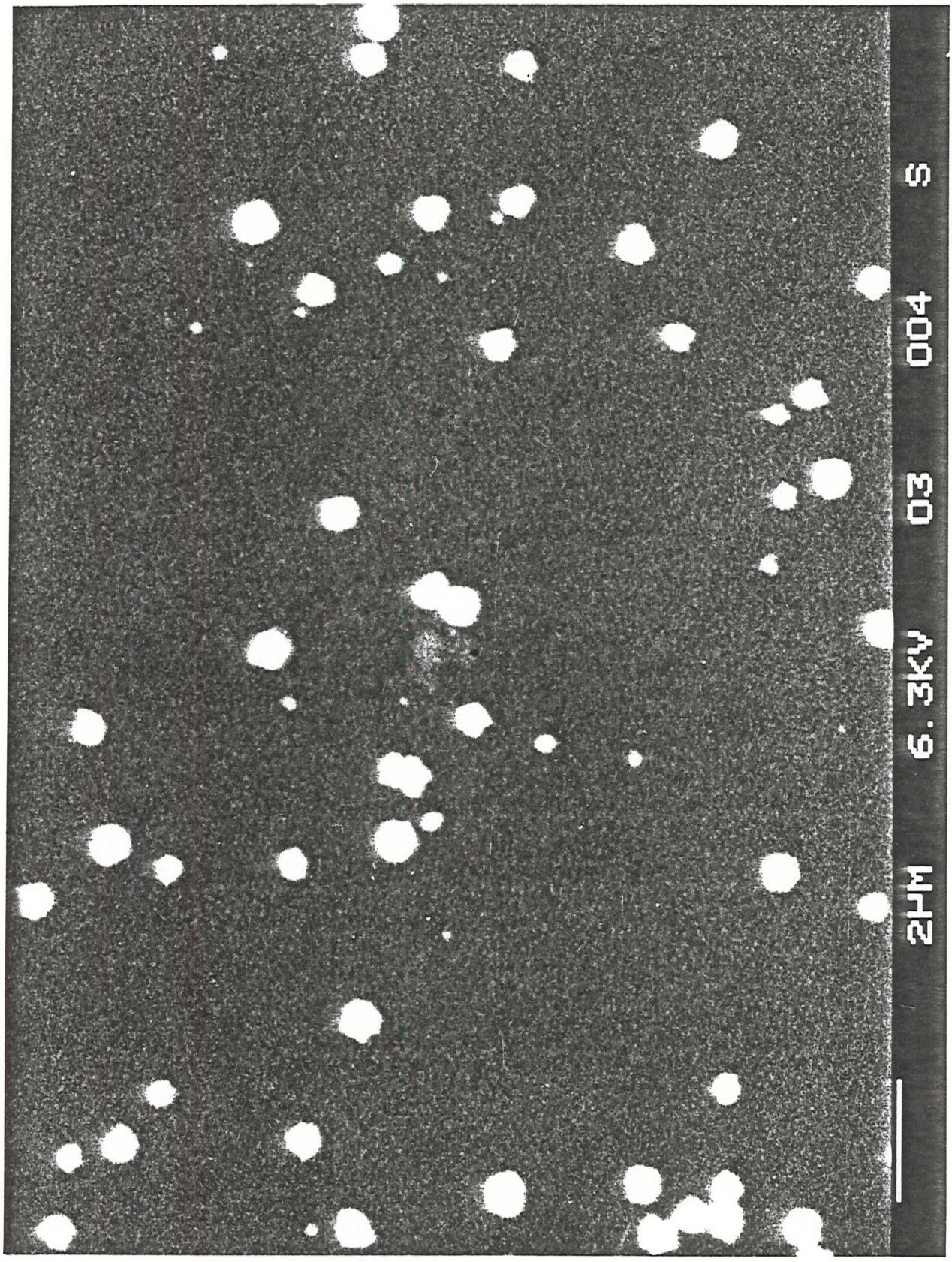

Figure 3.20 Electron micrograph of the palladium deposit at higher magnification

and platinum) were carried out using a one compartment, two electrode cell as shown in figure 2.3. A set of linear sweep voltammograms recorded for the reduction of palladium onto a carbon fiber electrode (area = 5×10^{-7} cm^2) from a solution of 20 mmol dm^{-3} palladium chloride in 1 mol dm^{-3} potassium chloride at pH 3.5 is shown in figure 3.21. In various experiments the secondary electrode which also acted as reference electrode was either a palladium or platinum wire (spiral electrode).

The I-E response for the reduction of palladium(II) at a microelectrode is quite different from that at a larger electrode. With a microelectrode, no peak is observed on the negative going sweep. Instead it is found that the current increases as the potential scan is continued and this trend is also seen during the early part of the reverse sweep. As a result the cathodic current during the reverse sweep is higher than on the forward sweep over a wide potential range. But as on the larger electrode, the deposition process continues until just negative to the reversible potential when reduction of palladium(II) stops. Moreover, in complete contrast to a larger electrode, at the microelectrode the current decreases with an increase in potential scan rate. All these differences may be understood if it is recognised that the rate of mass transport to the microelectrode is very high. Hence on the timescale of the experiments, mass transport control does not set in. There is therefore no peak on the forward scan while the correlation of the current with potential scan rate simply reflects the size of the growing center - the slower the sweep the more time for the growth of the centers. Therefore on microelectrodes the process is purely kinetically controlled. However the potentials for the deposition and dissolution phenomena were found to be independent of the size of the electrode. The potentials on macro and microelectrodes are comparable.

The nucleation potential was found to shift towards more negative potential with the increase in potential sweep rate (figure 3.21). The nucleation potentials were -200 mV, -300 mV and -400 mV at $5mVs^{-1}$, $10mVs^{-1}$ and $40mVs^{-1}$ respectively and this behaviour is similar to that observed during the reduction of palladium on a macroelectrode. The cathodic and anodic charges at all the sweep rates were estimated and the charge ratio was 0.90 which suggests that most of the palladium was dissolved anodically. Even so the electrode was polished (with 1-0.3

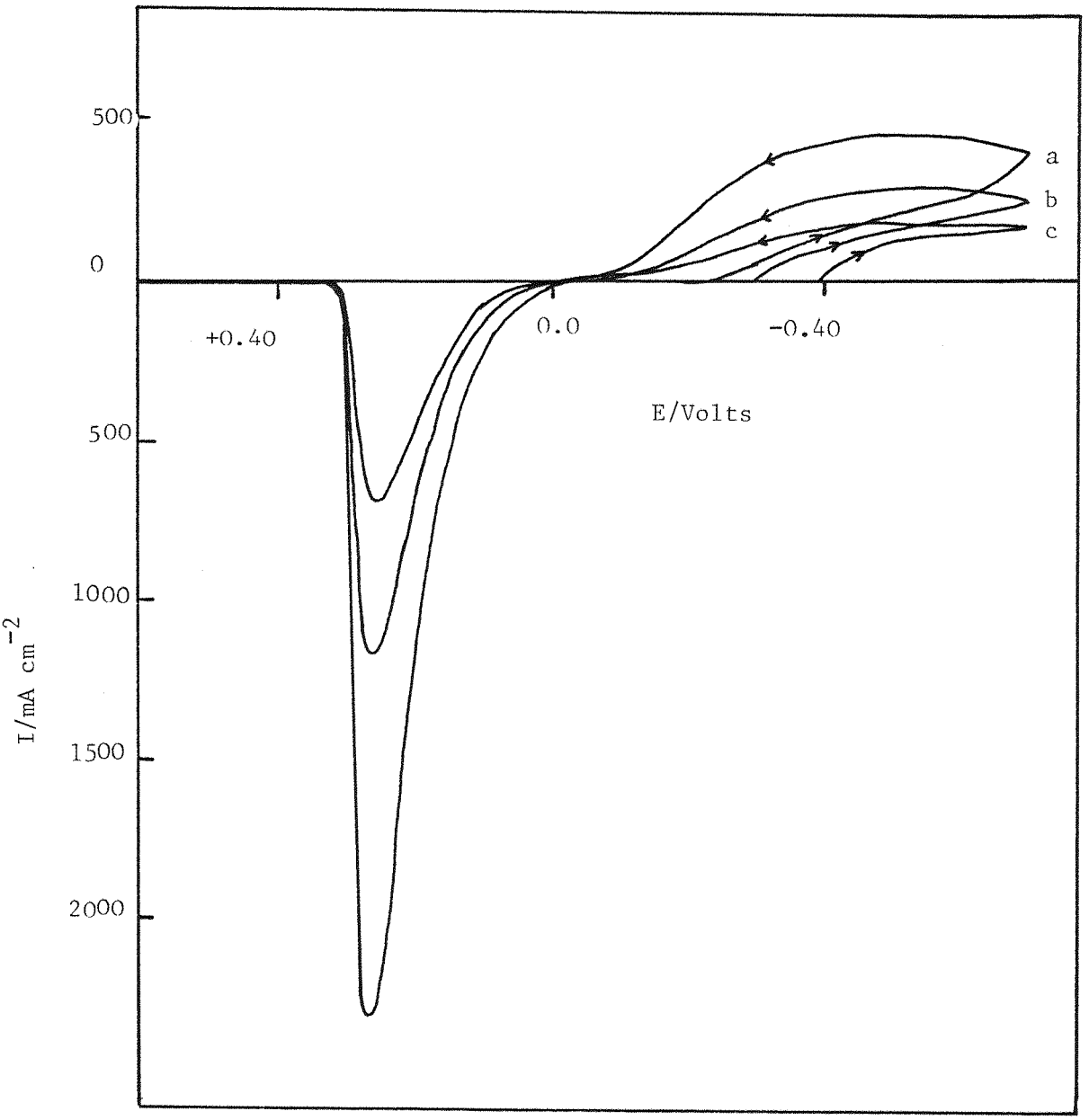

Figure 3.21 Cyclic voltammograms for the reduction of palladium(II) at a carbon fiber microelectrode (Area = 5 x 10^{-7} cm^2) from a solution of 20 mmol dm^{-3} $PdCl_2$ in aqueous 1 mol dm^{-3} KCl at pH ≈ 3.5, at potential sweep rates

(a) 5 mV s^{-1}

(b) 10 mV s^{-1}

(c) 40 mV s^{-1}

micron alumina) between every run.

Using similar potential limits and at a potential sweep rate of 30 mVs^{-1}, cyclic voltammograms for 10 and 50 mmol dm^{-3} palladium chloride were also recorded, figure 3.22, 3.23. The cathodic shift in nucleation potential could be noticed at low concentration of Pd^{2+}. The charge ratio of anodic and cathodic charges was again 0.90.

Figure 3.24 shows a linear potential sweep voltammogram for the reduction of 20 mmol dm^{-3} palladium chloride in 1 mol dm^{-3} potassium chloride at potential sweep rate of 10 mVs^{-1} onto a platinum microelectrode (area = 7.85×10^{-7} cm^2). The secondary electrode was again a palladium wire (spiral) electrode. The overall behaviour of the platinum microelectrode seemed to be very similar to the carbon fiber electrode. The nucleation potential was also similar to that at a carbon fiber for the same concentration and potential sweep rate. Similar cathodic and anodic current densities were also observed. The anodic stripping peak is slightly broader than that on the carbon fiber. The overall current densities on microelectrodes were found to be much higher than those observed on macroelectrode; this could be due to the high mass transfer to these electrodes.

3.4.2 POTENTIOSTATIC METHOD APPLIED TO THE MICROELECTRODES

The electrodeposition of mercury onto a carbon fiber microelectrode (area 5×10^{-7} cm^2) was reported earlier by Scharifker(134). Under a range of conditions, he obtained a transient such as that shown in figure 3.25. It can be seen that its shape is quite different to that on a macroelectrode; there is a sudden increase in current and the transient follows a $i\text{-}t^{\frac{1}{2}}$ form over a wide timescale. This type of transient was taken as evidence for the formation of a single nucleus as was predicted from the nuclei number density found from an experiment at a macroelectrode and the nucleus was shown to be growing under diffusion control. Moreover the delay before the rise in current varied widely from experiment to experiment showing the formation of a nucleus to be stochastic process and the formation of a single nucleus could be confirmed by electron microscopy. In some experiments the formation of two nuclei are to be expected and randomly a transient such as that figure 3.26 was observed.

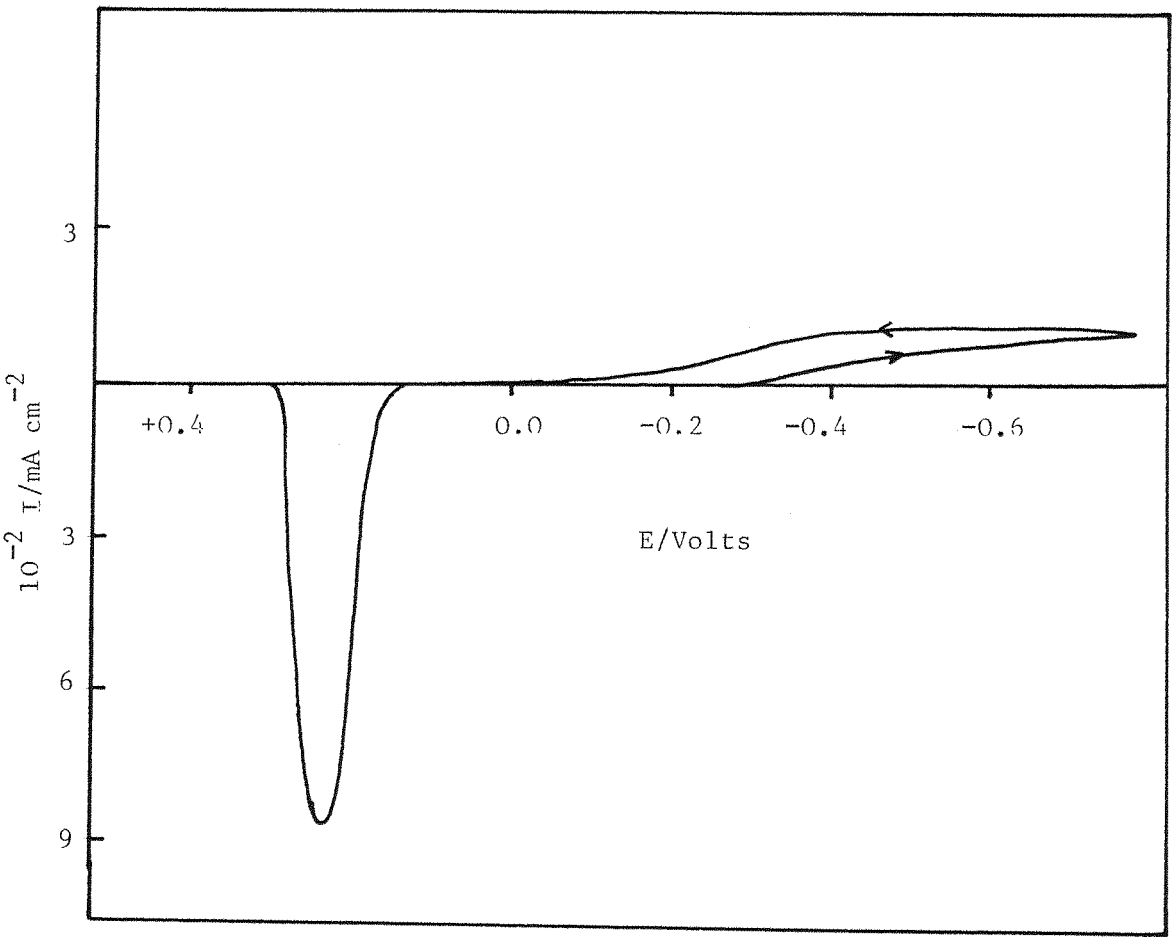

Figure 3.22 Cyclic voltammogram for reduction of palladium(II) at a carbon fiber microelectrode from a solution of 10 mmol dm^{-3} $PdCl_2$ in 1 mmol dm^{-3} KCl at pH ≃ 3.5, sweep rate = 30 mVs^{-1}.

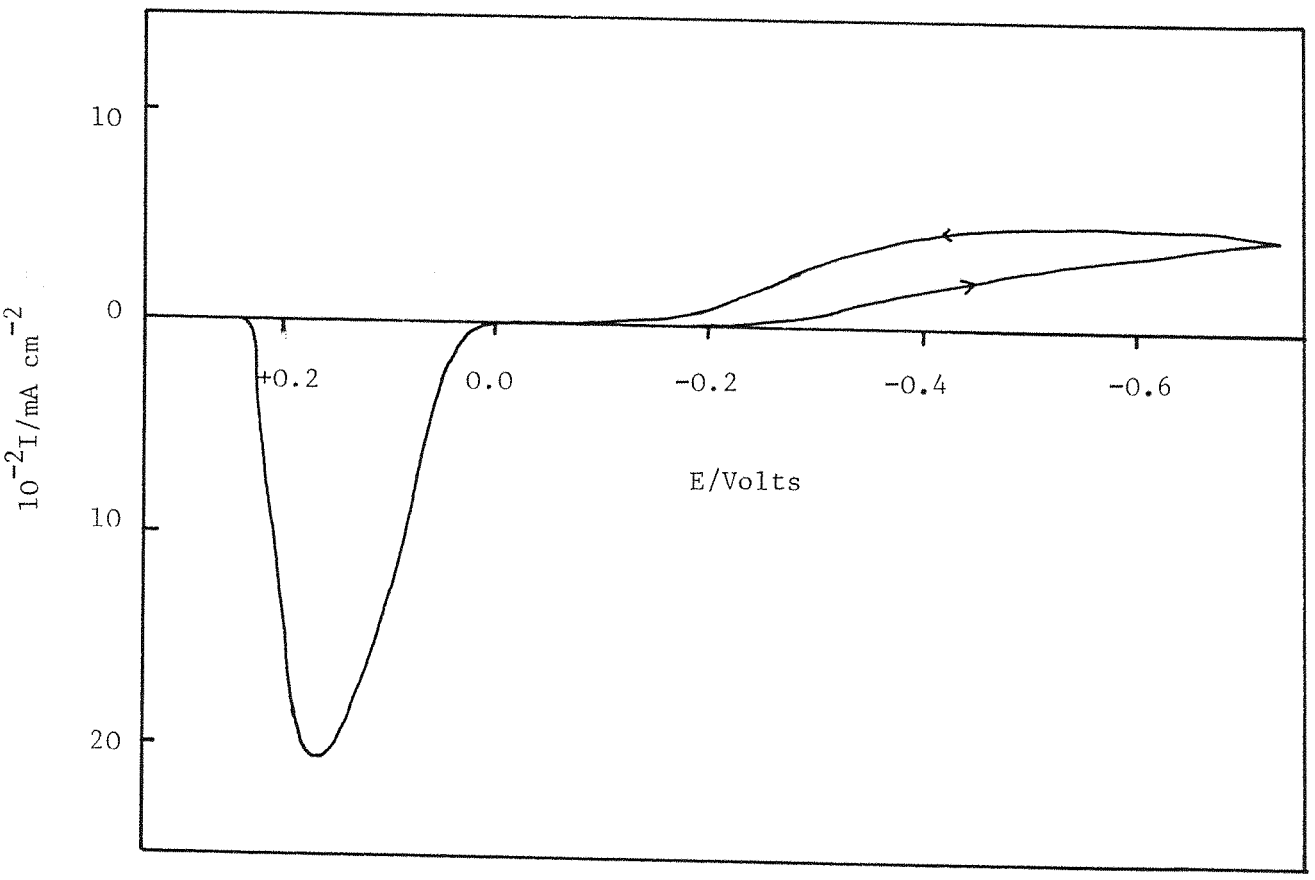

Figure 3.23 Cyclic voltammogram for the reduction of palladium(II) at a carbon fiber microelectrode from a solution of 50 mmol dm^{-3} $PdCl_2$ in 1 mol dm^{-3} KCl at pH ≈ 3.5, sweep rate = 30 mVs^{-1}.

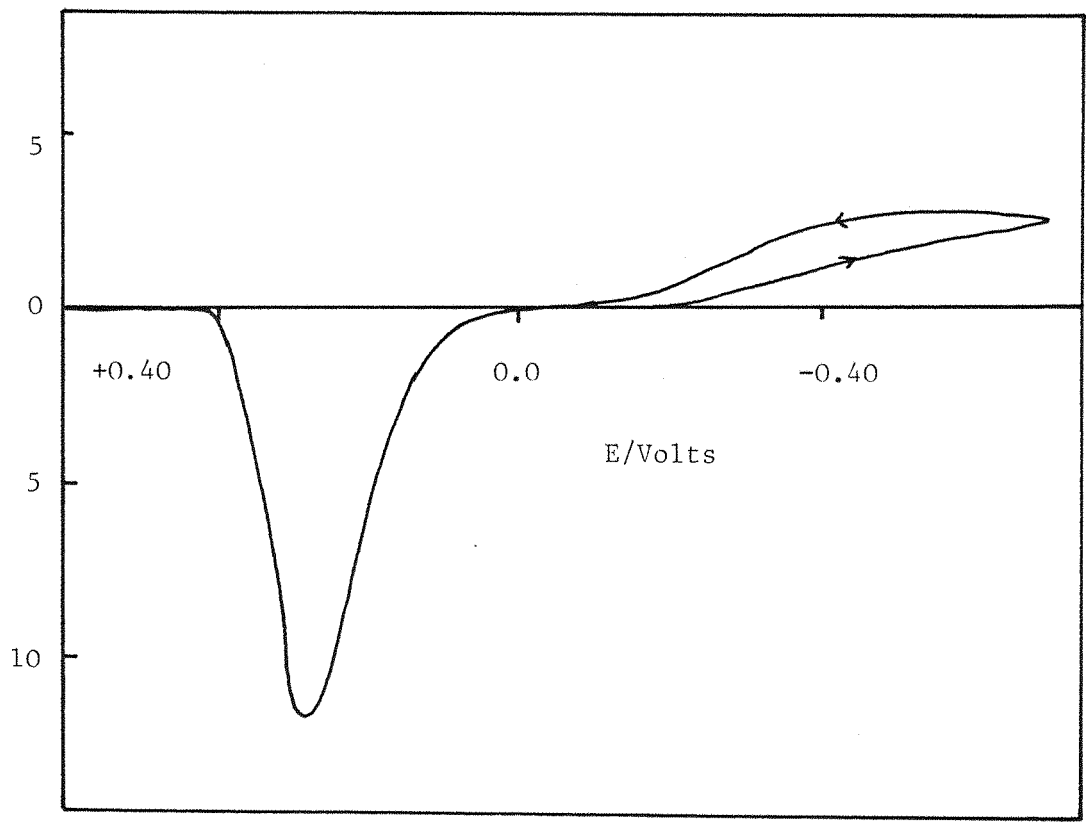

Figure 3.24 Cyclic voltammogram for 50 mmol dm^{-3} $PdCl_2$ (under similar conditions) on a platinum micro-electrode (Area = 7.85×10^{-7}) Sweep rate = 10 mV s^{-1}.

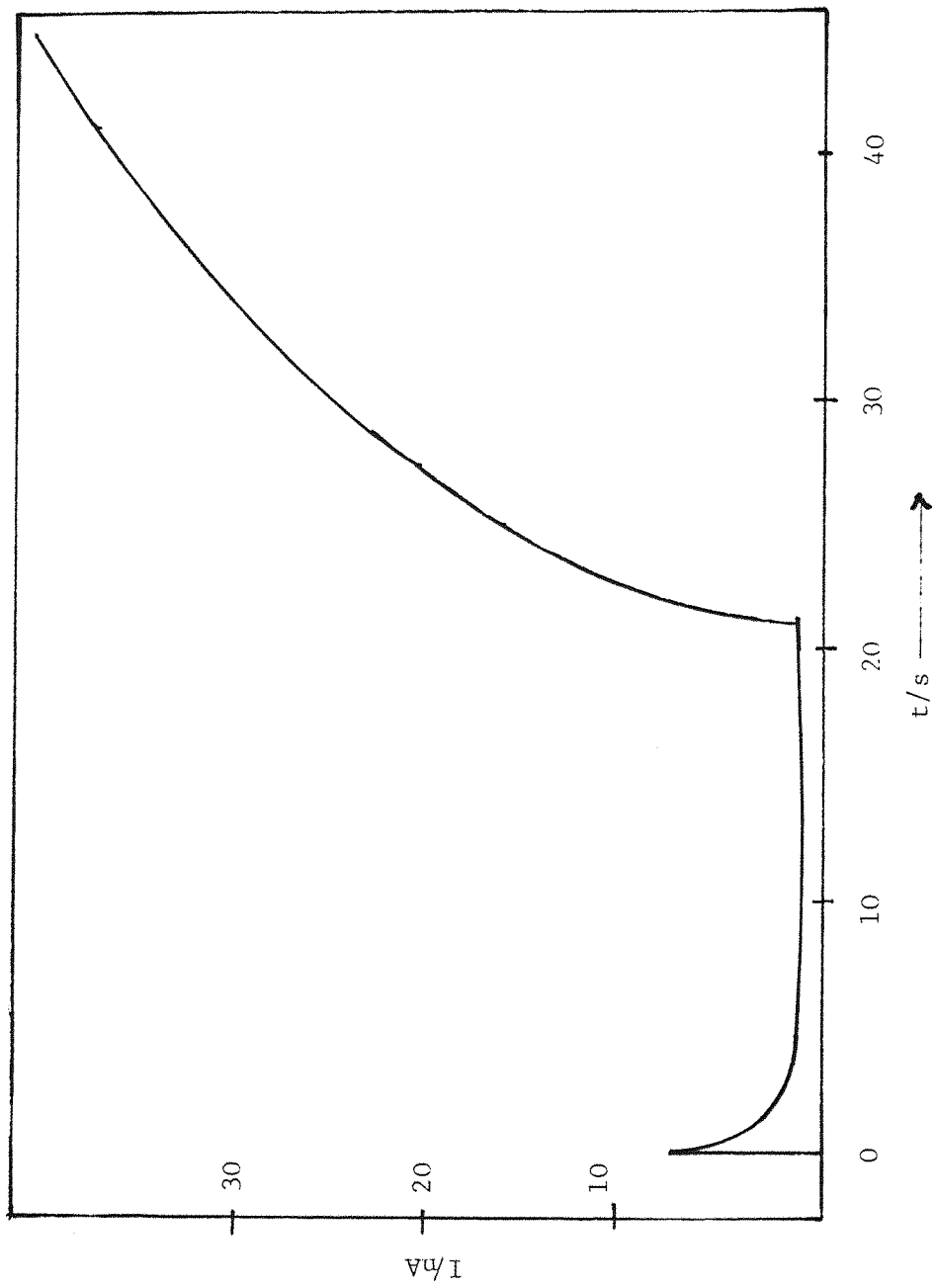

Figure 3.25 Potentiostatic current transient for the deposition of mercury on a carbon fiber microelectrode from a 10 mmol dm^{-3} solution of $Hg_2(NO_3)_2$ in aqueous potassium nitrate. n = 200 mV.

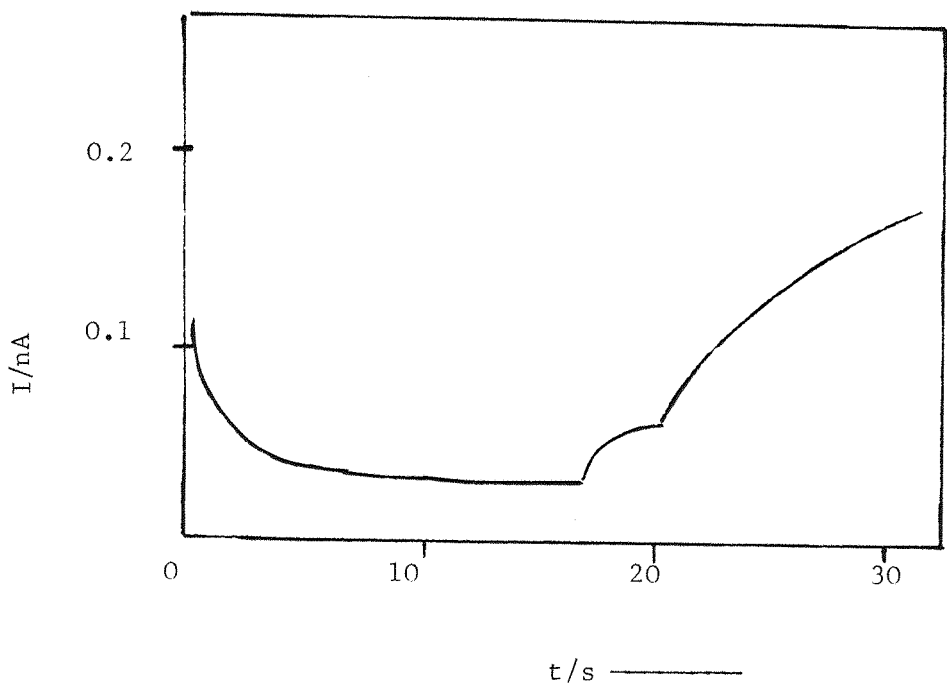

Figure 3.26 Potentiostatic current transient for the deposition of mercury from a solution of 1 mmol dm^{-3} $Hg_2(NO_3)_2$ in KNO_3(aq) on a carbon fiber microelectrode. η = 200 mV.

Here the two nucleation processes can clearly be seen.

In the palladium system the number of nuclei expected would be ten using the nucleus number density estimated from the electron scan microscopy (a calculation based on the number density found from the $I\text{-}t^{\frac{1}{2}}$ plots would, of course, be one). In fact, the transients are very similar in shape to those at a macroelectrode and are also quite reproducible. In other words, it must be concluded that in the palladium system there are always a large number of nuclei, even on the microelectrode, and the stochastic nature of the nucleation process is averaged out. Indeed the number of centers probably exceeds ten and this may be because of the surface of the fiber is not the same as the vitreous carbon rod.

A potentiostatic pulse method was applied to a carbon fiber electrode in solutions of 10-50 mmol dm^{-3} palladium chloride in 1 mol dm^{-3} potassium chloride. Some of the resulting current time transients for 20 mmol dm^{-3} palladium chloride at pH 3.5 are shown in figure 3.27. It was evident from the figure that the shape of the rising transients was similar to those obtained on macroelectrode, except that there was not a significant double layer charging current. After the potential step, the current starts increasing to give well defined rising current transients at the microelectrodes; the current densities reach a high value and no peak is seen in the transient. The current instead goes to a plateau. Both these features again reflect the very high rate of mass transport to the microelectrode.

The log i vs log t plot (figure 3.28) for the early parts of the transients from figure 3.25 give a slope value of 2, clearly indicating that the process is under total kinetic controlled and that instantaneous nucleation occurs. Therefore the current at very short time could be replotted as the square of time, and this produced a straight line shown in figure 3.29. From the slopes of the lines using equation (1.21) the value of rate constants were calculated and are listed in table 3.5. Moreover the values of the rate constants were found to be the same order of magnitude as were calculated from the data obtained on a large electrode (table 3.3). The rate constants are also potential dependent and a plot of log kN_o versus applied potential was a straight line, see figure 3.30, with a slope of 120 mV (again similar to large electrode) indicating a $1\bar{e}$ transfer as the rate determining step.

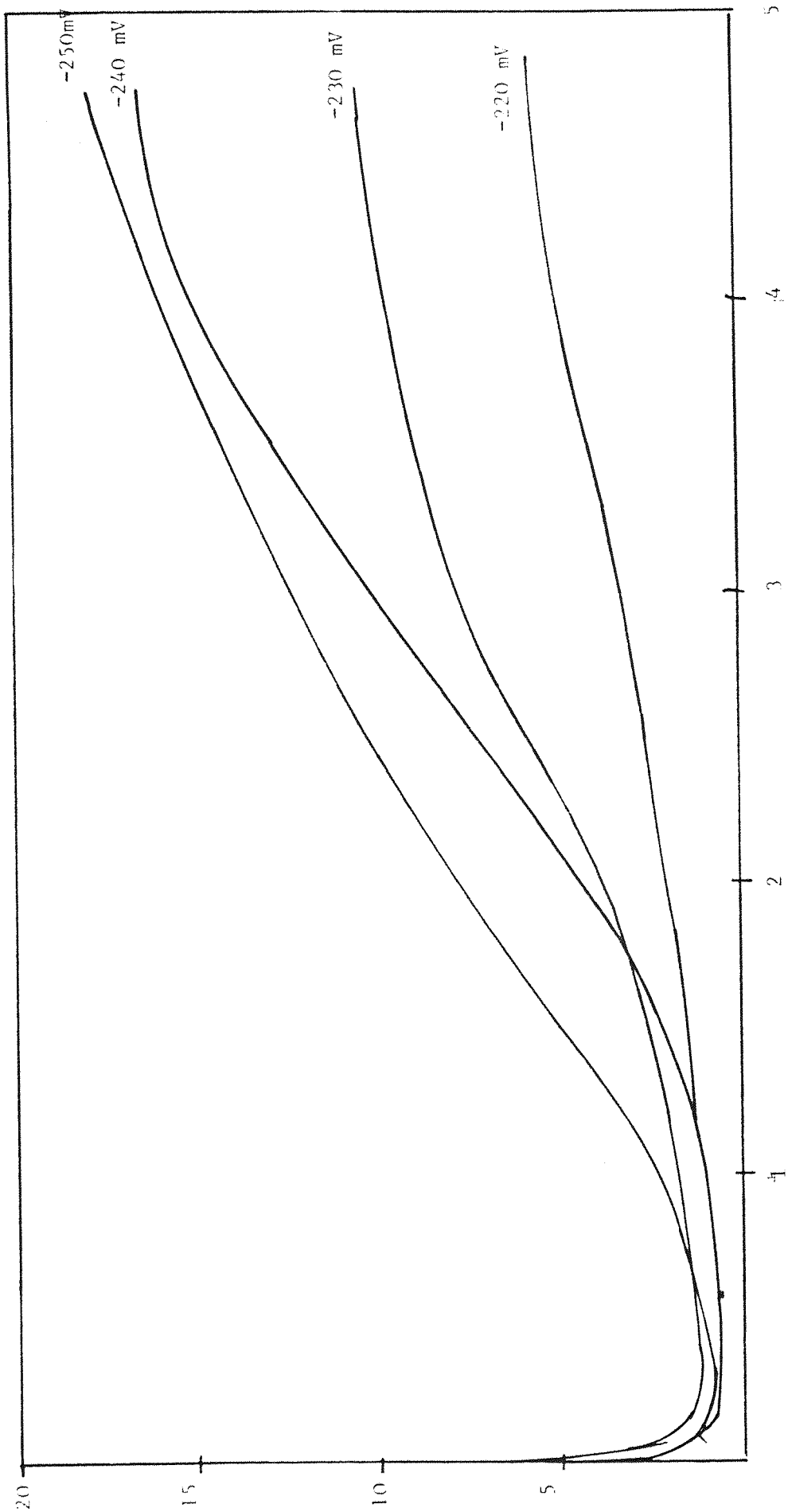

Figure 3.27 Potentiostatic current transient for the deposition of palladium on a carbon fiber from a solution of 20 mmol dm^{-3} $PdCl_2$ in 1 mol dm^{-3} KCl at pH ≈ 3.5. Potentials as shown.

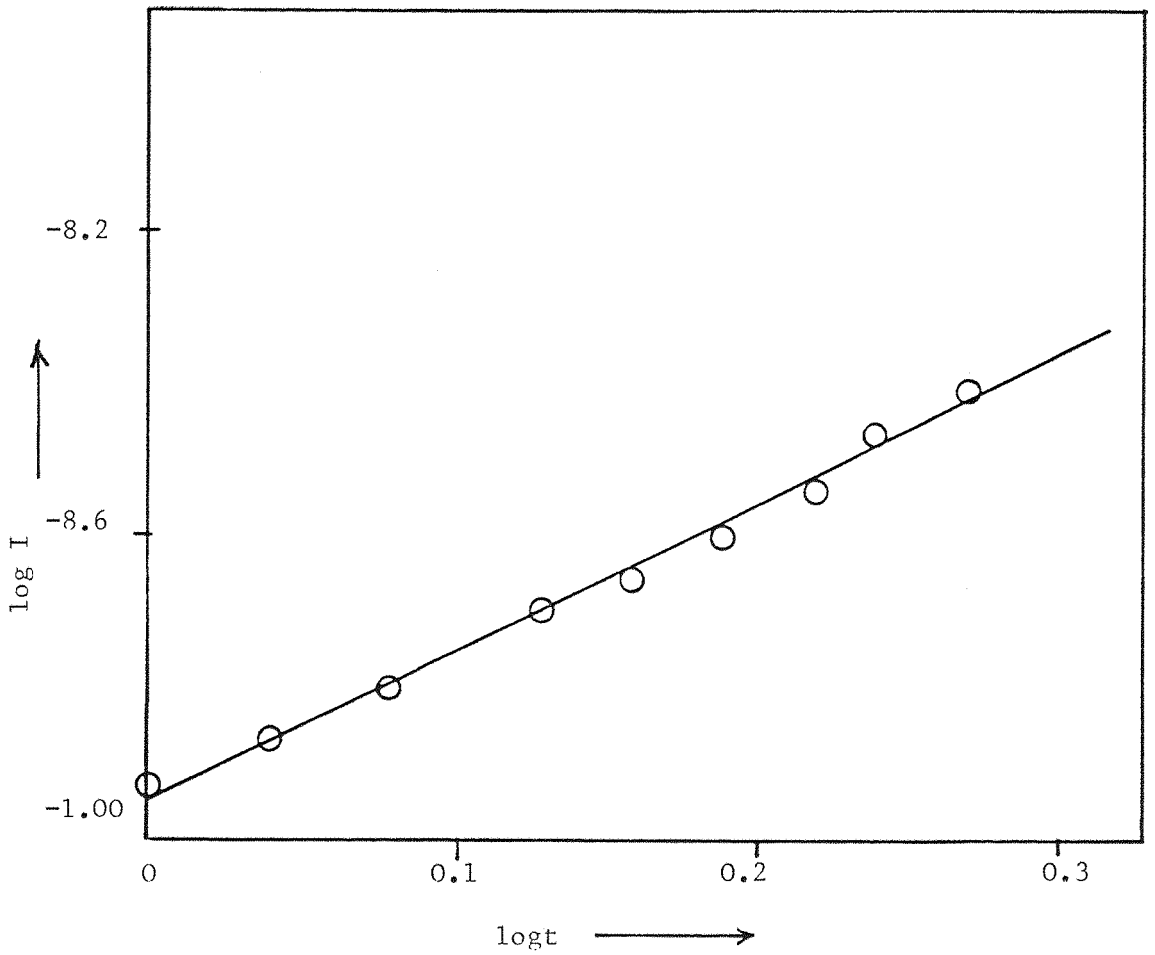

Figure 3.28 log i vs log t plot for the early part of the potentiostatic current transient (E=-240mV) for deposition of palladium, figure 3.25.

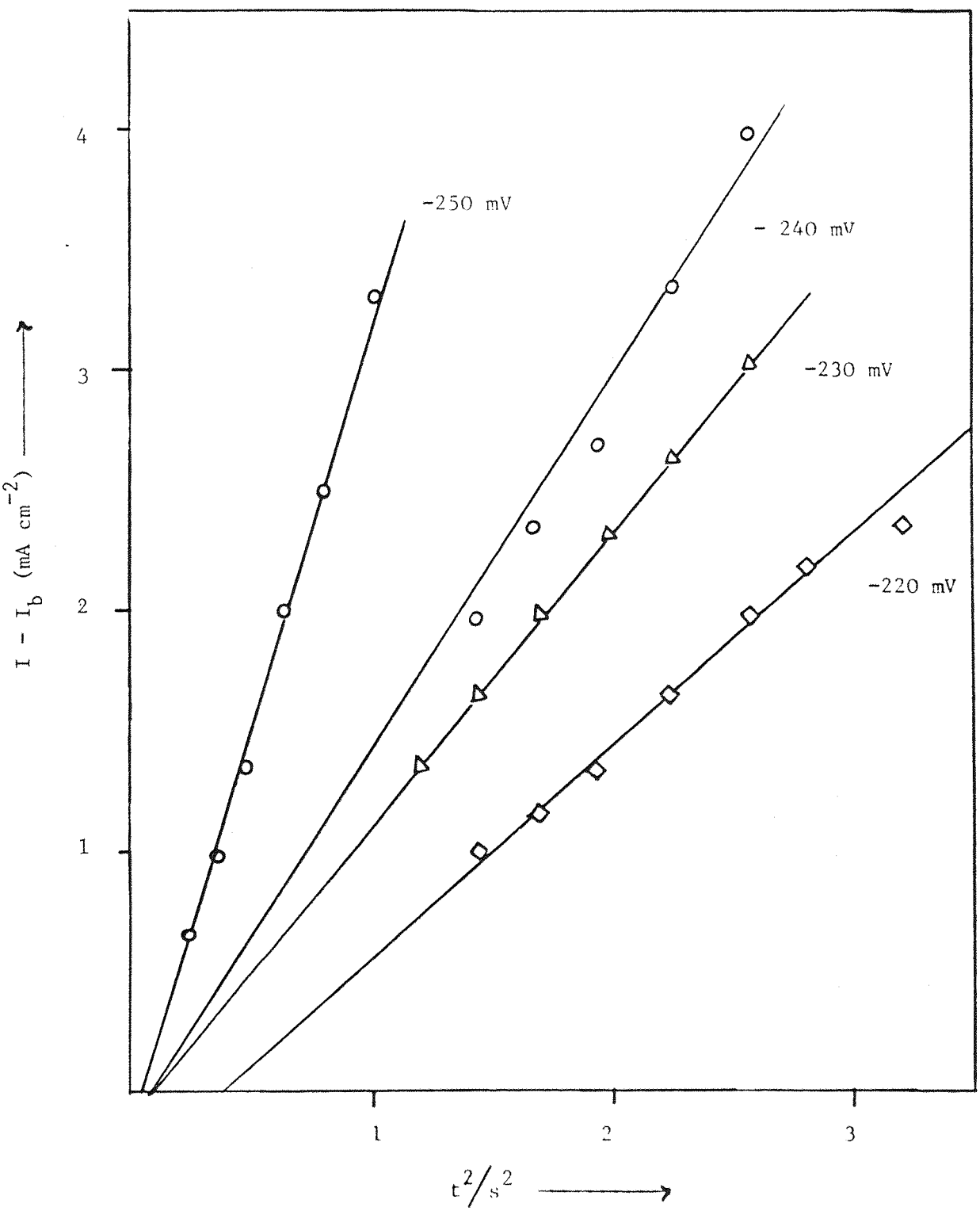

Figure 3.29 I vs t^2 plots for the early rising part of the transients from figure 3.27. I_b is the current flowing immediately before the rise

50 mmol dm^{-3} $PdCl_2$ + 1 mol dm^{-3} KCl				10 mmol $PdCl_2$ + 1 mol dm^{-3} KCl			
-E /mV	$10dI/dt^2$ mA $cm^{-2}s^{-2}$	10^3 kN_o mol $cm^{-2}s^{-1}$	$\log N_o k$	-E mV	$10^3 dI/dt^2$ mA $cm^{-2}s^{-2}$	$10^4 kN_o$ mol $cm^{-2}s^{-1}$	log kN_o
188	4.75	1.80	-2.74	150	0.57	4.15	-3.37
193	5.42	1.88	-2.72	155	1.05	5.11	-3.29
203	5.89	1.93	-2.71	175	1.4	5.62	-3.25
				185	1.8	6.14	-3.21
				195	2.5	6.81	-3.16

Table 3.5 Calculated potential dependent rate constants for a range of potentials. Solutions are 10 mmol dm^{-3} $PdCl_2$ and 50 mmol dm^{-3} $PdCl_2$ in 1 mol dm^{-3} KCl.

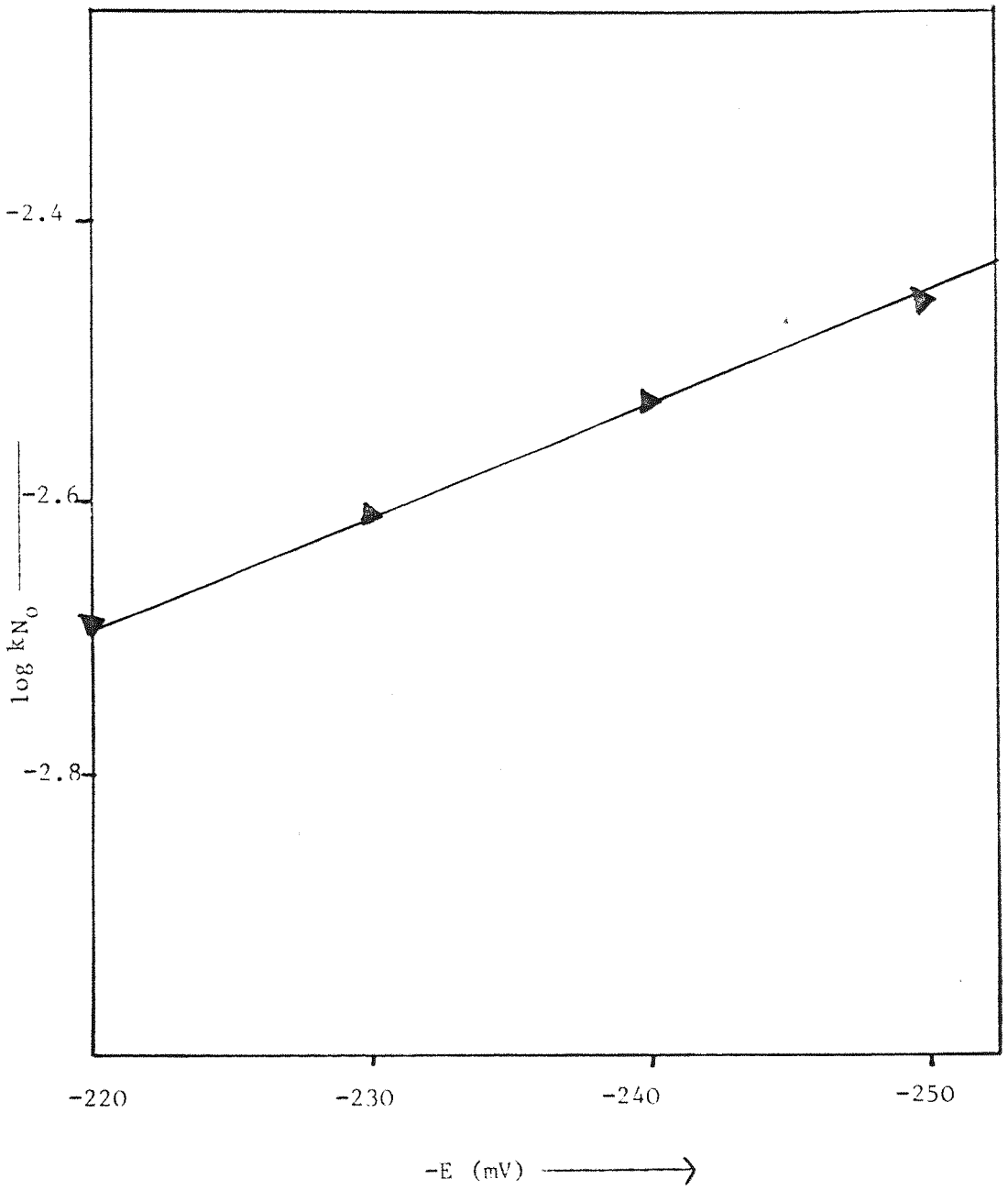

Figure 3.30 logkN$_o$ vs -E(mV) for the transients in figure 3.27.

The current time transients for 50 mmol dm^{-3} and 10 mmol dm^{-3} palladium were also recorded and analysed using same method to calculate the values of rate constants from I vs t^2 plots. The results obtained showed reasonable agreement with those reported in table 3.3. and 3.5. The values of rate constants corresponding to various potentials are summarized in table 3.5 .

The potentiostatic pulse method was also applied to a platinum microelectrode (area 7.85 x 10^{-7} cm^2) using a platinum spiral reference electrode, in a solution of 50 mmol dm^{-3} palladium chloride in 1 mol dm^{-3} potassium chloride at pH 3.5. A set of current time transients for a range of potential (-100 to -130mV) is shown in figure 3.31. The shape and behaviour of the transients is similar to those obtained at a carbon fiber electrode and well defined rising transients can be seen with a high current density. The current again goes to a plateau relecting the high rate of mass transport.

PART TWO - ELECTRODEPOSITION OF INDIUM

3.5 LINEAR SWEEP VOLTAMMETRY

3.5.1 EFFECT OF CONCENTRATION

The results were obtained for the solutions of 10-50 mmol dm^{-3} concentrations of indium chloride at pH=4.3, at a potential sweep rate of 50 mV s^{-1}. The supporting electrolyte was 1 mol dm^{-3} potassium chloride. The data obtained from cyclic voltammograms is summarised in table 3.6 while the I-E curves for two extreme cases are shown in figure 3.32-a and 3.32-b.

At low concentration (10 mmol dm^{-3}) a sharp cathodic peak is observed at -840mV vs S.C.E. A cathodic current crossover range is again observed i.e. between -430 and -510 mV on the reverse sweep,but is smaller than in case of palladium. The potential difference between where deposition stops and dissolution commences is small and hence the reaction is quite reversible. The cathodic reaction must be

$$In^{3+} + 3e \longrightarrow In \qquad (3.1$$

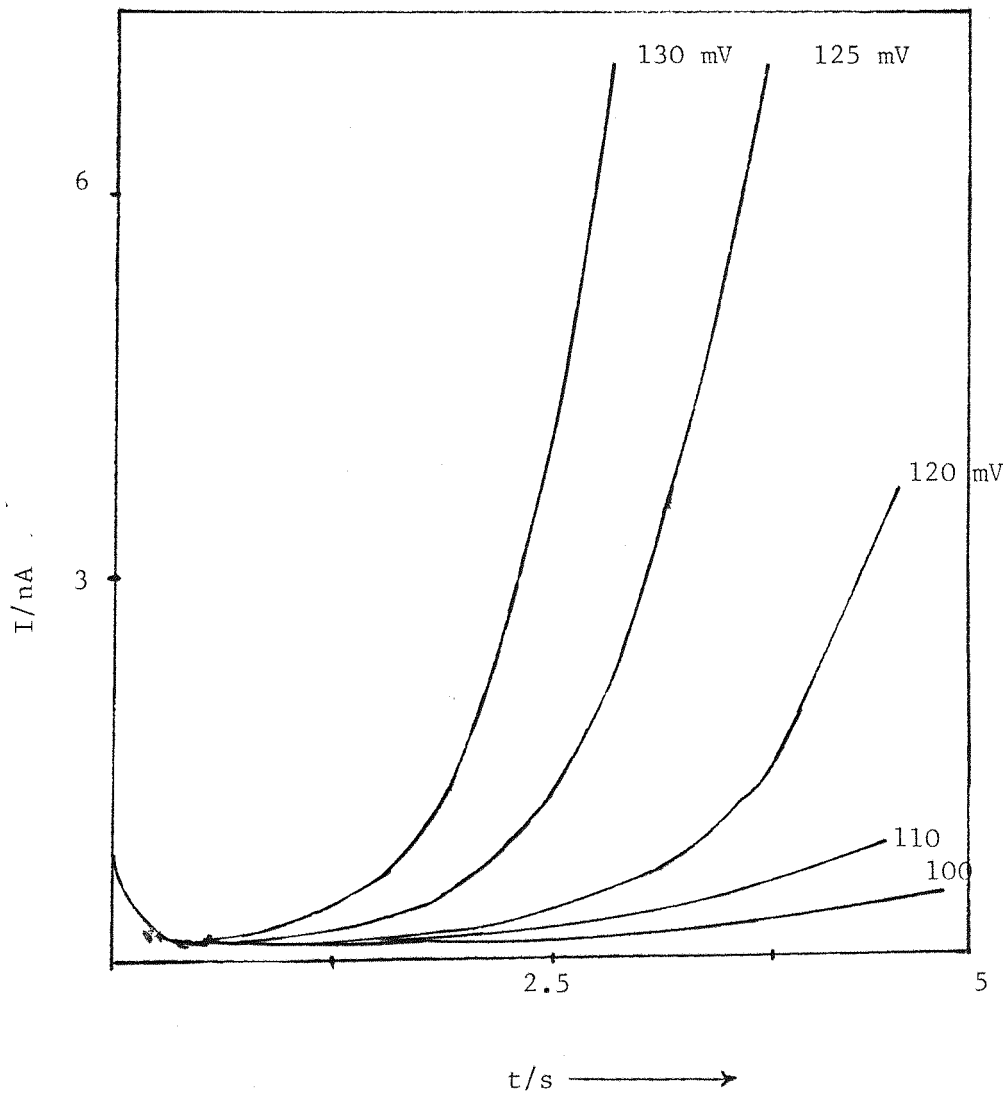

Figure 3.31 Potentiostatic current transients for the deposition of palladium on a platinum microelectrode ($A=7.85 \times 10^{-7}$ cm^2). Solution is 50 mmol dm^{-3} $PdCl_2$ in 1 mol dm^{-3} KCl.

Conc mmole dm^{-3}	I_{Pc} mA cm^{-2}	E_{Pc} mV	I_{Pa_1} mA cm^{-2}	I_{Pa_2} mA cm^{-2}	E_{Pa_1} mV	E_{Pa_2} mV	Width of anodic peak at half peak height $(\Delta E_{\frac{1}{2}})_A$ mV	Q_C mC cm^{-2}	Q_A mc Cm^{-2}	Q_A/Q_C
10	6.0	-840	2.0	1.5	-700	-650	25	23.1	4.71	0.2
20	11.6	-810	10.5	-	-680	-	30	52.4	10.3	0.2
30	15.5	-810	20.1	-	-640	-	50	76.1	25.7	0.3
50	27.4	-810	50.3	-	-630	-	70	128.5	85.3	0.6

TABLE 3.6 Table of the parameters obtained from cyclic voltammograms as a function of indium concentration.

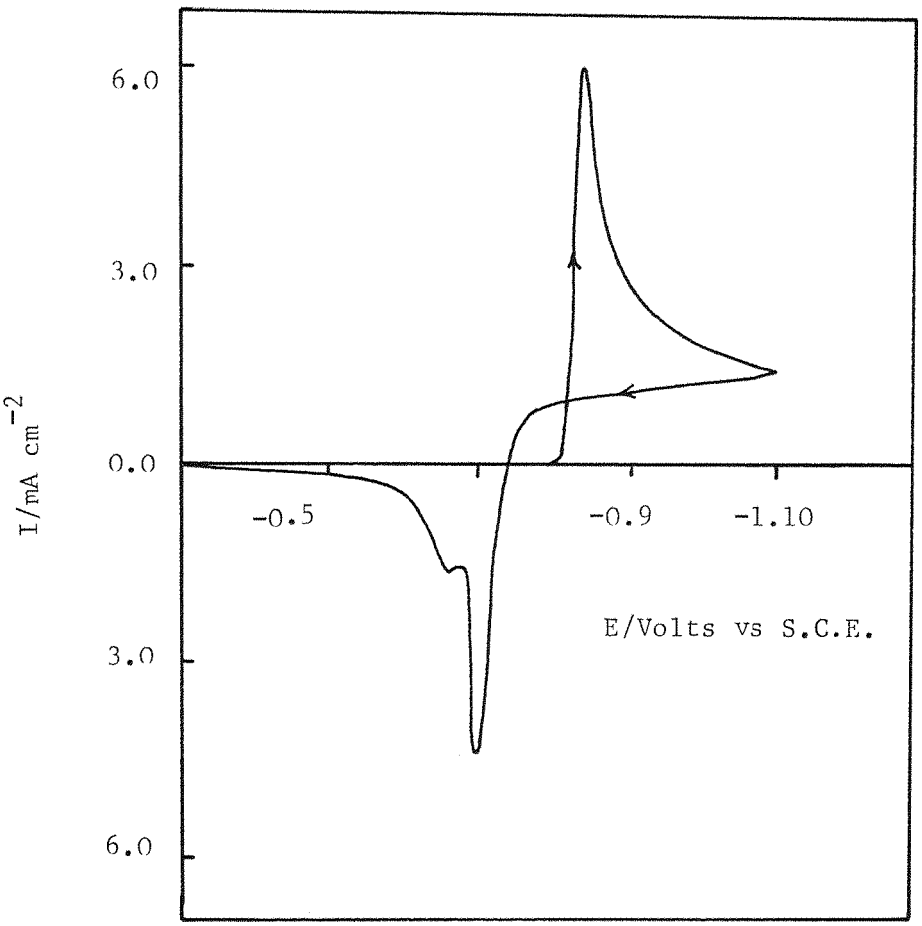

Figure 3.32(a) Cyclic voltammogram for the reduction of In(III) onto vitreous carbon electrode (Area = 0.07 cm^2) from a solution of 10 mmol dm^{-3} $InCl_3$ in 1 mol dm^{-3} KCl at pH 4.3, at potential sweep rate = 50mVs^{-1}.

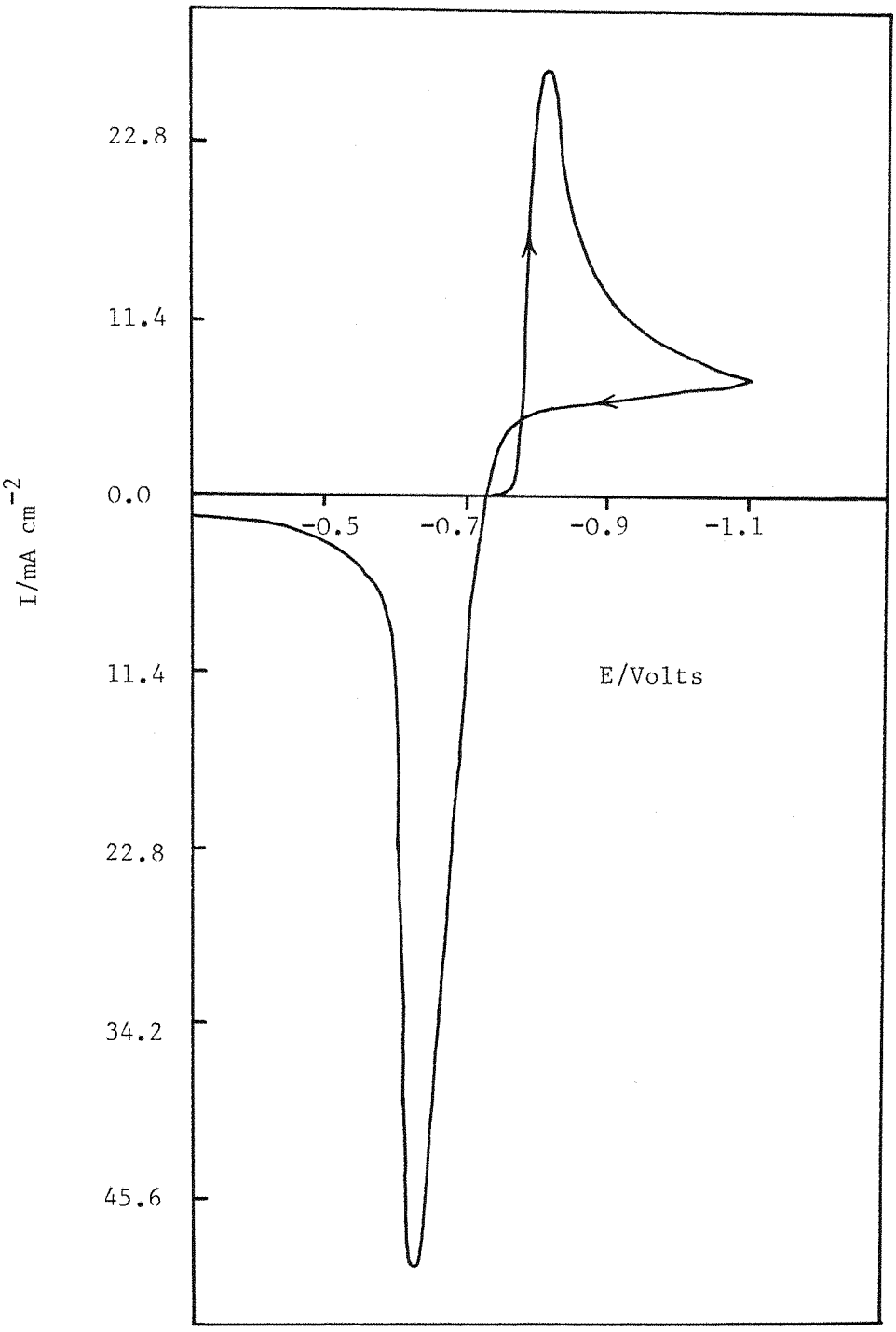

Figure 3.32(b) Cyclic voltammogram for the reduction of indium(III) from 50 mmol dm^{-3} $InCl_3$ + 1 mol dm^{-3} KCl at pH 4.3, at potential sweep rate = 50 mVs^{-1}.

At low concentration (10 mmol dm^{-3} $InCl_3$) the anodic dissolution leads to two peaks, the first is at -700 mV and second anodic peak was at -650 mV vs SCE.

At high concentration (20-50 mmol dm^{-3}) the anodic dissolution gives only one peak which seemed to shift towards more negative potential with the increase in concentration which is -700 mV, -680 mV, - 670 mV and -630 mV, for 10, 20, 30 and 50 mmol dm^{-3} indium chloride solution in aqueous 1 mol dm^{-3} potassium chloride. However, there was no second anodic peak observed at these higher concentrations which leads us to the conclusion that there must be some complex formation of indium or step wise dissolution at low concentration. The peak currents for these split peaks was found to be slightly different, (Ip_{A_1} = 2mA cm^{-2}, Ip_{A_2} 2 1.5 mA cm^{-2}). The results obtained from varying concentrations are summarized in table 3.7.

The cathodic and anodic charges were also calculated by using, simultaneously, an integrator and it was found that anodic dissolution of indium was more efficient at high concentration of In(III) but was not 100%. The maximum charge ratio (0.66) was for 50 mmol dm^{-3} indium concentration. At low concentration it was only 0.2.

Linear potential sweep voltammetry was also carried out for 10 mmol dm^{-3} indium chloride in 1 mol dm^{-3} potassium chloride (pH≈4) with increasing sweep rate. The cathodic peak current and peak potential was sweep rate dependent as expected. Only the cathodic part of the voltammograms were recorded and are shown in figure 3.33. The cathodic peak current could be plotted against square root of sweep rate, to give a straight line (see figure 3.34a), from the slope of the line the value of diffusion coefficient was calculated, D = 6.3 x 10^{-6} $cm^2 s^{-1}$. Furthermore the cathodic peak current is proportional to the concentration of indium (3.34-b).

3.5.2 EFFECT OF pH

Experiments were also carried out for different solutions of various pH (pH2-4.2) for 50 mmol dm^{-3} indium chloride. To attain the different pH, a few drops of HCl were added to the supporting electrolyte before adding the indium salt, so that it should not effect the concentration. The results obtained are summarised in table 3.7 and the cyclic voltammograms

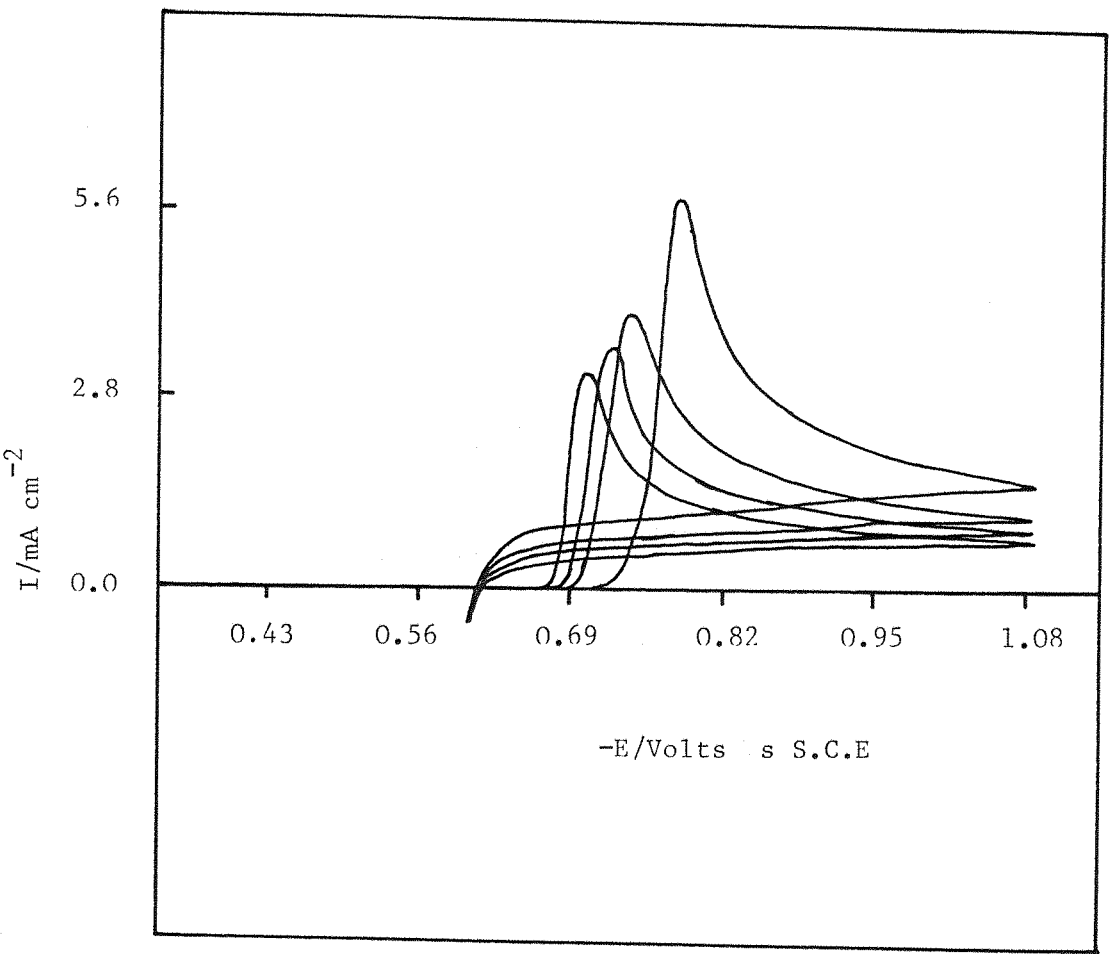

Figure 3.33 Cyclic voltammogram for indium(III) reduction for a solution of 10mmol dm^{-3} $InCl_3$ + 1 mol dm^{-3} KCl, pH = 4.3 at various potential sweep rates

(a) 10 mVs^{-1}
(b) 15 mVs^{-1}
(c) 25 mVs^{-1}
(d) 50 mVs^{-1}

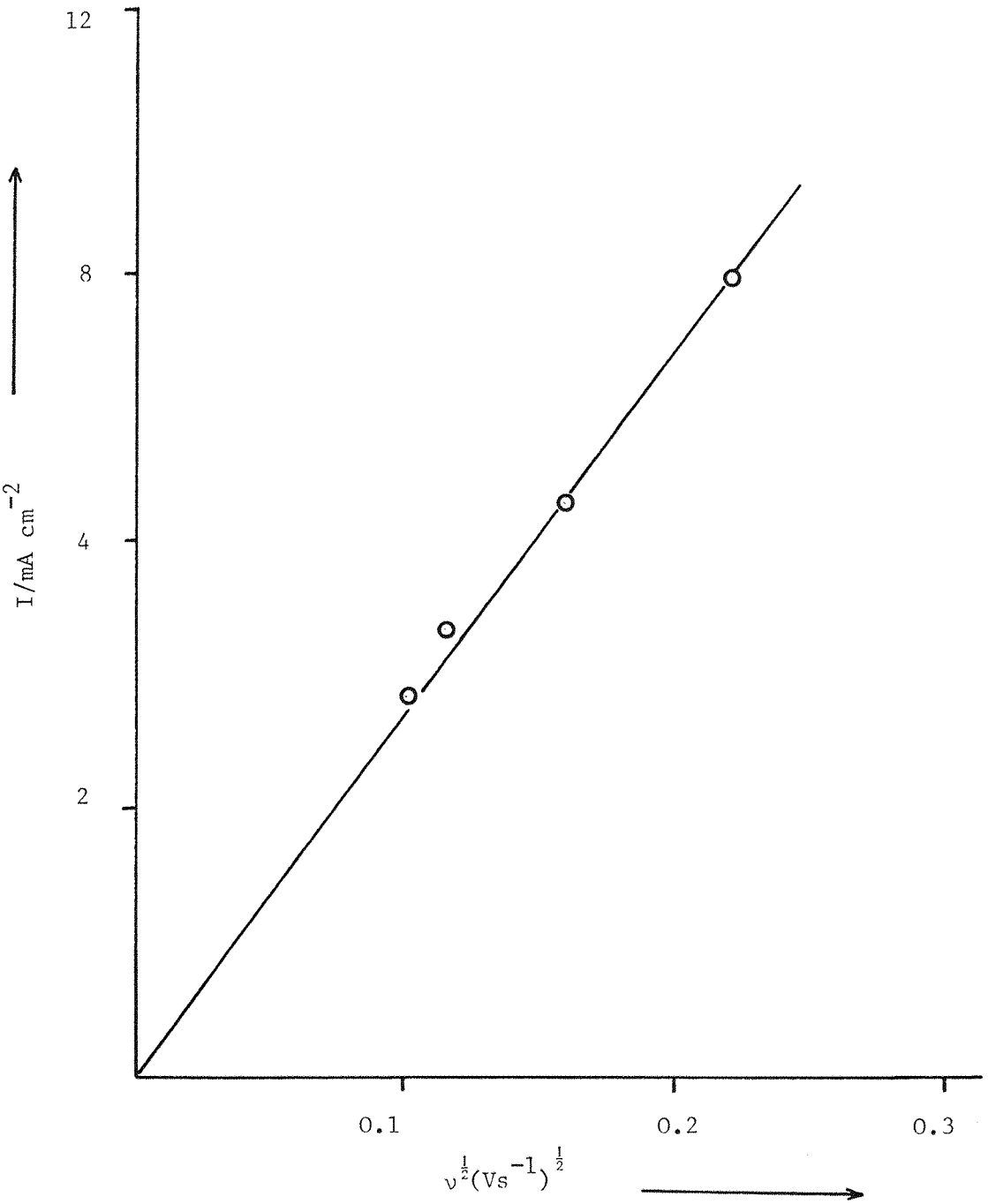

Figure 3.34(a) Cathodic peak current density versus square root of potential sweep rate plot, from figure 3.3.

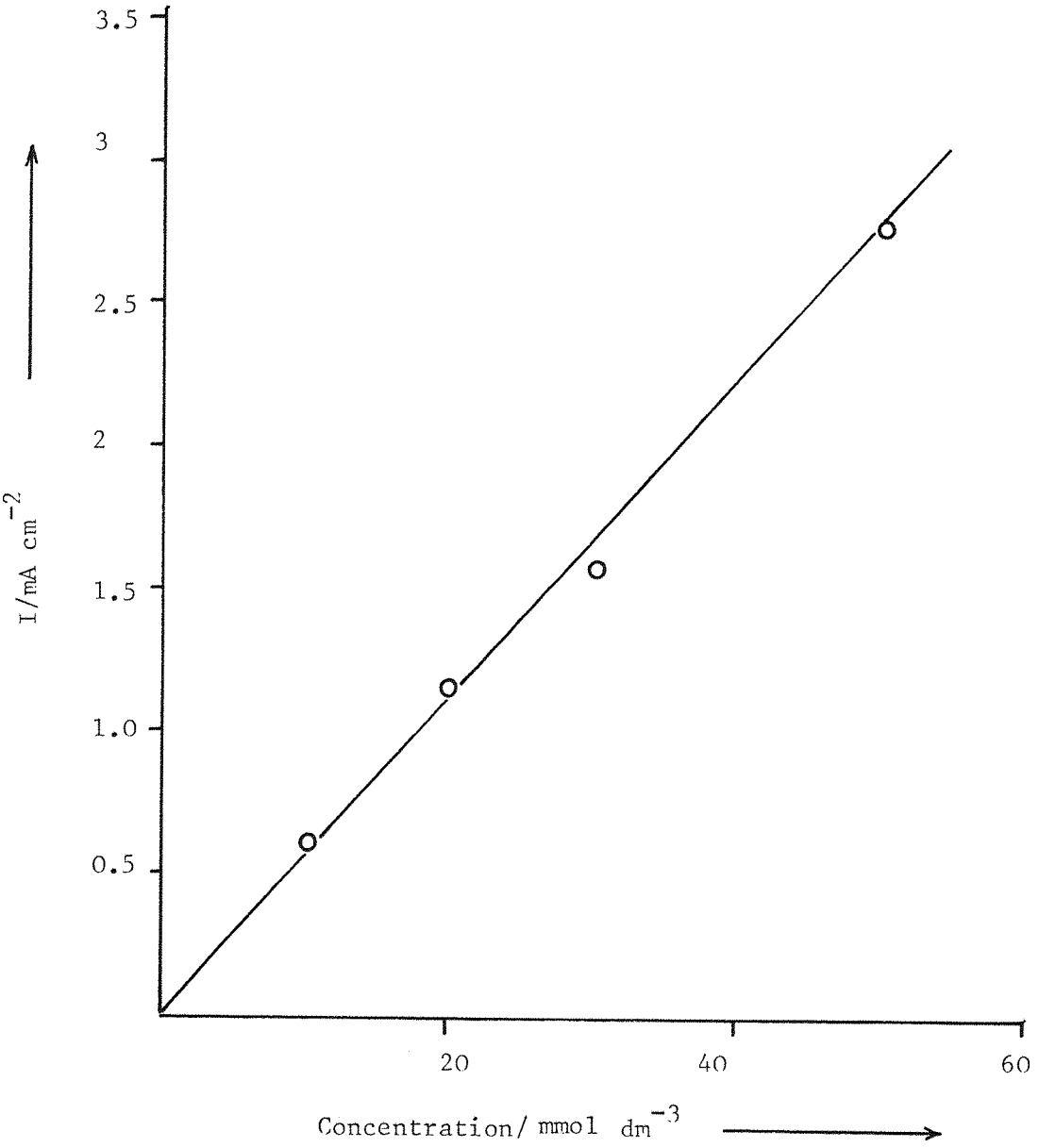

Figure 3.34(b) A plot of cathodic peak current versus concentration of indium

pH	I_{Pc} mA cm^{-2}	E_{Pc} mV	I_{Pa} mA cm^{-2}	E_{Pa} mV	Width of E_{Pa} at half height $(\Delta E_{\frac{1}{2}})_A$ mV	Q_C mC cm^{-2}	Q_A mC cm^{-2}	Q_A/Q_C
2	24.3	-826	80	-593	90	116	112	0.96
2.5	24.3	-826	74.3	-593	90	124	111	0.90
3.0	25.7	-826	80	-593	80	124	112	0.90
3.7	26.2	-816	42.8	-634	60	125	85	0.68
4.2	27.4	-810	50.3	-630	70	128	85	0.66

TABLE 3.7 Table of the parameters obtained from cyclic voltammograms as a function of pH

for two extreme cases are shown in figures 3.35-a and b. For all the pH, a single anodic peak was observed which shifts towards more negative potential at high pH. The other significant change with pH was the charge ratio Q_a/Q_c which is at its maximum value 0.96 at pH≈2 but decreases to 0.66 for pH 4.2. It is clear that the dissolution of indium is more quantitative in acidic media.

3.6 POTENTIOSTATIC PULSE EXPERMENT

Figure 3.36 shows a family of current transients for single potentiostatic pulses for the electrodeposition of indium onto a carbon electrode form a solution of 50 mmol dm^{-3} indium chloride in 1 mol dm^{-3} potassium chloride. The range of potentials applied was -700 mV to -770 mV. The curves were very similar to those for palladium described earlier. At very short time a double layer charging spike can be seen. Then the current start increasing, and for short time the process of nucleation was kinetically controlled. Therefore the current density can be replotted versus the square of time. Plots were obtained for corresponding increasing potentials, which can be seen in figure 3.37. From the slopes of the lines,the values of rate constants were calculated and are given in table 3.8. The rate constants were found to be potential dependent as shown in the table. A plot of logkNo vs E is a straight line, with a slope value of 145 mV, figure 3.38.

The later portion of the rising transients obeys the $I/t^{\frac{1}{2}}$ growth law, the plot of which is shown in figure 3.39. I vs $t^{\frac{1}{2}}$ rectilinear relationship are indicative of three dimensional growth under diffusion control, and from the corresponding slopes of the lines, the number densities were calculated using equation (1.26), are given in table 3.10.

Some of the transients in figure 3.36, especially those corresponding to high overpotential, show a well pronounced maxima. This could be because of the overlapping of the individual hemispherical zones giving rise to a planar diffusion layer. A linear I vs $t^{\frac{1}{2}}$ dependence of these parts of the transients further justifies this explanation. Therefore from the falling past of the transients diffusion coefficient can be evaluated. The value of $D = 1.10 \times 10^{-5}$ cm^{-2} s^{-1} was calculated using equation (1.1).

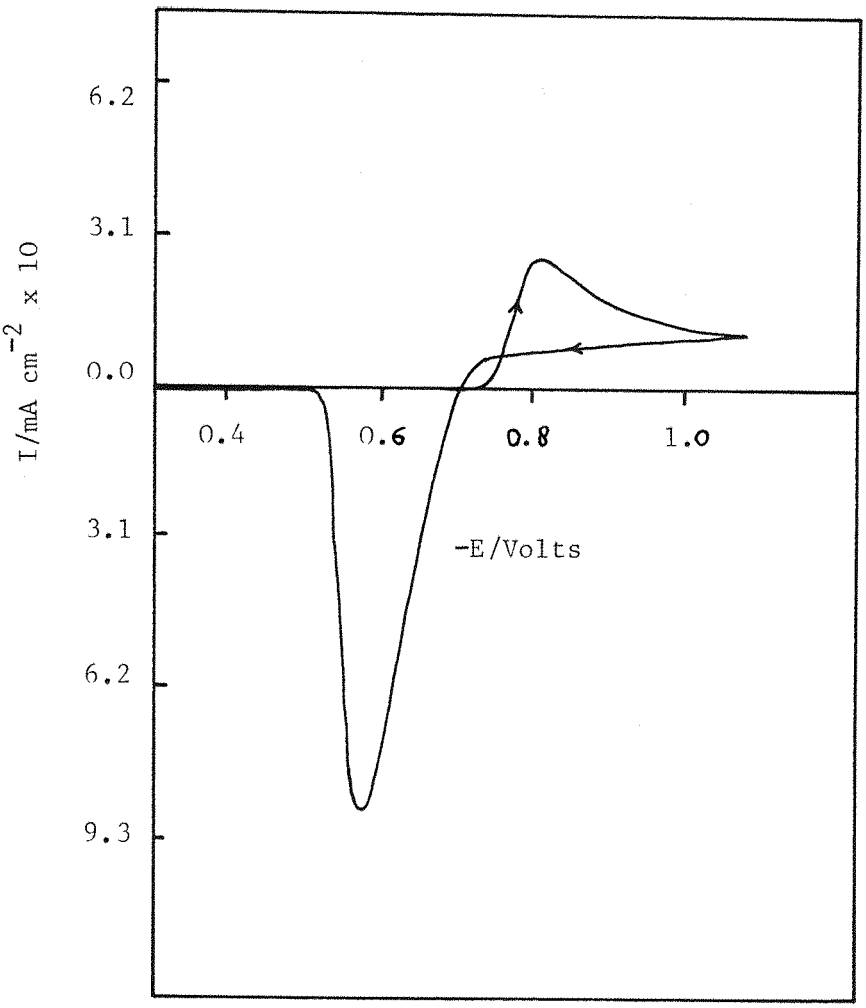

Figure 3.35(a) Cyclic voltammograms for the reduction of In(III) from 50 mmol dm^{-3} $InCl_3$+1 mol dm^{-3} KCl, at potential sweep rate 50 mVs^{-1} (a) at pH ≃ 2

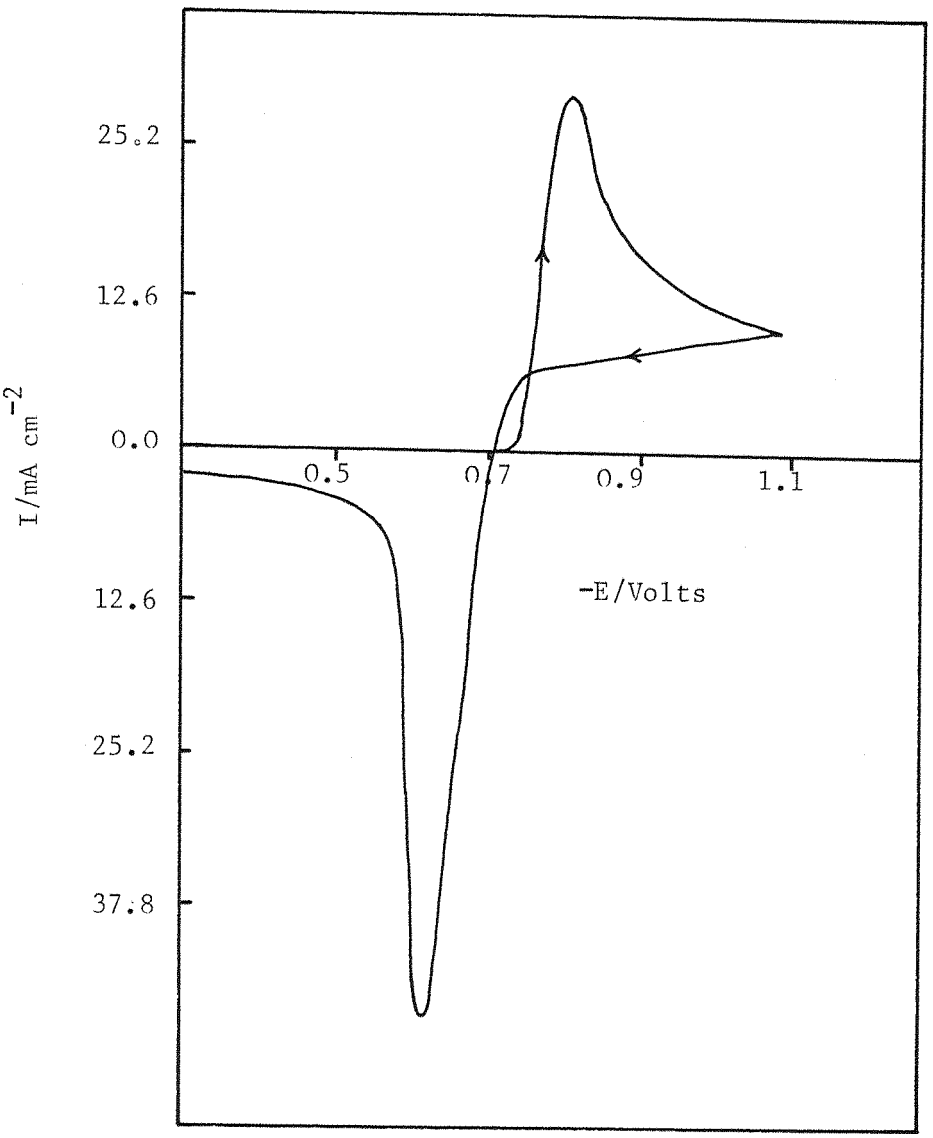

Figure 3.35(b) As Figure 3.35(a)
(b) at pH ≃ 3.7

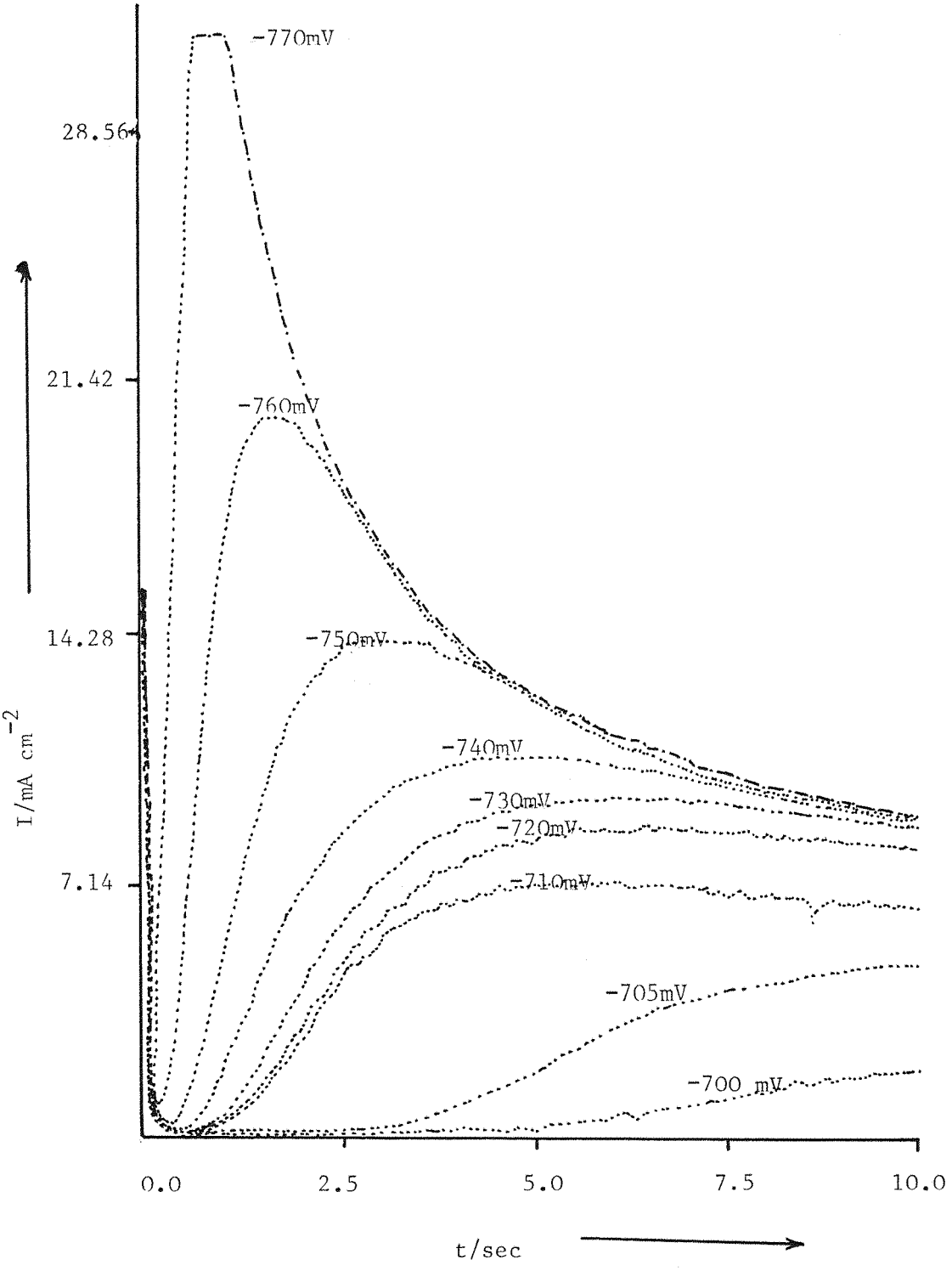

Figure 3.36 Potentiostatic current transients for the deposition of indium at various potential from a solution of 50 mmol dm^{-3} $InCl_3$ in 1 mol dm^{-3} KCl

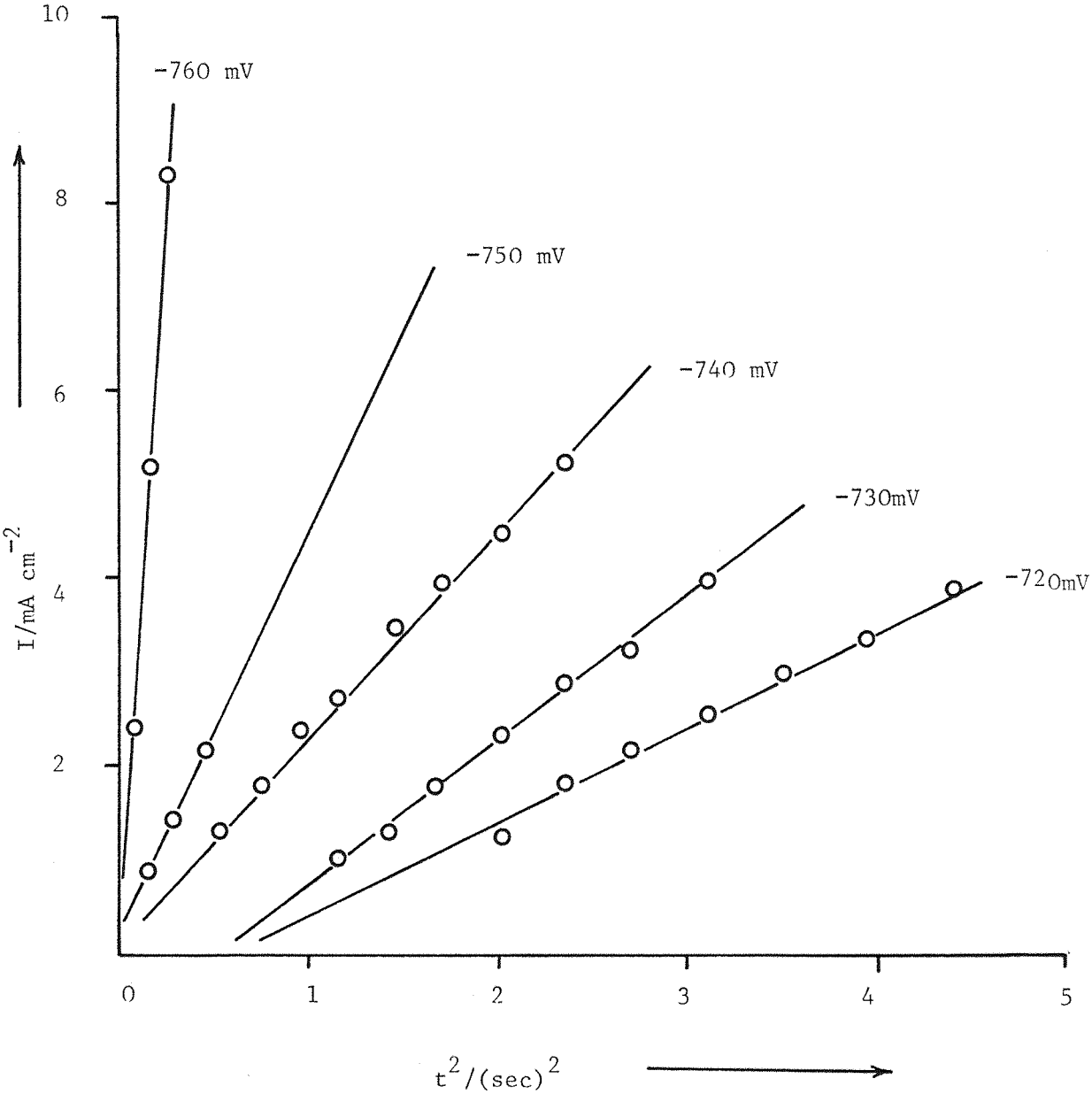

Figure 3.37 I Vs t^2 plots for the early parts of the current time transients in figure 3.36

E (mV)	dI/dt^2 $mAcm^{-2}sec^{-2}$	10^4 N_ok $mol\ cm^{-2}\ s^{-1}$	$logkN_o$
750	4.09×10^{-3}	2.35	-3.62
740	2.22×10^{-3}	1.92	-3.71
730	1.57×10^{-3}	1.72	-3.76
720	1.0×10^{-3}	1.48	-3.82

TABLE 3.8 $logkN_o$ as a function of potential applied.

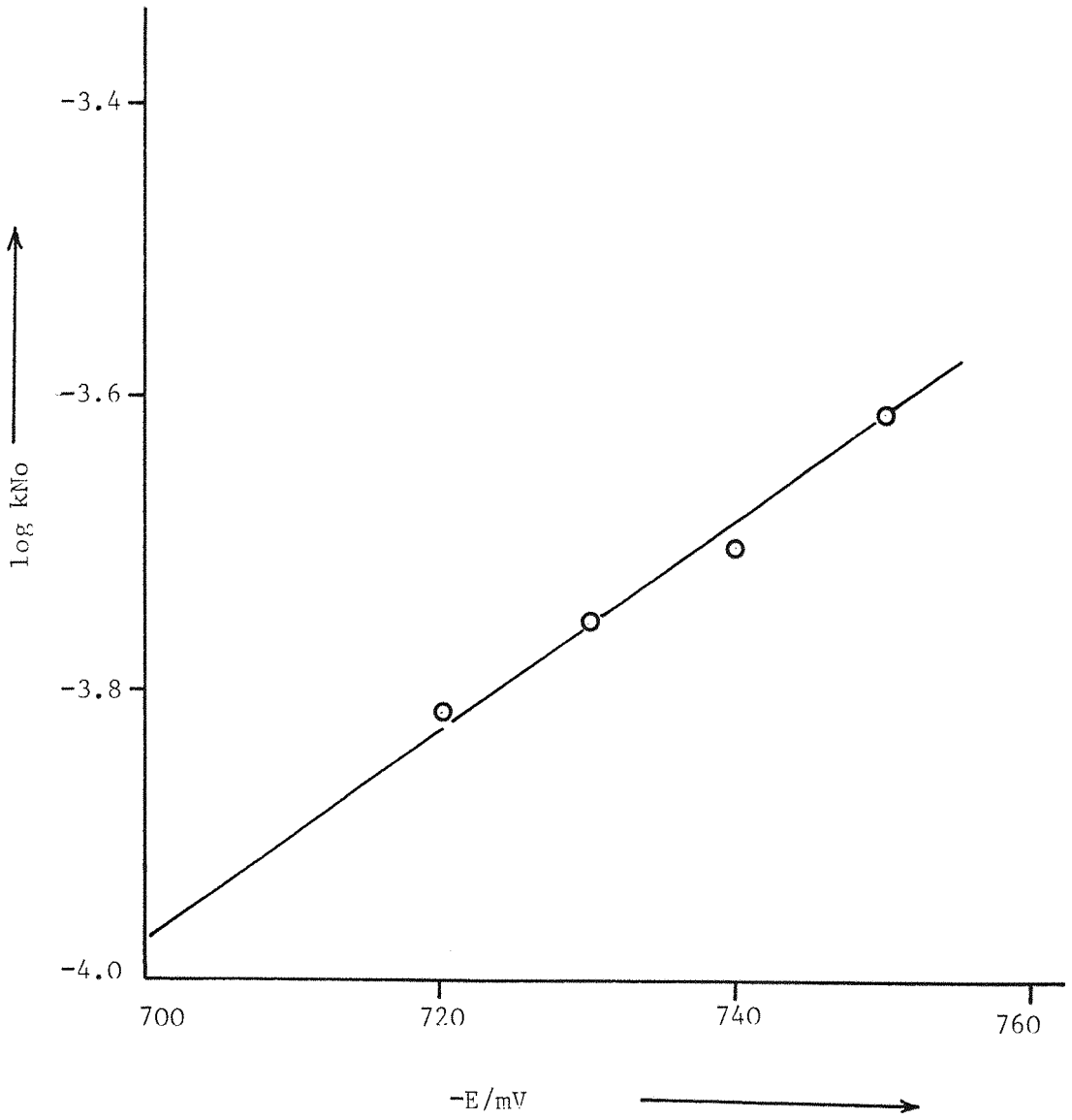

Figure 3.38 $\log kN_o$ versus E plot. The values are calculated from the slopes of the lines in figure 3.37

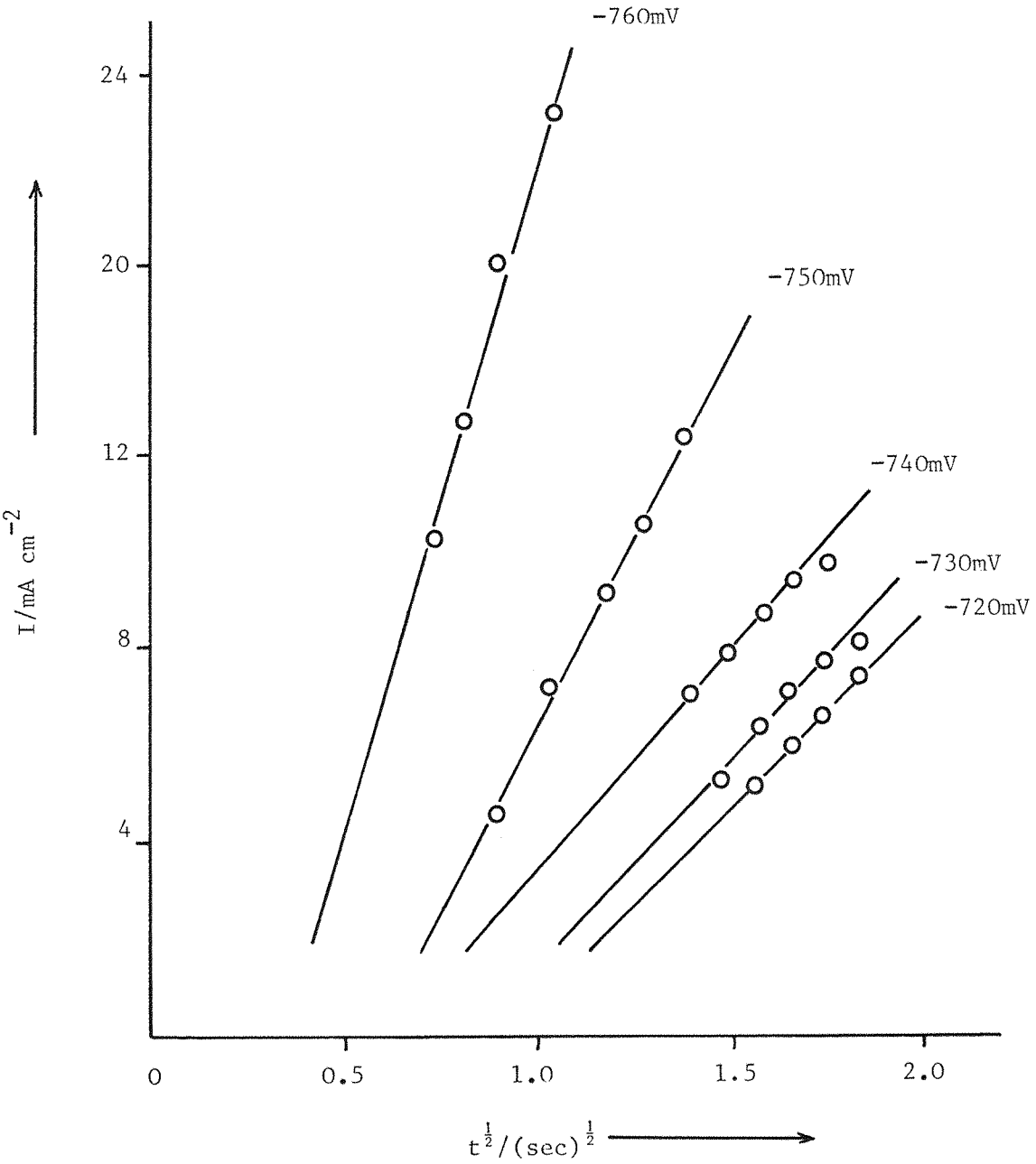

FIGURE 3.39 I versus $t^{\frac{1}{2}}$ plot from Figure 3.36

-E (mV)	$dI/dt^{\frac{1}{2}}$ mA cm^{-2} $s^{-\frac{1}{2}}$	$10^{-5}N_o$
720	10.19×10^{-3}	1.86
730	10.58×10^{-3}	1.93
740	11.72×10^{-3}	2.14
750	2.05×10^{-2}	3.76
760	3.73×10^{-2}	6.82

TABLE 3.9 Nuclear number densities as a function of potential applied calculated from the slopes of the lines in Figure 3.39.

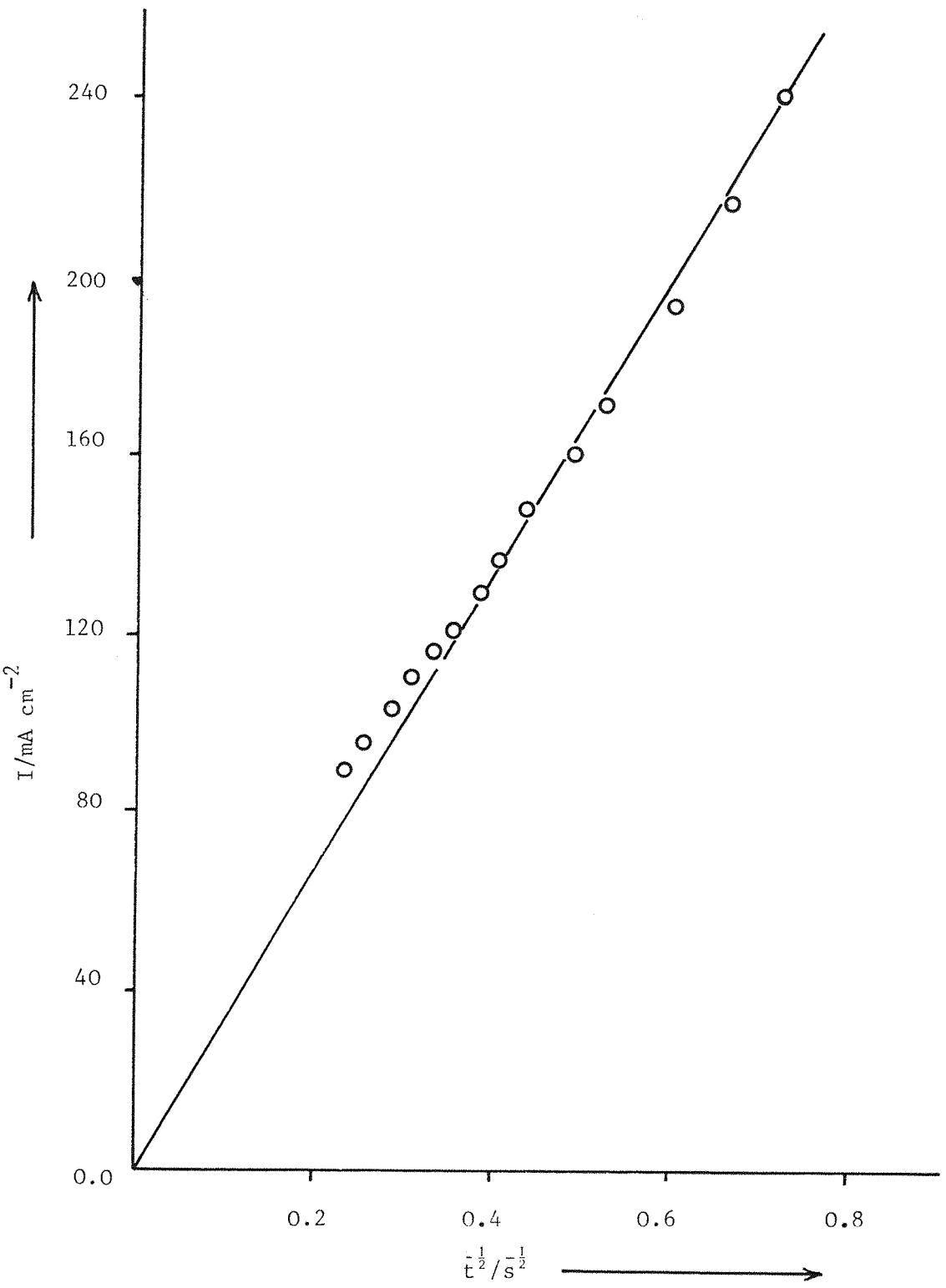

FIGURE 3.40 I versus $t^{-\frac{1}{2}}$ plot for the transient at -770 mV from Figure 3.36

3.7 NUCLEATION AND GROWTH OF INDIUM ON MICROELECTRODE

3.7.1 LINEAR SWEEP VOLTAMMETRY

Figure 3.41 shows a cyclic voltammogram for 50 mmol dm^{-3} indium chloride in 1 mol dm^{-3} potassium chloride at pH 3.7. The microelectrode used was again a carbon fiber (area 5 x 10^{-7} cm^2) and the potential sweep rate was 10 mVs^{-1}. As mentioned earlier for the reduction of palladium, the voltammogram does not show the typical features of nucleation and growth phenomena observed onto a large vitreous carbon electrode. In the case of the microelectrode the rate of diffusion is very high (as the electrode area is small) and therefore the growth is purely kinetic controlled. The cathodic and anodic current were also found to be time dependent (through sweep rate)aswell as the potential sweep dependent. Hence high current densities were observed in all the experiments carried out on microelectrodes.

It was noticed that the potential limits applied to the system are similar to those on amacroelectrode and the deposition and dissolution potentials were comparable too. The cathodic current rises abruptly at -978 mV and the reverse potential was found to be -965 mV. The cathodic and anodic charges were also determined by using an integrator. The ratio Q_{a/Q_c} was calcaulated and was 0.72 which is comparable to that calculated for large electrode which was 0.68.

3.7.2 POTENTIOSTATIC METHOD APPLIED TO MICROELECTRODE

A set of potentiostatic current transients for the nucleation and growth of indium from 50 mmol dm^{-3} indium chloride at pH ≃ 2 are shown in figure 3.42. The supporting electrolyte was 1 mol dm^{-3} potassium chloride. The shape of the transients did not show any resemblence either with the one shown in figure 3.25 nor to that figure 3.26, (for the growth of single nuclei and for two nuclei). Therefore it is evident that in this case also the number of nuclei formed on the electrode surface are more than one or two and the I-t transients show a shape very similar to those obtained for a macroelectrode system. Moreover the nuclear number densites calculated for both indium and palladium from the I-E response obtained on large electrode were of same order of magnitude. Later on it was proved from the observ-

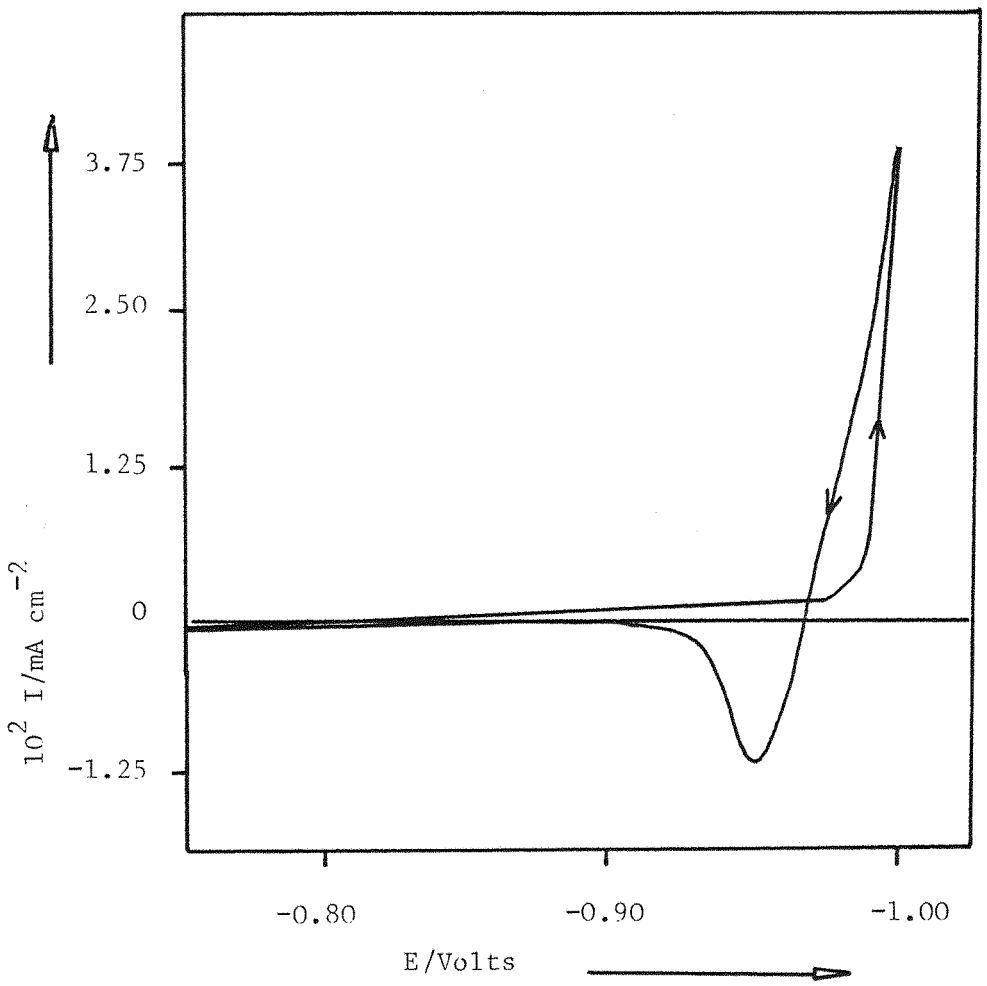

Figure 3.41 Cyclic voltammogram for the reduction of indium(III) at a carbon fiber microelectrode (Area = 5 x 10^{-7} cm^2). Solution is 50 mmol dm^{-3} $InCl_3$ in 1 mol dm^{-3} KCl, pH ≈ 3.7. Potential sweep rate = 10 mVs^{-1}

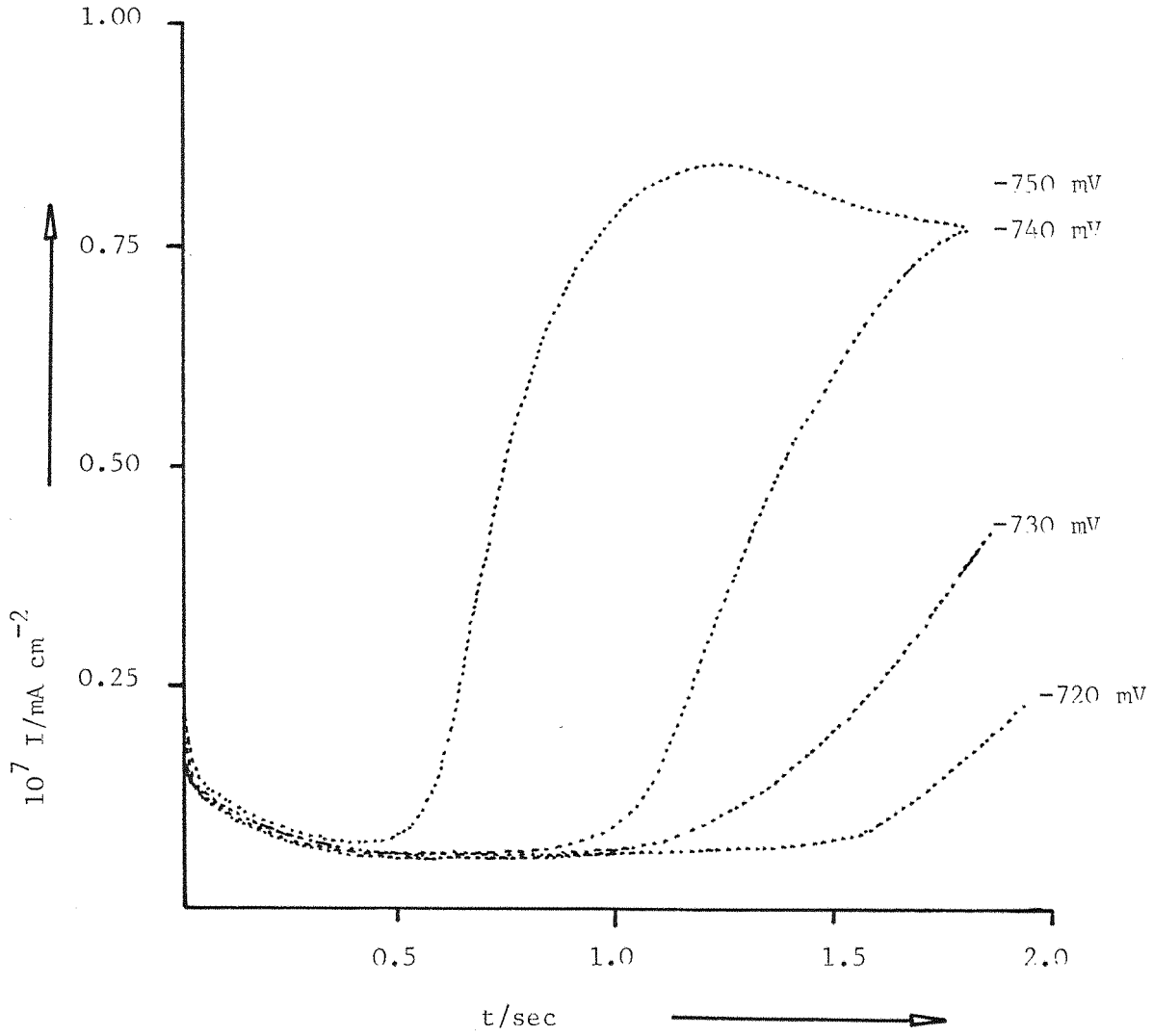

Figure 3.42 Potentiostatic current transients for the deposition of indium on to a carbon fiber microelectrode from a 50 mmol dm^{-3} $InCl_3$ solution in 1 mol dm^{-3} KCl, pH ≃ 2.

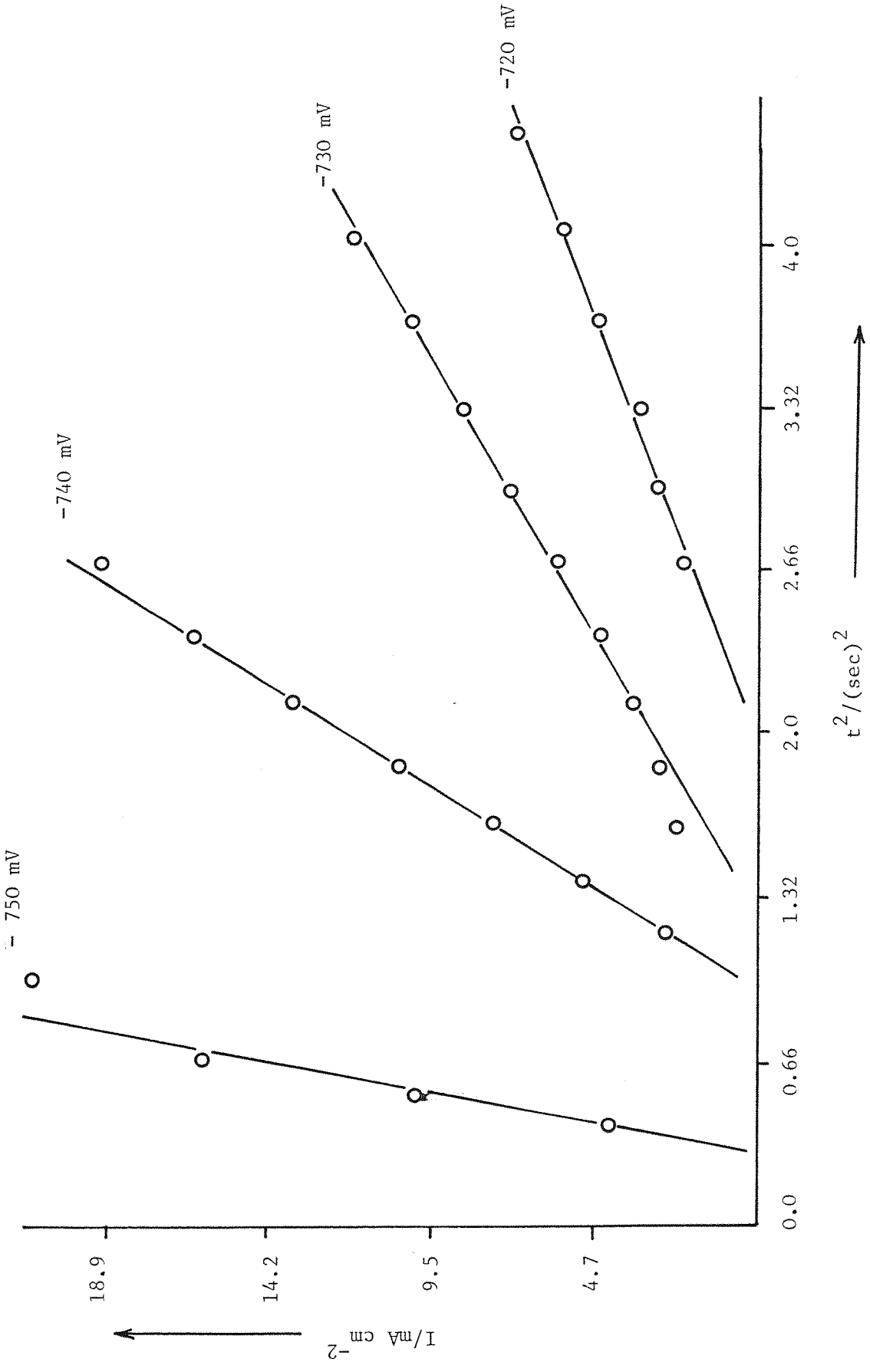

Figure 3.43 I vs t^2 plots for the early part of the rising transients in figure 3.42

ations and calculations from electron scanning microscopy that the number of nuclei are ∿ 10. Therefore it is possible that the number density could be same for indium system, and the instantaneous nucleation followed by the three dimensional growth should be considered. A similar treatment of the data was used to that for palladium. The i vs $(t-\tau)^2$ plot gives a straight line figure 3.43, from the slope of the lines the values of $N_o k$ have been calculated using equation 1.21. The potential dependent rate constants are given in table 3.10. Moreover the plot of log $k N_o$ vs E (figures 3.44) produced a straight line. The slope is, however, 72 mV.

3.8 DISCUSSION

All the experimental results for the reduction of palladium (II) and indium(III) suggest the presence of an electron transfer process characteristic of the nucleation and growth of a new phase on the electrode surface. The evidence from

(a) The shape of the cyclic voltammogram on a large electrode
(b) I - t transient
(c) Electron scan microscopy
(d) Cyclic voltammetry on microelectrode

all lead to the same conclusion. The shape of both the cathodic and anodic stripping peak and their separation (the peak separation for both processes is greater than 60 mV table 3.7, 3.8), the crossing over of the cathodic current during the reverse sweep and the shift in the foot of the cathodic peak to move negative potential with increasing sweep rate can all be seen on the cyclic voltammograms. Similar results have been reported by Bell and Harrison(49) while studying the reduction of palladium(II) in a chloride medium. With a microelectrode the rate of mass transfer is much higher and instead of a current "crossover", a large current loop is seen as the current increases with deposition time. The cyclic voltammograms for both micro and macroelectrodes show a marked difference between the indium and palladium systems. The In/In(III) system is quite reversible. On the back sweep the current crosses the I=o axis directly from a deposition current into the dissolution peak. With Pd/Pd(II) there is a potential region, where no current flows between where the deposition process switches off and dissolution starts. Hence the Pd/Pd(II) couple

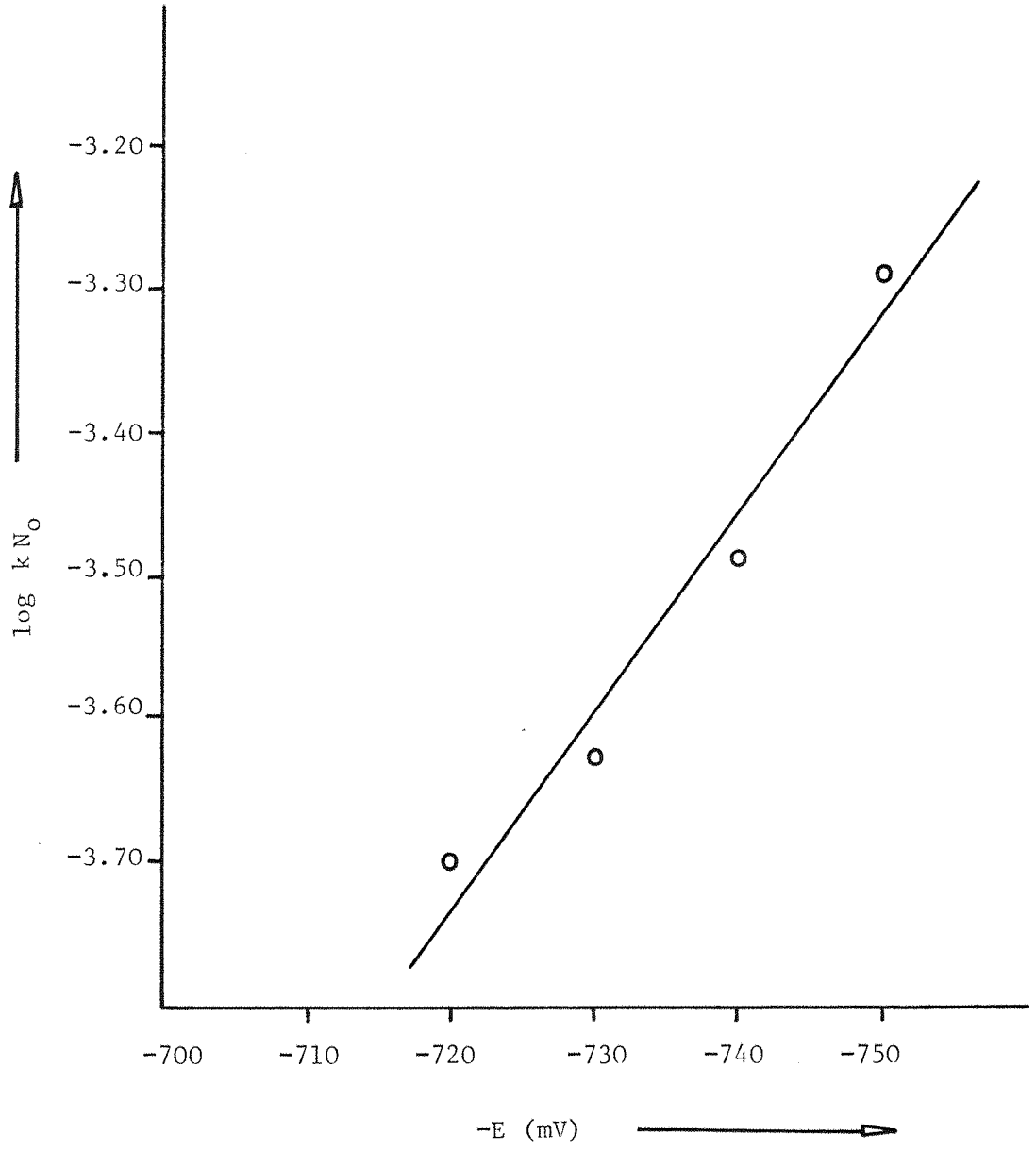

Figure 3.44 log k N_o vs -E plot, (values estimated from figure 3.42)

is irreversible. Of course,however, in both cases,there is a nucleation overpotential which can be seen on the forward sweep. The I - t transients show all the typical features of nucleation and growth, the rise in current with time and the change in the shapes of the transients with overpotential. Finally, of course the scanning electron microscopy allows one to see the nuclei and follow their growth with time.

3.8.1 NUCLEATION AND GROWTH

The principal feature of the transient is the rising current with time corresponding to the formation of nuclei and their subsequent growth. The shape of the transients immediately leads to the conclusion that the process is three dimensional growth, while the fit of the data to I - t^2 plots, i.e. equation 1.21, gives the evidence for instantaneous nucleation followed by three dimensional growth(28). The form of the responses for instantaneous nucleation and two dimensional growth (equation 1.20), as well as for progressive nucleation both with two and three dimensional growth, are explained in section 1.2.4, where the process of nucleation and growth is completely charge transfer controlled and the kinetics of the nucleation can be studied. The I - t response provides information about the potential dependent rate constants for the nucleation and growth as described by Fleischmann etal(28). The rate constants for growth were determined by fitting the slopes of the I - t^2 plots in equation (1.21), see table 3.3, 3.8, for palladium and indium. Moreover the results obtained from the microelectrodes, where the growth phenomena is totally kinetic controlled, agreed well with those obtained from large electrodes. In both cases the order of magnitudes of $N_0 k$ value is 10^{-3}-10^{-4} for palladium and indium respectively.

When the rate of electron transfer is sufficiently high for continuous growth of the nuclei, then the rate controlling step becomes mass transfer. This statement is applicable to the middle rising part of the I - t transients where the current is continuously increasing with the increasing size of the nuclei. The total current density for the growth of N nuclei within a hemispherical diffusive flux under mass transport controlled is given by equation (1.26), for instantaneous nucleation and 3 - D growth. The equation 1.26 fits very well for both systems providing further evidence for instantaneous nucleation and three dimensional growth. Also scanning electron microscopy confirms that all the nuclei formed are of similar size

at a particular time. In contrast, Astley etal(45) and Harrison etal(49) have studied the growth of palladium (onto glassy carbon from 2.72×10^{-2} m$PdCl_2$ in $HClO_4$ + HCl) and concluded that progressive nucleation followed by three dimensional growth occurs ($I - t^3$ plot) at longer time i.e. 2 minutes. Hence at short times (30 sec) the relationship changes to $I - t^2$, the t^2 dependence has been interpreted as a lattice growth at growing three-dimensional centers. They have further investigated the rate of reaction by plotting $(i/t^2)^{1/3}$ against η, which is comparable to one of k against η, and the nuclear number density obtained from scanning electron microscopy was 4×10^4 cm^{-2}. This value of N_o is much lower than the values obtained from results calculated here from scanning electron microscopy and the $I - t^{\frac{1}{2}}$ plots, but one must note that the solution was slightly different as well as the pulse technique (prepulse method) and the substrate. The other factor is the overlapping of the centers which could effect the total number of countable nuclei. Harrison and Bell(49) have also considered the palladium growth to be progressive nucleation and three dimensional growth and again the nuclear number density is potential dependent. The N_o value reported are $\sim 10^8 cm^{-2}$ which are now higher than those reported here. The nuclear number densities can be calculated by using equation 1.26, where the current is the result of planar diffusion to the electrode surface, so that the growth of nuclei is diffusion controlled. From a knowledge of the diffusion coefficient and concentration, N_o can be calculated. The nuclear number densities for silver and mercury(173,174), (all these values have been calculated from $I - t^{\frac{1}{2}}$ plots by various workers in these laboratories(173-174)), palladium and indium have been included in table 3.1 . The values of the nuclear number densites are of comparable order of magnitude, although only a low overpotential was required for silver deposition. The nuclear number densities for palladium was also calculated from scanning electron microscopy, the order of magnitude is $10^{-6} cm^{-2}$ and $10^{-7} cm^{-2}$ from the $I - t^{\frac{1}{2}}$ plots and scanning electron microscopy respectively, a tenfold difference is seen in these values. The values obtained for the deposition of silver onto vitreous carbon were of the same order by both methods(174). Therefore, for palladium, there must be some problem in the $I - t^{\frac{1}{2}}$ fitting procedure or the forms of carbon used to make the electrodes must lead to different surfaces. Later on the results obtained on microelectrodes also provide the evidence that the N_o value is large because the transients are not those for a single

Mercury 2.6×10^{-5} mol cm^{-3} + KNO_3		Silver 2.5×10^{-5} mol cm^{-3} + KNO_3		Palladium 2.5×10^{-5} mol cm^{-3} + KCl		Indium 2.5×10^{-5} mol cm^{-3} + KCl	
η mV	$10^{-6}N_o$ cm^{-2}	η mV	$10^{-6}N_o$ cm^{-2}	η^* mV	$10^{-6}N_o$ cm^{-2}	η^* mV	$10^{-5}N_o$ cm^{-2}
-190	5.5	-12	0.3	-373	0.3	-152	1.86
-200	12.3	-14	4.7	-383	0.5	-162	1.93
-210	15.5	-16	5.1	-393	0.65	-172	2.14
-220	20.8	-18	5.4	-403	0.86	-182	3.76
-230	27.0	-20	9.5	-413	1.18	-192	6.82
-240	33.8	-22	12	-423	1.43	-	-
-250	42.7	-24	19.9	-433	1.79	-	-
-260	55.0	-26	25.2	-	-	-	-

TABLE 3.10 Nuclear number densities as a function of overpotential, calculated from I versus $t^{\frac{1}{2}}$ plots, (the values for mercury and silver are taken from ref; 173,174)

$^*\eta = E-E_{M^+/M}$

$E_{Pd^{+2}/Pd} = 383mV$ vs S.C.E.

$E_{In^{+3}/In} = -578mV$ vs S.C.E.

nucleus while astley etal(45) has considered the nucleation and growth for these three metals follows entirely different mechanisms and the rate controlling factor is different in each case. Hg has no crystallive lattice, gives $I - t^{\frac{1}{2}}$, growth is dominated by diffusion in solution and the electrochemical step is fast. For silver the I-t dependence is kinetically controlled and consequently silver has a crystal structure and Pd shows an $I \& t^2$ dependence, lattice growth in three dimensions.

3.8.2 MECHANISM OF $M^{n+} \longrightarrow M$

From the transient analysis, the potential dependent rate constants were calculated. The plots of log k vs E always give a slope (Tafel slope) of approximately 120 mV which leads to the conclusion that the rate determining step in both palladium(II) and indium(III) reduction is the first electron transfer. When Astley etal(45) plotted $(i/t^2)^{1/3}$ against η,a plot comparable to one of k against η, the slope was 50 mV^{-1} which suggestedthat two electrons were transferred in the rate determining step with α=0.6. They further suggested that $PdCl_2$ is the complex involved in the electrochemical reaction. This contrasting behaviour could be because of slight changes in the nature of the complexes in solution. Both palladium and indium readily form complexes in aqueous solutions either in the form of oxide and hydroxides or in complexing media they form complexes with variable stoichiometery as has been considered in section 1.1. The species present in the solutions of palladium(II) used for these studies are demonstrated in figure 1.2. The major speciesis $PdCl_4^{2-}$ and likewise for indium the dominating species is $InCl_3$. Therefore the question arises as to whether all the species in solution reduce together or whether only one of the species is electroactive. All the experiments lead to only a single reduction peak. Moreover, it was potential sweep rate dependent, and a plot of I vs $\nu^{\frac{1}{2}}$ gave a straight line with a slope which led to a reasonable value of the diffusion coefficient ($D= 1.08 \times 10^{-5}$) indicating that the reduction process consumes all the palladium(II) and by a similar argument, all the indium(III) in solution. It is possible that all the species are in rapid equilibrium with the electroactive species. In the case of palladium the overall process

could follow the pathway

$$PdCl_4^{2-} \underset{}{\overset{-Cl^-}{\rightleftharpoons}} PdCl_3^- \xrightarrow{-Cl^-} PdCl_2 \xrightarrow{-2e} Pd+2Cl$$

as proposed by Douglas and Magee(34). But Zelensikii and co-worker(40,44) have concluded that in $PdCl_2$ solution, the major reducible species is $PdCl_4^{2-}$ and the reduction of palladium was found to be in the forms $InCl_2^+$, and $InCl_3$ (figure 1.6) and the major species was $InCl_3$. Therefore the electrode reaction may be as follows:

$$InCl_3 \xrightarrow[+e]{-Cl^-} InCl_2 \xrightarrow[+e]{-Cl^-} InCl \xrightarrow{+e\ -Cl^-} In$$

The successive one electron transfer mechanism has been proposed by many other workers(53,55). Equally our data cannot rule out the possibility that several of the species in solution are electroactive.

3.8.3 THE ANODIC DISSOLUTION

The anodic dissolution of the electrodeposited metal in some solutions of palladium(II) and indium(III) give very simple results. For example, the cyclic voltammograms have only one reduction peak followed by a single anodic dissolution peak. It is concluded above that the reduction always takes place through a nucleation and growth process. For palladium solutions at pH less than or greater than 3, only one dissolution peak was observed (figure 3.5-b). For the reduction of indium for all pH and concentrations, except very low concentration, a single anodic dissolution peak has been observed. In media without Cl^- no dissolution peak was observed. In general three other features were sometimes observed.

(i) Two anodic peaks even though there was always one reduction peak.

(ii) The anodic charge is less than the cathodic charge

(iii) A shift in anodic peak potential

Whilst most metal deposits give single peak anodic stripping there are examples in the literature of systems where several peaks are observed. For example multiple peaks for the stripping of zinc in a solution containing glycine as a complexing agent has been reported by Belenkii(176), and Nicholson(177) has shown than the anodic dissolution of deposited nickel exhibit two peaks in solution containing KSCN. The average thickness of the deposits appears to be the critical factor in determining the shape of the dissolution curve. An increase in the thickness shifted the charge distribution towards the first peak, such behaviour can be observed from table 3.1 where for high concentration of palladium the peak separation is 50 mV while for the low concentration the peak separation is 80 mV. It is obvious from the cathodic peak currents (table 3.1) that with an increase in concentration the deposit thickness increases. One author(177) further suggested that the double peak pattern was a surface phenomena where the first peak corresponds to the removal of nickel atoms from what was effectively a nickel surface while the second stage involved atoms attached directly to the substrate electrode surface.

The two anodic arrests could also be the result of the formation of two different complexes during dissolution or metal oxide formation. It is known that both palladium(II) and indium(III) form stable oxides and hydroxides (section 1.1) in solution and as solids. Thus the anodic dissolution may be effected either by (i) a surface oxide film since passivation by an oxide layer (124) could explain the two distinct anodic peaks observed in for example figure 3.1. The second peak usually occurs as a shoulder which is evident from figure 3.1 or 3.5-c, and may be explained by the pathway described in section 1.5 or (ii) hydroxide ions; figure 3.32-a may be explained on the basis of the formation of a metal hydroxide during the anodic process. The two anodic peaks could also be due to the formation of metal oxide of different phases.

The stepwise oxidation of a metal would result in more than one anodic dissolution peak. The stepwise dissolution of indium in acid solution was proved using a rotating ring-disc electrode (122,61) the reaction mechanism is described in section 1.5. The effective valency of indium

depends on the rate of reaction. At low pH the valence leads to one and the shift in indium potential is towards more negative potential (122,178) and can be seen in table 3.8.

The charge ratio Qa/Qc was never equal to unity, but at high concentration of palladium it was 0.95. For indium even at high concentration it was 0.66. This might be due to the fact that the reduction potential is just positive to the hydrogen potential and there was always a chance of co-deposition of hydrogen. Moreover on microelectrode the charge ratio was also 0.9. More likely, however, the charge ratio might be effected by the passivation of palladium and indium the ratio Qa/Qc depends on concentration and pH of the solution (table 3.1, 3.2, and 3.7, 3.8). An increase in concentration and the decrease in pH both cause an increase in total Cl^- ions in solution and both of these factors have known to be effective on the rate of dissolution of metals.

CHAPTER 4

STUDY OF CATALYTIC EFFECT OF PALLADIUM DEPOSIT

CHAPTER FOUR

4.1 THE STUDY OF THE HYDROGEN EVOLUTION REACTION ON PALLADIUM USING MICROELECTRODES

The technique used to study the hydrogen evolution reaction consisted of (a) depositing Pd onto a carbon fiber microelectrode, area 5×10^{-7} cm^2 using a potential step from 0.0V to -0.190V and a deposition time in the range of 1 to 3 seconds. The solution was 50 mmol dm^{-3} palladium chloride in 1 mol dm^{-3} potassium chloride, (b) transferring this Pd on carbon electrode to a solution of aqueous acid and running a cyclic voltammogram at a sweep rate of $0.030V/s^{-1}$. In practice two similar cells, each two electrode with a platinum wire spiral counter/reference electrode, were used for the experiments.

The I-E curve for the carbon electrode in 1 mol dm^{-3} H_2SO_4 is shown as curve (a) in figure 4.1. The hydrogen evolution current commences at -0.8V but no adsorption peaks are seen. A series of experiments were then carried out where Pd was deposited onto the carbon for different periods (the transients are shown in figure 4.2) and cyclic voltammograms were then recorded for each electrode in 1 mol dm^{-3} H_2SO_4. The curves are again shown in figure 4.1. It can be seen that there is an increase in the hydrogen evolution current beyond -0.8V (see figure for carbon itself) and at less negative potentials a single adsorption and desorption peak appear on the forward and reverse sweeps respectively. The size of these peaks and the H_2 evolution current increases with the Pd deposition charge. It can also be seen that the adsorption peaks become broadened and shift to negative potentials with increasing charge. But the current certainly drops to zero beyond the peaks.

The charge under the transients of figure 4.2 were used to estimate the surface area of deposited Pd assuming that 10 nuclei were formed and grow (as estimated from the electron scan micrographs). This assumption may not be entirely correct due to the different carbons used for the electron microscopy and to prepare the microelectrodes but is best available to estimate the surface area of Pd. Figure 4.3 shows the plots of the adsorption peak current density versus the estimated area of the 10

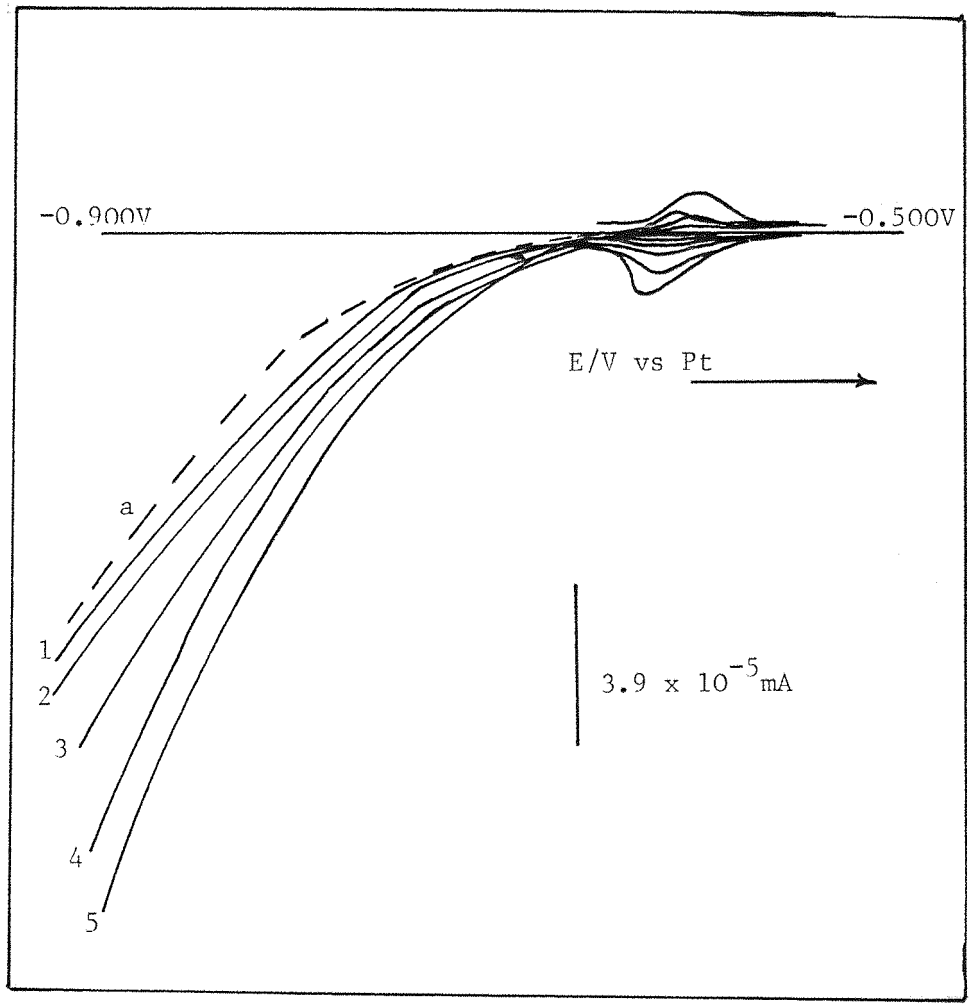

Figure 4.1 Linear sweep voltammograms for hydrogen evolution on carbon fiber microelectrode from the solution of 1 mol dm^{-3} H_2SO_4 at potential sweep rate of 30 mVs^{-1}
(a) C.V on a clean carbon fiber
(b) C.V on palladium deposited onto a carbon fibre

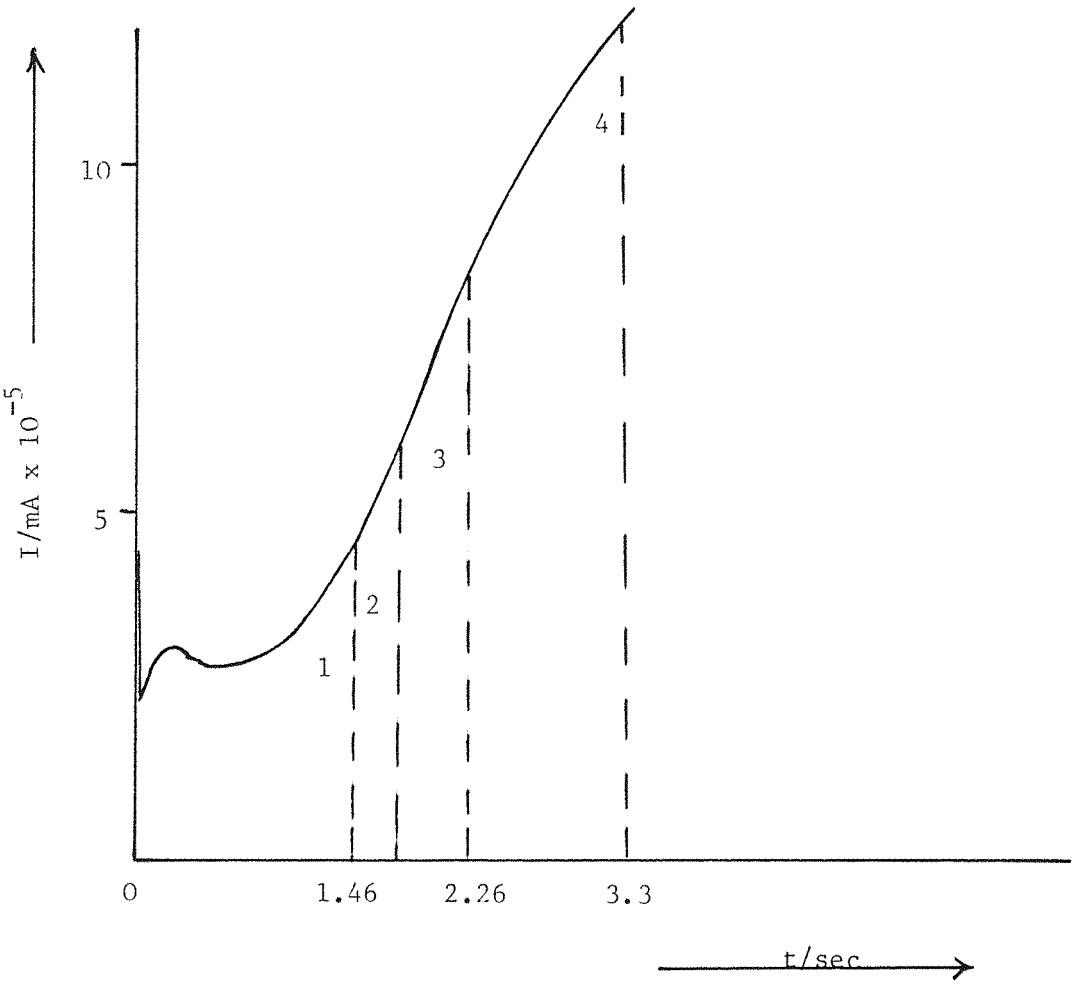

Figure 4.2 Potentiostatic current transients for the preparation of the Pd nuclei on the Carbon fiber deposition from 50 mmol dm^{-3} $PdCl_2$ in 1 mol dm^{-3} KCl

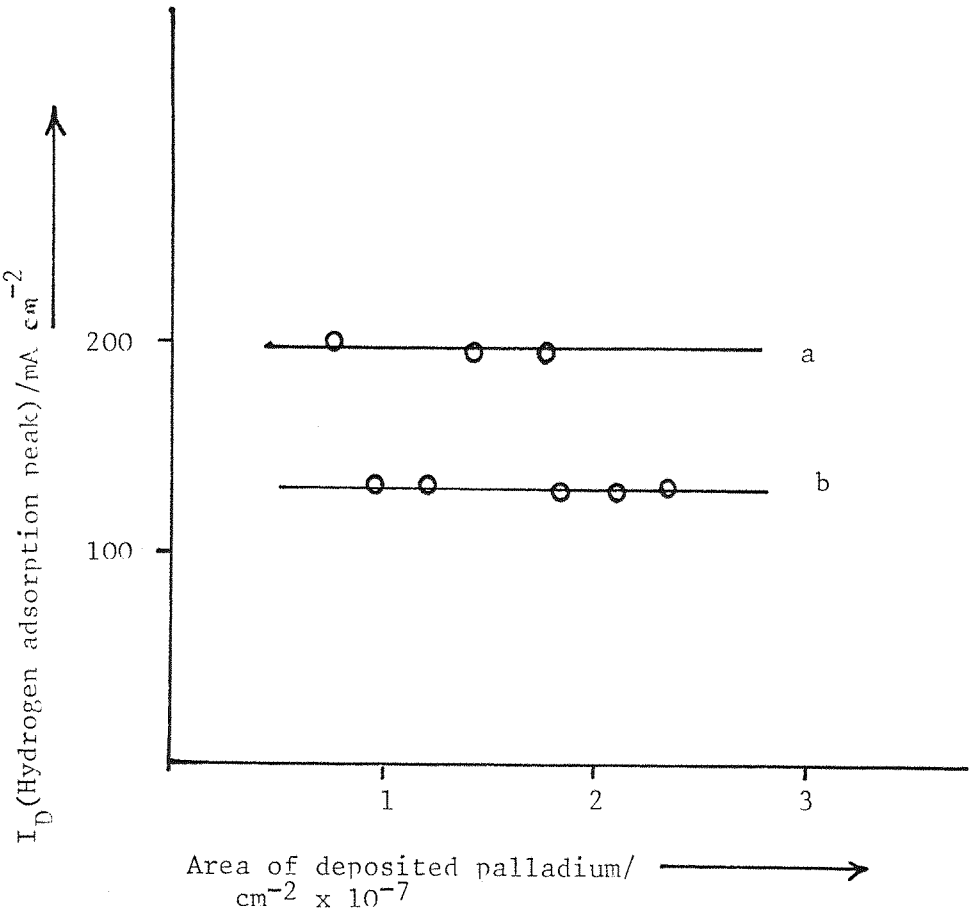

Figure 4.3 The plot of hydrogen adsorption peak current density as a function of area of deposited palladium from

(a) 1 mol dm^{-3} H_2SO_4; platinum microelectrode (Area = 7.85 x 10^{-7} cm^2)

(b) 1 mol dm^{-3} $HClO_4$; carbon fiber microelectrode (Area = 5 x 10^{-7} cm^2)

nuclei for both H_2SO_4 and $HClO_4$. It can clearly be seen that the peak current density is invariant with surface area confirming the adsorption nature of the process. This conclusion is consistent with the general shape of the cathodic and anodic peaks.

Similar sets of experiments was also carried out for palladium deposited onto a platinum microelectrode (area 7.85×10^{-7} cm^2). Surprisingly no adsorption peak was seen with the clean platinum microelectrode but this is probably because of the scale of the current density axis; the area of the deposited palladium is much larger than the actual platinum microelectrode. Linear potential sweep voltammograms were then recorded for a palladium deposited platinum electrode and a single hydrogen adsorption peak appears at about -430mV. The peak current density is proportional to potential scan rate (figure 4.4) confirming that the peaks are indeed due to the adsorption process.

The data in figure 4.1 were also used to construct Tafel plots for the H_2 evolution reaction. The currents at potentials -800 to -900 mV were negative and were used to construct the log I vs E plots. The current densities were again based on the surface area of Pd estimated from the curves of figure 4.2 assuming that 10 nuclei of the same size are growing on the carbon microelectrode. Figure 4.5 shows the set of Tafel plots for the various sizes of Pd nuclei. It can be seen that the straight lines are obtained with Tafel slope of 120 mV which is similar to that of massive Pd electrodes. This suggests a first order, 1 $\bar{e}$ transfer process as the rate determining step as reported by Bockris etal(147).

Also the current densities seem to depend on the size of the Pd nuclei, at least for the smaller sizes. This is more clearly seen by the plots of I Vs r (radius of Pd nuclei) at constant E for two such experiments shown in figure 4.6. It would seem that below a critical size, the smaller nuclei are less active for H_2 evolution. The critical size for the Pd nuclei, below which the activity for H_2 evolution varies with r (radius) is approx. 6×10^{-5} cm. It is interesting to note that Fleischmann etal(180) and Pletcher etal(181) have reported a dependence of the activity for H_2 evolution on the size of nuclei, for the systems Ru on carbon in aqueous acid solution and Ni on carbon in acidic EtOH.

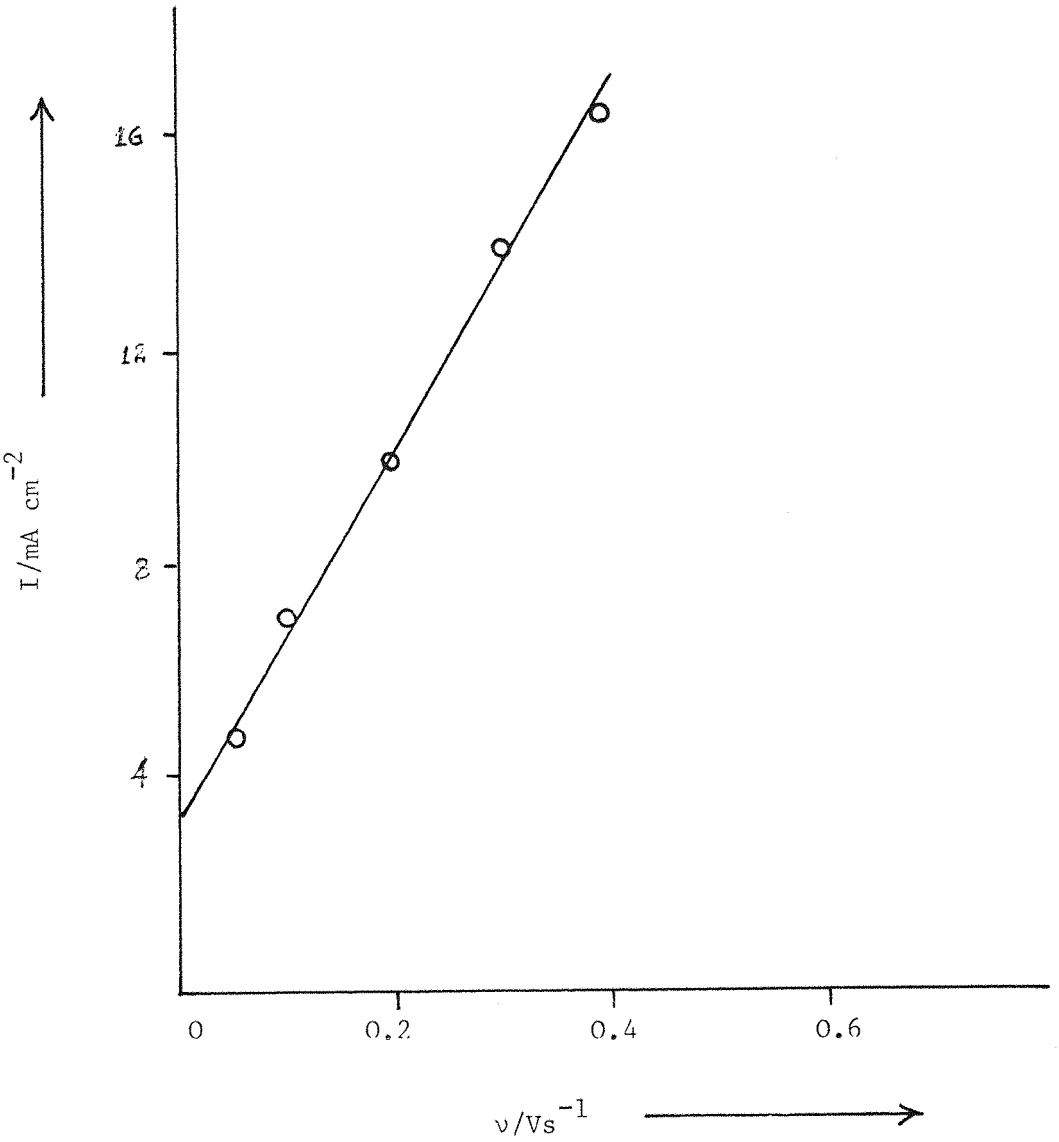

Figure 4.4 A plot of hydrogen adsorption peak current density versus potential scan rate.
1 mol dm^{-3} $HClO_4$ Pd on Pt microelectrode.

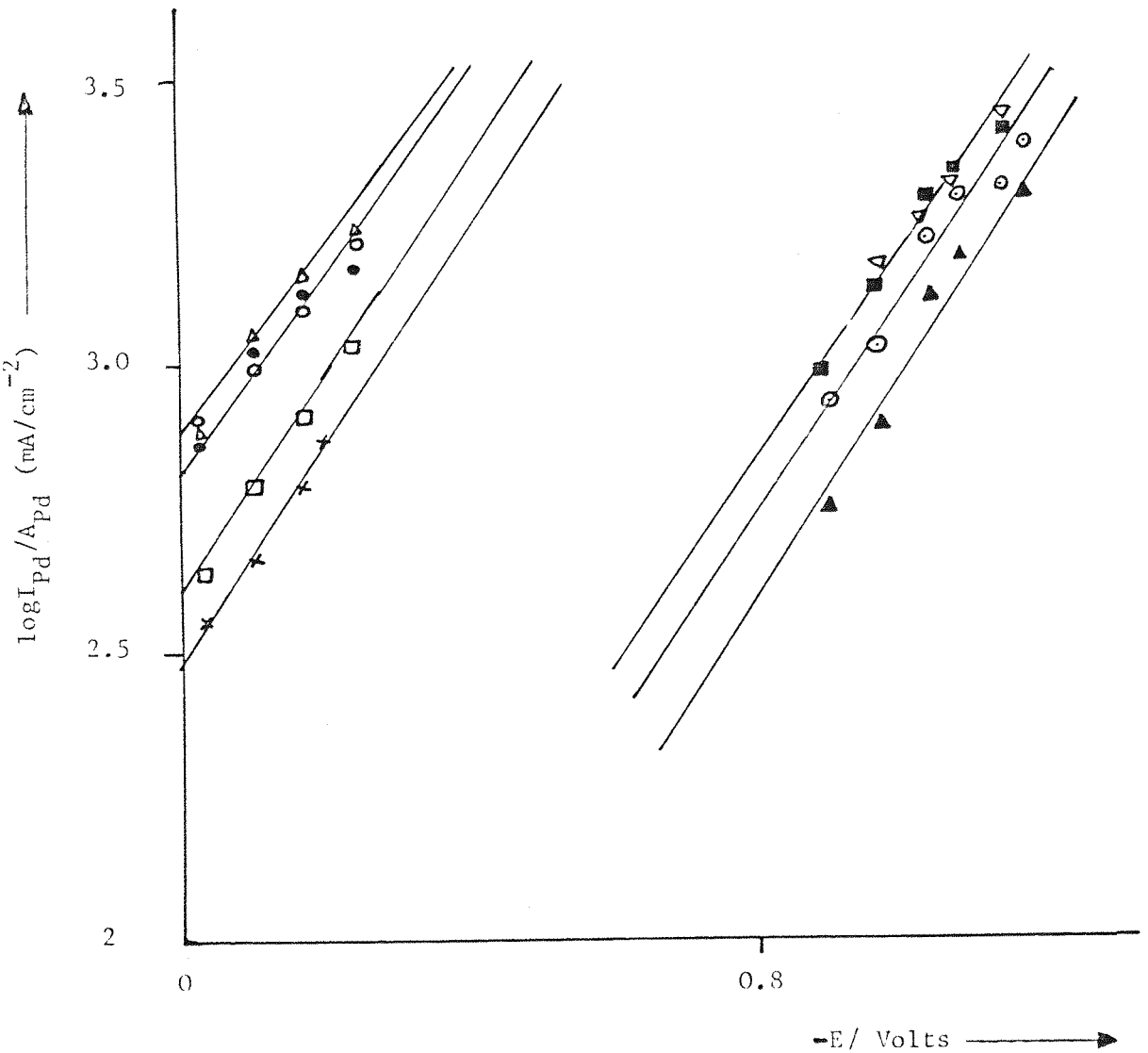

Figure 4.5 log I versus -E plots for the hydrogen evolution reaction on carbon fiber microelectrodes with deposited palladium nuclei of various dimensions.

Δ r = 8.34×10^{-5} cm	∇ r = 8.79×10^{-5} cm
o r = 7.65×10^{-5} cm	■ r = 6.88×10^{-5} cm
● r = 6.48×10^{-5} cm	⊙ r = 5.83×10^{-5} cm
□ r = 6.35×10^{-5} cm	▲ r = 5.24×10^{-5} cm
× r = 6.30×10^{-5} cm	

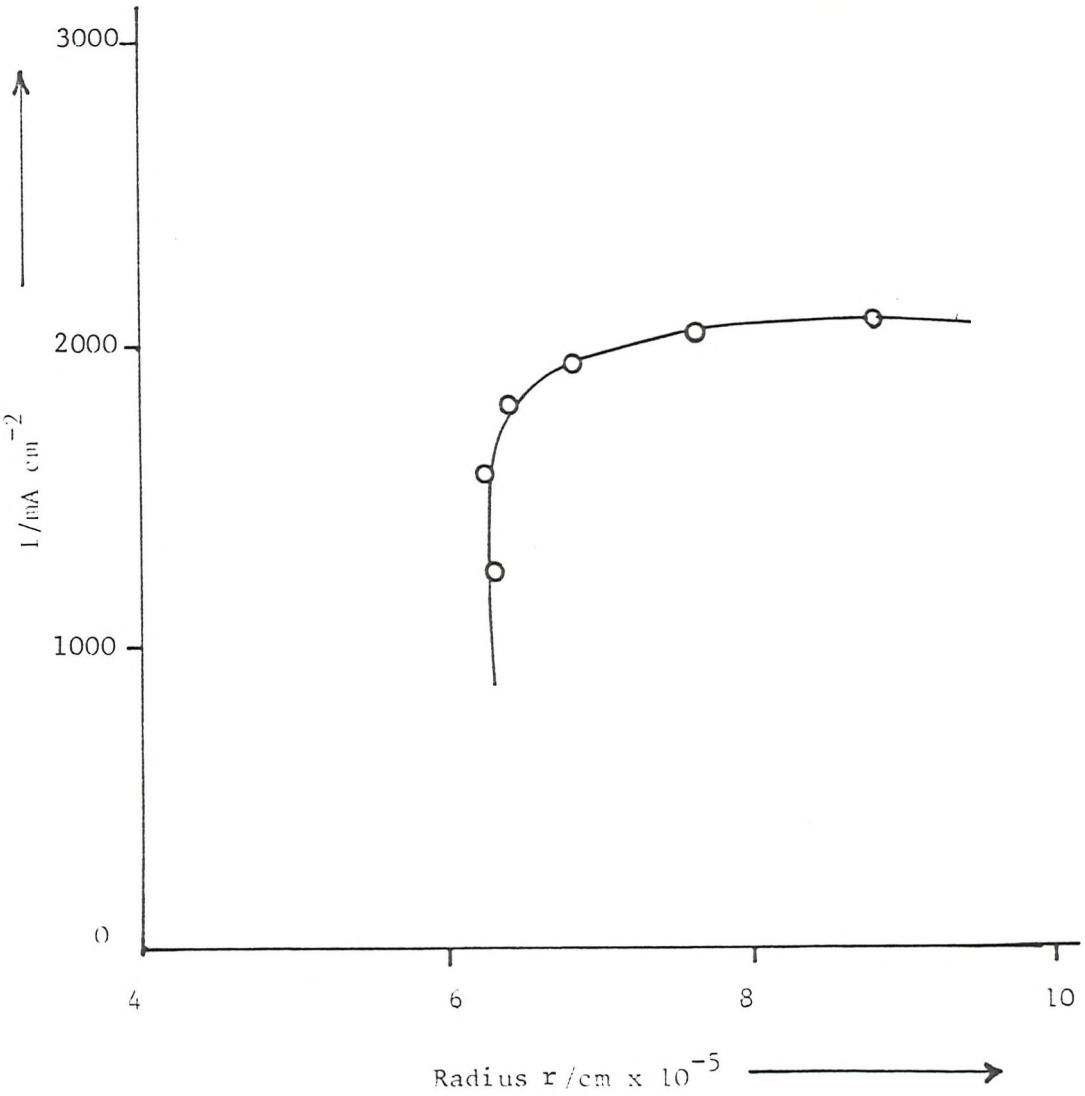

Figure 4.6 A plot of the current for H_2 evolution reaction at a constant potential versus the radii of deposited palladium nuclei.

In their cases, however, the critical radius is much smaller than r = 200A°. However, the conclusions of this study, if confirmed in other related studies would be important in fuel cell technology where a great effort is made to disperse the Pt as much as possible.

It may be noted that the radii calculated from the charge under the transients assuming 10 nuclei fall in the range 5 - 10 x 10^{-5} cm^2; the value of r taken from the electron scan microscopy is 6 x 10^{-5} cm. It can be seen that the agreement is good, supporting the assumption of 10 nuclei on each microelectrode.

4.2 THE STUDY OF THE CATALYTIC EFFECT OF PALLADIUM FOR THE OXIDATION OF FORMIC ACID

A method similar to that used for the study of the hydrogen evolution reaction on electrodeposited palladium on platinum and carbon fiber microelectrodes (A = 7.85 x 10^{-7} and A = 5 x 10^{-7} cm^2 respectively) was used. A potential pulse was applied from 0 to -160 mV to deposit palladium from 50 mmol dm^{-3} palladium chloride in 1 mol dm^{-3} KCl. Two, two electrode cells were used throughout, one containing $PdCl_2$ solution for the deposition and the other containing 1 mol dm^{-3} formic acid in 1 mol $HClO_4$ solution to study the oxidation of formic acid. In both cases a platinum wire spiral electrode was used as a reference electrode.

Figure 4.7 shows a cyclic voltammogram for a platinum microelectrode in 1 mol dm^{-3} HCOOH in 1 mol dm^{-3} $HClO_4$. The potential sweep rate was 0.100 Vs^{-1}. The shape of the curve is very similar to that observed with a platinum macroelectrode. However the reference electrode is a platinum wire electrode, not the normally used NHE, and therefore the peak potentials are shifted. Figure 4.8 represents a I-E curve for a palladium electrode (palladium wire sealed in glass with an exposed area of 4.90 x 10^{-4} cm^2 which is much larger than that of the platinum microelectrode). The curve is in good agreement with that reported by Capon and Parsons (166,167)for a Pd electrode in 1 mol dm^{-3} HCOOH. The first anodic peak is at 0.05V with a peak height of 14.5mA cm^{-2}, while the anodic peak potential on the reverse sweep is slightly shifted towards positive potentials and the peak height is 20.8 mA cm^{-2}.

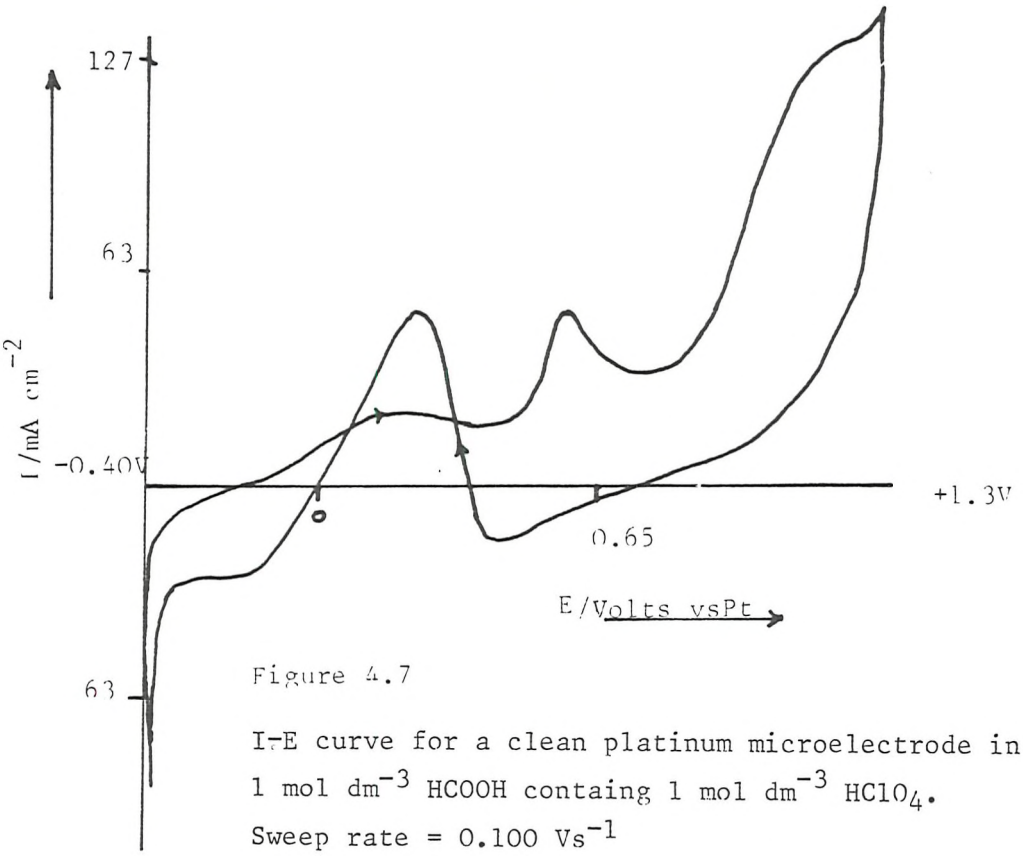

Figure 4.7

I-E curve for a clean platinum microelectrode in 1 mol dm^{-3} HCOOH containg 1 mol dm^{-3} $HClO_4$.
Sweep rate = 0.100 Vs^{-1}

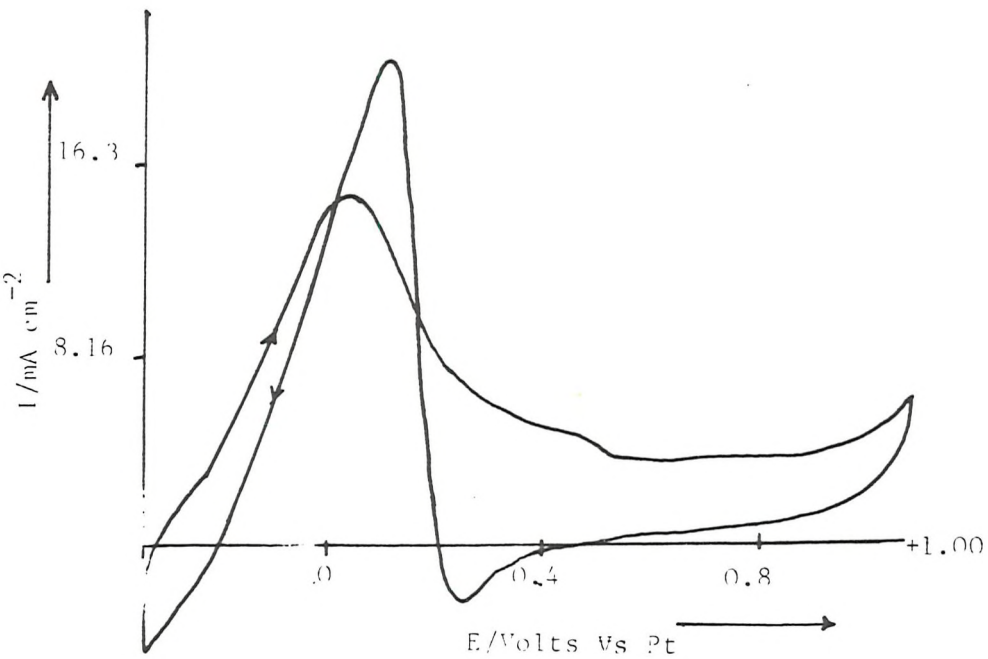

Figure 4.8 I-E curve for palladium electrode (4.90 x 10^{-4} cm^2) in 1 mol dm^{-3} HCOOH + 1 mol dm^{-3} $HClO_4$.
Sweep rate = 0.100 Vs^{-1}

Experiments were then carried out to study the oxidation of formic acid on Pt and C microelectrodes with palladium deposits. A cyclic voltammogram was recorded at a Pt/Pd electrode in 1 mol dm^{-3} HCOOH at a potential sweep rate of 0.200 V/s^{-1} (figure 4. 9). The shape of the curve is similar to that of figure 4.8. However the peak potentials on the forward and reverse sweeps, Ep_{a1} = -0.187V and Ep_{a2} = -0.100V vs Pt are less positive than those observed at Pd or Pt electrodes (see figure 4.7 and 4.8). Moreover, the peak current densities are much higher approximately 400 and 300 mA cm^{-2}. (The current densities were again calculated assuming there are 10 nuclei, based on ESM). The peak current density on Pd/Pt is,in fact, very close to the peak current density for a diffusion controlled process and the shape of the peak confirms this conclusion. Although one could be confident about the general conclusion that the palladium deposit leads to a very strong catalytic effect, problems of reproducibility prevented the study of the catalytic activity as a function of nucleus size. At some stages the data seemed to show that the smaller nuclei were more active than the larger ones but the data was not reproducible enough to confirm this statement. All experiments during these studies, however, confirmed that palladium on platinum electrodes are good catalysts at least on a short time scale. Further studies of such systems would be rather interesting, maybe using a platinum macroelectrode where it is easier to overcome the problem of reproducibility.

A number of experiments were performed on a clean carbon fiber microelectrode and carbon fibers with a palladium deposit. It was found that a clean carbon electrode is entirely inactive for formic acid oxidation and no currents were observed. With a palladium deposit on the carbon surface (formed potentiostatically as above) the electrode becomes somewhat more active and an anodic peak was observed at much more positive potential than with a Pt substrate or massive Pd and Pt electrodes. Figure 4.10 represents a cyclic voltammogram for the Pd/C electrode in 1 mol dm^{-3} HCOOH containing 1 mol dm^{-3} $HClO_4$ at a potential sweep rate of 0.100 V/s^{-1}. The I-E curves a,b,c and d corresponds to the cathodic potential limits -100, -200, -300 and -400 mV respectively. It can be seen that the behaviour of Pd/C electrode is quite different from Pd/Pt electrode. The peak potential is much more positive i.e. approximately

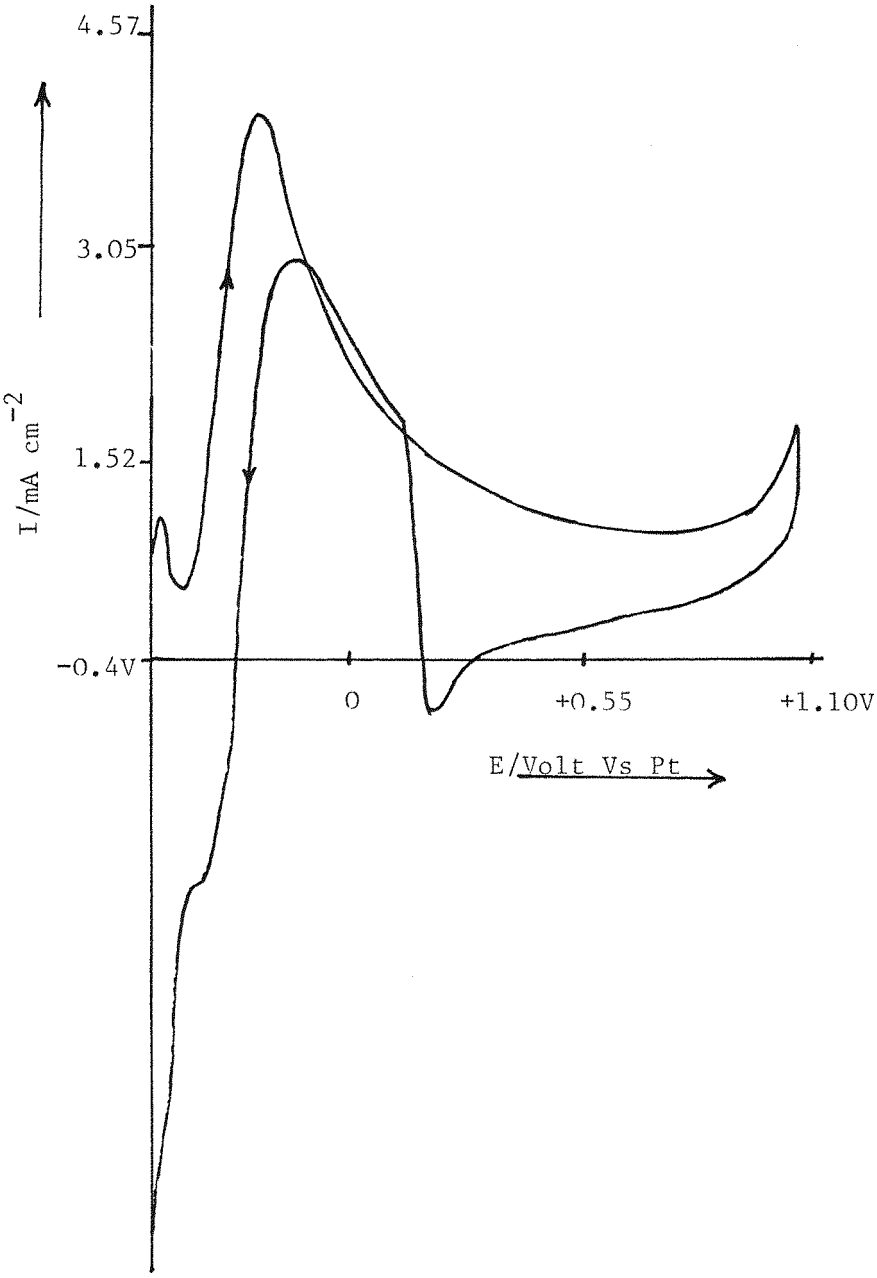

Figure 4.9 Cyclic voltammogram for a palladium deposited Pt electrode (Q=7 x 10^5mC) for 1 mol dm^{-3} HCOOH + 1 mol $HClO_4$, sweep rate = 0.200 Vs^{-1}

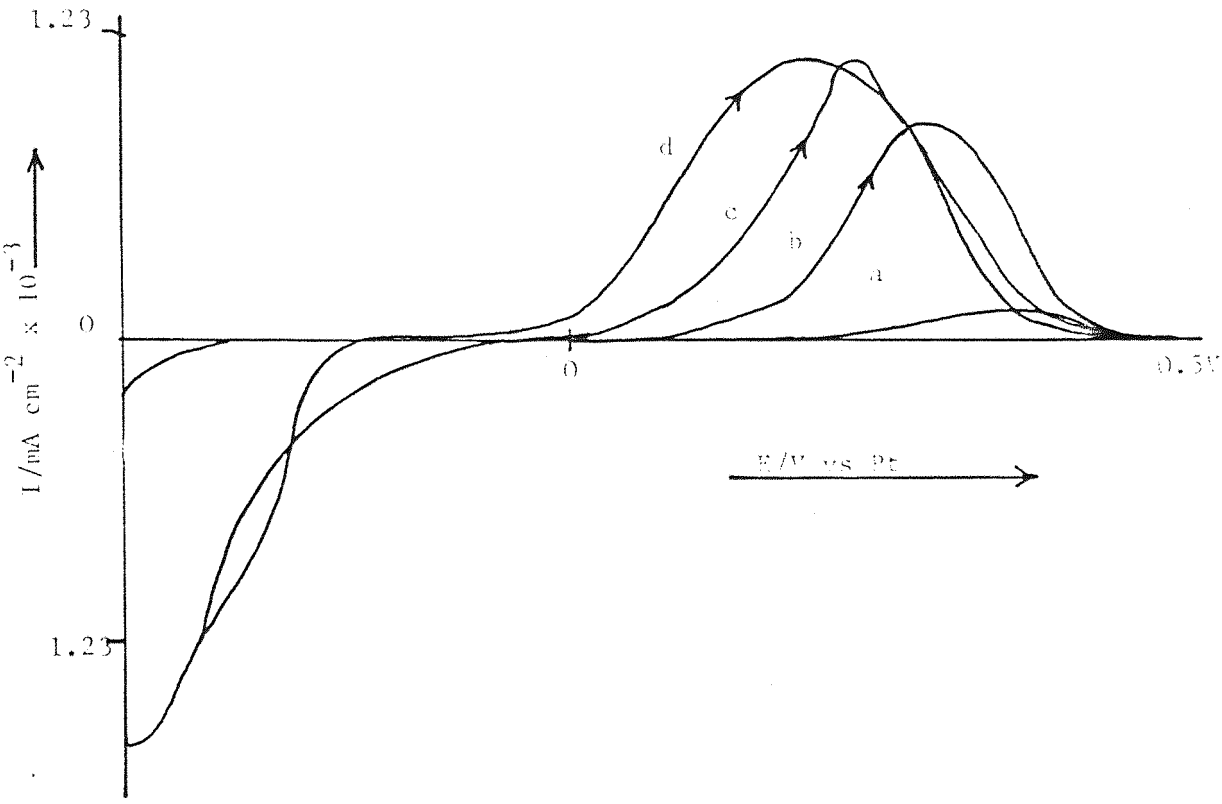

Figure 4.10 Cyclic voltammogram for palladium deposited carbon electrode in 1 mol dm^{-3} HCOOH + 1 mol $HClO_4$, sweep rate = 0.100 Vs^{-1}.

+250mV and Ip is much more smaller than Ip at Pd/Pt. Particularly when the sweep is commenced just negative to the peak the oxidation rate is almost negligible which can be seen from curve a, where the potential sweep was started at -100 mV.

There certainly appears to be a substrate effect as the nuclei seem to know the difference between Pt and C electrodes, showing entirely different behaviour. Similar behaviour of platinum deposits on carbon and gold substrates was observed by Pletcher etal(182). However, if a large amount of palladium is deposited on carbon (a long time potential step was applied) the I-E curves again have the characteristics of the curves obtained at a Pd electrode.

APPENDIX

1. INTRODUCTION

The anodic oxidation of formic acid at platinum electrodes has been a subject of many studies over the past 25 years. Platinum itself is a good catalyst but it very quickly gets poisoned by strongly adsorbed intermediates. Since it was reported that submonolayer amounts of mercury on the platinum(183) surface catalysed formic acid oxidation, a number of efforts have been made to examine the effect of metal adatoms on this reaction e.g. Bi, Cd, Pb, Ti, (151, 184-188). It should also be noted that catalysis can be obtained by the adsorption of some organic and inorganic molecules onto the surface(183) while some metal adatoms do not catalyse, and may even inhibit, the oxidation of formic acid(186). Intensive investigations of the properties of adatoms and of the underpotential deposition of metals have also been summarised by Kolb(190). More recently Motoo and coworkers(191) have made an extensive study of the effect of adatoms on electrode reactions. They have shown that in a monolayer of lead on platinum, the adatoms are loosely arranged with each adatom occupying two platinum sites and with geometrical space between(189); this result indicates that at a lead coverage $\theta_{Pb} = 0.5$ (where the maximum rate of formic acid oxidation is observed) there are two free platinum atoms for each lead adatom. They also distinguish clearly between adatoms such as Bi, Hg or Pb and others such as As, Ge or Ru which catalyse the oxidation process by oxygen adsorption at a lower potential. Finally they have shown that electrocatalysis is a function of surface properties rather than the bulk metal structure(191).

The mechanism proposed by Capon and Parsons(192) for the oxidation of formic acid has been widely accepted. They suggested that oxidation occurs by the sequence

$$HCOOH + 2Pt \longrightarrow Pt - H + Pt-COOH \qquad (1)$$

$$Pt - H \xrightarrow{-e} Pt + H^+ \qquad (2)$$

$$Pt - COOH \xrightarrow{-e} Pt + CO_2 + H^+ \qquad (3)$$

where step (1), the dissociative adsorption process, is the slow

step and the oxidation of the adsorbed species is very rapid at the potential where oxidation occurs. In fact, the current density observed for the oxidation of formic acid at a clean Pt surface is relatively high and hence the rate of step (1) is quite fast (in contrast to the other organic molecules). On Pt however, the rate of oxidation of formic acid drops rapidly due to the formation of surface poisons. This probably forms by a reaction such as

$$Pt - COOH + HCOOH \longrightarrow \begin{matrix} Pt \\ Pt \\ Pt \end{matrix} \!\!\diagdown\!\!\diagup\!\!\!= CHO + H_2O + CO_2 \quad (4)$$

where one of the products is a strongly adsorbed species which cannot be oxidised at a significant rate. It has been suggested that the reaction leading to poison formation requires several adjacent Pt atoms (151,187,188). The role of metal adatoms such as Pb is hence to prevent the formation of surface poison, by arranging themselves over the surface so as to create a large number of sites where there are two adjacent Pt atoms available for reaction (1) to occur but there are few sites where there are sufficient adjacent Pt atoms for the poison to form. The most active Pb/Pt electrode is one where $\theta_{Pb} = 0.5$ (184-187), which since each Pb atom interacts with two Pt sites, corresponds to a surface where the "average site" is 1Pb + 2 Pt atoms as sketched in figure A.1.

Most of the studies of the oxidation of formic acid on Pt have been made using linear potential sweep methods. Recent studies have emphasised potential step methods (151,187,188), because linear potential sweep data cannot be analysed quantitatively; several factors (e.g. metal adatom coverage, rate of oxidation of formic acid) change simultaneously with potential. Therefore, potential step methods have been preferred for the study of formic acid at Pt/M surfaces and it has been demonstrated that analysis of the transients can lead to the rate constant for step (1) in the mechanism above. The electrode surface is first cleaned by potential cycling, then held at a potential where a complete monolayer of adatoms forms (and hence neither dissociative adsorption of formic acid or formation of adsorbed hydrogen can occur). A potential step is then applied to a potential where partial oxidation of the adatom layer occurs and the oxidation of formic acid can take place on the Pt/M surface. The I-t response for the potential step can then be analysed.

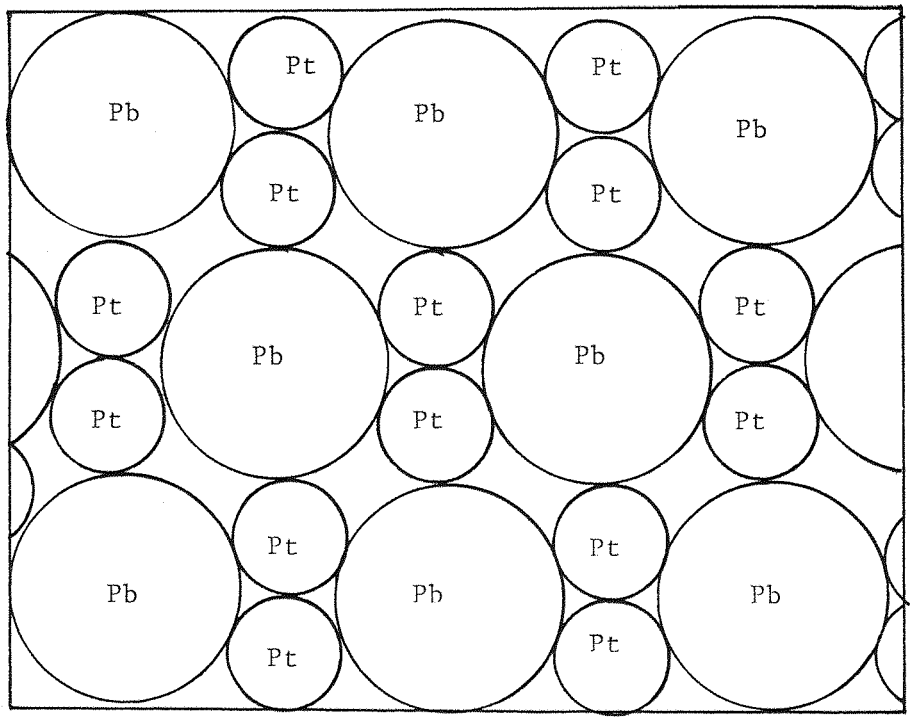

Figure A.1 Sketch illustrating the arrangement of Pb adatoms on a Pt surface when $\theta_{Pb} = 0.5$

The observation of falling I-t transients leads to the conclusion that the oxidation of formic acid at such surface is partially diffusion controlled. A range of experiments with different adatoms and at various potentials shows

(a) At short times, the current densities are variable depending on the choice of metal adatom and potential

(b) At long times, the current densities tend to the same value and these parts of the transients can be replotted to give linear $I\text{-}t^{-\frac{1}{2}}$ plots, from which the diffusion coefficient for formic acid can be estimated.

This behaviour indicates that the process is diffusion controlled at long times but under mixed control by diffusion and a chemical step at short times. Hence the rate of oxidation of formic acid at platinum partially covered by metal adatoms can either be determined by diffusion of HCOOH to the surface or a chemical step whose rate depends on the nature of the surface. With Pb/Pt surfacesthe rate of the chemical step varies with the number of sites where the combination of one lead and two platinum surface atoms is to be found. It has been suggested that the dissociative adsorption process (1) is the rate determining step. Such a mechanism can be described by the equation

$$\frac{\partial C}{\partial t} = D\frac{\partial^2 C}{\partial x^2} \qquad (5)$$

with initial conditions

at $t = o$, $C = C^{\infty}$ at all x

and the boundary conditions, $t>o$

$x = \infty$, $C = C^{\infty}$

$x = o$

$$I = nF\left(\frac{\partial C}{\partial x}\right)_{x = o} \qquad (6)$$

or $$I = nFk\theta_{Pb}\left(1 - \theta_{Pb}\right) C^{\sigma} \qquad (7)$$

Where k is the rate constant for reaction (1)

C^{∞} is the concentration of formic acid in solution

C^{σ} is the concentration of formic acid on the electrode surface

θ_{Pb} is the coverage by lead at potential where formic acid is oxidized

The solution to these equations is, by analogy with similar sets of equations(193),

$$I=nFkc^{\infty}\theta_{Pb}(1-\theta_{Pb})\exp\left[k^2\theta_{Pb}^2(1-\theta_{Pb})^2t/D\right]\operatorname{erfc}\left[k\theta_{Pb}(1-\theta_{Pb})t^{\frac{1}{2}}/D^{\frac{1}{2}}\right] \quad (8)$$

At long times this equation may be approximated to

$$I_D = \frac{nFD^{\frac{1}{2}}C^{\infty}}{\pi^{\frac{1}{2}}t^{\frac{1}{2}}} \quad (9)$$

while at short times the kinetics of reaction (1) and hence the coverage of platinum by lead adatoms will predominate.

To obtain the kinetic parameters for reaction (1) the transient can be treated according to the procedure of Delahay and Oka(194). Division of equation (8) by equation (9) leads to

$$\frac{I}{I_D} = \pi^{\frac{1}{2}}\lambda \exp \lambda^2 \operatorname{erfc} \lambda \quad (10)$$

where

$$\lambda = \frac{k\theta_{Pb}(1-\theta_{Pb})\ t^{\frac{1}{2}}}{D^{\frac{1}{2}}} \quad (11)$$

Hence current time transients can conveniently be analysed from a plot of $It^{\frac{1}{2}}$ against $t^{\frac{1}{2}}$. For a diffusion controlled process $It^{\frac{1}{2}}$ is independent of $t^{\frac{1}{2}}$ while a partially diffusion controlled process will give a curve. At short times $It^{\frac{1}{2}}$ will have a lower value but at long times the value of $It^{\frac{1}{2}}$ will tend to the value for diffusion control. The values of λ are found from a standard plot of $\pi^{\frac{1}{2}} \exp \lambda^2 \operatorname{erfc}\lambda$ against λ shown in figure A.2. From the ratio of I/I_D the corresponding value of λ can be found using figure A.2. The values of λ can then be replotted against $t^{\frac{1}{2}}$, a plot which should be linear and from the slope, the rate constant can be obtained, see equation (11).

The purpose of the experiments carried out here was to compare the rate of the dissociative adsorption of HCOOH and DCOOH and hence to comment on the controversy between electrochemists and chemists interested

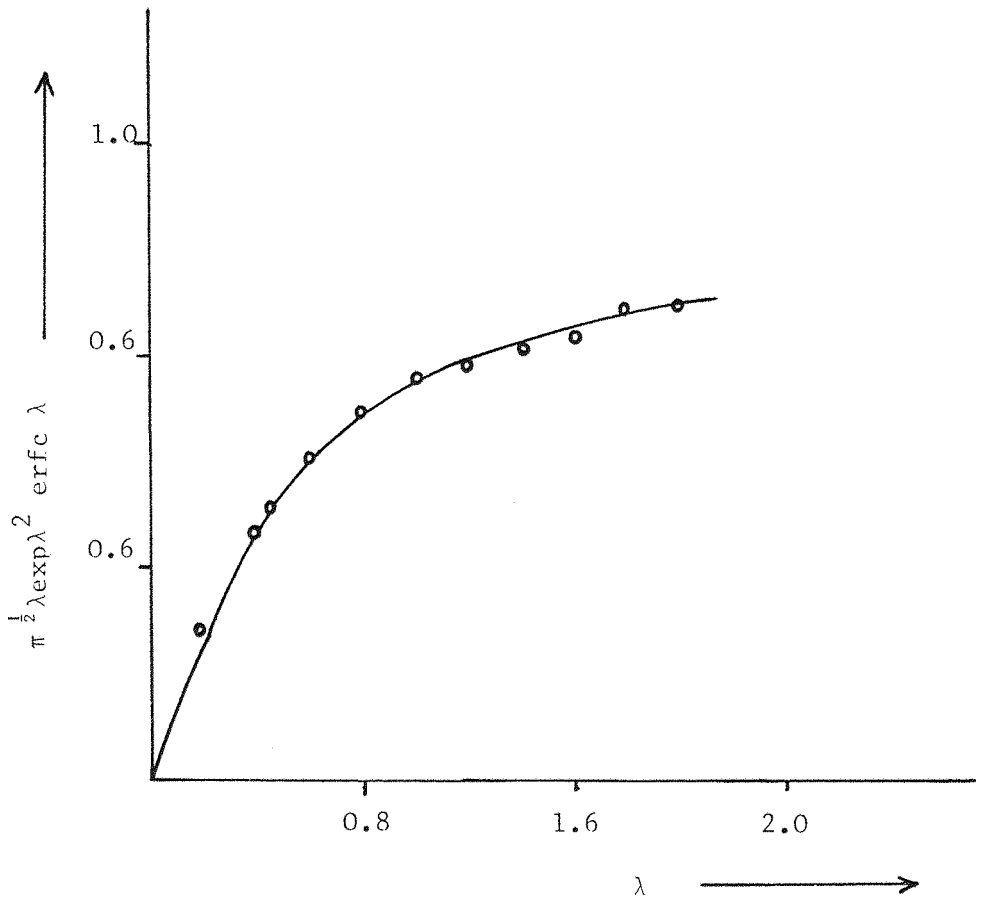

Figures A.2 A plot of $\pi^{\frac{1}{2}}$ λ exp λ^2 erfc λ vs λ, used for the determination λ values from the experimental data

in heterogeneous catalysis over the mechanism of formic acid oxidation.

According to the reaction scheme proposed by Capon and Parsons(192) and generally by the electrochemists, the first step involves the cleavage of the C-H or C-D bond at the metal surface i.e.

$$H\text{-}COOH + 2Pt \longrightarrow \overset{H}{\underset{|}{Pt}} + \overset{COOH}{\underset{|}{Pt}} \qquad (12)$$

In contrast to electrochemists, the mechanism proposed in studies of heterogeneous catalysis(195) for the kinetics of the decomposition of formic acid and DCOOD in the gas phase involves the cleavage of the O-H bond e.g.

(a) Adsorption step

$$DCOOH + * \xrightarrow{\text{fast}} (DCOOH)_{ads} \qquad (13)$$

(b) Dissociation

$$2(DCOOH)_{ads} \xrightarrow{\text{fast}} (DCO\overset{O}{\overset{\|}{C}}\overset{O}{\overset{\|}{C}}D)_{ads} + H_2O_{(g)} \qquad (14)$$

(c) Decomposition

$$(DCO\overset{O}{\overset{\|}{C}}\overset{O}{\overset{\|}{C}}D)_{ads} + * \xrightarrow[\text{slow}]{k} 2D_{ads} + CO_{(g)} + YCO_g + (1-Y)CO_{ads} \qquad (15)$$

$$2D_{ads} \xrightarrow{\text{fast}} D_{2(g)} + 2* \qquad (16)$$

$$CO_{ads} \xrightarrow{\text{slow}} CO_g + * \qquad (17)$$

where * represents the surface site. Studies of the rate of CO_2 and D_2 formation and $CO(\alpha_2)/DCOOH$ ratio show the value of Y in equation(15) to vary between 0 and 1 since it depends on the surface covered by complex formate.

They also suggest that formic acid can adsorb dissociatively with the direct cleavage of the O-H bond. Hirota etal(196) suggested that the hydrogen atoms remained on a fresh metal surface but Madix etal(195)

do not agree and suggested the scheme

$$HCOOH \longrightarrow HCOO_{ads} + H_{ads} \quad (18)$$

$$HCOO_{ads} \longrightarrow H_2 + CO_2 \quad (19)$$

Hence the oxidation of HCOOH and DCOOH was studied at a Pt anode. If the rate constant for the dissociative adsorption of HCOOH and DCOOH showed a large kinetic isotope effect, it was felt that it would be strong evidence that the rate determining step involves the cleavage of the C-H bond. The Pt adatom effect was used to overcome the poisoning of the Pt surface.

RESULTS AND DISCUSSION

The results of studies of formic acid oxidation can be badly effected by impurities in solution and also depends upon the history of the Pt surface. Hence the glassware were carefully cleaned by soaking it in hot 1:2 sulphuric acid - nitric acid solution, followed by rigorous rinsing and boiling in triply distilled water. The electrolytic cells employed were of conventional three electrode design. The working electrode was a smooth platinum wire of 0.25 cm^2 geometric area and the counter electrode was a platinum gauze placed around the working electrode in the same solution. A normal hydrogen electrode, with hydrogen electrochemically generated in situ, was used as the reference electrode. Between series of experiments, the platinum electrode was cleaned chemically in H_2SO_4/HNO_3 solution and then electrochemically by the application of a repetative triangular potential sweep between + 0.03V and 1.50V until a voltammogram showing the characteristic response described in ref (197). For the purpose of maintaining a clean surface, two cells were used, one filled with 1 mol dm^{-3} $HClO_4$ for cleaning cycles and the other with the solution under study. Triply distilled water was used to prepare the solutions. The chemicals used were Analar grade and were not further purified. The deuterated acid used was DCOOD (Merck Urasol Grade) which in an aqueous solution of 1 mol dm^{-3} $HClO_4$ exchanges protons rapidly

$$DCOOD \xrightarrow{H+} DCOOH \qquad (20)$$

The real surface area of the Pt electrode was estimated from the area under the hydrogen adsorption peaks and the roughness factor was approximately 4.

Figures A3 and 4 show cyclic voltammogram run at a Pt electrode for 0.1 mol dm^{-3} formic acid and 0.1 mol dm^{-3} DCOOH in 1 mol dm^{-3} $HClO_4$ respectively. Whereas figure A5 and A6 report the I-E curves for the oxidation of HCOOH and DCOOH in the presence of 10^{-3} mol dm^{-3} $Pb(NO_3)_2$. The curves for HCOOH are almost identical to those reported earlier (151,186,187). In the absence of Pb^{2+} in solution, the I-E response has a complex form. On the sweep to positive potentials, three low current

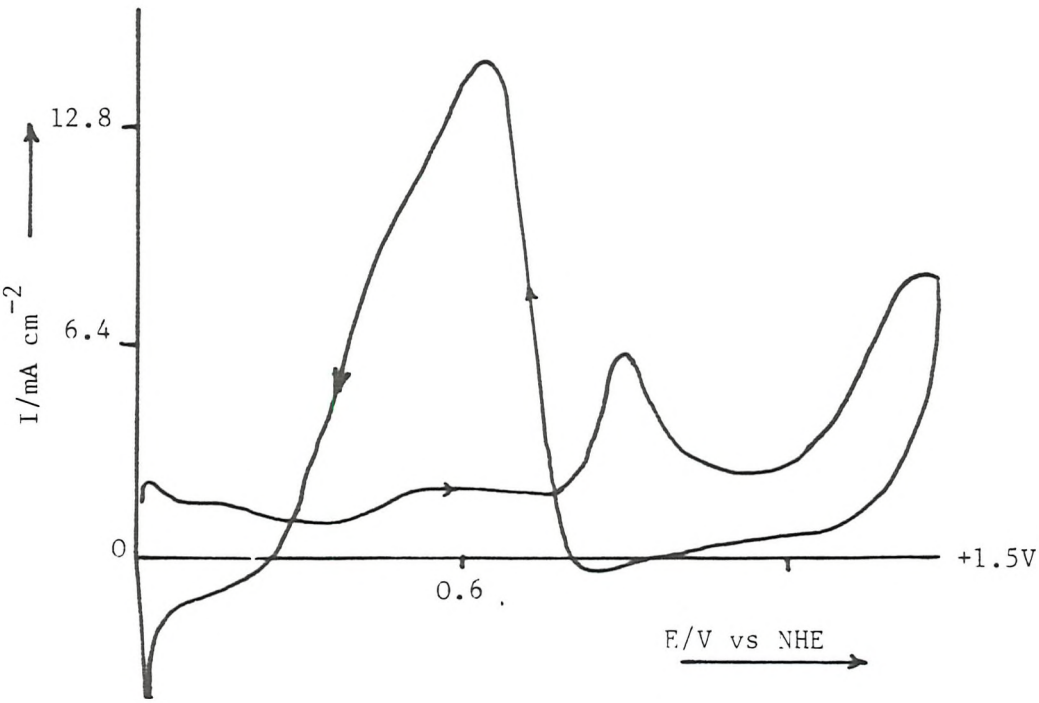

Figure A.3 Cyclic voltammogram for the oxidation of 0.1 mol dm^{-3} HCOOH in 1 mol dm^{-3} $HClO_4$ at platinum wire electrode, sweep rate = 0.1Vs^{-1}.

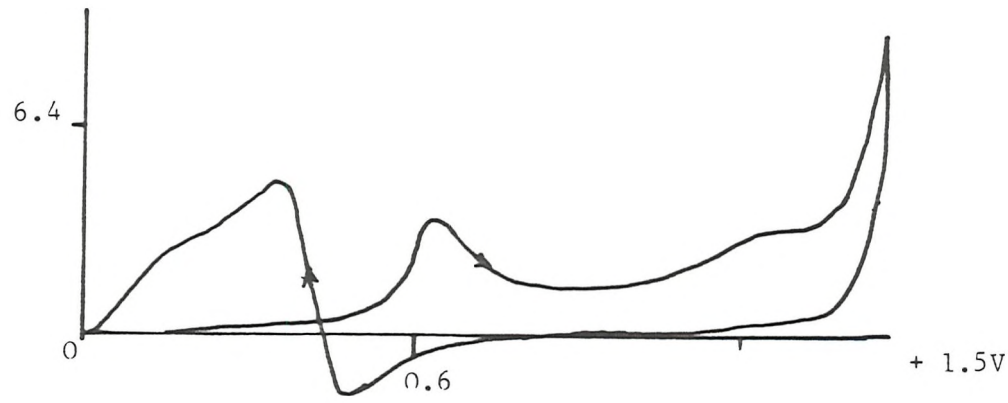

Figure A.4 Cyclic voltammogram for a platinum wire electrode in 0.1 mol dm^{-3} DCOOH in 1 mol dm^{-3} $HClO_4$. Sweep rate = 0.1Vs^{-1}.

density oxidation peaks are seen, the first at +0.400V to + 0.600V is a plateau, the second is well defined but with a low current density at +0.900V and the third anodic peak occurs in the potential region +1.4 to +1.5V. On the reverse sweep a much larger anodic peak is seen at +0.600V. A similar behaviour was observed for the oxidation of the deuterated acid (figure A.4) but with smaller current densities than HCOOH. The difference in current densities is of the order of two. The other difference is the shift in peak potentials. This first anodic peak is negligible, the second anodic peak is at +0.640V and the third anodic peak is at +1.5V. The reverse anodic peak is shifted towards less positive potential, i.e. +0.330V. The plateau at low current density on the positive going scan may be due to the low rate of oxidation of *COOH

$$*COOH \longrightarrow CO_2 + H^+ + e \qquad (21)$$

Angerstein - Kozlowska etal (183) have demonstrated that this slow oxidation process allows more time for the formation of an intermediate such as formic anhydride. The second anodic peak is related to oxidation of an adsorbed species. The peak on the reverse scan is the oxidation of formic acid on a fresh platinum surface because the cathodic dissolution of PtO at this potential reforms the Pt surface.

After addition of Pb^{2+}, both the forward and back sweeps show a single oxidation peaks; their current densities are much higher and the peak potentials are very similar (Ep=0.59V) see figure A.5, A.6. Earlier workers have suggested that these peaks were from a rapid oxidation of HCOOH at a Pt/Pb surface and that the current density at each potential reflects the coverage by Pb. The peak potential corresponds to θ_{Pb}= 0.5; lower potentials correspond to θ_{Pb}>0.5 where some of the surface has no uncovered Pt atoms while at higher potential, θ_{Pb}<0.5 and some of the surface becomes poisoned.

The peak current density for DCOOH is about half that for HCOOH. The lower value is to be expected if the initial cleavage is of the C-H/C-D bond. The cyclic voltammograms do not,however, allow quantitative estimation of this effect. Hence the potential step method was applied. The I-t response for the oxidation of formic acid was obtained

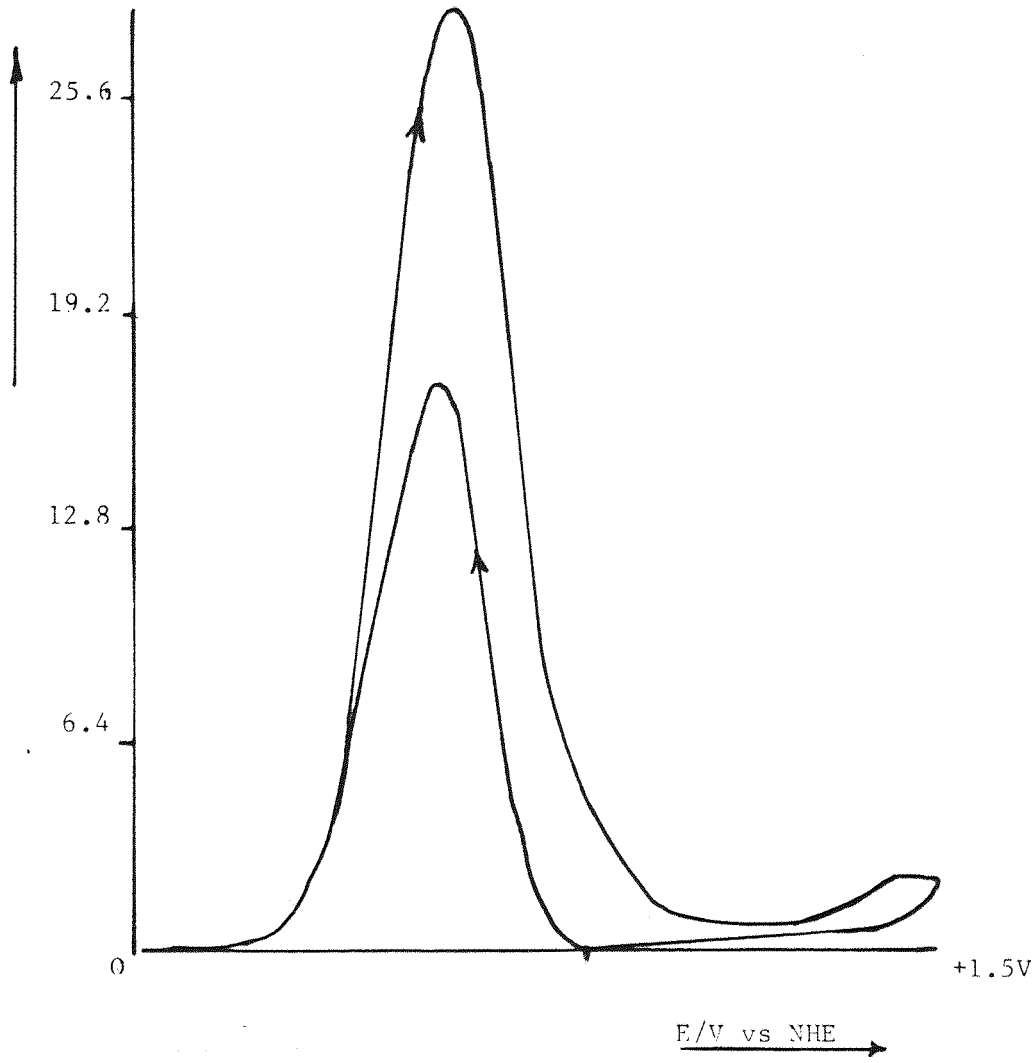

Figure A.5 I-E curve for oxidation of 0.1 mol dm^{-3} formic acid in $HClO_4$ in the presence of 10^{-3} mol dm^{-3} Pb^{2+}. Sweep rate = $0.1Vs^{-1}$.

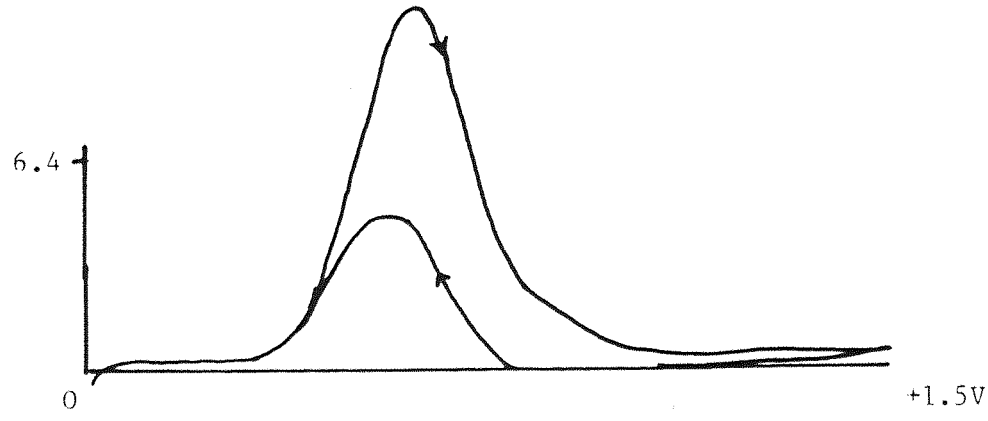

Figure A.6 I-E curve for 0.1 mol dm^{-3} DCOOH in the presence of 10^{-3} mol dm^{-3} Pb^{2+}(in $HClO_4$). Sweep rate = $0.1Vs^{-1}$.

by using a rather complex potential-time profile. It may be divided into three parts (a) ensuring a clean surface, (b) forming the monolayer of Pb, (c) partially oxidising the monolayer and observing the oxidation of formic acid. The I-t transients for 0.1 mol dm^{-3} HCOOH in 1 mol dm^{-3} in the presence of 10^{-3} mol dm^{-3} $Pb(NO_3)_2$ are shown in figure A.7. Figure A.8 shows the corresponding I-t transients for the oxidation of DCOOD. A potential step from 0.2 to 0.6V was applied, 0.6V being chosen since earlier workers had shown $\theta_{Pb}=0.5$ at this potential, and falling transients are obtained in both cases. The transients were recorded over the time scale from 0.1 to 100 seconds.

The transients were analysed by plotting $It^{\frac{1}{2}}$ vs $t^{\frac{1}{2}}$, see figure A.9. It can be seen that the data for HCOOH follows closely that expected from theory, i.e. at short times $It^{\frac{1}{2}}$ increases with $t^{\frac{1}{2}}$ and beyond sixteen seconds the plot reaches a plateau. Moreover the diffusion coefficient calculated from the plateau is 0.8×10^{-5} cm^2 s^{-1}. With DCOOH the situation is not as clear. At short times $It^{\frac{1}{2}}$ increases with $t^{\frac{1}{2}}$ but it reaches to maximum and thereafter drops with increasing t never reaching the expected diffusion limit, i.e. the same plateau value as that for HCOOH. A likely explanation of this behaviour is that the electrode surface is more rapidly poisoned because of the impurities in DCOOD. The HCOOH employed was Analar but similar quality DCOOD cannot be purchased. In fact even with HCOOH a slight drop in the value of $It^{\frac{1}{2}}$ is observed at very long times, approaching 100 seconds and this is also probably a slow poisoning effect. Hence the data for HCOOH was analysed using the procedure described in the introduction but for DCOOH the analysis was carried out using the value of I_D found for HCOOH. Below 4 seconds this procedure gave excellent results and plots of λ versus $t^{\frac{1}{2}}$ are linear for both acids see figure A.10. Deviation becomes large for DCOOD beyond 4 seconds. The good agreement at short times is also emphasised by the curves drawn in figure A.9, which were computed from the values found for D and k. The values of k_{DCOOH} and k_{HCOOH} found from the slopes of the lines in figure A.10 were 2.9×10^{-3} cm s^{-1} and 7.6×10^{-3} cm s^{-1} respectively. Hence the ratio k_{HCOOH}/k_{DCOOH} is 2.6. This clearly shows the cleavage of the C-H and C-D bond in the rate determining step confirming the mechanism proposed by Capon and Parsons(192) and widely accepted by electrochemists.

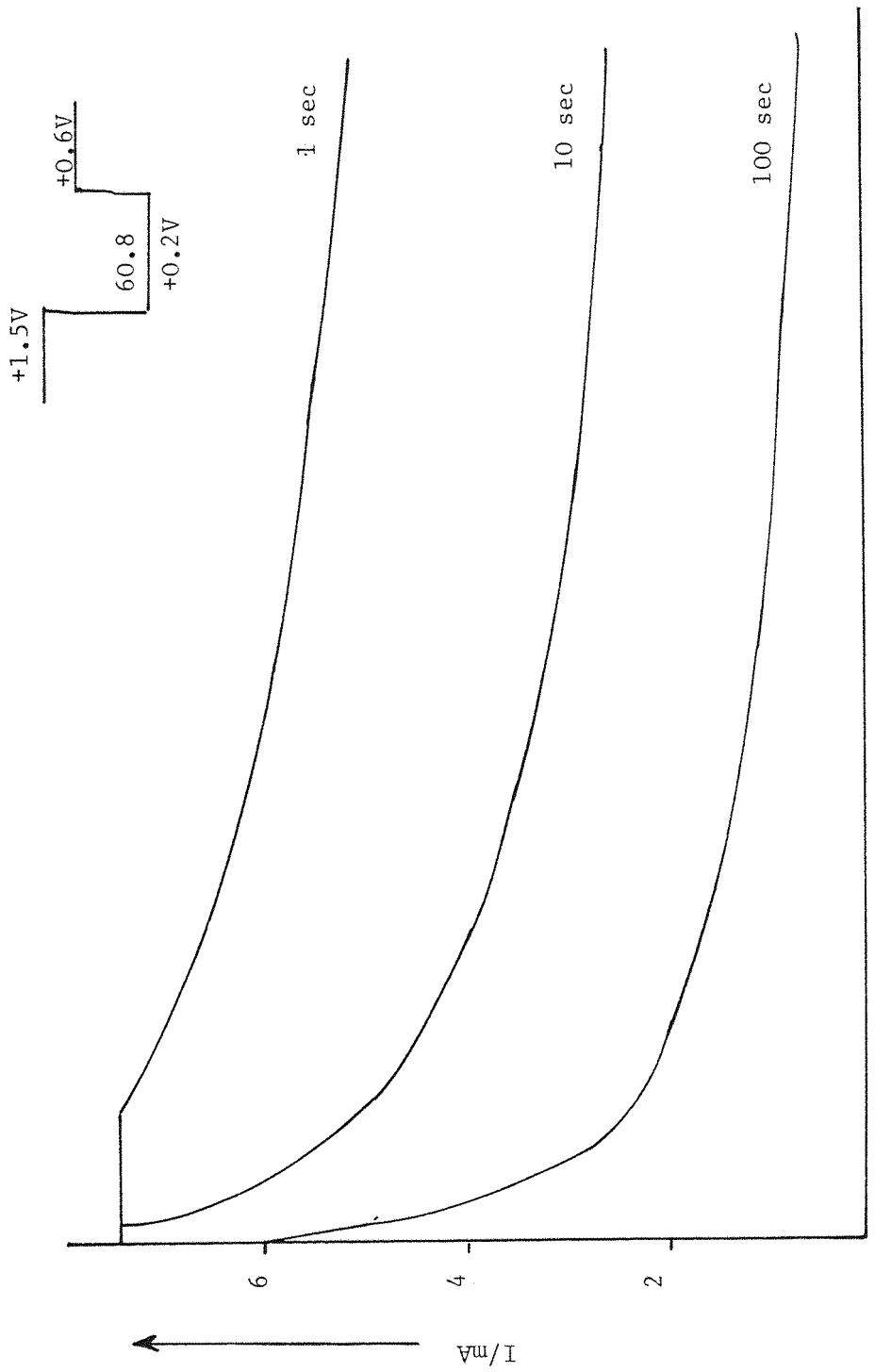

Figure A.7 I-t transients resulting from a potential step experiment from +0.2V to +0.6V. The solution is same as Fig. A.5. The potential profile is shown in the figure.

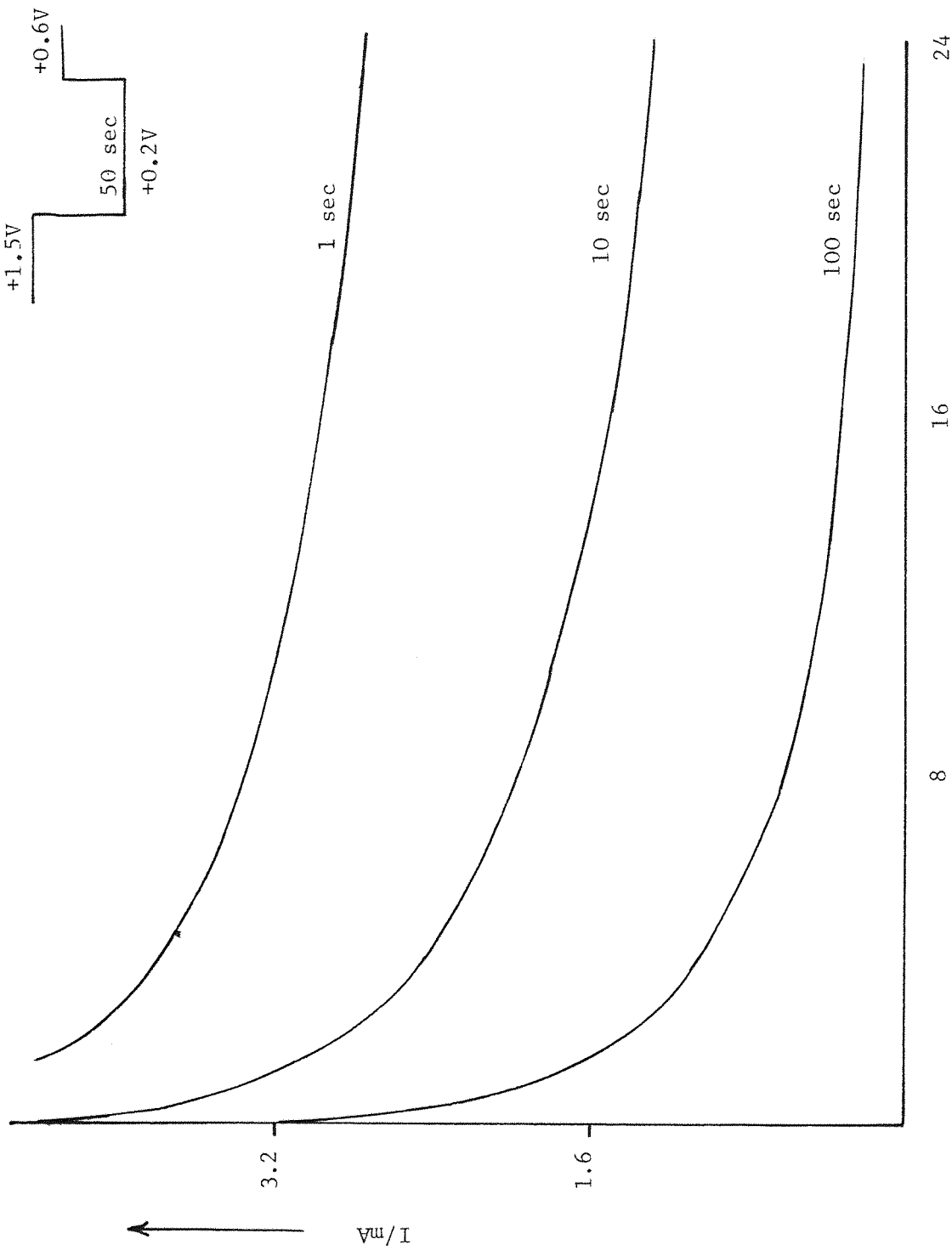

Figure A.8 I-t transients resulting from potential step applied to a platinum electrode in solution as in figure A.6.

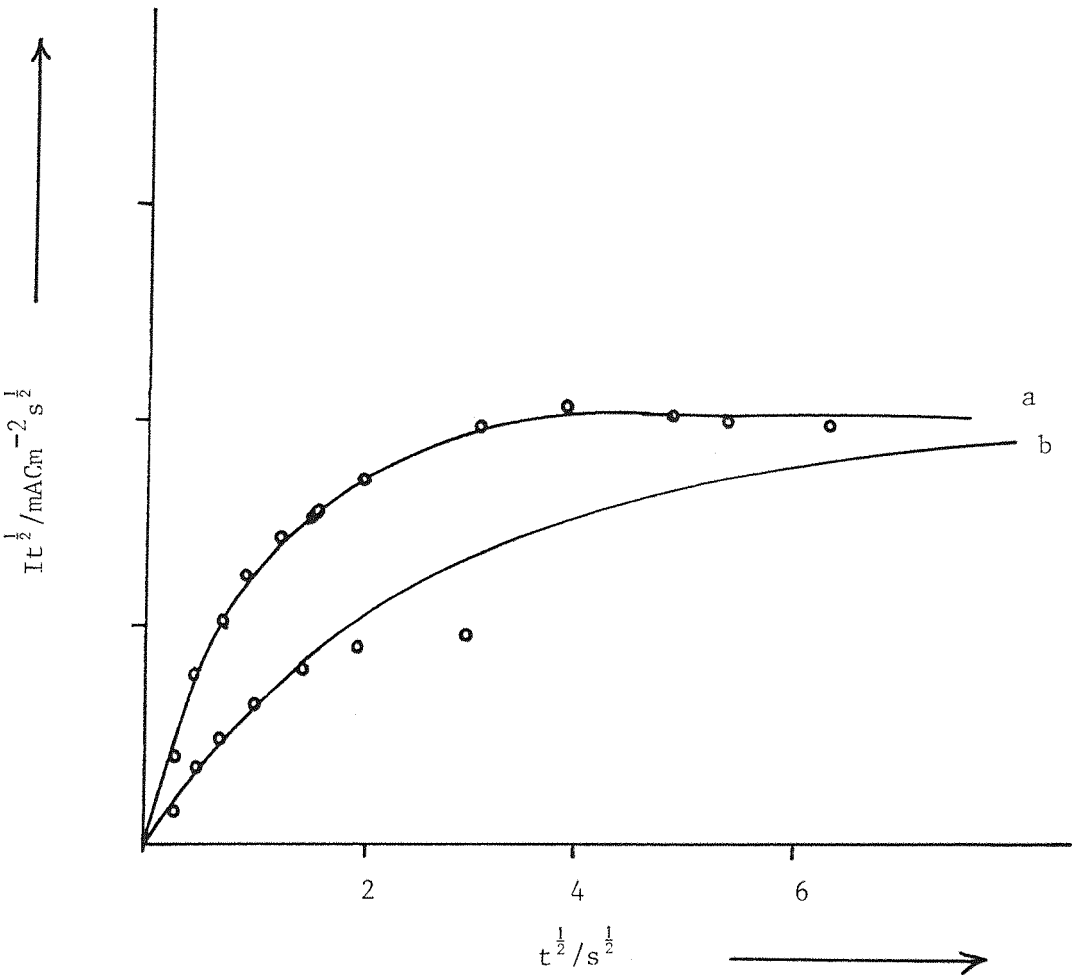

Figure A.9 A plot of $It^{\frac{1}{2}}$ vs $t^{\frac{1}{2}}$ plot for the data obtained from Figure A.7 and A.8.

(a) For formic acid

(b) For Dueterated acid

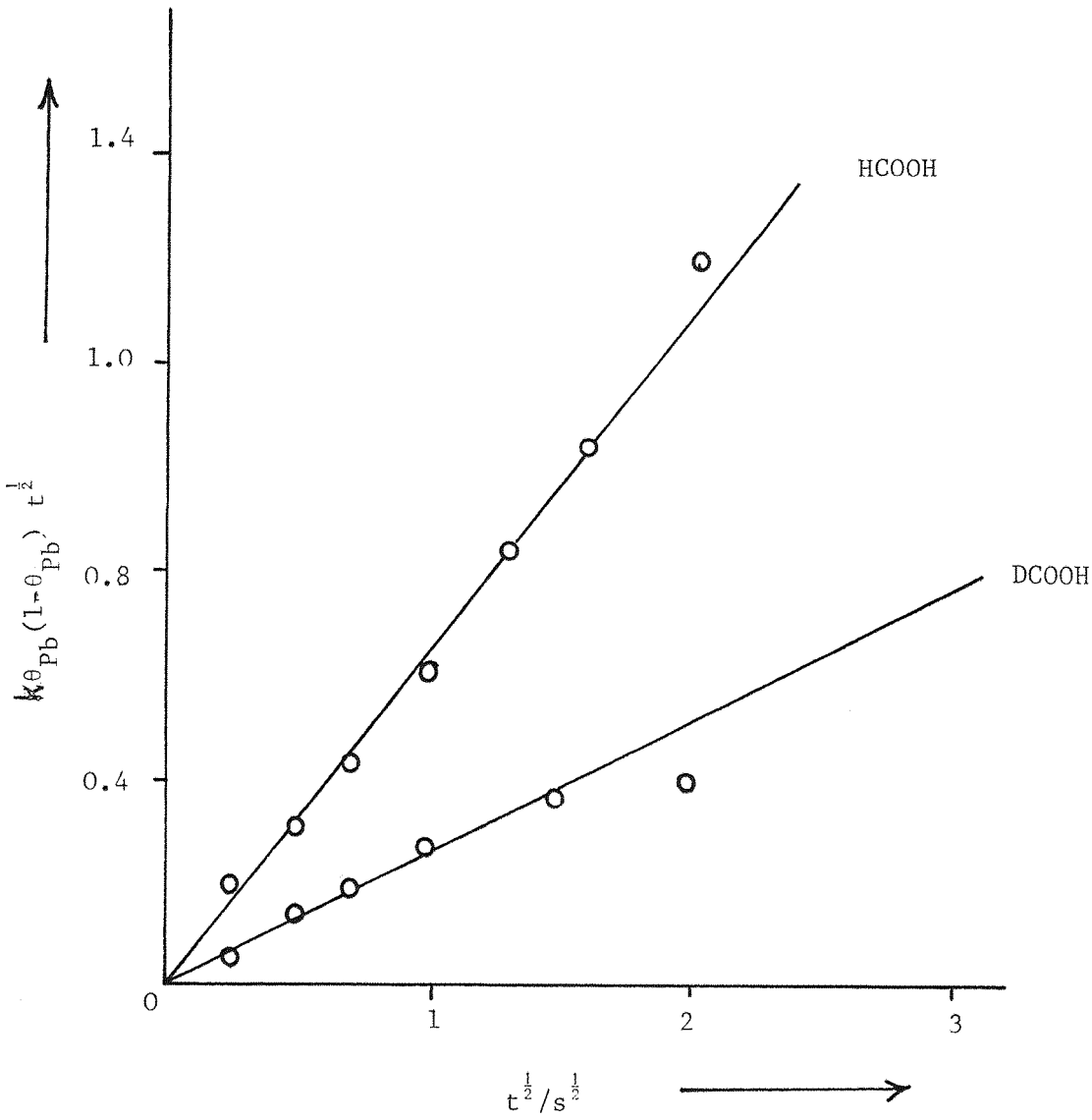

Figure A.10 A plot of $\frac{k\theta_{Pb}(1-\theta_{Pb})t^{\frac{1}{2}}}{D^{\frac{1}{2}}}$ (λ obtained from Figure A.2 for various times) versus $t^{\frac{1}{2}}$.

REFERENCES

1. Atlas of Electrochemical Equilibria in Aqueous Solutions by Marcel Pourbaix. Pergammon Press (1966)
2. H.A.Droll, B.P.Block and W.C.Ferleius. J.Phys.Chem.6 (1957) 1000.
3. A.K.Sundaram and E.B.Sandell, J.Amer, Chem.Soc.77 (1955) 855.
4. Critical Stability Constants, Vol.4. Inorganic Complexes, Robert M. Smith and Arthur E. Martell. Plenum Press (1976).
5. A.I.Busev, The Analytical Chemistry of Indium, Pergammon Press. 1962
6. G.Beidermann, Rec. Trav. Chim.Pays - Bas, 75 (1956) 716; Ark.Kem 9 (1955) 277.
7. T. Moeller, J.Amer. Chem. Soc. 63 (1941) 1206
8. T.Moeller, J. Amer. Chem. Soc. 63 (1941) 2625
9. B.G.F.Carlson, and H.Irving, J.Chem. Soc. (1954) 4390
10. D. Ferri, Acta Chem. Scand. 26 (1972) 733
11. T.P.Radhakrishnan and A.K.Sundaram, J.Electroanal. Chem. 5 (1963) 555.
12. J.W.Gibbs, Collected Works, Vol. 1, Thermodynamics, Yale University Press, New Haven, 1948.
13. W.Kossel, Nachr, Ges. Wiss Gothingen, Math, Physic K.I., (1929) 135
14. I.N.Stranski and R.Kaishev, Physical Z., 36 (1935) 393.
15. A.Bewick., M. Fleischmann and H.R.Thirsk, Trans. Faraday Soc. 58 (1962) 2200
16. W.K. Burton., N. Cabrera and C.F. Frank. Discussion Faraday Soc. 5 (1949),33, 40,48.
17. H. Seiter and H. Fischer, Z. Electrochem. 63 (1959) 249
18. V. Kohlschutter and A. Torricelli, Z. Electrochem. 38 (1932) 213
19. F.C.Frank, N. Cabrera and D.A.Vermilyea, Growth and Perfection of Crystals, Willey, New York (1958)
20. P.B.Price, D.A. Vermilyea and M.B.Webb, Acta Met 6 (1958) 524.
21. J.L.Barton, and J.O.M. Bockris, Proc. Roy. Soc. London, Ser. A (1962)
22. M. Fleischmann and H.R.Thirsk, Electrochim; Acta, 2 (1960) 22
23. H.S.Carslaw and J.C.Jaegar, Conduction of Heat in Solids, Clarendon Press, 1959.
24. F.C.Frank, Proc. R. Soc. Lond., A201 (1956) 586
25. D.J.Astley, J.A.Harrison and H.R.Thirsk, Trans Faraday Soc. 64 (1968) 192
26. G.J.Hills, J. Thompson and D.J.Schiffrin 19 (1947) 657.
27. M.Fleischmann, and H.R.Thirsk, Electrochinica Acta 1 (1959)146
28. M.Fleischmann, and H.R.Thirsk, Advances in Electrochemistry and Electrochemical Engineering Vol,3, Interscience New York 1963
29. J.Willis., J.Amer. Chem. Soc. 67 (1945) 547

30. A.Ruis and M.Molera, AnR. Soc. Fis. Quim (Madr) 45B(1949) 1151
31. R.B.Simpson., R.L. Evans and H.A.Sarof., J. Amer. Chem. Soc.77 (1955) 1438
32. W.H. Douglas and R.J. Magee. J. Electroanal chem. 5 (1963) 171.
33. W.Watt and J.A.Cunningham. J. Electrochem. Soc,, 110 (1963) 716
34. R.J.Magee and W.H. Douglas, J. Electroanal. Chem. 6 (1963) 261
35. R.Wilson and R.Daniel. Anal. Chem. 27 (1955) 906
36. S.I.Woodburn, T.J. Carmell., and R.J. Magee.Recl; Trav. Chim. Pay - Bas 88 (1969) 1167.
37. I. Kravtsov and M.I.Zelenskii, Elektrokhimiya 2 (1966) 1138
38. I. Kravtsov and M.K.Zelenskii, Elektrokhimiya 5 (1969) 247
39. I. Dravtsov and I.I. Shereshevskaya. Elektrokhimiya 5 (1969) 985
40. M.I. Zelenskii and V.I.Dravtsov, Elektrokhimiya 6 (1970) 793
41. V.I. Kravtsov and I.I. Shereshevskaya, Elektrokhimiya 7 (1971) 99
42. V.I. Kravtsov and I.I. Shereshevskaya, Elektrokhimiya 7 (1971) 618
43. V.I. Kravtsov and I.I. Shereshevskaya, Elektrokhimiya 7 (1971) 407
44. M.I.Zelenskii and V.I. Kravtsov, Elektrokhimiya 6 (1970) 1057
45. D.J. Astley, J.A.Harrison and H.R.Thirsk, Trans. Faraday. Soc. 64 (1968) 192
46. J.A.Harrison, R.P.J.Hills, J. Thompson, J. Electroanal.Chem. 47 (1973) 431
47. J.A.Harrison, J. Thompson, J. Electroanal. Chem.,40 (1972) 113
48. J.A.Harrison, J. Thompson, J. Electroanal. Chem.,43 (1973) 405
49. M.F.Bell, J.A.Harrison, J. Electroanal. Chem.,41 (1973) 15
50. R.K.Astakhova, B.S.Krasikov., Fiz Khim, 4 (1969) 116 (Russ)
51. F. Domenech, J. Genesea, L.Victori, Rev. Metal 14 (1978) 321 (Span).
52. J.J. Lingane., J. Amer. Chem Soc. 61 (1939) 2099
53. D.G.Tuck and M.K.Yang, J. Chem. Soc. A (1971) 3100
54. S.A.Lavitskaya, S.A. Zebreva and A.I.Palagutuna. Izv. Uyssh. Ucheb. Zaved. Khim Tekhnol. 14 (1971) 1468
55. L. Kiss, A. Korosi and J. Farkas, Nagy. Kem Falyoriat 75 (1969) 66.
56. G.M. Budov and V.V.Losev, Dokl.Akad. Nauk SSSR 129 (1959) 6
57. V.V. Losev and A.I. Molodov, Dokl. Akad. Nauk SSSR 135 (1960) 111
58. A.P. Pchel'nikov and V.V. Insev., Elektrokhimiya. 5 (1969) 284.
59. R.E.Visco, J. Phys. Chem. 69 (1965) 202
60. R.E.Visco, J. Electrochem. Soc. 112 (1965) 932, 113 (1966) 636
61. B. Miller and R.E.Visco. J. Electrochem. Soc., 115 (1968) 251
62. V.Markovac and B. Lovrecek. J. Electrochemical Soc. 113 (1966) 838
63. G.A.Wright, J. Electrochemical Soc. 114 (1967) 1263.
64. Tedeschi, J. Benjamin, J. Precious Met (Proc. Int. Precious Met inst conf, 5th, 1981) Pub 1982, Edited by Zysk, Edward D. Pergmon
65. R.W.Johnson. J. Electrochem. Soc. 108 (1961) 632

66. Speciality Inorganic Chemicals. R.T.Thompson. Royal Society of Chemistry London 1981.
67. Mayer Ursula, Metalloberfaeche 3 (1978) 32 (Ger)
68. N.O. Tomashov., G.P. Chernova, T.A. Fedoseera. Zashch Met.13 (1977) 164 (Russ) (86, 1626802)
69. W.Keitel and H.E.Zchiegner. Trans. Electrochem. Soc, 59 (1931) 273
70. J.S.Stevenson, Trans, Inst. met, Finish, 59 (1981) 113
71. R.H.Reid, Plating 52 (1965) 531
72. L.A.Heathcote, Plat Met. Rev, 9 (1965) 80
73. Ch.J.Raub. Plat, Met, Rev., 26 (1982) 158
74. Ronald. J. Morrisey. Plat. Met. Rev. 27 (1983) 10
75. Technic. Inc. British Patent 1, 014, 045 (1965)
76. N. Hopkin. Inc British Patent 965, 859, (1969)
77. R.H.Atkinson and A.R.Rapaer. J. Electrodeposits. Tech. Soc. 8, 1, (1933)19
78. A. Brenner, G.E. Riddell, J.Res. Natn, Bur, Stand, 37 (1946) 31
79. G. Gutzeit, Plating, 46 (1959) 1158, 1275, 1377,- 47 (1960) 63
80. A. Brenner, Met. Finish, 52 (1954) 68.
81. R.N.Rhoda, , Trans Inst; of Met Finish 36 (1959) 82
82. R.N. Rhoda, , J. Electrochemical Soc; 108 (1961) 707
83. F. Pearlstein, Met Finish 53, 59 (1959)
84. F. Pearlstein, and R.F. Weightman, Plating, 56 (1969) 1158
85. Kawagoshi Saka. Japan Kokai 77, 60, 733 (CI, C23, C_3/02)
86. Miscioscio, Kathleen B., Smith Paul T., Fr Demande FR2, 496, 129.
87. Crosby, Jaffrey Norman (Inco Europe Ltd) Eur Pat.
88. Miscioscio, B.Kathleen, T. Smith Paul., Fr. Demande FR2, 496, 127 (U.S.Patent)
89. Yahlom Joseph (Bell Telephone Laboratories, Inc) U.S; U.S. 4,299,67 (chem ab; 96, 26376)
90. Lamaczyk, J.Robert,(Bunker Ramo corporation) Porit, U.K. Pat. App. G.B. 2, 065, 175.
91. J.M. Stevens, Trans. Inst. Met. Finish 46, (1968) 26
92. Branik, Michael. (Heraeus, W.C. G.M.6.4) Ger.Offen.2,939,920
93. M.A.Whitehead. Metal Finishing 4 (1944) 405.
94. C.F.Smart. Trans. Am. Inst. Min. Metal. Eng. Inst. Met. Div, 128 (1938) 295.
95. B.E.Scot. Proc. Am. Electroplat. Soc.45 (1958) 93.
96. G.L.Schnable and J.G. Janes. Electrochem. Technol, 2(1964) 201
97. H. Suzuki, J. Met. Finish. Soc. Japan, 15 (1964) 283
98. J. Ota, T. Ishikama and K. Kosakai, J. Met. Finish. Soc, Japan 16 (1965) 246

99. Hitach Ltd; Japanese Patent 20 (1966) 806.
100. O.P.Bespalko and I.D.Volvenko. Russian Patent 244,058,(1967)
101. Ya.P.Akmens, D.L.Mikhlovenko, S.I. Rikman, I.M. Ozolinski and D.A. Udem Russian Patent 264, 095,(1968)
102. J.A., F.B and L.E. Lisowski., U.S. Patent 3, 440, 152 (1969)
103. A.J. Certa, T.V. Manns, G.L. Schnable and H.S.Segal. J.Electrochem.SOC 106 (1959) 690
104. N.A.Marchenko, L.S. Ionycheva, and H.V.Batyak, Russian Patent, 160, 410 (1963)
105. R.G.Benham, U.S.Patent 3, 311, 547 (1967).
106. N.G. Rakhmatullah and R.R.Kadyrov, Uzbeksk. Kain, Zh. 13 (1969) 20
107. A. Voronko, R.N. Visomirskis and A.M.Moleadsky, Zascita. Met, 6 (1965) 703.
108. V.M.Gershov and B.A.Purin, Izv.Akad. Nank. Latv. SSSR Ser.Khim No,2 (1969) 175
109. D.Gray. U.S.Patent 1, 935,630 (1933)
110. D.Gray Trans Electrochem. Soc. 65 (1934) 377
111. W.S.Murray and D.Gray. U.S.Patent, 1, 965, 251 (1934)
112. R.L.Westbrook, Trans. Am; Chem. Soc; 57 (1930) 57
113. C.G.Fink and R.H. Lester. Trans Electrochem. Soc; 78 (1930) 289
114. H.B.Linford. Tran Electrochem. Society 78 (1941) 443
115. W.E.Murray. Proc. Am. Electroplat Society June (1944) 160
116. V.V.Losev and A.P.Pchelnikov. Electrochinica Acta 18 (1973) 589
117. T.M.Salem; A.A.Ismail, J.Chem. Soc.A11 (1970) 2415, 2419
118. P. Jones, R. Lind and W.F.K.Wynn-Jones, Trans. Faraday Soc.50 (1950) 972
119. P. Jones, H.R.Thirsk and W.W.K.Wynn-Jones ibid 52 (1956) 1003
120. E.C.Potter, J.Sci; Inter., 29 (1952) 160
121. R.Piercy, P.D.Stokes and N.A.Hampson. Br.Corr.J. 8 (1973) 275
122. V.V.Losev, Electrochim, Acta 15 (1970) 1095
123. A.P.Pchelnikov and V.V. Losev, Elektrochimia, 5 (1969) 284
124. F. Goodridge and C.G.H.King. Trans Faraday Soc; (1970) 2889
125. B. Macdougall and M.J.Graham, Electrochimica Acta 27 (1982) 1093
126. B. Macdougall. J. Electrochemical Society 127 (1980) 789
127. T.Tokuda and M.B.Ives, Corros. Sci; 11 (1971) 297.
128. Z. Szklarska - Smialouska and M.Janik - Czachar,Corros. Sci. 7 (1967) 65
129. Z. Szklarska - Smialouska, Corrosion (Houston) 27 (1971)2231
130. D.N. Swan, Ph.D. Thesis, Southampton University (1980)

131. P. Bindra, A.P. Brown, M. Fleischmann and D.Pletcher. J. Electroanal Chem. 58 (1975) 31

132. P.Bindra. A.P. Brown, M. Fleischmann and D. Pletcher. J. Electroanal Chem. 58 (1975) 39

133. P. Bindra, M. Fleischmann, J.W. Oldfield, and D. Singleton, Chem.Soc. Faraday Dicuss, 56 (1973) 180

134. B.R.Scharifker Ph.D. Thesis Southampton University (1980)

135. M.W. Bayes Ph.D. Thesis Southampton University (1982)

136. A.M.Kavenpour Ph.D. Thesis Southampton University (1982)

137. R. Mark Wightman. J. Analytical Chem. 53 (1981) 1125A

138. J.L.Ponchon, K. Cespuglio, F. Gonan, M. Jouvet, J.F. Pujal. Analchem. 51 (1979) 1483

139. R.S.Robinson, R.L. McCrery. Anal Chem. In Press

140. J.O.M.Bockris, I.A.Ammar and A.K.M.S.Huq. J. Phys. Chem. 61 (1957) 879

141. J. Horiuti and M. Molanyi, Acta Physico Chem. U.R.S.S. 2, (1935), 505

142. R.Parsons and J.O'M Bockris, Trans. Faraday Soc. 47 (1951) 914.

143. J.C.P. Mignolet, J. Chim. Phys., 54 (1957) 19

144. R. Suhrmann, G.Wedler and H. Gentsch, Z. Phys. Chem 17 (1958) 350

145. W.A.Pliskin and R.P. Eischens, ibid., 25 (1960) 69

146. B.E.Conway and J.O'M. Bockris, J. Chem. Physics 26 (1957) 532.

147. A.M. Azzam and J.O'M. Bockris, Trans. Faraday Soc. 48 (1952) 145

148. A.Capon and R.Parsons J. Electroanal Chem. 39 (1972) 275

149. M. Mordart, J. Am. Chem. Soc. 74 (1952) 1531 and 3556

150. F.G.Will and C.A.Kron. Z. Electrochem. 64 (1960) 270

151. I. Fonseca Jiang Lin-Cai, D.Pletcher. J.Electrochem Soc. in press

152. J.Horken., J. Electroanal Chem, 106 (1980) 245.

153. N.Fruya, S. Motoo, Denki Kagasu 41 (1973) 384 (Japan)

154. I. Morcos, J.Elect. Chem Soc. 122 (1975) 1492

155. I. Morcos, J. Electroanal Chem., 72 (1976) 389.

156. I. Morcos, Electrochimica Acta, 22 (1977) 497

157. E. Keren. A. Soffar, J. Electroanal Chem. 44 (1973) 53

158. G.I. Shterev, Zh. Glozhahka, D. Naveh. Tr. Plovdivski, Univ. Mat, Fiz, Khim. Biol. 10 (1972) Bulg) 107

159. A. Capon and R. Parsons J. Electronanal Chem. 45 (1973) 205

160. S. Brummer. J. Electrochem. Soc. 113 (1966) 1043.

161. A.Bewick, K. Kunimatsu, J. Robinson and J.W.Russel. J. Electroanal Chem. 119 (1981) 175

162. A.Bewick and J.W.Russel, J. Electroanal Chem, 132 (1982) 329

163. B. Beden, C. Lanny, A. Bewick and K. Kunimatsu, J. Electroanal Chem 121 (1981) 343

164. B. Beden, A.Bewick, M. Razaq and J.Webber. J. Electroanal Chem. 139 (1982) 203

165. A. Bewick and M. Razaq. To be published

166. A. Capon and R.Parsons, J.Electroanal. Chem. 44 (1973) 239

167. A. Capon and R. Parsons, J. Electroanal. Chem. 65 (1975) 285

168. J. Giner. Electrochim Acta, 8 (1963) 985, 9 (1964) 835

169. A. Kutschker and W. Vilslich, Electrochimica Acta 8 (1963) 985 and 9 (1964) 835.

170. M.W.Brieter, Electrochimica Acta 8 (1963) 973

171. D.A.J.Rand, R.Wood, J.Electroanal Chem, 31 (1971) 29

172. A.G.Poliak, Yu.B.Varisiliev, V.S.Bagoskii and R.M.Smirnova, Electrokhim 3 (1967) 1076.

173. G. Gunawardena, G.J.Hills, and I. Montenegro and B.R.Scharifker. J. Electroanal. Chem 138 (1982) 255

174. G. Gunawardena, G.J.Hills and I. Montenegro. J. Electroanal Chem. 138 (1982) 241

175. G. Gunawardena, G.J.Hills, I. Montenegro and B.R.Scharifker. J. Electroanal Chem. 138 (1982) 225

176. Belenkii, V.N. Vkr, Khim. Zh. (Russ.Ed) 46 (10)(1980) 1032.

177. M.M.Nicholson. Anal. Chem. 32 (1960)

178. A.P.Pchelnikov and V.V.Losev, Zashch Metal 1 (1965) 482. Proc.3rd Int, Cong on Metallic corrosion. Mowcow 1966, P.H1, Moscow(1968)

179. Ermin Langale and Norman Hackman. J. Electrochem. Soc. 18 (1971) 1273.

180. M. Fleischmann, J. Koryta and H.R.Thirsk, Trans. Faraday Soc., 63 (1967) 1261

181. M.J.Lian - unpublished results

182. Jiang Lin - Cai, J. Electrochem. Soc. in press.

183. H. Angerstien - Kozlowska, B. MacDougall and B.E.Conway, J. Electrochem. Soc. 120, (1973), 756

184. R.R.Adzic, K.I.Popov and M.A. Pamic, Electrochim. Ecta. 23 (1978),1191

185. R.R.Adzic, W.E.O'Grady and S.Srinivasan, J. Electrochem Soc. 128 (1981),1913

186. R.R.Adzic, D.N.Simic, D.M.Drazic and A.R.Despic. J.Electroanal chem. 61 (1975) 117, 65 (1975) 587, 80 (1977), 81.

187. D.Pletcher and V.Solis, J.Electroanal Chem, 131 (1982) 309.

188. D.Pletcher.J. Electrochemical. Soc. in Press.

189. N.Furaya and S.Motoo. J. Electroanal. Chem 98 (1979) 189.

190. D.M.Kolb, Advance in Electrochemistry and Electrochemical Engineering 11 (1979) 125

191. S.Motoo and M.Watanabe, J.Electroanal Chem. 98,(1979), 203

192. A.Capon and R.Parsons. J.Electroanal Chem, 45 (1973) 205

193. D.D.MacDougall, Transient Techniques in Electrochemistry. Plenum Press 1977.

194. P.Delahay and S.Oka, J.Am.Chem Soc. 82 (1960 329.

195. J.L.Falconer and R.J.Madix. Surface Science 46 (1974) 473.

196. K. Hirota, K. Kunata, T. Olakai and S.Asai,in: Proc. Second Intern. Cogr. Catalysis, Paris, 1961, p.809.

197. R. Woods in A.J.Bard (Ed), Electroanalytical chemistry, Vol.9, Plenum Press, 1976.